Rotten Hill: A Late Triassic Bonebed In The Texas Panhandle, USA

By: SPENCER G. LUCAS1, LARRY F. RINEHART1, **ANDREW B. HECKERT**2, ADRIAN P. HUNT3 AND JUSTIN A. SPIELMANN3

Abstract

The Rotten Hill bonebed is a Late Triassic fossil locality in the Texas Panhandle discovered by Floyd V. Studer in 1926, and collected primarily by WPA-funded excavations during the late 1930s and early 1940s. This locality is in the lower part of the Tecovas Formation (Chinle Group) and is of Adamanian (late Carnian) age. Forensic taphonomic analysis indicates it is a mass death assemblage that was hydraulically concentrated. The Rotten Hill bonebed is a low diversity multitaxic and monodominant bonebed; the vast majority of the bones are of the metoposaurid Koskinonodon perfectum. It closely resembles other Chinle Group metoposaurid-dominated bonebeds that suggest aggregation of a group of metoposaurids, followed by catastrophic mortality, complete disarticulation and disassociation of the skeletons, culminated by rapid transport and burial. Fossil taxa from the Rotten Hill bonebed are the unionoidan bivalve Plesioelliptio sp., the coprolite ichnogenera Alacocopros, Eucoprus and Heteropolacopros; various fishes known from ichthyoliths; a rhynchosaur; a sphenodontid; the archosauriform Vancleavea; the trilophosaurs Trilophosaurus and Spinosuchus; the phytosaur Smilosuchus; a probable poposaurid (cf. Postosuchus), the aetosaurs Desmatosuchus and cf. Stagonolepis; a shuvosaurid; and the metoposaurids Apachesaurus gregorii and K. perfectum. K. perfectum is represented by numerous skulls, lower jaws, vertebrae, girdle and limb bones representing a minimum number of 68 individuals based on recovered interclavicles. We describe the osteology and variation of these bones, which allows us to present a revised diagnosis of Koskinonodon that employs new postcranial characters to differentiate it from other metoposaurid genera. We also compiled and analyzed a morphometric database of the Rotten Hill Koskinonodon to conclude that bone growth varied from isometry to allometry and suggests a loss in limb robustness during ontogeny that likely indicates a transition from a partly terrestrial to a more aquatic lifestyle. Probability plotting to test for size groups in the Rotten Hill Koskinodonon identifies 10-11 groups that we interpret as yearly age cohorts and use to plot a growth curve. This indicates indeterminate growth in K. perfectum and that the Rotten Hill sample represents a population of breeding adults, some of which survived at least 10-11 years after reaching sexual maturity. This is a growth curve also characteristic of some living salamanders. We infer that K. perfectum employed some mechanism, such as disparate feeding strategies, or another ecological factor that enforced separation of adults and juveniles, to reduce predation on juveniles by conspecifics and minimize the competition for food resources between the ontogenetic stages.

Heckert, Andrew & P. Hunt, Adrian & Lucas, Spencer & A. Spielmann, Justin & Rinehart, Larry. (2016). *Rotten Hill: A Late Triassic Bonebed in the Texas Panhandle, USA*. New Mexico Museum of Natural History and Science Bulletin. Version of record available at: https://www.researchgate.net/publication/321826539_Rotten_Hill_A_Late_Triassic_Bonebed_in_the_Texas_Panhandle_USA

ROTTEN HILL: A LATE TRIASSIC BONEBED IN THE TEXAS PANHANDLE, USA

SPENCER G. LUCAS[1], LARRY F. RINEHART[1], ANDREW B. HECKERT[2], ADRIAN P. HUNT[3] AND JUSTIN A. SPIELMANN[3]

[1]New Mexico Museum of Natural History, 1801 Mountain Road N. W., Albuquerque, NM 87104; [2]Department of Geology, Appalachian State University, ASU Box 32067, Boone, NC 28608-2067; [3]Flying Heritage Collection, 3407 109th St. SW, Everett, WA 98204

Abstract—The Rotten Hill bonebed is a Late Triassic fossil locality in the Texas Panhandle discovered by Floyd V. Studer in 1926, and collected primarily by WPA-funded excavations during the late 1930s and early 1940s. This locality is in the lower part of the Tecovas Formation (Chinle Group) and is of Adamanian (late Carnian) age. Forensic taphonomic analysis indicates it is a mass death assemblage that was hydraulically concentrated. The Rotten Hill bonebed is a low diversity multitaxic and monodominant bonebed; the vast majority of the bones are of the metoposaurid *Koskinonodon perfectum*. It closely resembles other Chinle Group metoposaurid-dominated bonebeds that suggest aggregation of a group of metoposaurids, followed by catastrophic mortality, complete disarticulation and disassociation of the skeletons, culminated by rapid transport and burial. Fossil taxa from the Rotten Hill bonebed are the unionoidan bivalve *Plesioelliptio* sp., the coprolite ichnogenera *Alacocopros*, *Eucoprus* and *Heteropolacopros*; various fishes known from ichthyoliths; a rhynchosaur; a sphenodontid; the archosauriform *Vancleavea;* the trilophosaurs *Trilophosaurus* and *Spinosuchus*; the phytosaur *Smilosuchus*; a probable poposaurid (cf. *Postosuchus*), the aetosaurs *Desmatosuchus* and cf. *Stagonolepis*; a shuvosaurid; and the metoposaurids *Apachesaurus gregorii* and *K. perfectum*. *K. perfectum* is represented by numerous skulls, lower jaws, vertebrae, girdle and limb bones representing a minimum number of 68 individuals based on recovered interclavicles. We describe the osteology and variation of these bones, which allows us to present a revised diagnosis of *Koskinonodon* that employs new postcranial characters to differentiate it from other metoposaurid genera. We also compiled and analyzed a morphometric database of the Rotten Hill *Koskinonodon* to conclude that bone growth varied from isometry to allometry and suggests a loss in limb robustness during ontogeny that likely indicates a transition from a partly terrestrial to a more aquatic lifestyle. Probability plotting to test for size groups in the Rotten Hill *Koskinodonon* identifies 10-11 groups that we interpret as yearly age cohorts and use to plot a growth curve. This indicates indeterminate growth in *K. perfectum* and that the Rotten Hill sample represents a population of breeding adults, some of which survived at least 10-11 years after reaching sexual maturity. This is a growth curve also characteristic of some living salamanders. We infer that *K. perfectum* employed some mechanism, such as disparate feeding strategies, or another ecological factor that enforced separation of adults and juveniles, to reduce predation on juveniles by conspecifics and minimize the competition for food resources between the ontogenetic stages.

INTRODUCTION

The Chinle Group in the western United States contains one of the world's most extensive, stratigraphically superposed, Late Triassic vertebrate fossil records (Long and Murry, 1995; Lucas, 1997). This record includes several well known bonebeds, including the *Placerias* quarry in eastern Arizona (Camp and Welles, 1956; Kaye and Padian, 1994; Fiorillo et al., 2000), the *Coelophysis* (or Whitaker: Colbert, 1989; Rinehart et al., 2009), Canjilon (Long et al., 1989; Hunt and Downs, 2002; Zeigler et al., 2002a), Snyder (Heckert et al., 2000; Zeigler et al., 2003a) and Hayden (Irmis et al., 2007; Nesbitt et al., 2009a) quarries in north-central New Mexico (see also Heckert et al., 2005), the Lamy amphibian quarry in central New Mexico (Romer, 1939; Colbert and Imbrie, 1956; Zeigler et al., 2002b; Lucas et al., 2010) and the *Trilophosaurus* quarries in West Texas (Gregory, 1945; Spielmann et al., 2008). Another significant Chinle Group bonebed is the Rotten Hill bonebed, an amphibian-dominated fossil locality, located in the Texas Panhandle (Fig. 1). The Rotten Hill and Lamy bonebeds, as well as another bonebed documented by Case (1932) in Scurry County, Texas, are the three largest accumulations of metoposaurids known, not only from North America, but from all of Late Triassic Pangea.

Discovered in 1926 and collected in the 1930s and 1940s, the Rotten Hill amphibian fossils have been discussed in various publications devoted to metoposaurid amphibians, such as Colbert and Imbrie (1956) and Hunt (1993), and some of the other tetrapods were documented by Murry (1982, 1986, 1989a) and Long and Murry (1995). However, the entire quarry fossil assemblage and its taphonomy and paleobiological significance have never been published. Here, we present a complete study of the Rotten Hill fossil assemblage, review its stratigraphic context, analyze its taphonomy, establish its taxonomic composition and present complete osteological data on the metoposaurid fossils that dominate the assemblage. This metoposaurid sample provides new information on metoposaurid taxonomy and ontogeny that improves our understanding of metoposaurid paleobiology.

INSTITUTIONAL ABBREVIATIONS

The following institutional abbreviations are used in the text: **NMMNH** = New Mexico Museum of Natural History and Science, Albuquerque, New Mexico; **PPHM** = Panhandle Plains Historical Museum, Canyon, Texas; **SMU** = Southern Methodist University, Dallas, Texas; **UMMP** = University of Michigan Museum of Paleontology, Ann Arbor, Michigan.

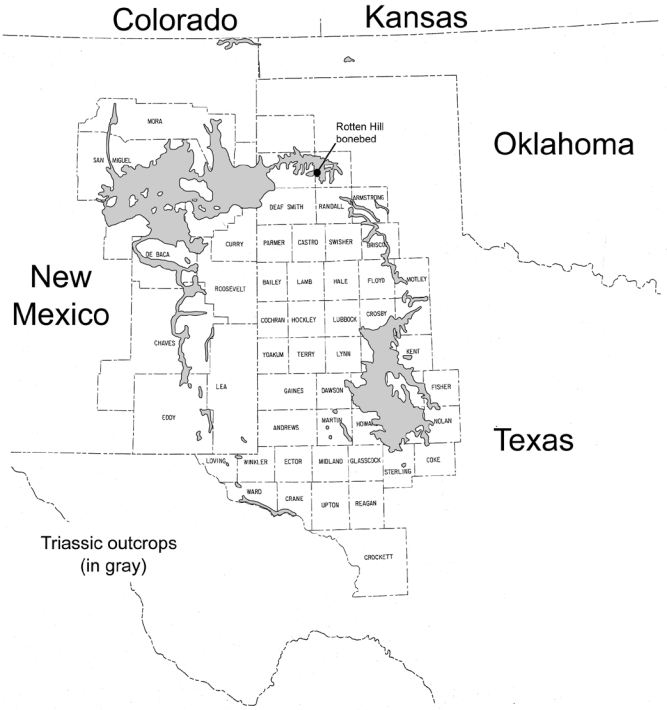

FIGURE 1. Map of West Texas showing outcrops of Chinle Group strata (after McGowen et al., 1979) and location of Rotten Hill bonebed.

The various fossils in the Panhandle Plains Historical Museum collection utilized in this study have a variety of numbers assigned to them, even though all elements illustrated and described are from a single quarry and single institution. We believe that this is a product of various cataloging systems being implemented over the 75+ years these specimens from Rotten Hill have been a part of the collection of the PPHM. Three numbering systems can be noted: WT, PPHM and X numbers.

The WT number consists of the letters "WT" (we assume this is an acronym for West Texas), and four digits (e.g., WT 2926, parts of three lungfish dental plates) followed occasionally by a dash and a single digit--this single digit is used to identify individual specimens within a multispecimen lot (e.g., WT3166-1, a complete skull of *Koskinonodon*). The PPHM number consists of the letters "PPHM," which is the acronym of the Panhandle Plains Historical Museum, followed by a single number (e.g., PPHM 6, a complete skull of *Koskinonodon*). The X numbers appear to be organized in a manner similar to an accession number with a four-digit year (typically 2000, suggesting that this is the most recent cataloging system used), a period, a two-digit number, a period and a three-digit number (e.g., coprolites numbered PPHM 1999.35.327 or PPHM 2000.10.82). Long and Murry (1995) typically prefaced specimens with WT designations with the PPHM acronym (e.g., PPHM WT 2961, osteoderm of *Desmatosuchus*), but this was probably to clarify the repository of WT specimens, and was not a combination used in the PPHM collections.

HISTORY OF STUDY

In 1926, Floyd V. Studer (1892-1966), an Amarillo resident, discovered Triassic fossil vertebrates, including what we call the Rotten Hill bonebed, along the Sierrita de la Cruz Creek in Oldham and Potter Counties, northwest of Amarillo (Fig. 1). Studer discovered the Rotten Hill bonebed while searching for a locality based on " a cowboy's story of finding 'sharks teeth' in the Rotten Hill area" (Studer, 1958, p. 5). Studer (1951, 1958) also stated that he oversaw excavation of the bonebed in 1937-1939, as it was quarried on behalf of the Panhandle Plains Historical Society and West Texas State College. (In evident contradiction, Murry [1989a, p. 132] states that the WPA excavation took place in 1941, but information in Appendix 1 demonstrates that at least some WPA excavation at Rotten Hill preceded 1941). Studer also noted that crews from the University of Michigan, Yale University and "Pennsylvania University" had collected in the area.

Studer (1951, p. 18) stated that the vertebrate fossils in the excavated quarry are "most abundant in the lavender shales that are the lowest part of the exposed section in the vicinity of the quarry," and his text indicates that a phytosaur skull came from the quarry, as did other phytosaur fossils that he assigned to *Brachysuchus megalodon*. Studer (1951, p. 20) also said that "vertebra [sic], teeth, and a claw of a small dinosaur have also been found at the quarry," as well as fossils of unionid bivalves.

Ermine Cowles Case (1871-1953) and his University of Michigan field crews collected along the Sierrita de la Cruz Creek during the late 1920s and early 1930s, securing specimens of metoposaurs, aetosaurs (holotype of *Stagonolepis wellesi* and specimens of *Desmatosuchus haplocerus*), a "rauisuchian," and phytosaurs, including specimens referred to *Leptosuchus crosbiensis* and *Smilosuchus gregorii* by Long and Murry (1995). At UMMP, these specimens are often described on labels as being from "Sierrita de la Cruz" or, informally, "Sweetly Cruize." According to Long and Murry (1995, p. 14), Case's field notes indicate that on 10 July 1931 he discovered a bone bed in "purple clay above the white layers" at Rotten Hill, from which he collected both phytosaur and metoposaur bones. We take this to indicate that Case may have independently located the Rotten Hill bonebed, five years after Studer's original discovery.

C. Stuart Johnston (1900-1939) obtained funding from the WPA (Works Progress Administration) to excavate the Rotten Hill bonebed. Johnston did this as part of his work at the West Texas State Teachers College, beginning in 1934, where he had started a Department of Geology and Paleontology (Lintze, 2003). It seems most likely that Johnston secured the funding, but that Studer actually oversaw the excavation, which was undertaken by otherwise unemployed men hired with the WPA money.

This is an important point, because those who actually undertook the excavation had no training in anatomy or paleontology, and the only trained paleontologist involved was Johnston, but he apparently did not participate regularly or directly in the excavation. It appears likely that these or similarly untrained personnel also undertook much of the preparation, although this is somewhat speculative based on the few records available. This may, in part, explain the composition of the collection from the bonebed, which is definitely biased against smaller bones—metoposaur vertebral intercentra, neural arches and foot bones as well as tetrapod teeth are conspicuously under-represented (see below).

In the PPHM archives, three quarterly reports to the WPA are the only remaining written records that shed further light on the excavations (Appendix 1). Prepared after Johnston's sudden death, they appear to represent final reports that closed the WPA-funded excavation. They refer to the Rotten Hill bonebed as being located 25 miles (40 km) northwest of Amarillo on the Herring Ranch lease. They note the domination of the material in the bonebed by "stegocephalian material" and indicate the presence of bones of phytosaurs and of the aetosaur *Desmatosuchus*. They also list lungfish toothplates as part of the collection.

A literal reading of the 1940 reports makes it sound like a new quarry had been located, different from the quarry discovered some 15 years earlier by Studer, but that seems highly unlikely. A key passage in the March 1941 report reads "the fossils found [in the quarry] are disarticulated and belong almost entirely to water-loving animals. Many different individuals are found crowded together and todate [sic] over ten thousand specimens have been found. As would be expected a large number of these are fragments, however, a large majority are complete specimens."

The Rotten Hill bonebed fossils have never been fully published. The large metoposaurid sample from the bonebed has figured in taxonomic studies of metoposaurids (e.g., Colbert and Imbrie, 1956; Hunt, 1993; Long and Murry, 1995), but has escaped others (Olsen, 1951; Gregory, 1980; Davidow-Henry, 1989). Some of the coprolites have been illustrated by Hunt et al. (2013), and a few elements of the non-metoposaurid vertebrates from the quarry have been published on by Murry (1982, 1986, 1989a), Long and Murry (1995) and Spielmann et al. (2008). The locality "Rotten Hill," either to refer to the bonebed or to the area around it, has figured as a prominent vertebrate fossil locality in reviews of Texas Late Triassic vertebrate fossils (e.g., Murry, 1982, 1986, 1989a; Long and Murry, 1995), and Long and Murry (1995) provided some history of the site that complements what we provide here.

STRATIGRAPHIC CONTEXT

The Rotten Hill bonebed is located in the Texas Panhandle near the border of Potter and Oldham Counties in the drainage and surrounding badlands of Sierrita de la Cruz Creek (Fig. 1). Finch and Wright (1983, p. 85) published the location of the bonebed, and locality data are also on file at the PPHM, as well as at the NMMNH as NMMNH locality 8997. The collections made by Murry (1982, 1986, 1989a) are reposited at SMU as their locality 121. Because of restrictions on land access, we were not able to visit the locality during the course of this study.

Studer (1951, 1958) noted that the Rotten Hill bonebed is in the Tecovas Formation, and that sandstone/conglomerate that caps ridges and buttes in the Sierrita de la Cruz area is Trujillo Formation (e.g., Gould, 1907; Finch et al., 1976; Finch and Wright, 1983; Lucas, 1993; Lucas and Anderson, 1993). Finch et al. (1976) and Finch and Wright (1983) measured a stratigraphic section at the bonebed that places it in the Tecovas Formation, approximately 36 m below the contact of the Tecovas with the overlying Trujillo Formation (Fig. 2). It thus is in a mudstone-dominated portion of the Tecovas Formation. Murry (1989a, fig. 8) published a similar stratigraphic section at the quarry (Fig. 2).

Fossil vertebrates from the Tecovas Formation establish its age as Adamanian (late Carnian) (Lucas and Hunt, 1993; Lucas et al., 1994, 2012; Lucas, 1998, 2010). The holotypes of both *Tecovasuchus chatterjeei* Martz and Small (2006) and of *Stagonolepis* (=*Calyptosuchus*) *wellesi* (Long and Ballew, 1985) were recovered from the Tecovas Formation in this region, and both are index taxa of the Adamanian land-vertebrate faunachron (Heckert et al., 2007a,b; Lucas, 2010). Parker et al. (2008) named a relatively small aetosaur, *Sierritasuchus macalpini*, for an incomplete skeleton at UMMP collected ~1.5 km east of Rotten Hill in 1939. They (Parker et al., 2008) also tentatively referred another specimen, also from the Tecovas Formation, which provides preliminary evidence that, if valid, *Sierritasuchus* may also be an index taxon of Adamanian age.

Furthermore, most of the vertebrate taxa from the Rotten Hill bonebed (Table 1) are indicative of an Adamanian age (Lucas, 1998, 2010). The associated fauna, based on collections from the Tecovas Formation regionally, includes several phytosaur and aetosaur taxa.

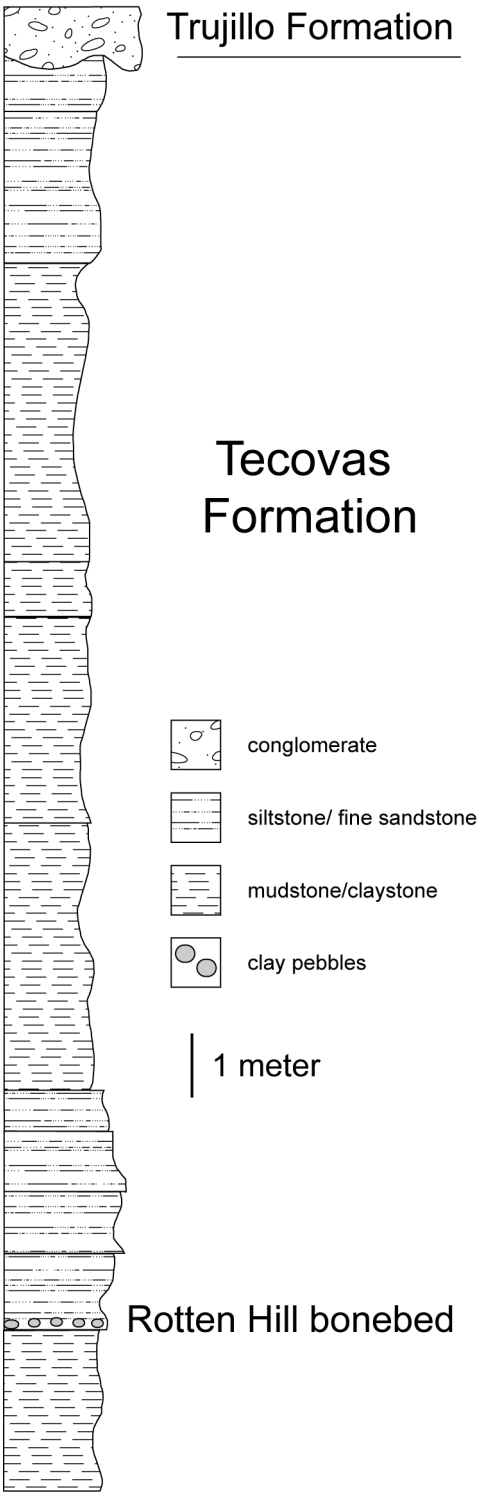

FIGURE 2. Measured stratigraphic section at the Rotten Hill bonebed (after Finch et al., 1976; Finch and Wright, 1983; Murry, 1989a).

Similarly, the phytosaurs *Leptosuchus* and *Smilosuchus* are known only from strata of Adamanian age, although they are identified using a wide range of generic names by different authors (e.g., *Machaeroprosopus*, *Leptosuchus*, *Smilosuchus*, *Rutiodon*, and others). Similarly, *Spinosuchus* is only known from strata of Adamanian age (Spielmann et al., 2009, 2013a). The microvertebarte shark "*Xenacanthus*" (=*Triodus*?) *moorei* was reported by Murry (1989a) and is an index taxon of the Adamanian (Heckert and Lucas, 2006).

Palynomorphs from the Tecovas Formation suggest a late Carnian age as well (Dunay and Fisher, 1974, 1979), as does the megaflora (Lucas et al., 2012; Lucas, 2013). The Tecovas Formation lacks tetrapods diagnostic of the Lamyan interval of the Adamanian, so it is probably of slightly older, Saintjohnsian, age (e.g., Hunt et al., 2005a; Lucas et al., 2012; Lucas, 2013). Therefore, the Rotten Hill bonebed is Adamanian, about 220-225 Ma.

TABLE 1. Faunal list of the taxa present in the Rotten Hill bonebed.

Microvertebrates (based on Murry, 1989a)
"*Xenacanthus*" *moorei*
Neoselachii indet.
Palaeoniscidae, cf. *Turseodus*
Redfieldiidae indet.
Colobodontidae(?)
Semionotidae—*Hemicalypterus*
Arganodus dorotheae
Macrovertebrates
Apachesaurus gregorii
Koskinonodon perfectum
Rhynchosauridae indet.
Sphenodontidae
Spinosuchus sp.
Trilophosaurus buettneri
Vancleavea campi
cf. *Postosuchus*
Shuvosauridae indet.
Smilosuchus gregorii
Desmatosuchus haplocerus
cf. *Stagonolepis wellesi*

TAPHONOMY

Relatively few records were kept of the excavations at the Rotten Hill bonebed, and no sort of quarry map appears to have been made. Also, because of restricted access, we were not able to examine the locality firsthand. Thus, all taphonomic inferences must be made from limited collection records, including the stratigraphic section (Fig. 2), a few field photographs (Figs. 3-4), and the collected fossils, including microvertebrates collected by Murry (1989a), who appears to be the most recent to revisit and collect the locality. We have referred to this as "forensic taphonomy" (Lucas et al., 2010), and we analyze the taphonomy of the Rotten Hill bonebed forensically.

Based on the limited data and other considerations, we address the following geological factors relevant to the taphonomy of the Rotten Hill bonebed: lithologic context, bone abrasion, bone deposition, bone alignment and hydrodynamics. Then, we discuss biological factors: associated non-metoposaurid vertebrates, association of skeletal elements, bone weathering, scavenging, bone fracture, MNI (minimum number of individuals) and age profiles (survivorshop) as biological evidence bearing on the taphonomic interpretation of the Rotten Hill bonebed.

Geological Factors

Lithologic Context

Some of the quarried blocks from the Rotten Hill bonebed containing metoposaur material in the PPHM collection have not been fully prepared, and contain some rock matrix of the bonebed. This matrix is a clay-pebble conglomerate that is color mottled pale reddish brown (10R4/2), grayish red (10R4/2), pale yellowish green (10GY7/2) and grayish green yellow (10GY7/2). The clasts are rip-ups of mudstone, siltstone and calcrete that are mostly 1-3 cm in diameter. The conglomerate is clast supported, and the matrix includes some quartz grains that are fine to medium grained and subangular/subrounded. A historic photograph of part of the bonebed (Fig. 4) suggests a similar

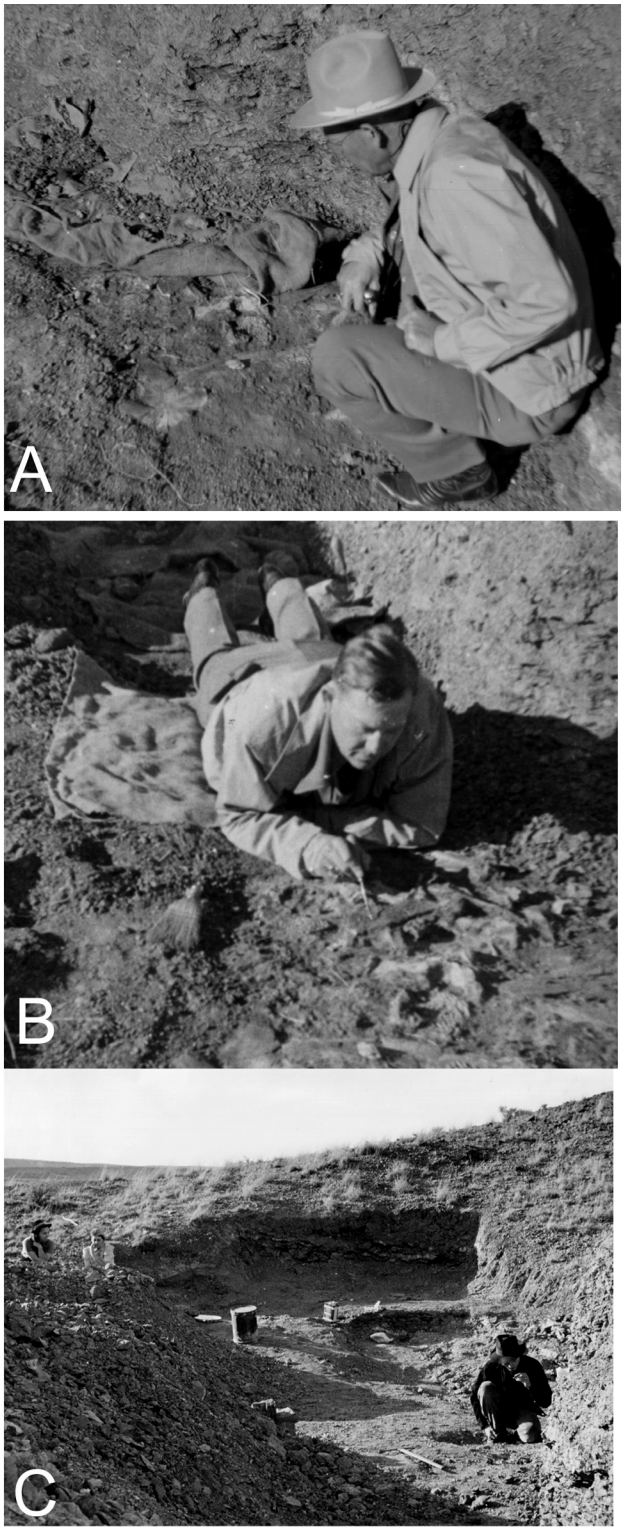

FIGURE 3. Photographic overviews of the Rotten Hill bonebed, Floyd V. Studer in the photos. **A-B**, bones in place and **C**, overview of the excavation site. Scanned from PPHM archives.

conglomerate throughout, and Murry (1989a, fig. 8) also identified the bone-bearing horizon as a color-mottled, clay-pebble conglomerate.

The mudstone-dominated strata that contain the Rotten Hill bonebed (Fig. 2) are readily interpreted as floodplain deposits, which is consistent with similar interpretations of Chinle Group mudstone intervals (e.g., Blakey and Gubitosa, 1983, 1984; Dubiel, 1989; Newell, 1993; Lehman and Chatterjee, 2005; Tanner and Lucas, 2006; Lucas et al., 2010). The bonebed in floodplain deposits at Rotten Hill is thus

FIGURE 4. Photograph of the Rotten Hill bonebed matrix during excavation. Scanned from PPHM archives.

similar to the Lamy amphibian bonebed in north-central New Mexico (Lucas et al., 2010). Both bonebeds are in beds of mudstone of the distal floodplain (lithofacies Fm of Miall, 1996). However, the Rotten Hill bonebed differs in being in a clay-pebble conglomerate matrix, not in the pedogenically-modified mudstone seen at the Lamy bonebed (Lucas et al., 2010). We interpret this conglomerate as a fluvial deposit of either a channel or crevasse splay. We also note that Murry (1989a, p. 132) inferred that the Rotten Hill bonebed had seen "current influence."

Bone Abrasion

Bones from the Rotten Hill bonebed show no signs of abrasion, although we note that nearly all of the teeth are missing from the numerous metoposaurid skulls and mandibles. The teeth were probably lost shortly after death, during brief transport, which otherwise had little effect on the bone surfaces. Thus, all of the bones are in an excellent state of preservation and often preserve small, thin and delicate portions essentially undamaged. All natural breakage of the bones appears to be compression fracturing due primarily to sediment loading and unloading, and shrinkage/swelling of the clays that encased the bones. No indication of trampling is present, and the bones were not obviously abraded by sediment or other objects in flowing water.

Bone Deposition

The limited records from the excavation simply indicate a dense bonebed dominated by disarticulated remains of metoposaurs (Fig. 4; Appendix 1). The most taphonomically informative part of these records is a photograph of the bonebed (Fig. 4). It indicates wholly disarticulated specimens and suggests some alignment of the long axes of the bones (Fig. 4). The disarticulation, apparent alignment and the bonebed matrix indicate that the bones in the Rotten Hill bonebed were hydraulically sorted and transported.

Bone Alignment

All of the metoposaurid amphibian bones, which comprise the vast majority of the elements in the quarry, are disarticulated and mixed in a single layer (Figs. 3B, 4). Skulls, mandibles, clavicular and limb elements and vertebral centra dominate the collections, with manual, pedal, rib and pelvic girdle elements being absent or proportionally less common. Fourteen elongate elements, all at least four times longer than their diameter/width and thus suitable for establishing orientation, were identified in the field photograph (Fig. 4). These were enumerated, identified, and their azimuth recorded (Table 2). The orientation of the photo is unknown, so for this test we assume that north (0°) is at the top. Therefore, the azimuth directions are meaningless, but the degree of alignment of the elements is pertinent to the strength of the paleo-flow.

The elongate elements are highly aligned; 95% of the data occur within an 18° span (Fig. 5). Relatively strong paleo-flow is thus indicated. Some of the elements in the field photo (e.g., the mandibles) have a distinctly heavier end, and the alignment of the rest of the bone with respect to this end indicates flow direction was essentially from the

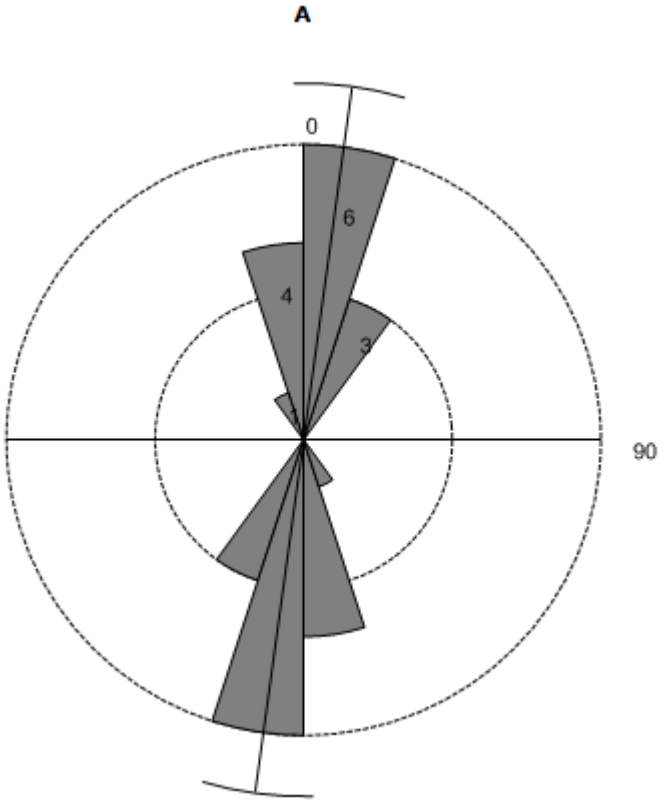

FIGURE 5. Rose diagram data from quarry photo (Fig. 4). Orientation unknown, so the plot shows only the degree of elongate bone alignment, not direction. For purposes of the plot the top of the photo is arbitrarily assigned to north. All measured elements at least four times longer than their diameter. N = 14.

bottom towards the top of the photo (mean direction 7.7°) (Figs. 4-5).

The complete disarticulation of bones at the quarry, and their alignment, strongly suggest some sort of hydraulic transport of the bones, and indicate a strong current to align the bones (e.g., Voorhies, 1969; Sander, 1987; Behrensmeyer, 1988; Fiorillo, 1991). However, the lack of abrasion of the bones and their completeness suggest that this was probably not transport over a long distance, though the degree of abrasion of bones does not always correspond to transport distance (Aslan and Behrensmeyer, 1996).

Hydrodynamics

Almost all of the bones of the metoposaurid skeleton are present in the quarry, from skulls (~ 60 cm long) to small vertebral centra (≤3 cm long). However, the smaller bones are under-represented–neural arches, smaller vertebrae and all bones of the manus and pes are absent. Voorhies (1969) defined three groups of modern mammalian bones distinguished by surface-area-to-volume ratios (SA:V). Group I bones have high SA:V ratios, and include vertebrae, ribs and foot bones, whereas group II bones have intermediate SA:V values and include the femur, tibia, ulna, radius and metatarsals. Group III bones have low SA:V ratios and include skulls and mandibles. The Voorhies groups reflect the hydrodynamic properties of the bones, so each group is moved by different current velocities–low velocity currents move group I bones, and high velocity currents move group III bones.

The Voorhies groups were based on mammal bones, so they do not necessarily apply equally to the bones of lower vertebrates (Blob, 1997). However, we apply them to the metoposaurid bones from the Rotten Hill bonebed, with the modification that we place metoposaurid clavicles and interclavicles (which are long, flat bones) into group III, not group II, where mammal clavicles and "interclavicles" (sternebrae) are placed. This was based on the idea that the metoposaur clavicles and interclavicles would be more difficult to transport because the flowing water would have less traction on the bone (i.e., lower SA:V than the corresponding mammal bones).

Lucas et al. (2010) assigned all the elements of a complete metoposaur skeleton (Sawin, 1945; Dutuit, 1976; Sulej, 2007) to Voorhies groups, so the expectation is domination of Voorhies group

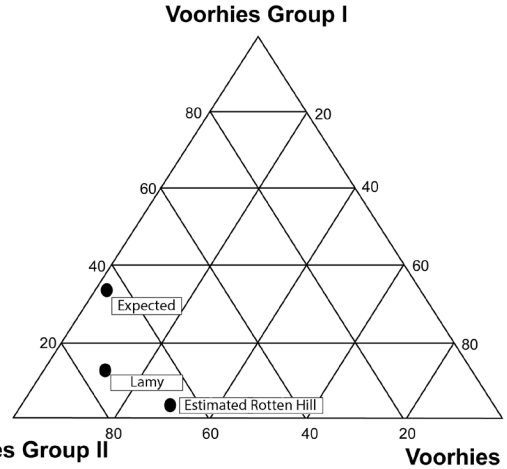

FIGURE 6. Ternary plot showing the expected (based on complete metoposaurid skeleton) and observed Voorhies Group percentages in the Lamy amphibian quarry (Lucas et al., 2010) as well as an estimate of the Voorhies Group percentages in the Rotten Hill bonebed.

II (64%), 34% group I and only 3% group III (Fig. 6). They showed, by actual count, that the Voorhies group proportions for the Lamy amphibian quarry are 75% group II, 13% group I and 12% group III, indicating winnowing of the deposit. In the Rotten Hill bonebed, actual bone counts were not made, but careful examination of the Lamy and Rotten Hill samples clearly showed a further reduction in the Voorhies group I bones at Rotten Hill. We also show an estimate of the Rotten Hill Voorhies group proportions based on the observed group I reduction over Lamy, and the congruent enrichment of groups II and III (Fig. 6). Enrichment of group II and group III elements suggests a low- to medium-velocity current that winnowed away group I elements, which are under-represented.

Biological Factors

Non-metoposaurids

The non-metoposaurid macrovertebrates in the Rotten Hill bonebed are primarily a typical array of Adamanian reptiles, most represented by one or a few elements, virtually all of which are disarticulated. Only phytosaurs are relatively numerous. These presumably amphibious reptiles, as well as the unionids and lungfish tooth plates, were likely washed into the bonebed by the fluvial source of the hydraulic concentration. The other reptile bones may also have been washed in from the floodplain. There is no evidence of predation, scavenging or any other sort of biotic interaction among the Rotten Hill bonebed taxa. We suggest, then, that the non-metoposaurid fossils in the bonebed were also hydraulically concentrated together with the metoposaurid bones.

Association of Skeletal Elements

As already stated, metoposaurid bones at the Rotten Hill bonebed are totally disarticulated and closely packed in the bonebed, but in no way associated. Even short strings of vertebral centra are essentially absent, which underscores the total disarticulation evident in the bonebed (Fig. 4). The only articulated specimens are a string of four metoposaurid dorsal vertebrae and the three articulated *Spinsouchus* vertebrae. The bonebed thus must have come from fully decayed carcasses that lacked any tissues to bind bones together (cf. Hill, 1979; Holz and Barberena, 1994).

Bone Weathering

None of the bones from the Rotten Hill bonebed show a significant degree of subaerial weathering. They thus correspond to stage 0 of Behrensmeyer (1978), in which bone surfaces are smooth and lack cracks other than those associated with post-depositional and post-fossilization stresses. Based on modern bones, this limits the duration of bone exposure to a maximum of ~ 3 years (Behrensmeyer, 1978). However, bone rapidly degrades in subaerial environments and must be buried quickly to appear unweathered when fossilized (Behrensmeyer, 1975). Thus, it seems likely that the Rotten Hill bones were only exposed for weeks or months. This low degree of bone weathering is

consistent with mass death and rapid burial whereby all of the bones were exposed to chemical and physical degradation at the same time (Fiorillo et al., 2000).

Scavenging

None of the bones from the Rotten Hill bonebed bears any evidence of vertebrate scavenging in the form of tooth marks. However, predators and scavengers are the greatest agents of dissociation of a carcass (Behrensmeyer, 1975), so it could be argued that scavengers played a large role in disarticulating the Rotten Hill bones. It has also been argued that the rarity of tooth marks on dinosaur bone relative to mammal bone may indicate differences in carcass utilization by Mesozoic scavengers (Hunt, 1987; Fiorillo, 1991), though taphonomic biases could also be a factor (Erickson and Olson, 1996). Thus, extensive scavenging in which little damage was done to bone may in part explain the dissociation of the Rotten Hill bones, though this can only be advocated as reasonable speculation.

Bone Fractures/Trampling

As noted above, metoposaurid bones from the Rotten Hill bonebed are very well preserved, but some are fractured. These fractures are perpendicular to bone long axes, and the break surfaces are straight and smooth. This indicates post-burial and post-fossilization damage, in part due to sediment loading and subsequent unloading, likely caused by swelling and shrinking of the clays that contain the bonebed (e.g., Dodson, 1971; Behrensmeyer, 1975). No fractures due to trampling (cf. Fiorillo, 1984, 1987) are evident.

MNI

The minimum number of individuals (MNI) of the metoposaurids collected from the Rotten Hill bonebed (based on counting prepared interclavicles) stands at >68. This sets an absolute minimum size on the sample of animals preserved at the quarry. The MNI of other tetrapods is more difficult to establish, as the fossils are fragmentary (and not all may have come from the primary bonebed), and there are few overlapping elements. Clearly, multiple phytosaur individuals are represented in the assemblage, but the metoposaurids numerically overwhelm all other vertebrates recovered from the site.

Survivorship

Mortality patterns, an important biological life history indicator, are best described by survivorship curves. Survivorship curves graphically depict the number of survivors in a population at any given life stage or age (Hammer and Harper, 2006). Such curves estimate the *survival function*, S(t), of a population, i.e., the number of individuals alive at time 0 that are still alive at any given later time. The survival function, then, represents the probability of any individual in a population surviving beyond time *t* (Glantz, 2005). Specifically:

S(t) = Number of individuals surviving longer than time *t* / Number in population.

Survivorship Curve Types

Pearl and Parker (1921) probably first studied survivorship in non-human populations. They produced survivorship data for wild populations of the fruit fly *Drosophila* living under various environmental conditions throughout most of the 1920s, publishing numerous papers that are referenced in Pearl and Miner (1935). In the 1935 work, Pearl and Miner studied survivorship in several extant invertebrate populations, producing theoretically possible types of survivorship curves plotted on linear axes (Fig. 7A).

In survivorship curves, the slope of the line indicates the mortality rate. High negative slopes show high mortality, whereas gentle negative slopes show low mortality. A horizontal slope indicates no mortality. Thus, in Figure 7A, curve A represents animals in which life starts with an expectation of high longevity, but all die at or near the same age. This is the negatively skewed rectangular curve of Pearl and Miner (1935). Curve B1 shows low infant/juvenile mortality, high mortality later in life, and then low mortality at advanced age. The B1 curve is rare in nature, but can be produced by such factors as parental care of infants and small juveniles. In curve B2, infant/juvenile mortality is high (concave up portion of the curve), there is then a "prime-of-life" period (central, near-horizontal portion of the curve) of low mortality, and finally the onset of senescence and high mortality at advanced age (concave down portion of the curve). Curve C, a decreasing exponential, represents a constant rate of mortality on a linear coordinate system. This curve would be a straight diagonal line on a logarithmic scale. Finally, curve D indicates very high infant/juvenile mortality followed by a reasonable expectation of long life (frequently the case with marine invertebrates). This is the positively-skewed rectilinear curve of Pearl and Miner (1935). All of these theoretical curves, or close variants of them, have been shown to exist in nature.

Deevey (1947) published theoretical survivorship curves after Pearl and Miner (1935) (Fig. 7B). He stressed the advantage of using a logarithmic survivor axis to show rate of mortality. Deevey's type I curve (Fig. 7B) is equivalent to Pearl and Miner's type A, and his type III curve is equivalent to Pearl and Miner's type D. Deevey's type II curve is equivalent to Pearl and Miner's type C, but here it presents a straight diagonal line because of the logarithmic survivor axis.

Survivorship in the Rotten Hill *Koskinonodon* Population

Here, we use the pectoral girdle bones and femora of the Rotten Hill *Koskinonodon* population to assess survivorship. The sample of measurable skulls was too small to give a reliable result.

Survivorship curves generated from the *Koskinonodon* bone metrics all show a concave down shape (Fig. 7C-E) similar to the negatively skewed rectangular curve (Type A) of Pearl and Miner (1935) and the type I curve of Deevey (1947). All are represented on linear age and logarithmic survivor axes as recommended by Deevey (1947). The samples of clavicles and interclavicles (Fig. 7C-D) are substantially larger than the femur sample (Fig. 7E) and probably yield the most accurate representation. Similar behavior in the three different data sets increases confidence in the result.

At first glance, these concave-down survivorship curves (Fig. 7C-E) appear to approximate the type A or type I curve (Fig. 7A-B) in which infant/juvenile mortality is low, and most of the population dies at or near the same advanced age. Note that all of the measured survivorship curves (Fig. 7C-E) begin with the near-horizontal portion representing low mortality that persists for some time before the onset of senescence and high "old age" mortality.

However, given that there are no small juvenile animals in the Rotten Hill population, we interpret these curves to represent the second half of a type B2 curve (Fig. 7A). Typically, infant/juvenile mortality is very high in extant amphibians (discussed below), and there is evidence of high infant/juvenile mortality in the fossil record (Brinkman et al., 2007). Thus, we hypothesize that in the Rotten Hill *Koskinonodon* population, infant/juvenile mortality was quite high, but after adulthood was reached a relatively low mortality rate prevailed until the onset of senescence (Fig. 7F). The type B2 shape of the survivorship curve in Figure 7F represents the survival function, S(t), of *Koskinonodon*; survivorship as a function of time, the first half (dashed line) being hypothetical and the last half (solid line) measured based on the Rotten Hill sample.

This type B2 life history pattern is similar to that of extant urodeles and anurans in which survivorship of larval forms is very low, mostly

TABLE 2. Elongate bone alignment at Rotten Hill. The top of the photograph (Fig. 4) is considered to be 0° for this test.

Number	Element	Azimuth °
1	Unknown	34
2	Rib	16
3	Mandible	4
4	Mandible	358
5	Rib	353
6	Dermal bone	329
7	Unknown	27
8	Unknown	0
9	Clavicle	13
10	Rib	18
11	Rib	25
12	Unknown	9
13	Unknown	345
14	Unknown	10

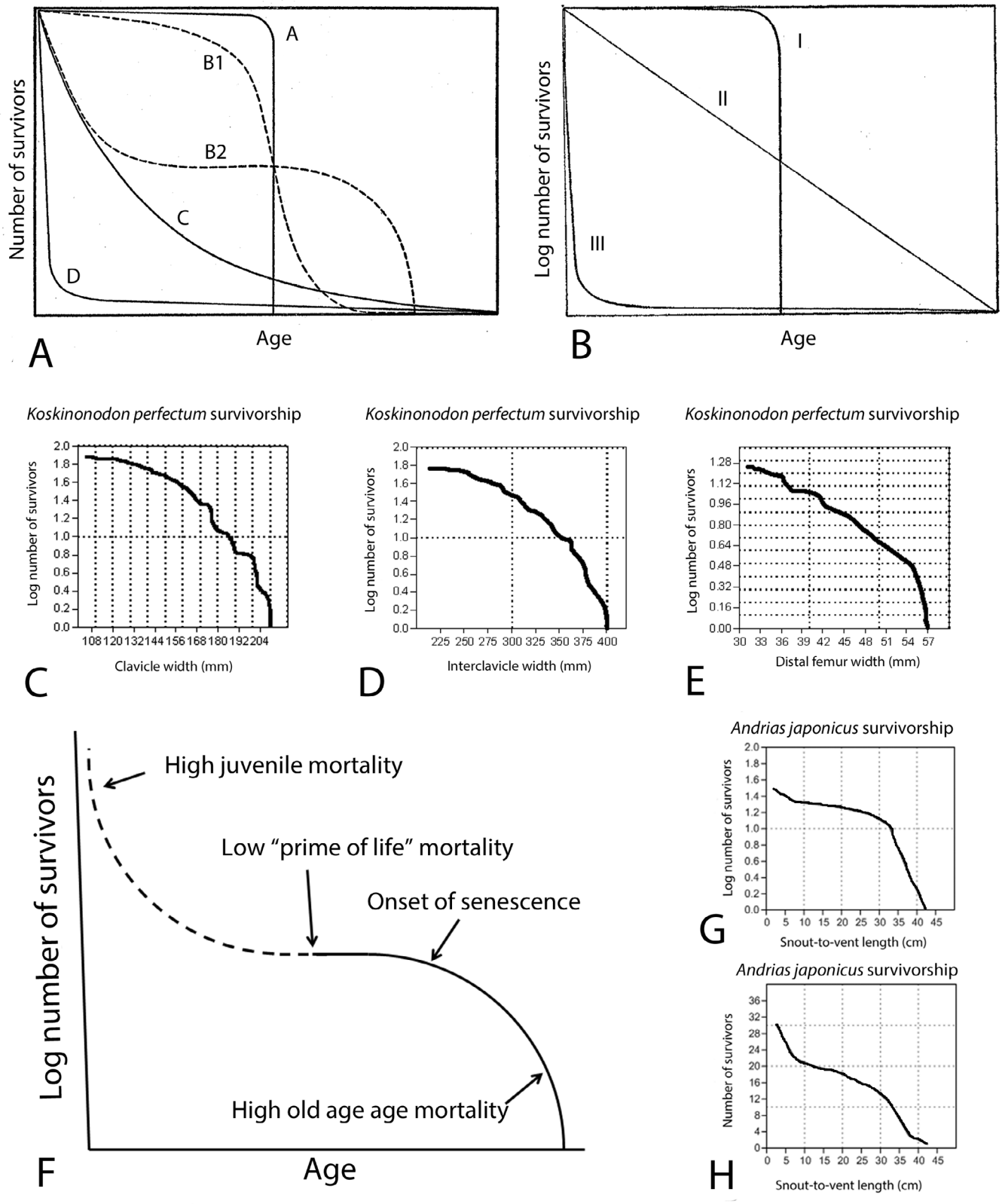

FIGURE 7. Survivorship. **A,** Survivorship curve types after Pearl and Parker (1921) on linear axes. **B,** Survivorship curve types after Deevey (1947), with logarithmic scale on the survivor number (y) axis. The Type I, II, and III curves of Deevey (1947) equal the Type A, C, and D curves of Pearl and Parker (1921), respectively. **C-E,** Survivorship in the Rotten Hill population based on **C,** clavicle widths, **D,** interclavicle widths, and **E,** distal femur widths. **F,** Hypothesized survivorship in the Rotten Hill *Koskinonodon* population is of type B2: high juvenile mortality (high negative slope); low prime of life adult mortality (low slope); and high old age mortality (high negative slope). The first half (dashed line) is hypothesized based on measured extant large amphibian survivorship curves. The second half of this curve (solid line) is based on the measured survivorship of the Rotten Hill population that is represented in C-E of this figure. **G,** An example of type B2 survivorship in the extant giant cryptobranchid salamander, *Andrias japonicus* (N = 87) based on snout-to-vent lengths of a wild population (logarithmic survivorship scale), extracted from Okada et al. (2008, fig. 3). **H,** The same *Andrias japonicus* data as G shown on a linear survivorship scale.

due to predation—typically, 1-10% survive the larval stage (Walls, 2007, fig. 14.9). But, upon reaching adulthood, annual survivorship increases to the 50% to 90% range (Walls, 2007). Such an annual survivorship is surprisingly high in wild populations. For example, the annual survivorship of adult passerine birds is 25% to 80% (Walls, 2007, citing Dorst, 1974), and small mammals show a relatively low annual survivorship of 10% or 15%, with a maximum of 45% (Walls, 2007). Walls (2007) posits that the relatively high survival rates of extant amphibians may be largely due to poison glands in the skin that discourage predation. As there is no evidence that temnospondyls had such glands, the analogy to extant amphibians should not be pushed too far.

Type B2 Survivorship in an Extant Giant Salamander

As an example of the type B2 survivorship pattern in a large extant amphibian, and for comparison to the Rotten Hill *Koskinonodon* data, we plotted survivorship in a wild population of the giant Japanese salamander, *Andrias japonicus*. There are many obvious differences between the giant cryptobranchid salamanders and *Koskinonodon*, but these animals may represent the best extant analog. The largest members of the genus *Andrias* (*Andrias japonicus*, known from Japan, and *Andrias davidianus*, from China), however, reach nearly the size of an "average" *Koskinonodon*. *Andrias japonicus*, the smaller of the two species, grows to at least one meter in total length, and the larger *Andrias davidianus* grows to 150-180 cm and weighs 45-55 kg (Browne et al., 2014). Whereas the bulk of the diet of these giant salamanders consists of aquatic invertebrates such as crayfish, crabs, and insects, they also consume fish, frogs, and water shrews (Browne et al., 2014). They are highly cannibalistic; Browne et al. (2014) found that in a wild population of *Andrias davidianus*, 27% of the stomach contents consisted of conspecifics.

We extracted snout-to-vent length data for 87 wild *Andrias japonicus* from Okada et al. (2008, fig. 3) and plotted survivorship for this animal on logarithmic and linear axes (Fig. 7G-H). The 87 individuals captured in Okada et al.'s (2008) study included 54 juvenile to adult animals and 33 larvae. The characteristic shape of the B2 curve is evident: high mortality in the smallest individuals (initial steep negative slope), a mid-life period of low mortality (central gentle slope), and high mortality in the oldest individuals (final steep negative slope).

Survivorship Summary

We have shown that the survivorship curve of the Rotten Hill *Koskinonodon* population superficially has a type I or type A form (Fig. 7A-E), but given that there are no juveniles present, this shape only represents the later portion of the actual survivorship function. Therefore, we hypothesize that the actual survivorship curve is almost certainly of type B2 (Fig. 7A, F), in which there is high infant/juvenile mortality, low mortality in midlife adults, and high mortality in old age. Our survivorship analysis of the giant cryptobranchid salamander, *Andrias japonicas,* exemplifies type B2 behavior (Fig. 7G-H), and provides a modern analog to the hypothesized survivorship function of the Rotten Hill *Koskinonodon* population.

Thus, in the measured survivorship curve for the Rotten Hill metoposaurids, the smallest recorded size is not the hatchling or even a juvenile size, but rather a relatively large, presumably young adult, animal (Fig. 7C-E). This observation appears typical of documented mass death assemblages of metoposaurs (Hunt, 1993; Lucas et al., 2010). Indeed, not only is this true of the North American assemblages, but also those in Argana, Morocco, Dutuit's site 1—*Dutuitosaurus* population N>70 (Dutuit, 1976); and Krasiejów, Poland—*Metoposaurus* population N>66 (Sulej, 2007); all the individuals in these bonebeds are apparently adults (Rinehart et al., 2008; Lucas et al., 2010).

Taphonomy of the Rotten Hill Bonebed--Summary

The Rotten Hill bonebed is a macrofossil bonebed that we see as a physical (hydraulic) concentration using the genetic framework for vertebrate skeletal concentration of Rogers and Kidwell (2007, fig. 1.1). The total disarticulation of skeletal elements in the bonebed and their evident preferred orientation (= current alignment) is prima facie evidence of hydraulic concentration. Thus, the Rotten Hill bonebed is a mass death assemblage with a hydraulic overprint (Rogers and Kidwell, 2007, fig. 1.6). Furthermore, as a hydraulic concentration, the Rotten Hill bonebed is in an intraformational conglomerate that is likely a fluvial channel deposit.

The near monotaxy of the Rotten Hill quarry assemblage suggests a biological concentrating mechanism (e.g., feeding?/mating?) of a metoposaur population prior to death, disarticulation and hydraulic concentration (Fig. 8). Behrensmeyer (2007) distinguished abiotic from biotic processes in bonebed formation. She argued that abiotically concentrated bonebeds are typically diverse, whereas biotically concentrated bonebeds have low diversity. This fits the idea that the Rotten Hill bonebed reflects an original biotic concentrating mechanism of the metoposaurs, followed by an abiotic overprint (Fig. 8).

In the Eberth et al. (2007a) classification of bonebeds, the Rotten Hill bonebed can be described as low diversity multitaxic and monodominant (one taxon numerically dominant). This is a fairly common type of bonebed, but Rotten Hill (like the Lamy amphibian quarry: Lucas et al., 2010) is unusual because of the complete disarticulation of skeletal elements. Eberth et al. (2007a, p. 123) note that "monodominant bonebeds most frequently form and develop in settings with low transport and reworking potential" and are often interpreted as catastrophic. This suggests that some sort of gregarious behavior underlies the formation of monodominant bonebeds.

Significantly, as Brinkman et al. (2007) argue, monodominant bonebeds are very useful for inferring paleobehavior. Thus, they note that "aggregation paleobehavior is frequently cited as an influence in the formation of bonebeds…, especially in those cases where a site contains enormous numbers of individuals of one species…" (Brinkmann et al., 2007, p. 231). However, as they note, attritional mortality can lead to monodominant bonebeds, and stress (e.g., drought, fire) can cause the aggregation of animals. Indeed, drought is commonly posited as a cause of aggregation (Brinkman et al., 2007, p. 238-239).

We have reviewed geological and taphonomic data on the Rotten Hill bonebed above based on the protocols of Eberth et al. (2007b, also see Munthe and McLeod, 1975; Behrensmeyer, 1991). Particularly important data include sedimentary context, sample size, individual counts, taxonomic representation and relative abundance, age profile, body size, skeletal articulation and association, skeletal completeness, bone orientation and bone modification. These data lead us to posit the following sequence of events leading to formation of the Rotten Hill bonebed (Fig. 8):

1. Aggregation of a large number of metoposaurid amphibians (cause of aggregation unknown, but by evidence presented here, they probably represent a breeding population) at a site distinct from the location of the Rotten Hill bonebed, though not distant.
2. Catastrophic mass mortality of the metoposaurids by an unknown agent.
3. Complete disarticulation and disassociation of the

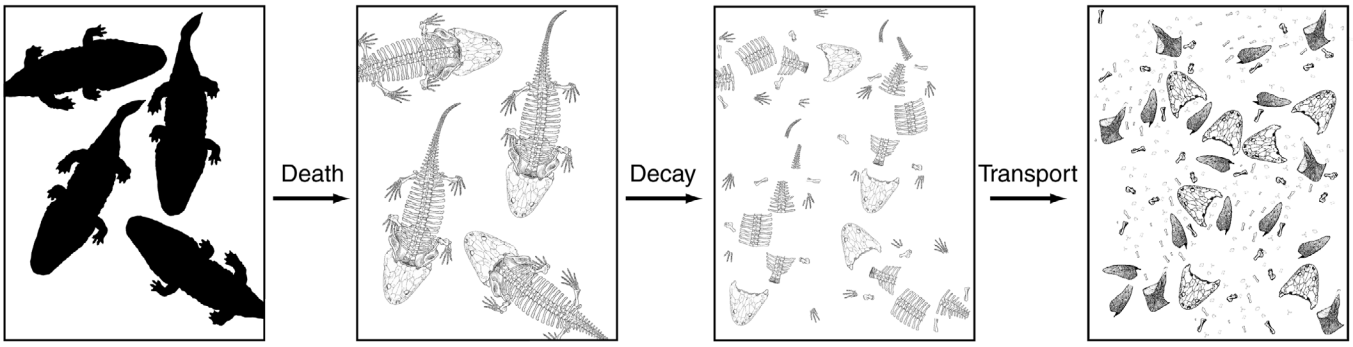

FIGURE 8. Schematic representation of events that led to the formation of the Rotten Hill bonebed (after Lucas et al., 2010). A population of metoposaurs died at one location, decayed to disarticulated bones, and these bones were transported to the location of the Rotten Hill bonebed.

metoposaurid skeletons.

4. Rapid transport of the disarticulated metoposaurid bones, as well as some bones of other taxa, onto a floodplain surface in a channel or sheetflood (crevasse splay) deposit.

5. Rapid burial of the bones.

Comparison to Other Metoposaur Bonebeds

Rotten Hill is one of four well-known metoposaur-dominated bonebeds in Upper Triassic strata; these are from the Upper Triassic Argana Group of Morocco and the Upper Triassic Chinle Group of the western USA (Case, 1932; Romer, 1939; Colbert and Imbrie, 1956; Dutuit, 1976; Long and Murry, 1995; Zeigler et al., 2002b; Lucas et al., 2010). One of these bonebeds, in Morocco, included articulated to associated skeletal material, so it differs fundamentally from the others (Dutuit, 1976). However, the other metoposaurid bonebeds, which are in the Chinle Group of the western USA, are characterized by totally disarticulated and disassociated bones. The Upper Triassic bonebed at Krasiejów, Poland, also contains totally disarticulated and disassociated metoposaurid bones (Sulej, 2007), but this bonebed also includes numerous skulls and other bones of non-metoposaurids (primarily archosaurian reptiles), so we do not compare it to the monodominant and nearly monotaxic metoposaurid bonebeds.

Thus, Dutuit's (1976) Argana, Morocco site 13 preserves an apparent catastrophic death assemblage that accumulated in a drying pond, much as Romer (1939) had suggested for the Lamy bonebed in New Mexico. Dutuit and his crews found a very high density, essentially monospecific assemblage of approximately 70 large individuals of the metoposaur *Dutuitosaurus ouazzoui* in a 30 m^2 area. The quarry itself did not contain mud cracks, but they were seen surrounding the quarry in the same facies. Most of the skeletons were articulated, and many were nearly complete. There was no imbrication of the bones or skeletons, and no calcrete pebbles were present. Significantly, all of the largest individuals were found in the center of the deposit surrounded by a ring of smaller individuals, which had apparently been forced out as the pond decreased in size.

In contrast, the metoposaurid bonebeds in Texas and New Mexico are characterized by disarticulated bones packed into beds that show clear evidence of hydraulic transport and sorting of the bones. The Texas bonebeds (Rotten Hill and Scurry County) preserve the metoposaurid bones in sandy and conglomeratic strata that are clearly fluvially-transported channel deposits. In contrast, the Lamy bonebed preserves the bones in a finer grained deposit that Lucas et al. (2010) interpreted as a floodplain surface onto which the bones were transported.

All of these metoposaurid bonebeds are monodominant and nearly monotaxic. They thus imply that metoposaurids aggregated in life to die suddenly and be preserved either at the site of death (Morocco) or to be transported to a final resting place (USA). The cause of aggregation in Morocco seems to have been a drought that forced the animals into a pond, whereas in the American bonebeds the cause of aggregation is less certain.

The likely cause of aggregation may be indicated by Rinehart et al. (2008), who investigated growth and age structure in *Koskinonodon perfectum* from the Lamy amphibian quarry and from Rotten Hill. They compared data from the metoposaurs in these mass death assemblages to extant salamander outgroups (e.g., *Andrias*, *Cryptobranchus*, *Chioglossa*, others) and other amphibians to show that growth was indeterminate, and that probably only sexually mature adults (marked by size, slow linear growth, and age distribution shape) were present in the fossil assemblages (also see discussion below). Their analysis of the Rotten Hill population showed that the diameter of *Koskinonodon* limb bones grew in strong negative allometry; e.g., the allometric constant for femur length versus midshaft diameter = 0.78, where a constant of 1.5 is required to maintain constant stress on the limb bones throughout growth. Thus, the weight-bearing capacity (strength) of the limbs relative to body size (stress) decreased drastically throughout adulthood.

Based on these results, Rinehart et al. (2008) hypothesized an ecological separation of juveniles and adults in *Koskinonodon,* similar to that seen in some extant amphibians. Such a separation could have served to reduce competition for food and conspecific predation on the juveniles. The decreasing relative strength of limb bones in the adults may have enforced such an ecological separation by making adults water-bound, while the juveniles could have been more terrestrial. The implication of this investigation is that mass death assemblages of metoposaurids, like that of the Rotten Hill bonebed, probably represent breeding populations.

COMPOSITION OF THE ROTTEN HILL BONEBED

Introduction

As already noted, bones of the metoposaurid amphibian *Koskinonodon perfectum* dominate the Rotten Hill bonebed. However, some other vertebrate taxa are present in the quarry (Table 1), notably various fishes, the small metoposaur *Apachesaurus*, a rhynchosaur, trilophosaurs, the archosauriform *Vancleavea*, phytosaurs, a shuvosaurid and aetosaurs. Unionoid bivalves and vertebrate coprolites complete the known quarry fossil assemblage. We describe and illustrate most of

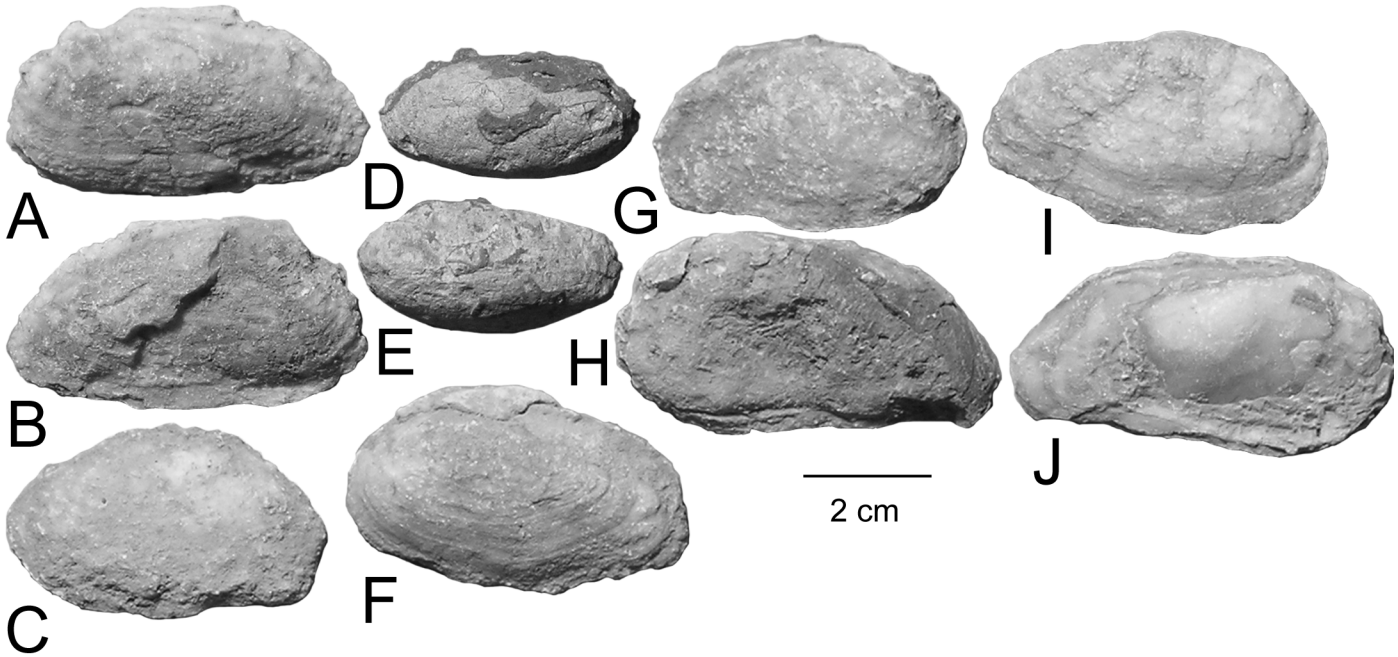

FIGURE 9. Unionoid bivalves (*Plesioelliptio* sp.), PPHM 1999.35.333, from the Rotten Hill bonebed, external views of valves.

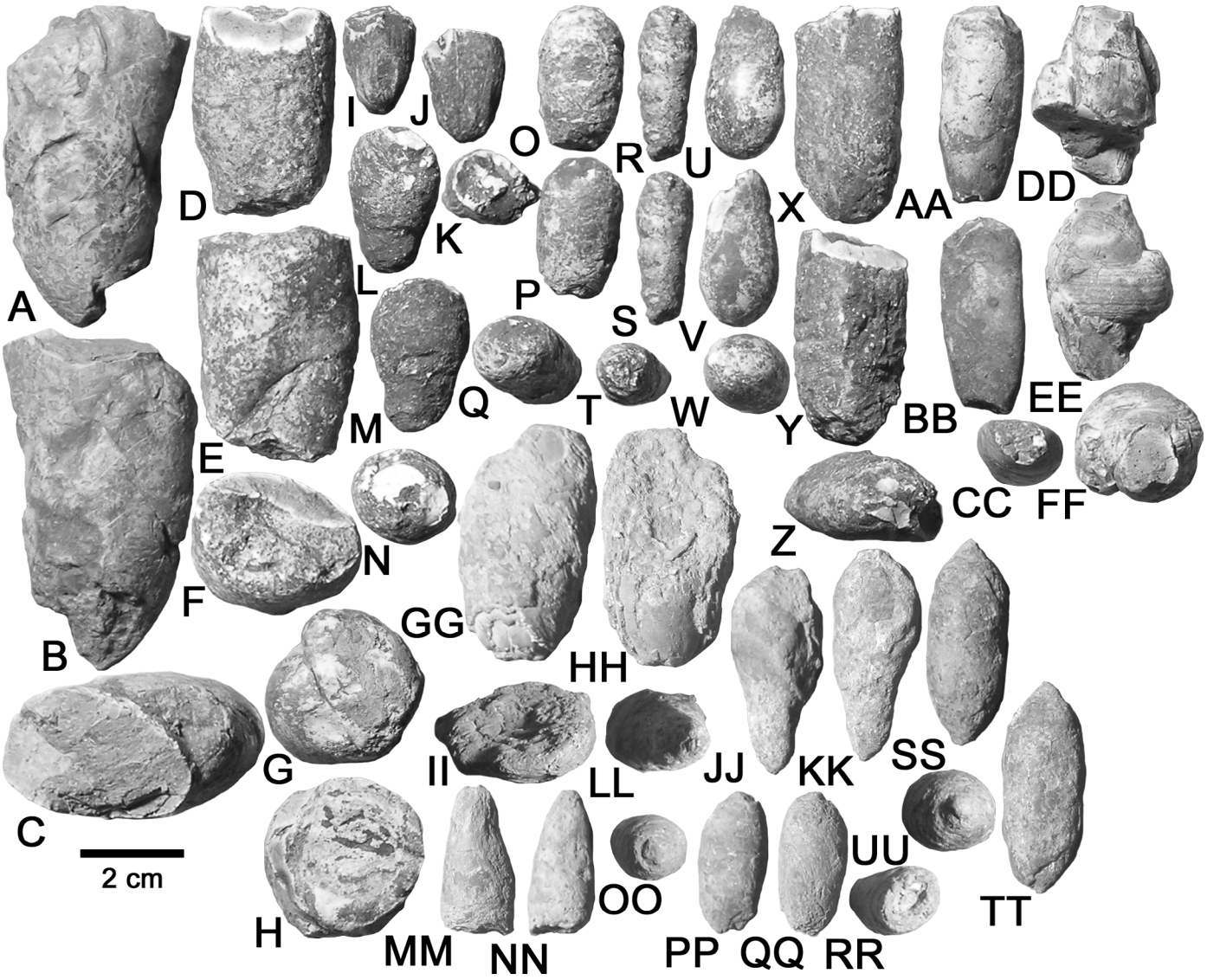

FIGURE 10. A selection of coprolites from the Rotten Hill bonebed catalogued as PPHM 1999.35.327, 1999.35.337 and 2000.10.82. **A-C**, cf. *Dicynodontocopros* isp. in lateral (**A-B**) and polar (**C**) views. **D-F**, cf. *Dicynodontocopros* isp. in lateral (**D-E**) and polar (**F**) views. **G-H**, Indeterminate coprolite in polar views. **I-K**, *Alococoprus triassicus* in lateral (**I-J**) and polar (**K**) views. **L-N**, *Heteropolacoprus texaniensis* in lateral (**L-M**) and polar (**N**) views. **O-Q**, *Eucoprus cylindratus* in lateral (**O-P**) and polar (**Q**) views **R-T**, Unidentified coprolite in lateral (**R-S**) and polar (**T**) views. **U-W**, *Eucoprus cylindratus* in lateral (**U-V**) and polar (**W**) views. **X-Z**, *Eucoprus cylindratus* in lateral (**X-Y**) and polar (**Z**) views. **AA-CC**, *Eucoprus cylindratus* in lateral (**AA-BB**) and polar (**CC**) views. **DD-FF**, Two connected specimens of *Alococoprus triassicus* in lateral (**DD-EE**) and polar (**FF**) views. **GG-II,** *Heteropolacoprus texaniensis* in lateral (**GG-HH**) and polar (**II**) views. **JJ-LL**, *Heteropolacoprus texaniensis* in lateral (**JJ-KK**) and polar (**LL**) views. **MM-OO,** *Heteropolacoprus texaniensis* in lateral (**MM-NN**) and broken polar view (**OO**) view **PP-RR**, *Heteropolacoprus texaniensis* in lateral (**PP-QQ**) and polar (**RR**) views. SS-**UU,** *Heteropolacoprus texaniensis* in lateral (**SS-TT**) and polar views (**UU**).

these fossils here (Figs. 9-26), followed by a separate treatment of the large sample of bones of *Koskinonodon* (Figs. 27-72).

One difficult item is establishing with certainty that all of the non-*Koskinonodon* fossils documented here came from the Rotten Hill bonebed, not just from the vicinity of Rotten Hill. Based on the aforementioned archival documents, we are confident that at least some of the lungfish, phytosaur and aetosaur fossils were collected from the main bonebed or its immediate vicinity (Appendix 1). Preservation and collection labels also suggest that the other fossils described here are from the actual bonebed, not just from "Rotten Hill," which has also been used to refer to Tecovas Formation outcrops near the bonebed (e.g., Long and Murry, 1995).

Murry (1989a, p. 128-133; also see Murry, 1982, 1986) discussed what he called the "Rotten Hill/Sierrita de la Cruz locality," noting that "a number of vertebrate fossils labeled 'Sierrita de la Cruz' are believed to be from or near the Rotten Hill Quarry" (p. 129), so he referred to all of these fossils collectively as the "Rotten Hill local fauna." It is clear that Murry screenwashed sediment from the quarry and from nearby, and in 1989 he reported a typical Adamanian assemblage of microvertebrate fossils from his sampling, notably fish ichthyoliths of "*Xenacanthus*" *moorei*, a putative neoselachian, cf. *Turseodus*, redfieldiids, colobodontids, and the semionotid *Hemicalypterus* as well as jaw fragments of a sphenodontid and *Trilophosaurus buettneri* (Murry, 1989a). We include these taxa in the faunal list of the Rotten Hill bonebed (Table 1) based on Murry's (1989a) report, noting that Mutter and Heckert (2006) cast doubt on at least some reports of "colobodontids" from the Upper Triassic of the American Southwest.

Long and Murry (1995, p. 221) listed the following vertebrate taxa from the "Herring Ranch/Rotten Hill locality, Sierrita de la Cruz Creek: "*Buettneria perfecta*, *Apachesaurus gregorii*, *Otischalkia elderae, Leptosuchus crosbiensis, Smilosuchus gregorii, Desmatosuchus haplocerus, Stagonolepis wellesi, Postosuchus kirkpatricki* and *Parrishia mccreai*." We can verify all of these taxa (although some with different taxonomic names) from the Rotten Hill bonebed except *Leptosuchus crosbiensis*, *Parrishia mccreai*, and, possibly *Stagonolepis wellesi*. Indeed, Long and Murry (1995, p. 227) state that the material

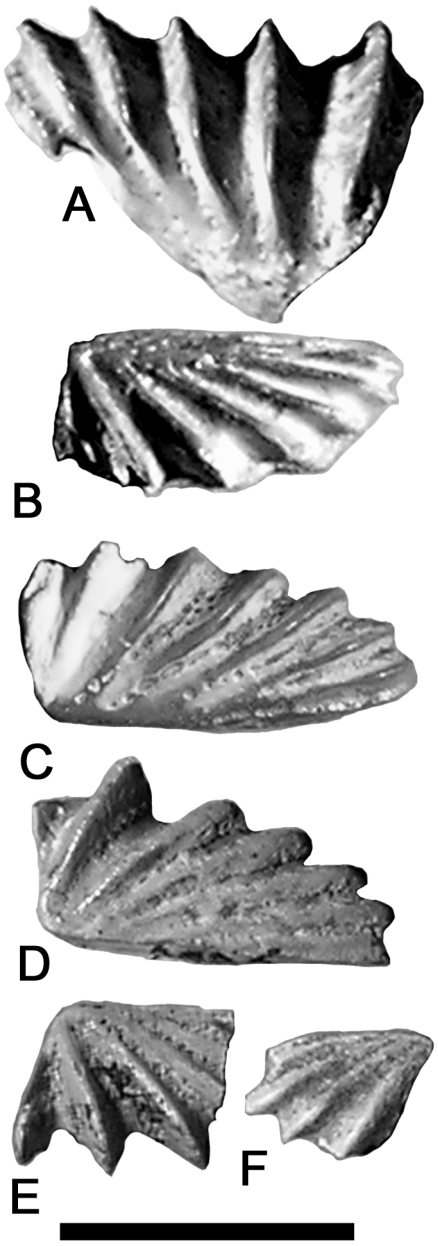

FIGURE 11. Lungfish dental plates, *Arganodus dorotheae*, from the Rotten Hill bonebed. **A-B**, two incomplete dental plates in occlusal view **A**, WT 2988; **B**, WT 2926. **C-D**, two complete upper (vomerine) tooth plates (WT 2926) in occlusal view. **E-F**, two incomplete tooth plates (WT 2988) in occlusal view.

of *Leptosuchus crosbiensis* found along Sierrita de la Cruz Creek is from "near Rotten Hill," not from the bonebed (also see Case and White, 1934). Also, Long and Murry (1995, p. 168) only list a Texas record of *Parrishia mccreai* from Crosby County, not from the Rotten Hill bonebed, which is in Potter County (Fig. 1). Osteoderms assigned to *Stagonolepis wellesi* by Long and Murry (1995) from the Rotten Hill bonebed likely pertain to that taxon, but are not diagnostic to species (see discussion below). Note that Long and Murry (1995), while focused on macrovertebrate tetrapods, did not refer to Murry's (1989a) records, thus not listing the fish, sphenodontian and *Trilophosaurus* specimens he described.

Aside from Murry (1982, 1986, 1989a), Long and Murry (1995) represent one of the few descriptions of non-metoposaurid taxa from the Rotten Hill bonebed. The other is Spielmann et al. (2009), who illustrated the vertebrae of *Spinosuchus caseanus* from the quarry. As

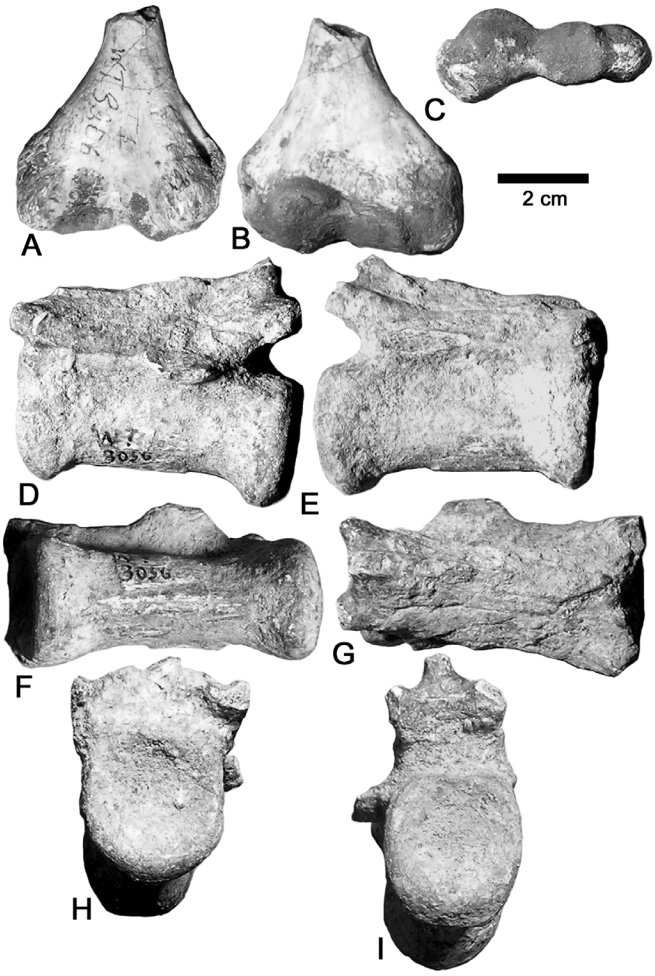

FIGURE 12. Reptiles from the Rotten Hill bonebed. **A-C**, Rhynchosauridae indet., WT 3206, distal right humerus in **A**, anterior, **B**, posterior and **C**, distal views. **D-I**, cf. *Postosuchus*, WT 3056, anterior caudal vertebra in **D**, left lateral, **E**, right lateral, **F**, ventral, **G**, dorsal, **H**, anterior and **I**, posterior views.

mentioned previously, other reports of aetosaurs from the Tecovas Formation in Potter County (Martz and Small, 2006; Parker et al., 2008) are of records from near, but not in, the bonebed.

Unionoida

Unionoid bivalves (Hyriidae: Rinehart and Lucas, 2013a) from the Rotten Hill bonebed encompass several compressed, nearly complete and bivalved specimens catalogued as PPHM 1999.35.333 (Fig. 9) and an incomplete articulated shell catalogued as PPHM 2000.10.119. These shells range in length from 42 to 58 mm and in height from 25 to 36 mm, following the measurement protocols of Good (1993; see also Good, 1998). They are relatively poorly preserved: crushed, partly encrusted with matrix and recrystallized. Their narrow ovoid shape, lack of an abrupt anterior end and lack of radial lirae supports identification as *Plesioelliptio*, not as *Antediplodon*, which is the most common genus of Chinle Group unionoids (Marshall, 1929; Good, 1998; Rinehart and Lucas, 2013a).

Coprolites

There are more than 150 complete or incomplete vertebrate coprolites from Rotten Hill that are catalogued as PPHM 1999.35.327, 1999.35.337 and 2000.10.82. Hunt et al. (2013, fig. 9) illustrated a selection of these, and we repeat that illustration here (Fig. 10). Coprolites are the most common vertebrate trace fossils throughout the Chinle Group from Texas to Wyoming, except for some restricted lacustrine-margin facies where footprints are more numerous (e.g., Lucas et al., 2010).

The majority of the Rotten Hill coprolites are apatitic in

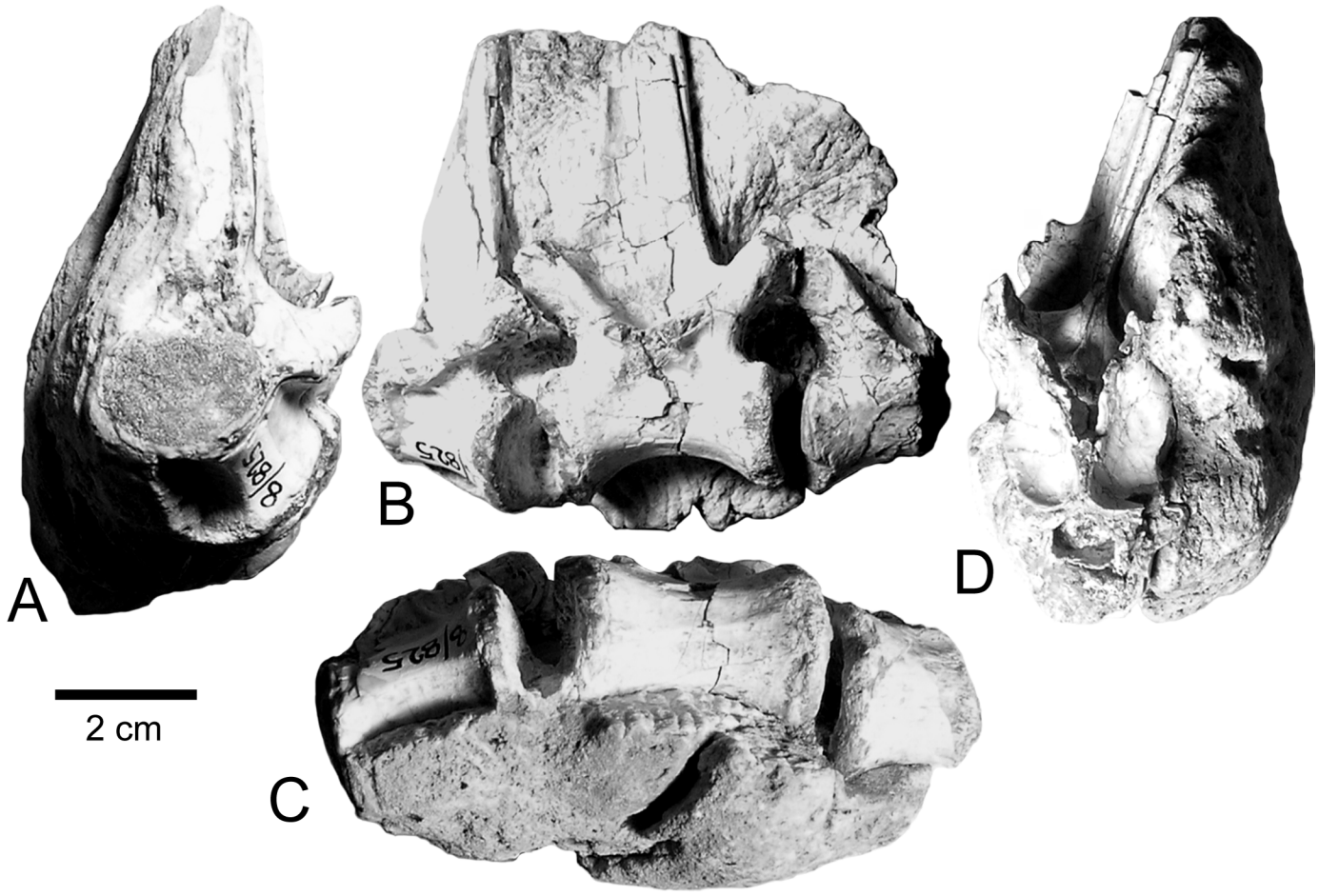

FIGURE 13. *Spinosuchus caseanus* from the Rotten Hill bonebed, WT 8/825, three articulated dorsal vertebrae in anterior (**A**), left lateral (**B**), ventral (**C**), and posterior (**D**) views.

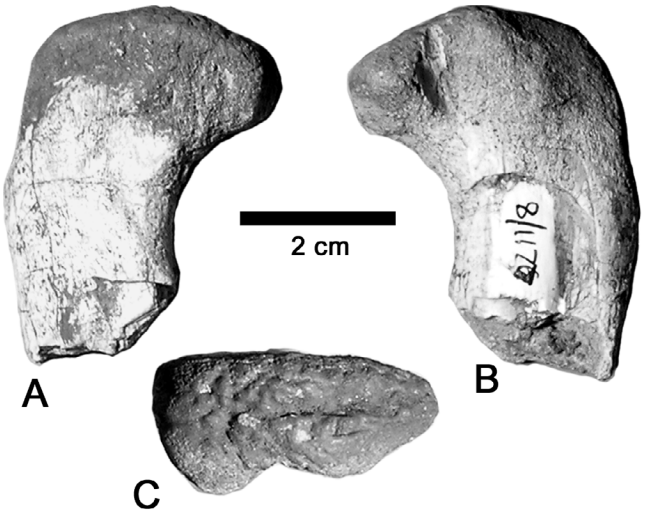

FIGURE 14. Shuvosaurid from the Rotten Hill bonebed, PPHM 8/1176, proximal left femur in **A**, lateral, **B**, medial and **C**, proximal views.

composition and were thus produced by carnivorous animals, which is the norm, with the notable exception of Pleistocene cave ichnofaunas (e.g., Hunt et al., 1994; Hollocher and Hollocher, 2012; Mead and Swift, 2012). Several of the Rotten Hill coprolites are weathered, which may suggest that they were surface collected. There are no specific locality data for the coprolites, which is unfortunate because the sample size is so large. Nevertheless, it is not surprising to find large numbers of coprolites associated with a bone bed. Coprolites of carnivores can be lithified very quickly and are common in bone beds of many ages, including the Late Triassic (Hollocher and Hollocher, 2012; Hunt et al., 2012). Coprolites are among the few ichnofossils that can be reworked (Hunt and Lucas, 2010).

Among the Rotten Hill coprolites, we can identify at least four ichnotaxa.The majority of coprolites are heteropolar and microspiral and can be assigned to *Heterapolacopros texaniensis* (Fig. 10L-N, GG-UU). These specimens are typically 3-4 cm long and circular in cross section. The anterior coil is elongate, and the posterior spire is relatively short (*sensu* Hunt and Lucas, 2012). This ichnotaxon was produced by a chondrichthyan.

Alococopros triassicus is characterized by an arcuate shape in lateral view, subrounded cross section and regularly spaced, thin long grooves along its long axis (Hunt et al., 2007). Specimens assignable to this ichnotaxon include an individual coprolite (Fig. 10I-K) and two conjoined ones (Fig. 10DD-FF). Conjoined specimens are known from the Late Triassic to the Paleocene. This is probably the coprolite of a crocodylomorph.

Eucoprus cylindratus (Fig. 10O-Q, U-W, AA-CC) is cylindrical with a subrounded cross section, rounded ends and lacks osseous inclusions (Hunt and Lucas, 2012). Several taxa produced coprolites of this morphology.

Cf. *Dicynodontocopros* isp. is large and coiled with acute tips and was probably produced by a dicynodont (Hunt et al., 1998). Two specimens from Rotten Hill show similarities to this ichnogenus, and we assign them to cf. *Dicynodontocopros* isp. (Fig. 10A-F).

One coprolite appears to be amphipolar in morphology (Fig. 10R-T) but cannot be assigned with confidence to a named ichnotaxon. Several other specimens, not illustrated here, are too poorly preserved to be assigned to any ichnotaxon.

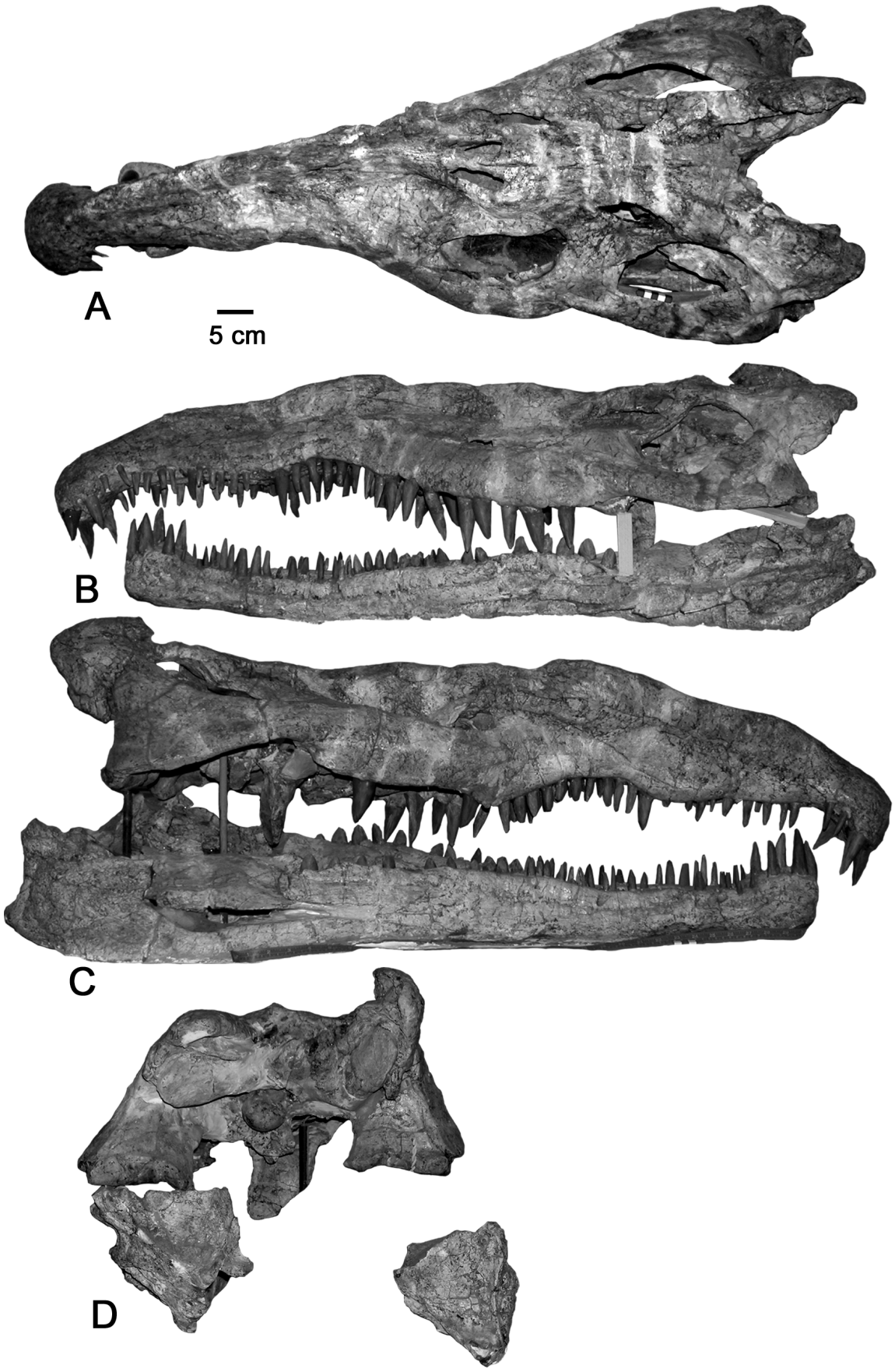

FIGURE 15. Phytosaur skull and lower jaws, *Smilosuchus gregorii*, from the Rotten Hill bonebed as mounted at the PPHM, WT 3217, **A**, dorsal, **B**, left lateral, **C**, right lateral and **D**, occipital views. The lower jaw pertains to a different individual than the skull (see text for details).

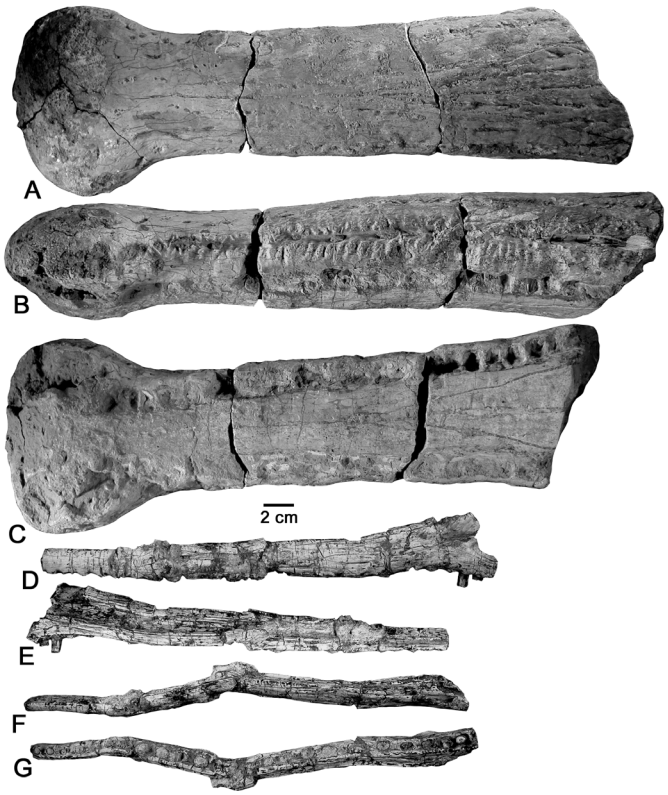

FIGURE 16. Phytosaur jaw and snout fragments from the Rotten Hill bonebed. **A-C**, X 1999.35.258, large phytosaur lower jaw fragment in **A**, ventral, **B**, lateral and **C**, dorsal (occlusal) view. **D-G**, X 2000.10.20, small left phytosaur premaxilla in **D**, lateral, **E**, medial, **F**, dorsal and **G**, ventral (occlusal) view.

Alococopros has a range from Early Permian to late Eocene, but *A. triassicus* is restricted to the Late Triassic to late Eocene. *Eucoprus* occurs from the Late Triassic to the Pleistocene. *Dicynodontocopros* and *Heterapolacopros* are common in the lower Chinle Group (Otischalkian-Adamanian) but are absent (*Dicynodontocopros*) or rare (*Heterapolacopros*) in the upper part of the unit (Revueltian-Apachean), so their co-occurrence is indicative of a pre-Norian age (Hunt et al., 1998, 2007). *Dicynodontocopros* is restricted to the Late Triassic, whereas *Heterapolacopros* has records dating back to the Pennsylvanian (Missourian) (Hunt et al., 2012).

Hunt et al. (1998, 2007) used a very small dataset to postulate that there was a Late Triassic *Dicynodontocopros* ichnocoenosis that was characteristic of areas of standing water, and a *Heterapolacopros* ichnocoenosis that was more common in fluvial settings. The coprolites in the Rotten Hill bonebed may have been transported and/or reworked, and they may suggest that the sources for the deposit might have included both lacustrine and fluvial paleoenvironments.

Lungfish

Six lungfish dental plates have been collected from the Rotten Hill bonebed, divided into two lots (WT 2926—Fig. 11B-D; WT 2988—Fig. 11A, E-F). Two of the six plates are complete (Fig. 11C-D), whereas the remainder are incomplete to various degrees (Fig. 11A-B, E-F). The complete dental plates are both upper (vomerine) plates, as the mesial surface of the first (mesial) ridge is not visible in occlusal view (Murry, 1989b). The complete plates both possess the seven distinct ridges that are diagnostic of *Arganodus* (Murry, 1989b), and the more fragmentary specimens, especially those in Figure 11A-B, are morphologically similar and probably pertain to the same taxon. The incomplete plates are missing portions of the first (shortest) ridge (Fig. 11B), the first and seventh (longest) ridge (Fig. 11A) and three or four of the ridges (Fig. 11E-F). The specimen illustrated in Figure 11B is also probably a vomerine plate. As noted by Heckert (2004) for other Chinle Group dental plates, the sixth and seventh ridges are offset lingually. Maximum crest lengths (for crest 6) are 23.2-24.6 mm. These are some of the larger dental plates of lungfish reported from the Chinle Group. Because lungfish only possess four dental plates that are not replaced, and the plates in Figure 11B-D all appear to represent upper left (vomerine) plates, they represent at least three or four (the plate in Fig. 11D may also be an upper left) individuals.

As enumerated by Heckert et al. (2012), the taxonomy of isolated lungfish dental plates is problematic, as most lungfish taxonomy is based on more complete cranial material, something lacking not only from the Rotten Hill bonebed, but from the Upper Triassic of North America as a whole. Although Kemp (1997) considered the type species of *Arganodus, A. atlantis* Martin (1979), part of her concept of *Asiatoceratodus*, Cavin et al. (2007) rejected this synonymy and found differences between dental plates they assigned to *Asiatoceratodus* and those of *Arganodus* (see also Soto and Perea, 2010). Thus, following Murry (1989b) and Heckert (2004), we identify the Rotten Hill lungfish toothplates as upper (pterygoid or pterygopalatine) toothplates of *Arganodus dorotheae* (Case). *A. dorotheae* is the only lungfish identified from the Carnian interval of the Chinle Group (Murry, 1986, 1989b; Huber et al., 1993; Heckert, 2004; Milner et al., 2006).

Amphibians

Apachesaurus

The small metoposaurid *Apachesaurus gregorii* is represented in the Rotten Hill collection by eight spool-shaped centra catalogued as PPHM 2000.11.27 (Fig. 25A-F). These centra range in length from 11.5 to 13.6 mm and in width from 13.2 to 16.6 mm. Most bear two rib facets. Note that these centra have been altered by drilling through their centers (at the notochordal pit), evidently to connect ("articulate") them together with wire or a metal rod, probably for exhibition.

The spool-shaped centra catalogued as PPHM 2000.11.27 are distinctively elongate (width/length<0.8) and so are readily assigned to *Apachesaurus gregorii* (Hunt, 1993, p. 85, fig. 14). *Apachesaurus* is found throughout the Chinle Group, but is much less common than *Koskinonodon* in Otischalkian-Adamanian strata, as is seen at Rotten Hill (Hunt and Lucas, 1993).

Koskinonodon

The large sample of *Koskinonodon perfectum* from the Rotten Hill bonebed is described in a separate section after the rest of the tetrapod assemblage.

Reptiles

Rhynchosauridae

A single, small rhynchosaurid distal humerus (WT 3206) was collected from the Rotten Hill bonebed (Fig. 12A-C). This humerus is somewhat dorso-ventrally flattened, but clearly possesses a bilobate distal articulation and lacks a hook-like process on its supinator crest. The lack of a hook-like process on its supinator crest precludes this specimen from being assigned to the rhynchosaur *Otischalkia elderae* (Hunt and Lucas, 1991; Spielmann et al., 2013b), *contra* Long and Murry (1995, p. 225).

This incomplete humerus appears very similar to the humerus that is part of the chimeric holotype of "*Malerisaurus langstoni*" (= *Trilophosaurus buettneri*, following Spielmann et al., 2006). Both humeri may belong to either a small, gracile adult rhynchosaur, heretofore undescribed from the Chinle Group of West Texas, or, more likely, a juvenile rhynchosaur, as originally posited by Spielmann et al. (2006). Thus, we assign WT 3206 to the Rhynchosauridae, based on its morphological similarity to other Chinle Group rhynchosaurs, but given its incomplete nature we do not provide a genus- or species-level identification.

Cf. *Trilophosaurus*

A small assortment of largely uncatalogued vertebrae and vertebral fragments (mostly centra) are most similar to those of *Trilophosaurus* known from other sites (e.g., Spielmann et al., 2007, 2008, 2013c). One of these is an incomplete dorsal vertebra, including much of the neural spine (Fig. 25G-L). The rest are a variety of elongate caudal vertebrae, some preserving neural arches (Fig. 25M-X). These are amphicoelous and are routinely ~4 times longer than the articular faces are tall. They range from 21 to 31 mm long and closely resemble the distal caudals of *Trilophosaurus buettneri* (cf. Spielmann et al., 2008, fig. 55), although they lack diagnostic features that would allow us to definitively assign them to *Trilophosaurus*. Note that Nesbitt et al. (2015) recently argued that not only is *Spinosuchus* closely related to *Trilophosaurus*, but in fact that it represents the same animal as *T. jacobsi*, a suggestion that needs further evaluation.

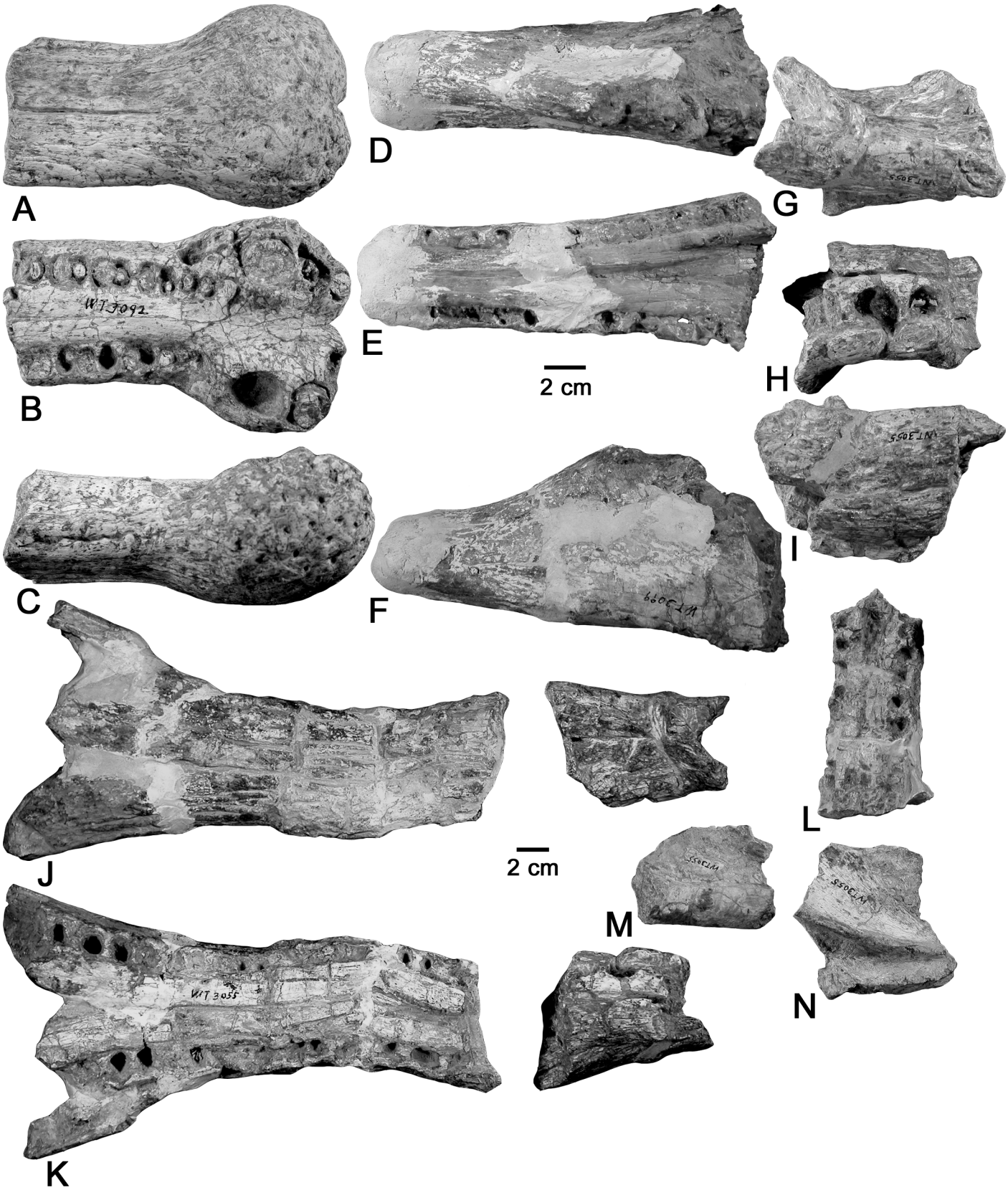

FIGURE 17. Phytosaur rostral/palate fragments from the Rotten Hill bonebed. **A-C**, WT 3092, phytosaur rostrum in **A**, dorsal, **B**, occlusal and **C**, lateral view. **D-F**, WT 3099, phytosaur snout fragment in **D**, dorsal, **E**, occlusal and **F**, lateral view. **G-N**, WT 3055, phytosaur skull fragments, **G-I**, maxilla? fragment in **G**, dorsal, **H**, ventral (occlusal) and **I**, lateral view, **J-K**, incomplete phytosaur lower jaw in two parts, in **J**, ventral, and **K**, dorsal (occlusal) view, **L**, snout fragment in occlusal view, **M-N**, miscellaneous phytosaur skull fragments. Upper scale bar for **A-I** and lower scale bar for **J-N**.

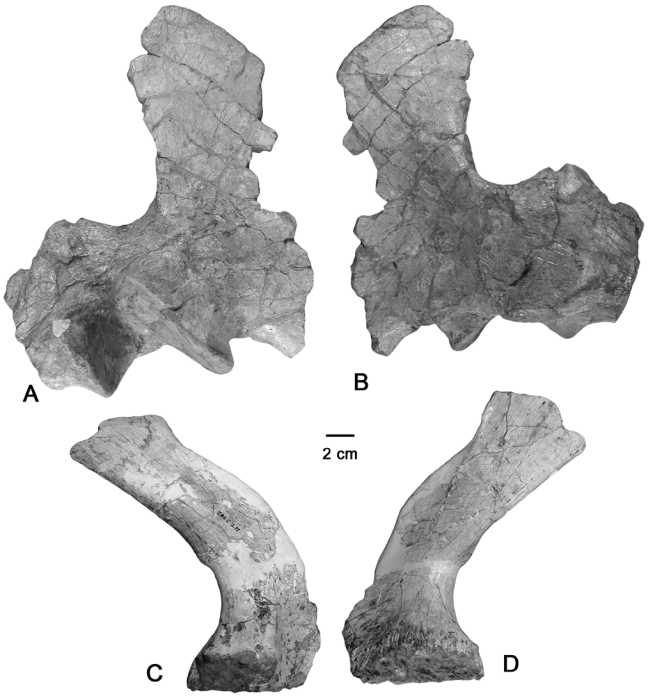

FIGURE 18. Phytosaur pectoral girdle elements from the Rotten Hill bonebed. **A-B**, WT 2908, incomplete left scapulacoracoid in **A**, lateral and **B**, medial view. **C-D**, WT 2902, right scapula in **C**, lateral and **D**, medial view.

Spinosuchus caseanus

Three articulated posterior dorsal vertebrae (PPHM 8/825: Fig. 13) from the Rotten Hill bonebed were described and illustrated by Spielmann et al. (2009, fig. 7c-f), who assigned them to *Spinosuchus caseanus* Huene. These vertebrae are relatively small (~24-28 mm long, ~17-19 mm wide). Although the centra and neural arch of *Spinosuchus caseanus* are strongly similar to those of *Trilophosaurus*, the neural spines, especially of the dorsal series, are extremely elongate—2-3 times longer than the centra and as much as 4 times taller—and terminate in wedge-shaped expansions that are narrowerest anteriorly (Spielmann et al., 2009). Dorsal vertebrae also typically bear sheet-like processes on the lateral sides of the neural spine (Spielmann et al., 2009; also see Case, 1927, fig. 6).

We follow Spielmann et al. (2009, p. 298) and assign these fossils to *Spinosuchus caseanus* based on the elongate neural spines with wedge-shaped, expanded tips, among other similarities (Fig. 13). *S. caseanus* is a relatively rare taxon restricted to Adamanian-age strata (Spielmann et al., 2009, 2013b).

Vancleavea campi

PPHM 2000.10.106 (Fig. 26) consists of seven relatively small vertebral centra that are amphicoelous and range in length from 16.4 to 31.5 mm and in width from 10.2 to 15.1 mm. These centra closely resemble those of *Vancleavea campi* (see Long and Murry, 1995, fig. 197; Hunt et al., 2005b, fig. 2; Nesbitt et al., 2009b, fig. 11), to which we refer them. These authors indicate the following features of *Vancleavea* that are also evident on the PPHM specimens: Cervical articular surfaces that are nearly square but with the corners rounded (Fig. 26C-D); weakly procoelous (Fig. 26B); bear a strongly developed ventral keel on the cervical vertebrae (Fig. 26B); and a sacral vertebra with a narrow groove between two thin ventral keels (Fig. 26F). The only vertebral autapomorphy of *Vancleavea* listed by Nesbitt et al. (2009b, p. 816) is the presence of twin keels on the ventral surface of some dorsal centra, a feature they note on the sacral and caudal centra as well, and that can be seen on several of the Rotten Hill specimens (e.g., Fig. 26F). These specimens, while fragmentary, are the only published record of *Vancleavea campi* from Texas other than an anterior dorsal centrum Long and Murry (1995, p. 195) listed from the Tecovas Formation near Home Creek in Crosby County.

cf. *Postosuchus*

Long and Murry (1995) referred WT 3056, a large caudal vertebra (Fig. 12D-I), to *Postosuchus kirkpatricki*. They also referred two other specimens to *P. kirkpatricki* in the PPHM collection that we did not locate: WT 3056, a dorsal vertebra and 3122.1, a cervical? vertebra. The large caudal centrum illustrated in Figure 12D-I is approximately 54 mm long, 29 mm across anteriorly, and 26.5 mm posteriorly. There are additional specimens of "rauisuchians," including probable poposauroids similar to *Postosuchus*, in the UMMP collections from the Tecovas Formation in this region (Long and Murry, 1995; ABH pers. obs.).

Shuvosauridae

PPHM 8/1176 is the proximal portion of a left femur (Fig. 14) that is slightly more than 48 mm long as preserved and compares well with a specimen of *Shuvosaurus* (= *Effigia*, = *Chaterjeea*: Lucas et al., 2007a) illustrated by Nesbitt (2007, fig. 44). The slender shaft appears to have a sigmoidal curve, and the proximal 14 mm is occupied by a well-developed head that is nearly 31 mm wide, has a distinct neck, and bears an elongate groove on the otherwise rugose proximal surface. Seen proximally, the anterior face of the head is nearly flat, whereas the posterior face has two processes separated by a cleft. The medial of these is the anterior medial tuber of Nesbitt (2007), although it is not as hook-like in proximal view as Nesbitt (2007, fig. 44) illustrated in *Shuvosaurus*. The more lateral process is an elongate ridge that is the posterior medial tuber. This appears more rounded and less elongate than the corresponding bone of *Shuvosaurus*, although this could be an artifact of preservation. As in *Shuvosaurus,* there is no obvious proximal lateral tuber on the smooth anterior face. In medial view (Fig. 14B), the head forms a well-defined sharp (slightly more than 90˚) angle, although the head itself is less robust than in *Shuvosaurus,* and the angle of the arc from the head down the shaft is more gentle than in *Shuvosaurus*.

Thus, this bone is a reasonable match to the femur of *Shuvosaurus* (see also Long and Murry, 1995, fig. 168), but we do not consider it diagnostic below the level of Shuvosauridae *sensu* Nesbitt (2007, 2011). This specimen appears to have escaped the attention of both Long and Murry (1995) and Nesbitt (2007), so it is the first record of a shuvosaurid from the Tecovas Formation of northwest Texas.

Phytosaurs

After *Koskinonodon*, the second most abundant fossils in the Rotten Hill collection at PPHM are of phytosaurs. The most informative phytosaur specimen is a large phytosaur skull (WT 3217—Fig. 15). Other phytosaur fossils from the Rotten Hill bonebed are either rostral or lower jaw fragments (Figs. 16-17) or various postcrania (Figs. 18-22).

Phytosaur Skulls and Lower Jaws

The most diagnostic specimen of a phytosaur from the Rotten Hill bonebed is WT 3217, an essentially complete skull and lower jaw on display at the PPHM (Fig. 15). Long and Murry (1995, fig. 29b) illustrated this specimen, referring it to *Smilosuchus gregorii*, a taxon considered valid in the last review of phytosaurs (Stocker and Butler, 2013). We note, though, that the skull and lower jaw of WT 3217 are of different colors and sizes, so we do not believe that they represent a single individual. Long and Murry's (1995, p. 16) interpretation of PPHM records suggests that the lower jaws are from a specimen designated WT 2899. Long and Murry (1995) also state that a large skull (1.14 m long) was found 0.8 km from the lower jaw, but they designate it WT 2900 in the main text, and refer to the skull and jaws illustrated here as WT 3217 in their illustration and appendix (Long and Murry, 1995, p. 229; fig. 29b). It is unclear if either is from the main bonebed.

As shown in Figure 15, the complete skull on exhibit is mounted in a manner that renders detailed examination, especially of key features such as the medial surface of the squamosals, difficult. As preserved, it is more than a meter (1010 mm) long from the tip of the snout to the occipital condyle, and approximately 1270 mm long to the posterior margin of the squamosals. Although the right side is somewhat crushed and deformed, the skull is still almost 400 mm wide at the quadrates. In general proportions, it is robust ("brachyrostral" condition of Hunt, 1989) and bears an elongate, low, narial crest that stretches nearly to the tip of the snout. The narrow, slit-like external nares are retracted so that they are essentially even with the anterior portion of the antorbital

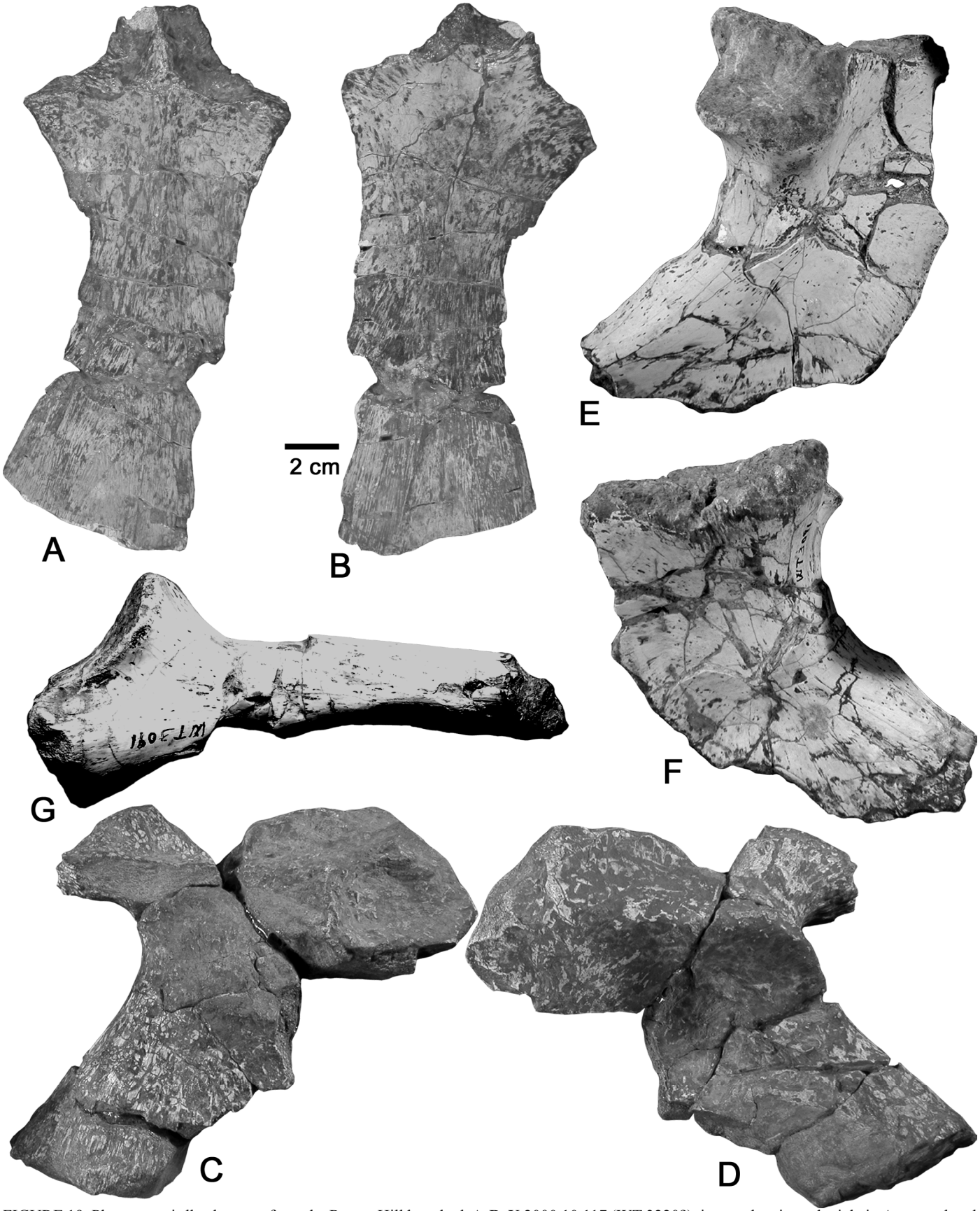

FIGURE 19. Phytosaur girdle elements from the Rotten Hill bonebed. **A-B**, X 2000.10.117 (WT 3220?), incomplete interclavicle in **A**, ventral and **B**, dorsal view. **C-D**, WT 2927, right ilium in **C**, medial and **D**, lateral view. **E-F**, WT 3091, right ischium in **E**, lateral, **F**, medial and **G,** ventral view.

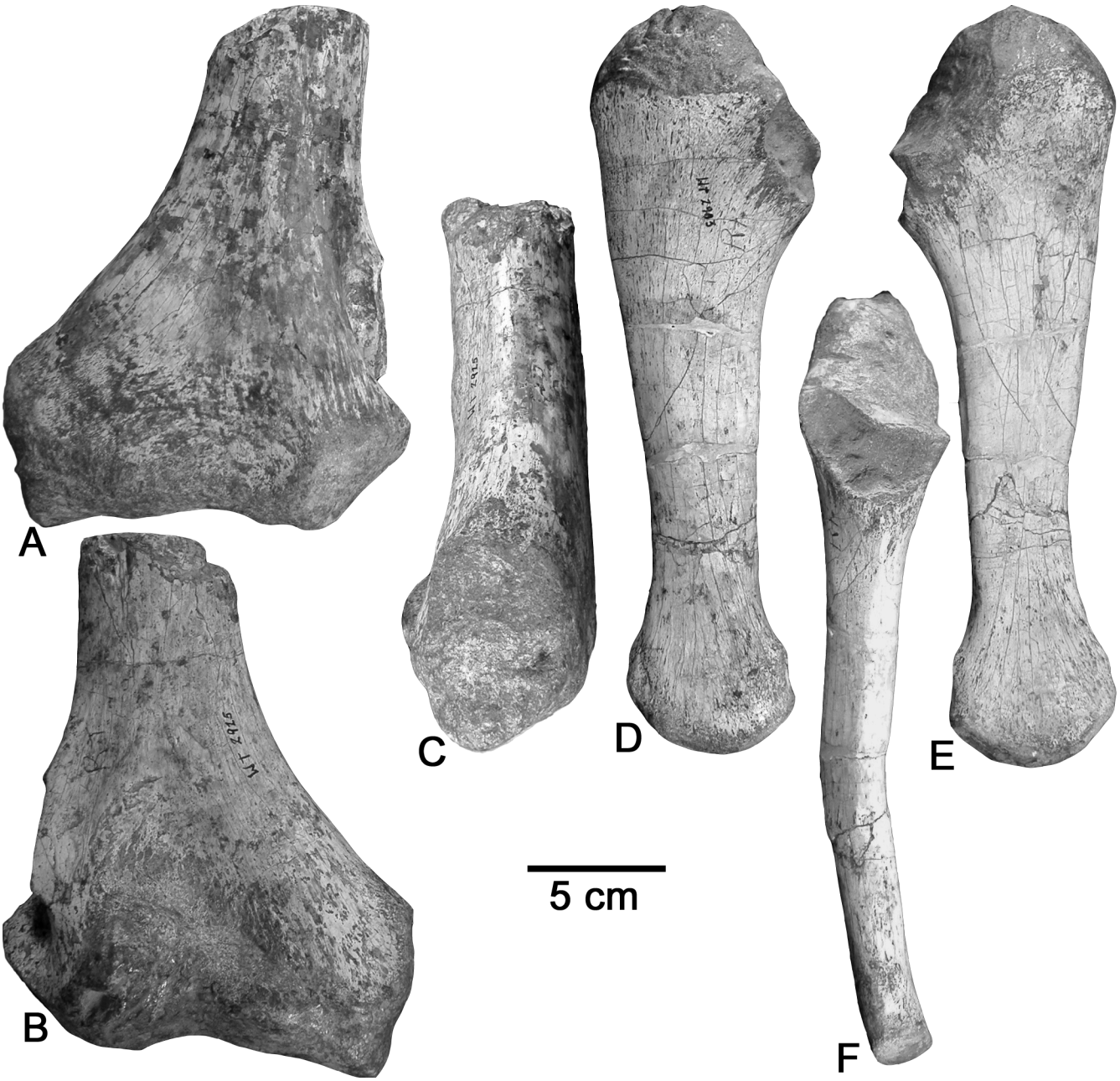

FIGURE 20. Large phytosaur fore limb bones from the Rotten Hill bonebed. **A-C**, WT 2925, distal left humerus in **A**, medial, **B**, lateral and **C**, anterior view. **D-F**, WT 2903, right ulna in **D**, lateral, **E**, medial and **F**, anterior view.

fenestrae, approximately 650 mm from the anterior margin of the snout. It is worth pointing out that the teeth evident in Figure 15 are "casts" implanted in the skull for display, and we could only verify ~34 tooth positions in the ~785 mm of tooth row on the skull.

With regard to the skull of WT 3217, Long and Murry (1995) drew attention to the very large size, extreme heterodonty, the premaxillary bulb that supports enlarged anterior premaxillary teeth, the massive and heavy rostrum and the dorsoventrally facing supratemporal fenestrae as the main diagnostic features of *Smilosuchus gregorii*.

The lower jaws are, as noted previously, the wrong size to articulate with the skull. Indeed, the mount has the skull articulating anterior to the mandibular condyle (Fig. 15). Furthermore, the jaw is preserved differently (a different color) and presumably came from differently colored matrix. As preserved, the lower jaw is 1080 mm long, and this would fit an even larger phytosaur than the skull. Based on Long and Murry's (1995, p. 16) interpretation of PPHM records, this jaw is properly designated WT 2899. A total of 36 tooth positions are evident on the left side, occupying 790 mm of the specimen's total length. The mandibular fenestra is 235 mm long as preserved and begins ~640 mm from the anterior edge of the specimen. The symphysis is 370 mm long, but the articulated nature of the mount obscures additional details.

A large lower jaw fragment bears the number X 1999.35.258 (Fig. 16A-C). This could be the specimen Long and Murry (1995, p. 229) referred to as "PPHM WT 3230, distal end of snout of very large individual" and assigned to *Smilosuchus gregorii*, apparently based on its large size. The preservation appears distinct from that of the more typical Rotten Hill sample so, like some other phytosaur specimens, it may not have been collected from the Rotten Hill bonebed *per se*. It is notable for its huge size—the preserved 370 mm long segment contains only 24 tooth sockets on each side and does not even reach to the posterior margin of the mandibular symphysis. The anterior "bulb" is 83 mm long, flares to as much as 120 mm wide, and contains three large and two smaller tooth sockets on each side. The rest of the specimen is similarly robust—75-90 mm wide and ~65 mm thick. It is widest posteriorly, which might reflect a lateral flaring that is common in robust phytosaurs. The splenials intrude well into the mandibular symphysis, beginning ~205 mm from the anterior margin near the 17th tooth socket. The splenials widen abruptly posteriorly and approach the

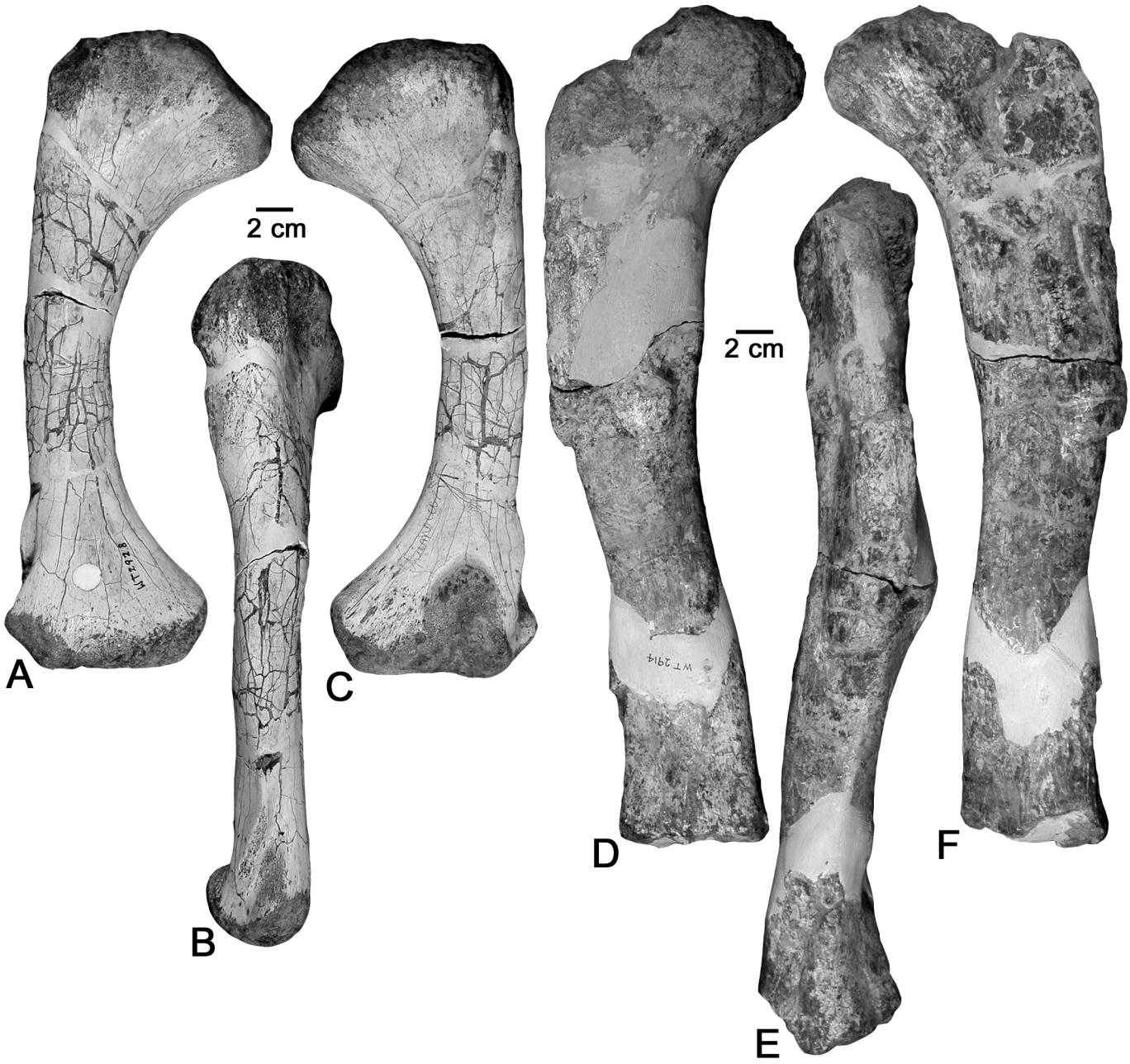

FIGURE 21. Phytosaur limb bones from the Rotten Hill bonebed. **A-C**, WT 2928, left humerus in **A**, anterior, **B**, lateral, and **C**, posterior view. **D-F**, WT 2914, incomplete left femur in **D**, posterior, **E**, lateral and **F**, anterior view.

tooth row. We have observed the splenials forming part of the medial margin of the tooth row in some phytosaurs (Heckert et al., 2013), a character that may have taxonomic significance, but the left side of this specimen is fractured just anterior to where this might occur.

A much smaller, presumably juvenile specimen is represented by an incomplete left premaxilla and maxilla (X 2000.10.20—Fig. 16D-G). We cannot discern the suture with certainty but it appears to cross the tooth row in the vicinity of the second (more posterior) break and offset at the widest part of the preserved bone. This specimen is broken posterior to the "bulb" and may include a sliver of the anterior margin of the antorbital fenestra. Although it is less than 270 mm long as preserved, it still preserves 28 tooth sockets, with the largest 8.2 mm long. Unlike some juvenile phytosaur specimens (Heckert et al., 2013; Lucas et al., 2013), these increase in size posteriorly (Fig. 16G). This strongly implies that this specimen, while juvenile, may represent a heterodont phytosaur such as *Smilosuchus*, although all of the preserved sockets are relatively circular. The anteriormost sockets are "paired" (likely reflecting ongoing tooth replacement) with the gap between positions 2-3 (as preserved) greater than the gaps between 1-2 or 3-4, a condition also typical of some juvenile phytosaur specimens (Heckert et al., 2013).

The anterior portion of a large phytosaur snout, WT 3092 (Fig. 17A-C) is only ~140 mm long but 91 mm wide across the anterior "bulb." The "bulb" bears three large tooth sockets on each side, followed by a single, smaller socket near its posterolateral corner. The rest of the tooth row begins from a position medial to the fourth tooth position, and extends for an additional nine tooth positions before the specimen is broken. As seen in some juvenile phytosaurs, the teeth posterior to the "bulb" appear to be paired, with teeth 5-6 and 7-8 closer to each other than 6 is to 7. In tooth positions 9-10 and 11-12, especially on the left side, this is carried to an extreme, and the wall between tooth sockets is missing. These teeth are, based on socket size, relatively small, circular in cross-section, and presumably homodont. We illustrate the specimen as if it is a lower jaw, but it could represent paired premaxillae.

A portion of a phytosaur snout (WT 3099—Fig. 17D-F) is ~185 mm long. The anterior portion of the preserved snout is 42 mm tall, but posteriorly this changes to 82 mm. The transition is rapid, occurring over 73 mm of length, and conforms to the pattern seen in hypothesized

FIGURE 22. Phytosaur limb bones from the Rotten Hill bonebed. **A-D**, WT 3116, left tibia in **A**, lateral, **B**, medial, **C**, anterior and **D**, posterior view. **E-H**, WT 3165, incomplete phytosaur femur in **E**, anterior, **F**, posterior, **G**, lateral and **H**, medial view. **I-L**, WT 3081, small right phytosaur femur in **I**, anterior, **J**, posterior, **K**, medial and **L**, lateral view.

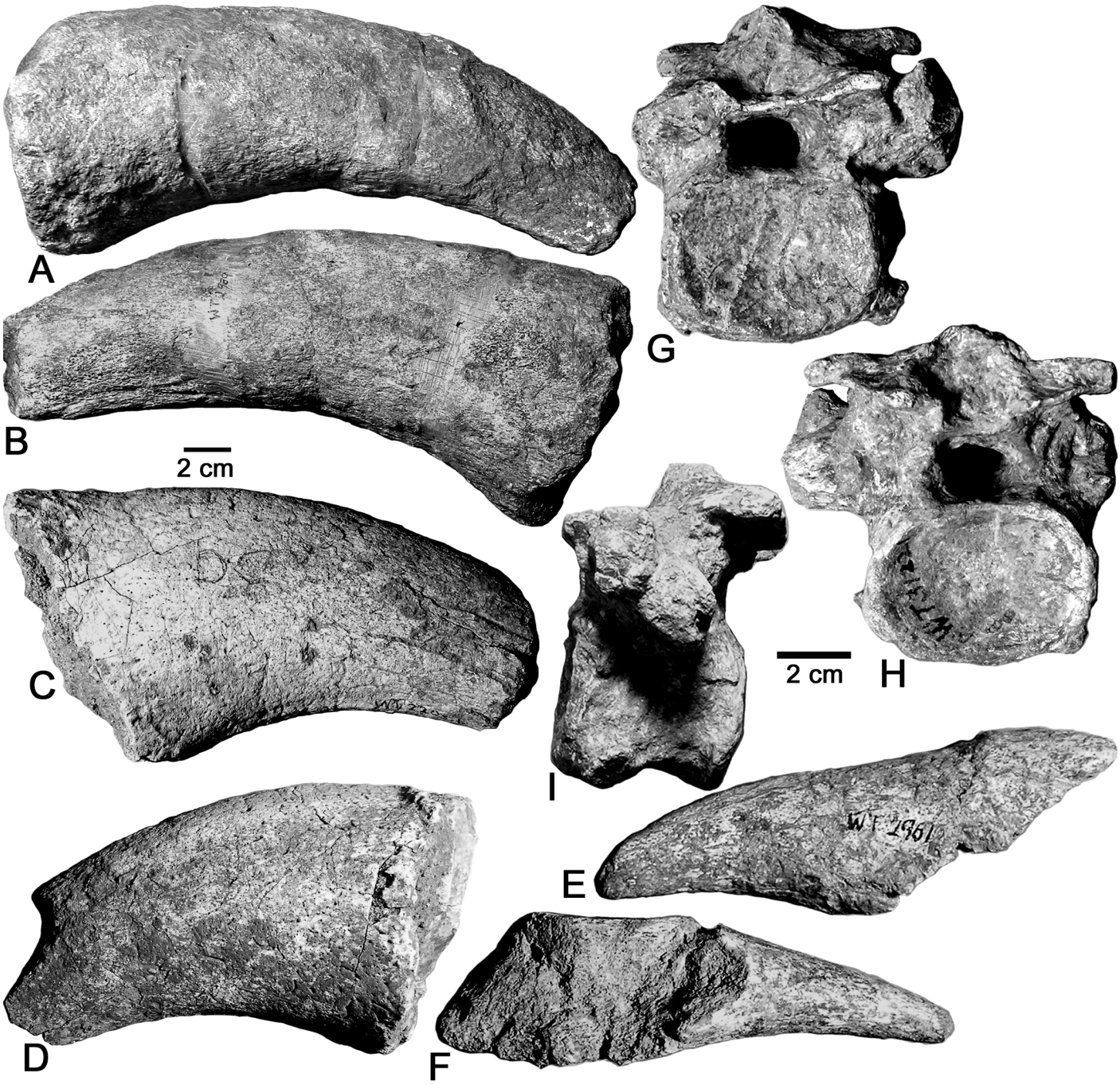

FIGURE 23. *Desmatosuchus haplocerus* from the Rotten Hill bonebed. **A-B**, WT 2939, left cervical lateral horn in **A**, ventral and **B**, dorsal view. **C-D**, WT 2203.1, right cervical lateral horn in **C**, dorsal and **D**, ventral view. **E-F**, WT 2961, left cervical lateral horn in **E**, dorsal and **F**, ventral views. **G-I**, WT 3132.1 anterior dorsal vertebra in **G**, anterior, **H**, posterior and **I**, left lateral view.

female phytosaurs (Zeigler et al., 2002a). The width also varies from 43 mm anteriorly to 73 mm posteriorly. The preserved specimen includes all or parts of 11-12 tooth sockets on each side.

A group of phytosaur skull and jaw fragments is assigned the number WT 3055, and some are illustrated here (Fig. 17F-N). We note that another fossil, a skull of *Koskinonodon* (Fig. 29A-B), also bears the number WT 3055, but the two specimens are easily distinguished, so we do not presume to renumber them here. The largest piece of the phytosaurian WT 3055 preserves about 255 mm of the mandibular symphysis (Fig. 17J-K). Another small fragment is from a more anterior portion of the symphysis. Together they show that the symphysis was nearly 30 cm long posterior to the bulb. It also appears that the jaw was complexly shaped, with a lateral bulge in the symphyseal region and another more posteriorly. This is clearly the brachyrostral condition. As noted for some of the other specimens, the splenial intrudes far anteriorly into the symphysis. Posteriorly, it forms the median wall of the four most posterior preserved sockets. Some other fragments with this number (Fig. 17G-I, L-N) may represent skull fragments, or else more posterior portions of the jaw.

Phytosaur Postcrania

In addition to the skulls and lower jaws, there is a modest assortment of phytosaur postcrania from the Rotten Hill bonebed in the PPHM collection. Most of these postcrania are of relatively large phytosaurs, so they likely are bones of specimens of *Smilosuchus gregorii*, and this large size is presumably the basis for Long and Murry's (1995, p. 229) assignment of much of this material to *Smilosuchus*. Unfortunately, essentially all systematic work on phytosaurs has focused on the skull, often to the exclusion of not just the postcrania, but even the lower jaws, in part because associated skeletons are extremely rare and few

have been described. Camp (1930) is an exception, detailing differences among some phytosaur taxa, particularly in the ilia, and other workers have documented postcrania that occur with more diagnostic material (e.g., Long and Murry, 1995; Lucas et al., 2002; Zeigler et al., 2003b; Kimmig, 2009; Spielmann and Lucas, 2012). Because phytosaur postcrania are not yet reliable for taxonomic purposes, we simply describe and illustrate a representative sample of the material recovered, in some cases amplifying or otherwise modifying the preliminary notes made by Long and Murry (1995).

A large, incomplete right scapulacoracoid (WT 2908—Fig. 18A-B) preserves much of the glenoid region and the more robust portions of the coracoid, but little else. This specimen pertains to a very large phytosaur. As preserved, the coracoid is 256 mm long and 156 mm deep, with the glenoid as much as 62 mm dorso-ventrally tall, and the length of the scapula-coracoid contact at the glenoid is ~93 mm. The large size and fusion of the scapula to the coracoid indicates that this was a skeletally mature individual. Long and Murry (1995, p. 229) referred this specimen to *Smilosuchus*, presumably based on its large size. The scapulacoracoid from Rotten Hill does not differ significantly from other scapulocoracoids of large phytosaurs illustrated by Camp (1930, fig. 15) and by Spielmann and Lucas (2012, fig. 61).

A much smaller scapula (WT 2902—Fig. 18C-D) is nearly completely preserved. It is 210 mm long and 74 mm across at the glenoid. It is typical of phytosaurian scapulae in being strongly posteriorly recurved, with a well-developed, thick contribution to the glenoid.

The only phytosaur interclavicle we encountered in the collection is catalogued as X.2000.10.117 (Fig. 19A-B), although we found 3220 written on one surface, so it may once have been WT 3220. It lacks the distal (posterior) portion but otherwise is typical of phytosaurs (cf. Camp, 1930, fig. 14). The proximal portion with the articulations for the clavicles is 95 mm wide, it tapers posteriorly to as little as 53 mm, and is approximately 195 mm long as preserved.

An incomplete, poorly preserved right ilium lacks much of the posterior acetabulum and posterior blade (WT 2927—Fig. 19C-D). The pubic peduncle is relatively long (91 mm). The very incomplete dorsal length is ~177 mm, and the specimen is ~131 mm tall, of which ~99 mm is acetabular height. It compares well to other illustrated ilia of large phytosaurs (Camp, 1930, fig. 16; Spielmann and Lucas, 2012, figs. 62-64), but the Rotten Hill ilium is too incomplete to allow detailed comparisons.

One of the best-preserved pelvic elements is a right ischium missing its distal blade (WT 3091—Fig. 19E-G). The total specimen length is ~168 mm, of which 98 mm are along the preserved symphysis. The acetabular contribution is ~46 mm across and distinct from a tongue of bone that probably articulated with the pubis. It compares well to an illustrated ischium of a large phytosaur from Arizona (Camp, 1930, fig. 16).

One large, fragment of a left humerus (WT 2925—Fig. 20A-C) is little more than the distal end but still 173 mm long and 142 mm across the condyles. The shaft is broken, so the midshaft diameters of 54 x 44 are probably larger than the actual minimal midshaft measurement. The ectepicondylar ridge is 80 mm long and 10-11 mm across, but the corresponding groove is nearly 93 mm long. It compares well to other illustrated humeri of large phytosaurs (Camp, 1930, fig. 17; Spielmann and Lucas, 2012, figs. 65-66).

A complete humerus (Fig. 21A-C) is 335 mm long and has a proximal width of 120 mm and a distal width of 109 mm. It has broad, flared ends and a bowed shaft. The proximal end is very rugose, and the ectepicondylar foramen is not pronounced, although the bone may be abraded in this area. It closely resembles the humeri of other large phytosaurs (Camp, 1930, fig. 17; Spielmann and Lucas, 2012, figs. 65-66).

A well preserved right ulna (WT 2903—Fig. 20D-F) is robust—261 mm long and 77 mm tall at the olecranon. Minimal midshaft measurements are 18 mm wide by 36 mm tall. The olecranon is robust for a phytosaur—46 mm across, with a facet 60 mm long. The distal end is 58 mm tall but only 20 mm wide. It differs from the ulna of *Redondasaurus* illustrated by Spielmann and Lucas (2012, fig. 67) in not having such a long olecranon process.

A nearly complete femur (Fig. 21D-F) is at least 380 mm long and has a proximal width of 120 mm. This bone has a slight sigmoidal flexure, and an expanded proximal end with a projecting head and a long fourth trochanter. It is similar to the femur of *Redondasaurus* illustrated by Spielmann and Lucas (2012, fig. 66). Two other, smaller femora (Fig. 22E-L) are similar. A tibia (Fig. 22A-D) has a broad, rounded proximal articular end and tapers to a much narrower shaft, expanding again to the rounded distal articular surface.

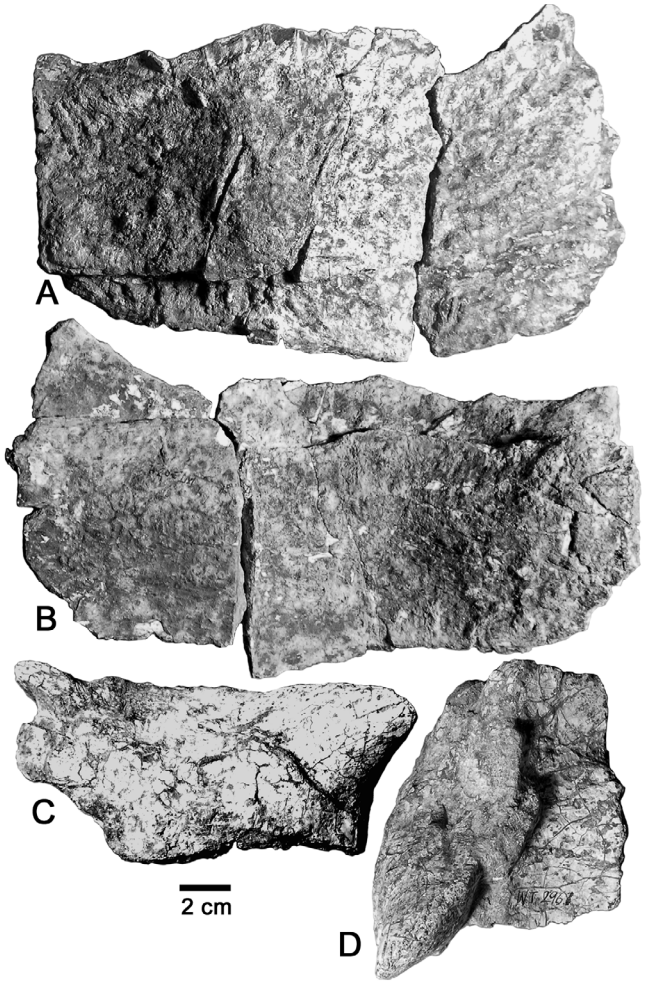

FIGURE 24. Aetosaurs from the Rotten Hill bonebed. **A-B**, cf. *Stagonolepis wellesi* osteoderms, WT 3034, **A,** two imbricated right anterior dorsal paramedian osteoderms in dorsal view. **B**, left dorsal paramedian osteoderm in dorsal view. **C-D**, *Desmatosuchus haplocerus,* osteoderms, WT 296. **C**, right lateral osteoderm in dorsal view. **D**, left(?) lateral osteoderm WT 2961, in dorsal view.

Additional, probable phytosaur fossils we do not illustrate or describe here include an array of centra catalogued as PPHM-209. These include centra from the dorsal and caudal series and range from 16-61 mm in length. Of these, P-209-151, the smallest specimen, may represent a juvenile phytosaur.

Desmatosuchus haplocerus

The largest and most identifiable specimens of aetosaurs are large, recurved lateral osteoderms of *Desmatosuchus* (Fig. 23A-F). There are also vertebrae (Fig. 23G-I) and other lateral osteoderms (Fig. 24C-D) that are less diagnostic but probably pertain to *Desmatosuchus haplocerus*. Long and Murry (1995, p. 233) referred several of these specimens to *Desmatosuchus haplocerus* as well.

A particularly robust lateral spine (WT 2939—Fig. 23A-B) is 99 mm in diameter, preserved for ~230 mm, but still incomplete, and badly abraded. As a result, much of the external surface, including the dorsal groove(s) described by Parker (2008) for other specimens, is missing. We tentatively identify it as a left based on the possible remnants of some grooves on the posterior surface (Fig. 23B). This specimen is a fifth lateral spike.

Another robust osteoderm, WT 2203, consists of the base of the large, recurved fifth lateral spike (Fig. 23C-D). It is also 99 mm in diameter, but is only 180 mm long as preserved. There are multiple grooves extending along the arc of the spike, although they are more posteriorly placed than Parker (2008, fig. 23f) described in a *Desmatosuchus* specimen from Arizona. Relatively little of the dorsal

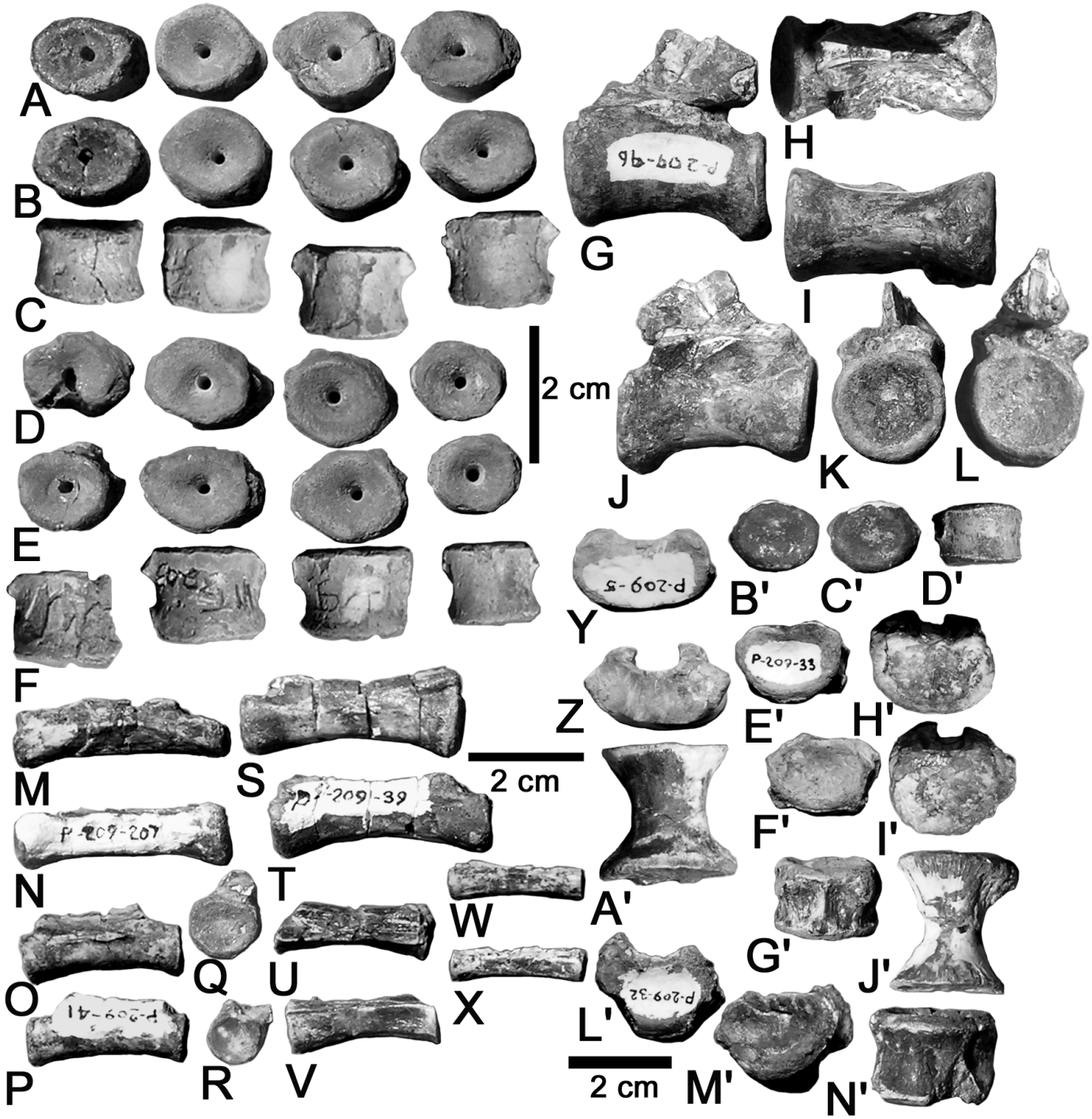

FIGURE 25. Tetrapod vertebrae from the Rotten Hill bonebed. **A-F**, *Apachesaurus gregorii*, eight centra in **A-B**, anterior (?), **D-E**, posterior (?) and **C, F**, ventral view. **G-L**, cf. *Trilophosaurus* sp., dorsal vertebra in **G**, left lateral, **H**, dorsal, **I**, ventral, **J**, right lateral, **K**, anterior and **L**, posterior view. **M-X**, cf. *Trilophosaurus* sp., caudal vertebrae in **M**, **O**, **S**, **U**, **W**, left lateral (?), **N**, **P**, **T**, **V**, **X**, right lateral (?), **Q**, anterior (?) and **R**, posterior (?) view. **Y-N'**, Reptilia inderminate, five centra in **Y**, **B'**, **E'**, **H'** and **L'**, anterior, **Z**, **C'**, **F'**, **I'** and **M'**, posterior and **A'**, **D'**, **G'**, **J'** and **N'**, ventral view. Upper scale bar for **A-L**, middle scale bar for **M-X** and lower scale bar for **Y-N'**. **A-F**, WT 3203; **G-N**, WT 209.

flange (which would articulate with the paramedian osteoderm) or the lateral flange is preserved.

Another spinose lateral osteoderm (WT 2961—Fig. 23E-F) may pertain to the cervical series, but is more likely one of the smaller (third, fourth, or sixth) lateral spines (e.g., Case, 1922; Long and Ballew, 1985; Long and Murry, 1995). The more elongate dorsal flange is incompletely preserved, and the ventral flange is missing. Not only is it considerably smaller than the other osteoderms, but the spine is essentially straight and lacks the curvature typical of fifth cervical spikes. Several other specimens with this number are incomplete lateral osteoderms that probably also pertain to *Desmatosuchus* but are not as diagnostic.

The large lateral osteoderms clearly pertain to *Demsatosuchus*, which has always been characterized by elongate, recurved lateral spines on its osteoderms (Case, 1922; Long and Ballew, 1985; Long and Murry, 1995; Heckert and Lucas, 2000). More recently Parker (2005, 2008) has split *Desmatosuchus* into at least two species and taken an alternative interpretation of the type material (compare to Heckert and Lucas, 2002). We do not accept his species-level taxonomy, though it was also followed by Desojo et al. (2013), so we refer all these Rotten Hill specimens to *Desmatosuchus haplocerus sensu* Heckert and Lucas (2000).

The other specimen we tentatively refer to *Desmatosuchus* is an anterior dorsal vertebra (WT 3122—Fig. 23G-I). This specimen is extremely similar to dorsal vertebrae of *Desmatosuchus* illustrated by Parker (2008, figs. 7-8). The articular facet is much broader (50 mm) than tall (38 mm), more like the cervicals, but the parapophysis is well above the centrum on the neural arch. The specimen is robust and relatively short (39 mm long) anteroposteriorly.

cf. *Stagonolepis wellesi*

We illustrate the incomplete remains of three aetosaur paramedian osteoderms from the PPHM collections. Two of these (WT 3034—Fig. 24A) are from the right side and tightly imbricated so that only the more anterior is visible in dorsal view. As preserved they are slightly more than twice as wide (218 mm) as long (89 mm), with a boss or dorsal eminence that is offset toward the straighter medial edge. The articular surface is slightly raised to form an anterior bar. The lateral side is not transversely thickened, and expands slightly antero-posteriorly, suggesting that this specimen is an anterior dorsal paraemdian, with a narrower osteoderm ahead and a wider one behind it. The ornamentation consists primarily of ovoid pits, not the irregular pits that typify *Desmatosuchus* and/or *Sierritasuchus*. These pits do not extend into the strongly radial ridges and grooves that are typical of many aetosaurs, but are arranged in a weakly radial pattern. This is the "anastomosing" pattern of Taborda et al. (2015).

A less complete left paramedian osteoderm (WT 3034—Fig. 24B) has similar proportions (250 mm wide and 84 mm long) but is less well preserved. The dorsal eminence is offset toward the medial margin but not strongly developed. The patterning is only faintly discernable, but consists of radially distributed elongate pits.

Long and Murry (1995, p. 232) referred these and some other osteoderm specimens with this number we did not locate to *Stagonolepis wellesi*. Indeed, these osteoderms are similar to those of *Stagonolepis wellesi*, but are not diagnostic, as the weakly radial pattern of an osteoderm with a low boss and moderately wide (width:length < 3:1) is characteristic of many aetosaurs (Heckert and Lucas, 2000; Desojo et al., 2013). We suspect that these osteoderms are the basis for Long and Murry's (1995) assignment of some fossils from Rotten Hill to *Stagonolepis wellesi*, but we more cautiously identify them as cf. *S. wellesi*.

KOSKINONODON PERFECTUM

Taxonomic Nomenclature

The Rotten Hill bonebed assemblage is dominated by fossils of the metoposaurid *Koskinonodon perfectum*. Unfortunately, no complete individual skeleton has been collected. However, enough isolated elements have been collected from the bonebed for us to provide a detailed osteology of *Koskinonodon perfectum* (see below). This osteology is based on the most complete elements available: 15 complete or nearly complete skulls, 2 lower jaws, 34 complete or nearly complete interclavicles, 27 clavicles, 18 atlases, 3 cervical vertebrae, 4 caudal vertebrae, 3 cleithra, 11 humeri, 3 radii, an ulna, 4 ilia, an ischium, 6 femora, 2 tibiae and 3 fibulae (Figs. 27-72).

The metoposaur long and widely known as *Buettneria perfecta* Case, 1922 is now properly known as *Koskinonodon perfectum* (Branson and Mehl, 1929). Mueller (2007) noted that *Buettneria* was a preoccupied taxonomic name, originally used for a bush-cricket from the Republic of the Congo, Africa, by Karsch (1889), who coined the name *Büttneria* (*Buettneria* by ICZN convention, ignoring diacritical marks). Mueller (2007) proposed that *Buettneria* should no longer be used for the metoposaurid amphibian and that the oldest available name and junior synonym *Koskinonodon* Branson and Mehl (1929) should instead replace it.

Lucas et al. (2007b) pointed out that *Buettneria* Karsch, 1889 had been a virtual *nomen oblitum*, nearly unused in the technical literature, while *Buettneria* Case, 1922 had been used in dozens (75+) of technical and more popular publications. A further comment by Hausdorf (2008) noted that Simroth (1888) had named an African gastropod *Buettneria* prior to Karsch's usage. Lucas et al. (2008), in a response to Hausdorf, noted that, much like *Buettneria* Karsch, 1889, *Buettneria* Simroth, 1888 was also a virtual *nomen oblitum*. Heckert (2008) provided citations of another 25 uses of *Buettneria* for the metoposaurid amphibian to the ICZN, showed that the only taxonomic use of the gastropod *Buettneria* has been relatively recent (since 1975), and that Simroth himself had switched to the term *Buettnerella* (Simroth, 1910). Thus, Lucas et al. (2008) and Heckert (2008) argued that the usage of *Buettneria* for the metoposaurid amphibian would produce a much more stable nomenclature for a long and widely used name, rather than either the bush-cricket or gastropod.

However, the ICZN (2010) ruled in favor of retaining *Buettneria* Simroth for the African land snail (and did not address what to do regarding *Buettneria* Karsch), so *Koskinonodon* (type species: *K. princeps* Branson and Mehl, 1929) appears to be the oldest available generic name to replace *Buettneria* (type species = *B. perfecta* Case, 1922). Due to grammatical rules, the specific epithet was modified from *K. perfecta* to *K. perfectum* (Mueller, 2007).

Revised Diagnosis

Based on the osteology of *Koskinonodon perfectum*, we are able to offer a revised diagnosis of *Koskinonodon*: a metoposaurid genus distinguished from other metoposaurid genera cranially by the lacrimal entering the orbital margin; and distinguished postcranially from the other metoposaurids with well known postcrania (*Metoposaurus, Dutuitosaurus*) by several features. Thus, in *Koskinonodon*, the atlas vertebra has a narrower and shorter neural canal and less prominent separation of the anterior articular surfaces than in *Metoposaurus*, and less deep and less cup-like anterior articular surfaces than are present in *Dutuitosaurus*. The caudal vertebral centra of *Koskinonodon* lack the deep notochordal notches seen in caudal centra of *Dutuitosaurus*. *Koskinonodon* has a much greater area of reticulate sculpture on the interclavicle than in *Metoposaurus*. The clavicle of *Koskinonodon* has a smaller and less prominent dorsal process and is relatively longer and more narrow than the clavicle of *Metoposaurus*. *Koskinonodon* has a flatter (less s-shaped curvature of the dorsal aspect of the shaft) ilium than in *Metoposaurus*, and a more hourglass-shaped tibia and a fibula with relatively shorter and thicker shafts than are present in *Metoposaurus* and *Dutuitosaurus*.

Previous diagnoses of *Koskinonodon* ("*Buettneria*") have only referred to the cranial character of the lacrimal entering the orbit margin (Hunt, 1993; Long and Murry, 1995; Schoch and Milner, 2000). The description of a large sample of postcrania of *Metoposaurus* (Sulej, 2007), the postcrania of *Koskinonodon* described here. and the description of a smaller sample of postcrania of *Dutuitosaurus* (Dutuit, 1976), have allowed us to identify several diagnostic features of the posctrania of these three metoposaurid taxa. We predict that further knowledge of the postcrania of these and other metoposaurid taxa will reveal other diagnostic features.

Osteology and Variation

Here we describe and illustrate the osteology of *Koskinonodon perfectum* based on the large sample of skulls, lower jaws and postcrania from the Rotten Hill bonebed. Our goal is not only to describe osteological elements, but also to document variation in morphology that appears to be both intraspecific in nature and/or of taxonomic significance.

Skull

The morphology of skull elements is the primary means for diagnosing the various genera and species of the family Metoposauridae (e.g., Hunt, 1993; Schoch and Milner, 2000). However, few analyses

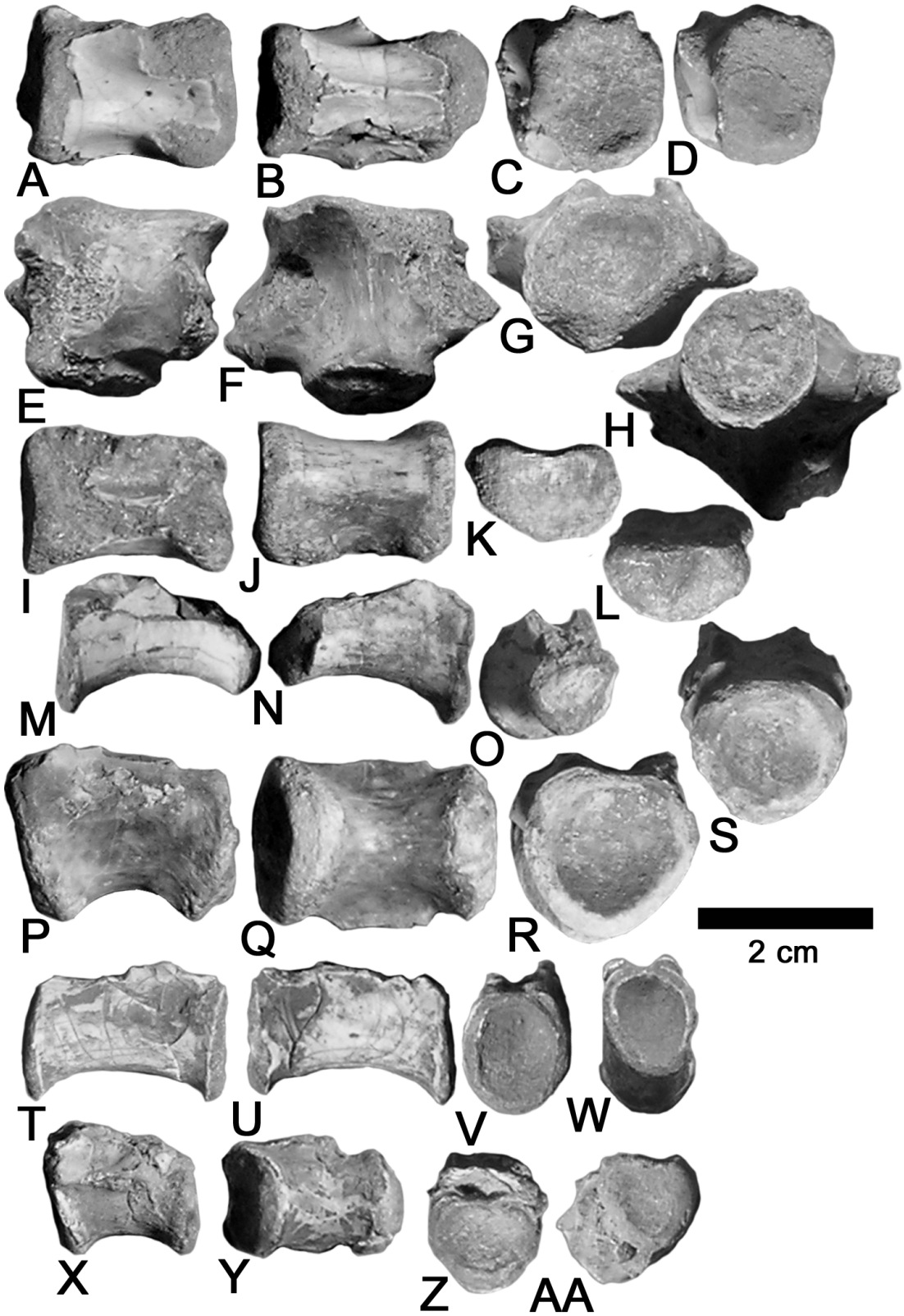

FIGURE 26. Vertebrae of *Vancleavea campi* from the Rotten Hill bonebed. PPHM 2000.10.106, **A-D**, cervical centrum; **E-H**, sacral centrum; **I-L**, dorsal centrum; **M-O**, dorsal centrum; **P-S**, caudal centrum; **T-W**, caudal(?) centrum; **X-AA**, anterior dorsal(?) centrum. These centra are illustrated in **A**, **M**, **P**, **T**, and **X**, right lateral; **B**, **F**, **J**, **Q** and **Y,** ventral; **C**, **G**, **K**, **O**, **R**, **V** and **Z**, anterior; **D**, **H**, **L**, **S**, **W** and **AA** posterior; **U**, left lateral and **E** and **I**, dorsal view.

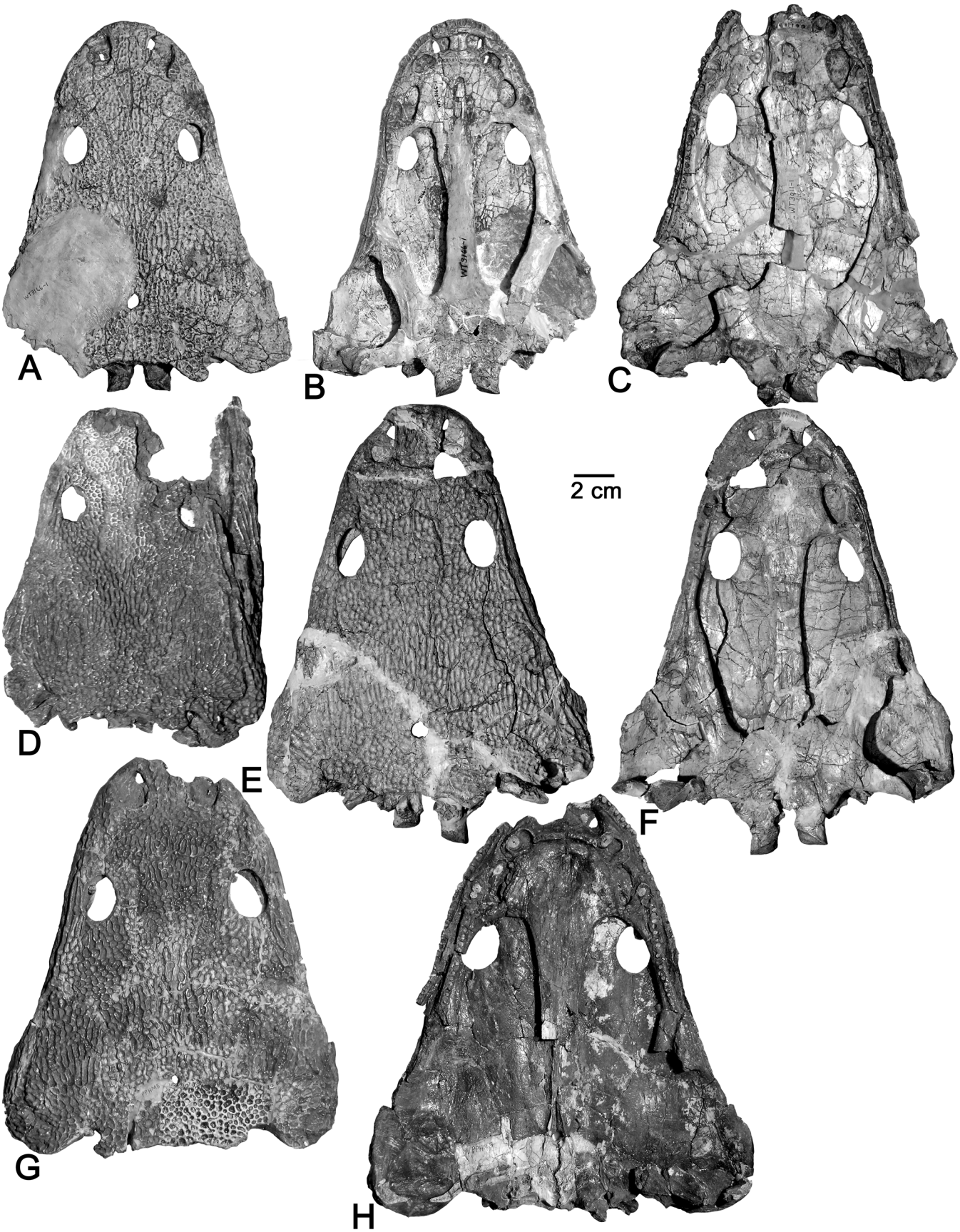

FIGURE 27. *Koskinonodon perfectum* skulls from the Rotten Hill bonebed. **A-B**, WT 3166-1, skull in **A**, dorsal and **B**, ventral view. **C**, WT 3011-1, skull in ventral view. **D**, PPHM 3, skull and right lower jaw in dorsal view. **E-F**, PPHM 6, skull in **E**, dorsal and **F**, ventral view. **G-H**, PPHM 5, skull in **G**, dorsal, and **H**, ventral view, with midline suture visible because the posterior portion of the palate is missing.

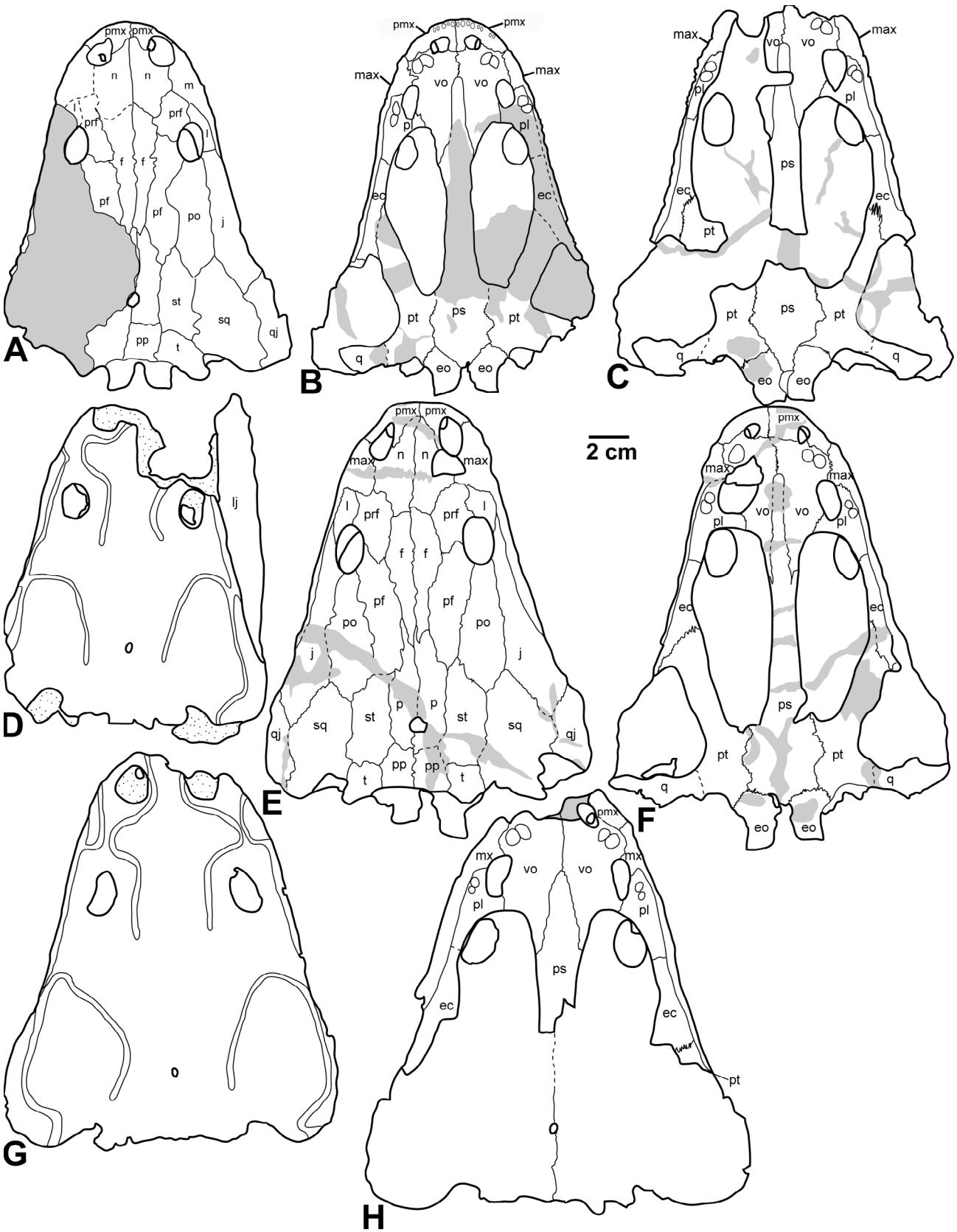

FIGURE 28. Interpretive drawings (bone maps) of the *Koskinonodon perfectum* skulls in Figure 27. **A-B**, WT 3166-1, bone map of skull in **A**, dorsal and **B**, ventral view. **C**, WT 3011-1, bone map of skull in ventral view. **D**, PPHM 3, dorsal outline of skull and right lower jaw with grooves for lateral lines drawn. **E-F**, PPHM 6, bone of map of skull in **E**, dorsal and **F**, ventral view. **G-H**, PPHM 5, **G**, Dorsal outline of skull with grooves for lateral lines drawn and **H**, Bone map of skull lacking posterior palate in ventral view, with midline suture drawn. Anatomical abbreviations are: ec = ectopterygoid; eo = exoccipital; f = frontal; j = jugal; lj = lower jaw; mx = maxilla; n = nasal; pa = palatine; pf = postfrontal; pmx = premaxilla; po = postorbital; pp = post-parietal; prf = prefrontal; ps = parasphenoid; pt = pterygoid; q = quadrate; qj = quadratojugal; sq = squamosal; st = supratemporal; t = tabular; vo = vomer.

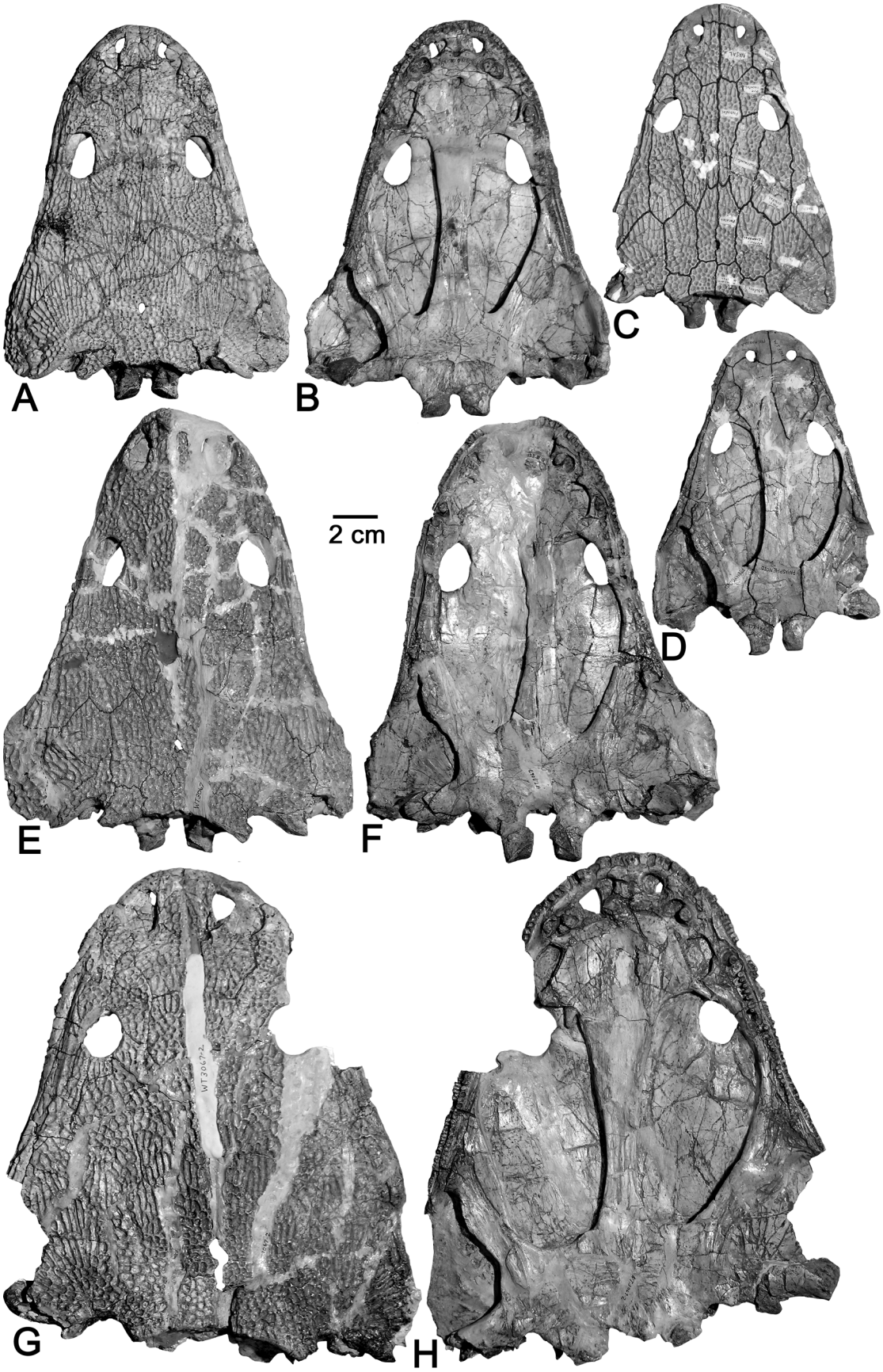

FIGURE 29. *Koskinonodon perfectum* skulls from the Rotten Hill bonebed**. A-B**, WT 3055, skull in **A**, dorsal and **B**, ventral view. **C-D,** WT 3011, skull in **C**, dorsal and **D**, ventral view. **E-F**, WT 3067, skull in **E**, dorsal and **F**, ventral view. **G-H**, WT 3067-2, skull in **G**, dorsal and **H**, ventral view.

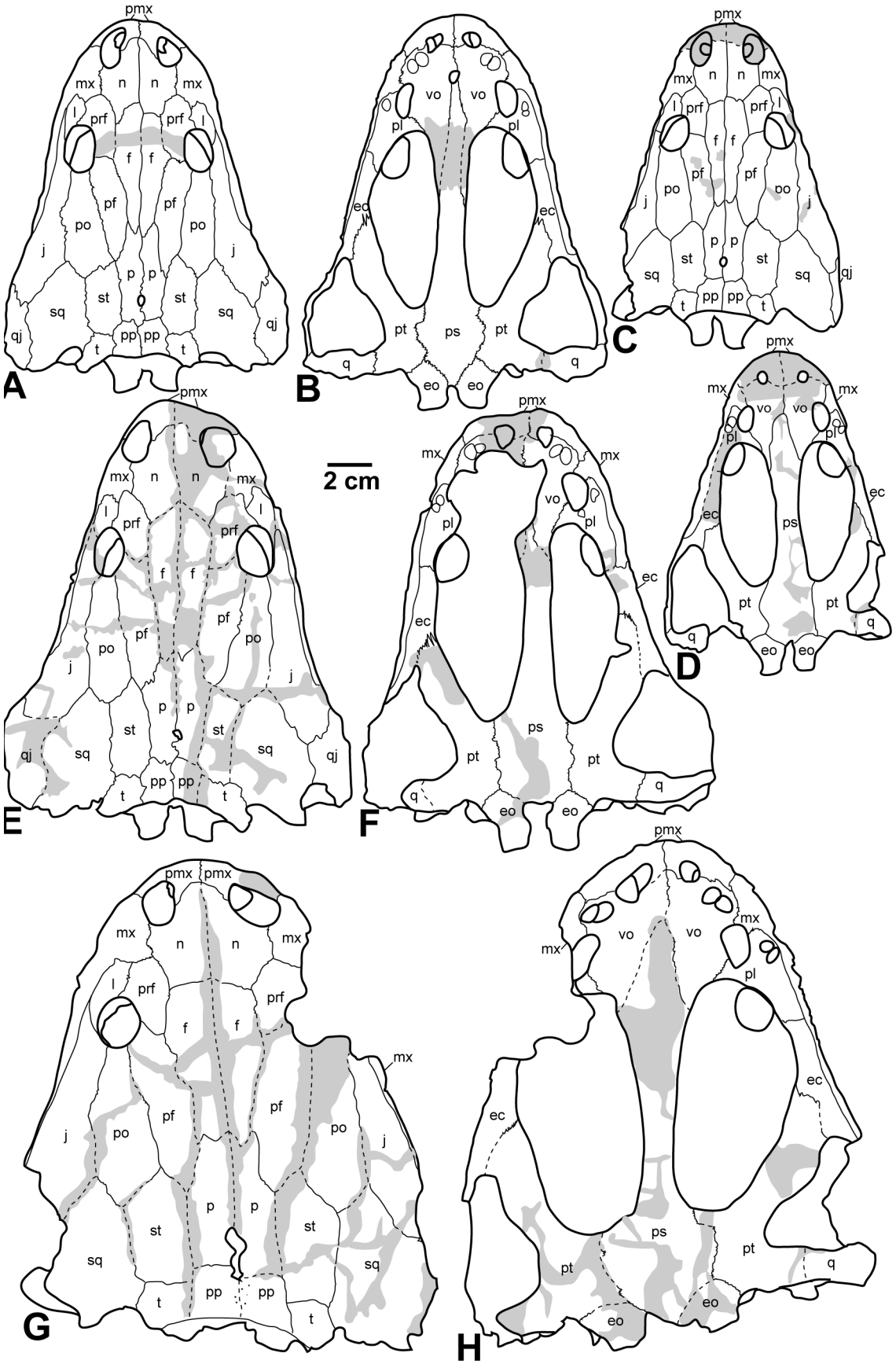

FIGURE 30. Interpretive drawings (bone maps) of the *Koskinonodon perfectum* skulls in Figure 29. **A-B**, WT 3055, bone map of a skull in **A**, dorsal and **B**, ventral view. **C-D,** WT 3011, bone map of a skull in **C**, dorsal and **D**, ventral view. **E-F**, WT 3067, bone map of a skull in **E**, dorsal and **F**, ventral view. **G-H**, WT 3067-2, bone map of a skull in **G**, dorsal and **H**, ventral view. Anatomical abbreviations as in Figure 28.

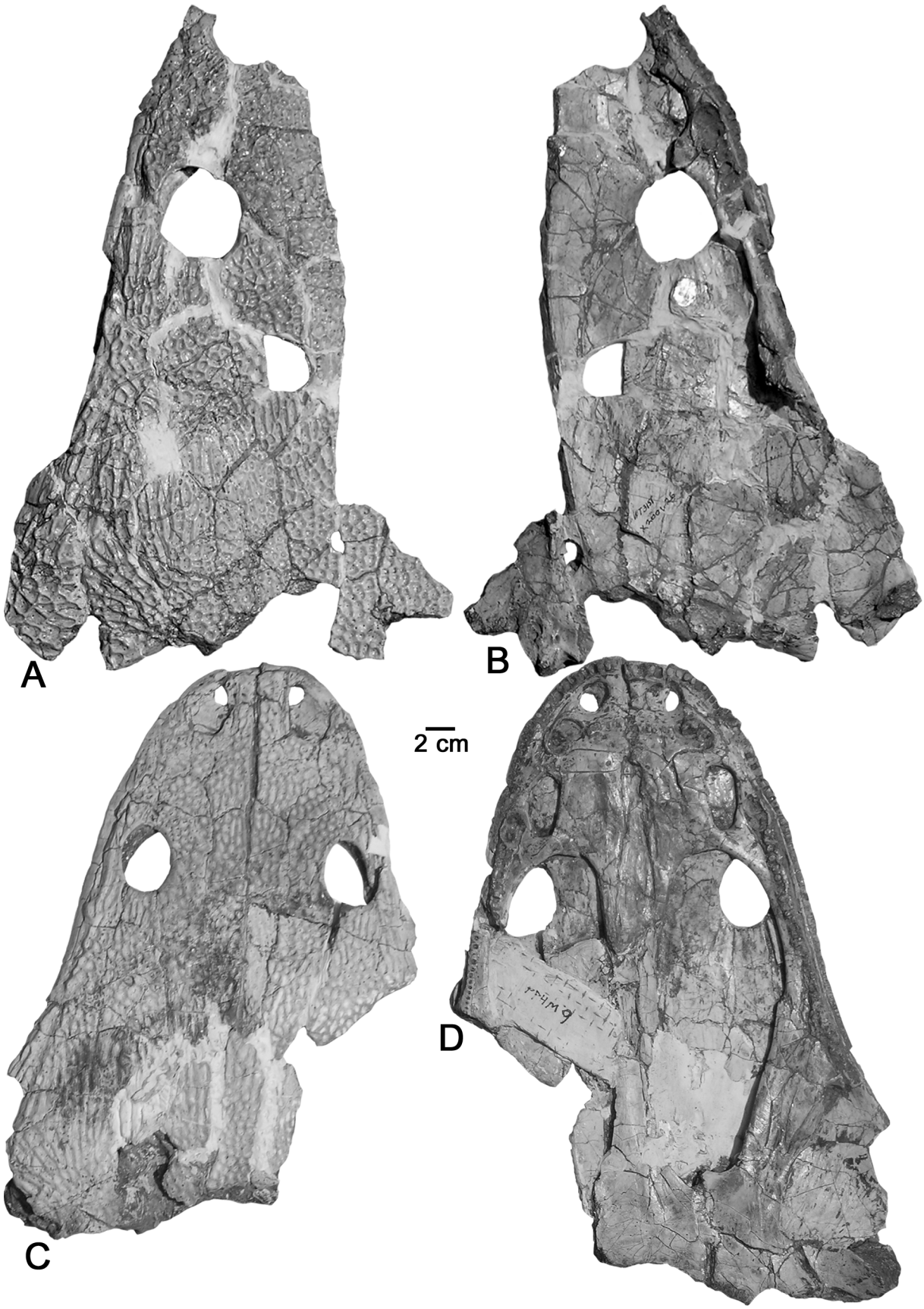

FIGURE 31. *Koskinonodon perfectum* skulls from the Rotten Hill bonebed. **A-B**, WT 3151, X2001.26, left half of skull in **A**, dorsal and **B**, ventral view. **C-D**, PPHM 9, skull in **C**, dorsal and **D**, ventral view.

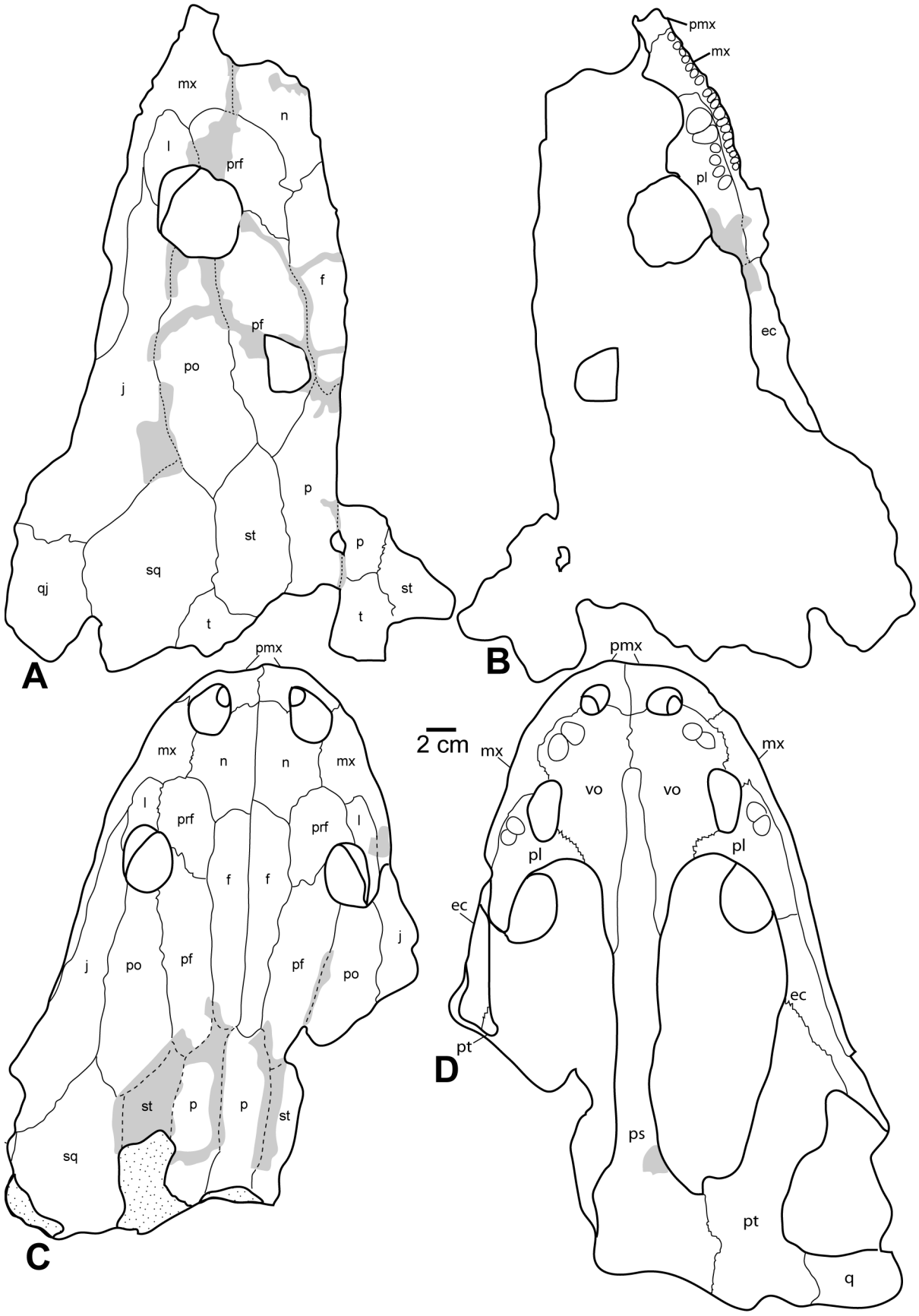

FIGURE 32. Interpretive drawings (bone maps) of the *Koskinonodon perfectum* skulls in Figure 31. **A-B**, WT 3151, X2001.26, bone map of left half of skull in **A**, dorsal and **B**, ventral view. **C-D**, PPHM 9, bone map of skull in **C**, dorsal and **D**, ventral view. Anatomical abbreviations as in Figure 28.

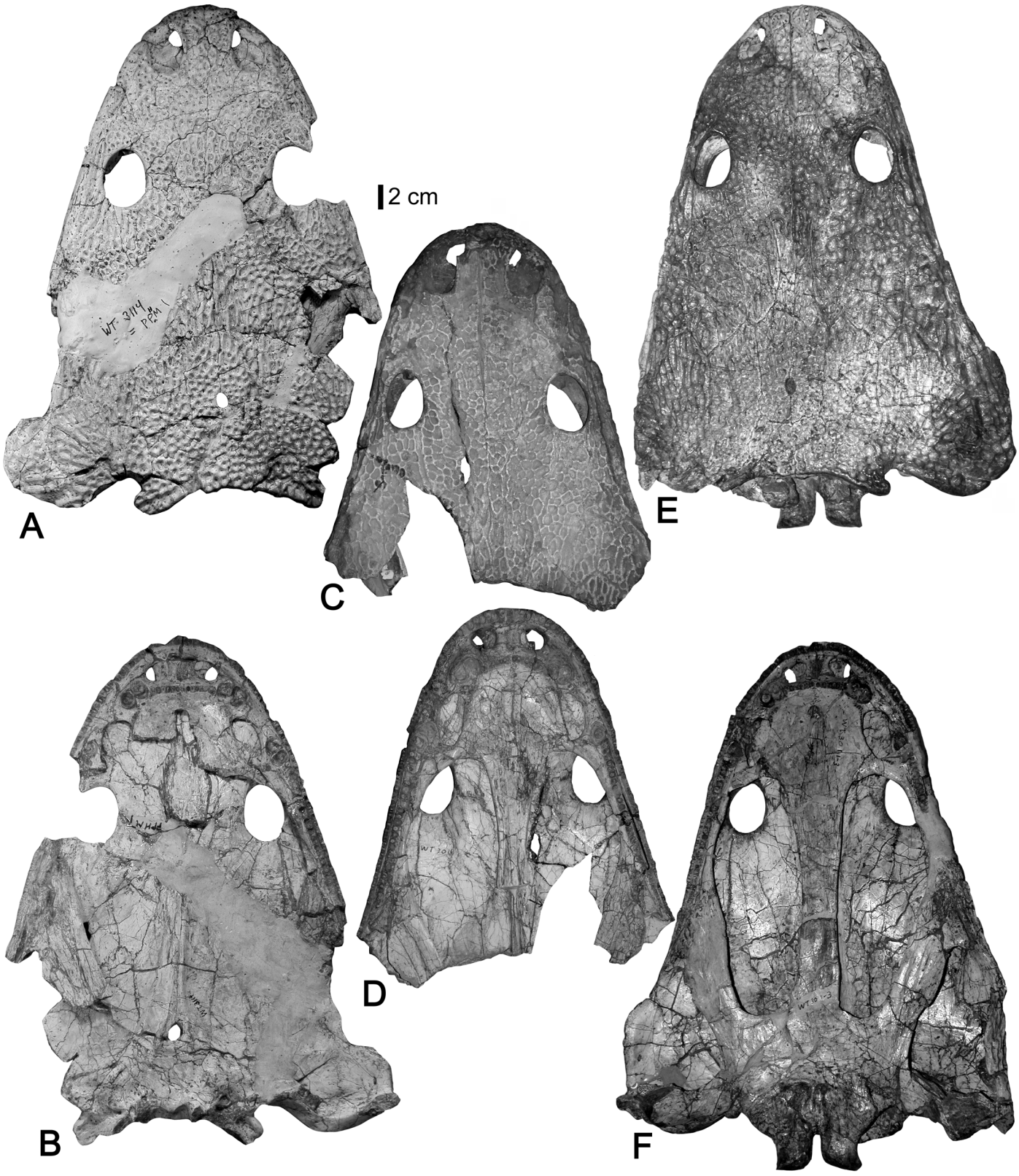

FIGURE 33. *Koskinonodon perfectum* skulls from the Rotten Hill bonebed. **A-B**, WT 3114, skull in **A**, dorsal and **B**, ventral view. **C-D**, WT 3011, skull in **C**, dorsal and **D**, ventral view. **E-F**, WT 3011-3, skull in **E**, dorsal and **F**, ventral view.

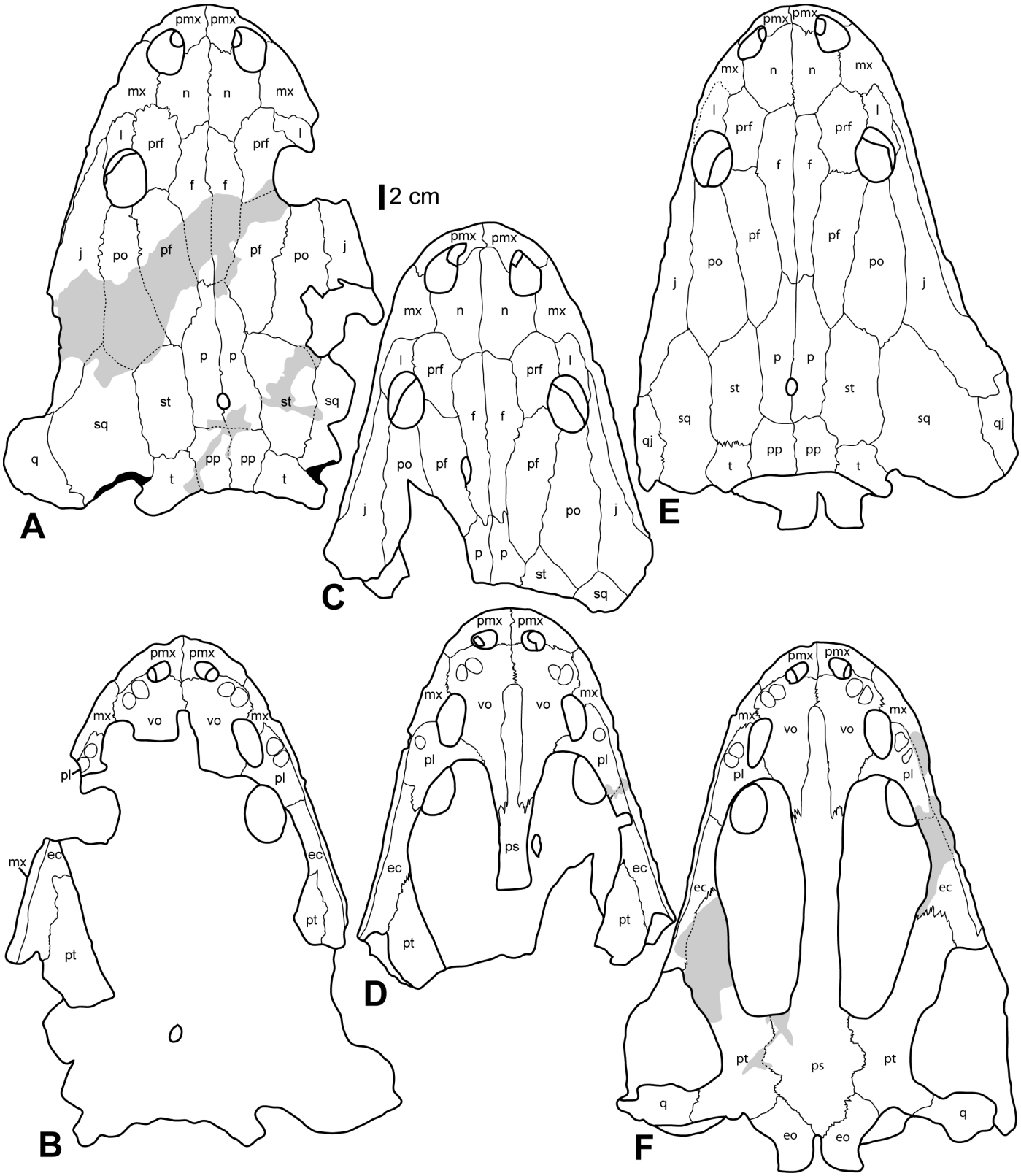

FIGURE 34. Interpretive drawings (bone maps) of the *Koskinonodon perfectum* skulls in Figure 33. **A-B**, WT 3114, bone map of skull in **A**, dorsal and **B**, ventral view. **C-D**, WT 3011, bone map of skull in **C**, dorsal and **D**, ventral view. **E-F**, WT 3011-3, bone map of skull in **E**, dorsal and **F**, ventral view. Anatomical abbreviations as in Figure 28.

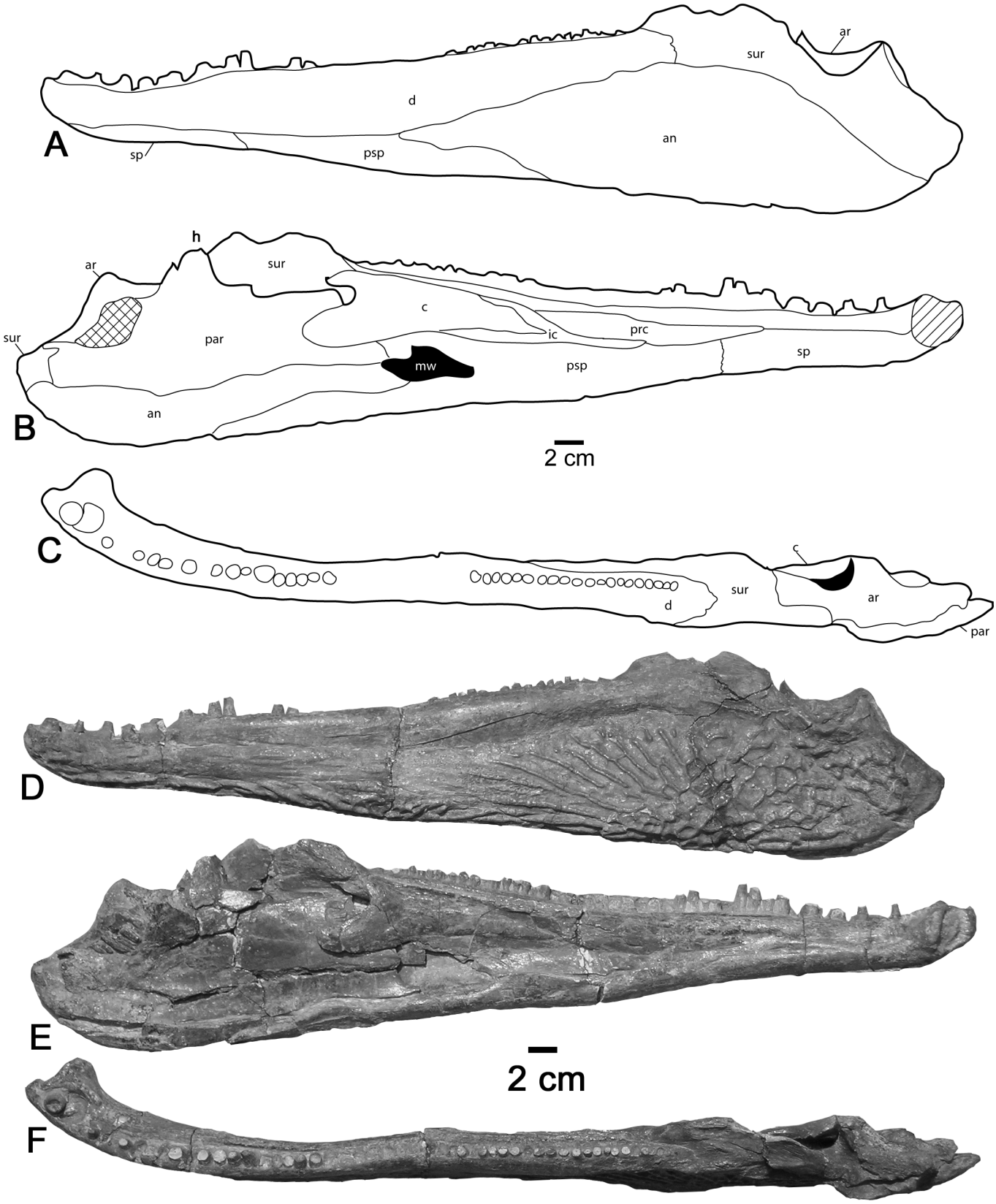

FIGURE 35. *Koskinonodon perfectum* lower jaw from the Rotten Hill bonebed. **A-F**, X 2000.10.110, large left lower jaw in **A, D**, lateral, **B, E**, medial and **C, F**, occlusal view. Anatomical abbreviations: an = angular; ar = articular; c = coronoid; d = dentary; h = hamate process; mw = Meckelian window; par = prearticular; prc = precoronoid; psp = postsplenial; sp = splenial; sur = surangular.

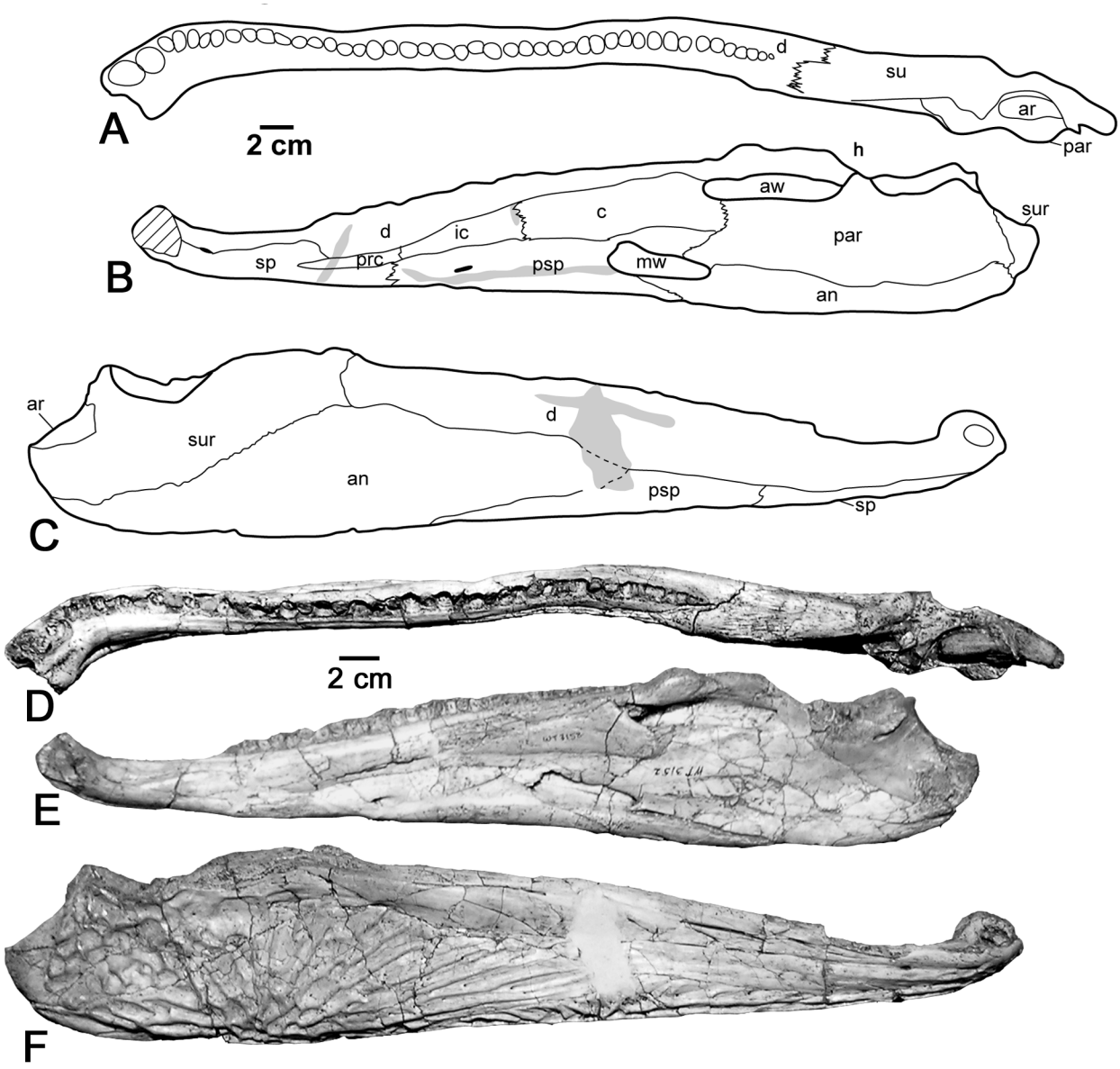

FIGURE 36. *Koskinonodon perfectum* lower jaw from the Rotten Hill bonebed. **A-F**, WT 3152, right lower jaw in **A**, **D**, occlusal, **B**, **E**, medial and **C**, **F**, lateral view. Anatomical abbreviations as in Figure 35.

have examined the meristic variation in skull elements within a single metoposaur taxon (Colbert and Imbrie, 1956, is an exception). Another issue in the case of *Koskinonodon perfectum* is that the most widely used osteological description is more than 70 years old (Sawin, 1945) and thus needs to be updated.

The reason that understanding variation in skull elements is so critical is that within the metoposaurids many of the taxa are diagnosed based on the morphology of single skull elements (e. g., Hunt, 1993; Long and Murry, 1995; Schoch and Milner, 2000). Only by examining a large statistical sample from a monospecific population, like that of the Rotten Hill bonebed, can a range a variation for a taxon be established.

In order to assess skull element variation in *Koskinonodon perfectum,* 10 of the most complete, best preserved, and/or informative skulls from the Rotten Hill quarry were photographed, bone mapped and/or outlined and compared to each other and to published illustrations and descriptions (Figs. 27-34). All of these skulls are nearly complete and exceptionally well preserved, so that details of sutural patterns are readily discerned. A variety of size ranges were examined from smaller (Figs. 27A-B, 28A-B, 29C-D) to larger (Figs. 27E-H, 29E-H). Also, we noted variation in the overall skull morphology ranging from relatively long and thin (dolicocephalic) (Fig. 29E-F) skulls through relatively short and wide (brachycephalic) skulls (Fig. 29G-H).

We attempted to examine, photograph and illustrate as many skulls as possible; however, some skulls were locked in their plaster cradles and could only be examined in a single view (e.g., Fig. 27C-D). A few skulls could not be completely bone mapped because their sutures are obscured by encrusting matrix (Fig. 27D, G). Even in cases when such bone mapping could not be accomplished, we generated outline drawings of the lateral line system (Fig. 28D, G).

Overview of Skull

Seen dorsally, the skull of *Koskinonodon perfectum* is shovel shaped, with a broad and arcuate anterior end and a more nearly flat (straight) posterior end (Figs. 27-34). The sides of the skull diverge regularly and gently away from the anterior end. The dorsal aspect of the skull is nearly flat (low and horizontal) and is ornamented with a reticulate texture of dermal bone. Five dorsally oriented openings are evident—the two external nares, the two orbits and a much smaller, medial pineal foramen. The occipital condyles project strongly from the posterior end of the skull, and there are distinct reentrant otic notches.

Lateral Line Canals

The lateral line canals comprise three pairs of shallow sulci that housed the water-motion-sensing, lateral line organs (Fig. 28D, G).

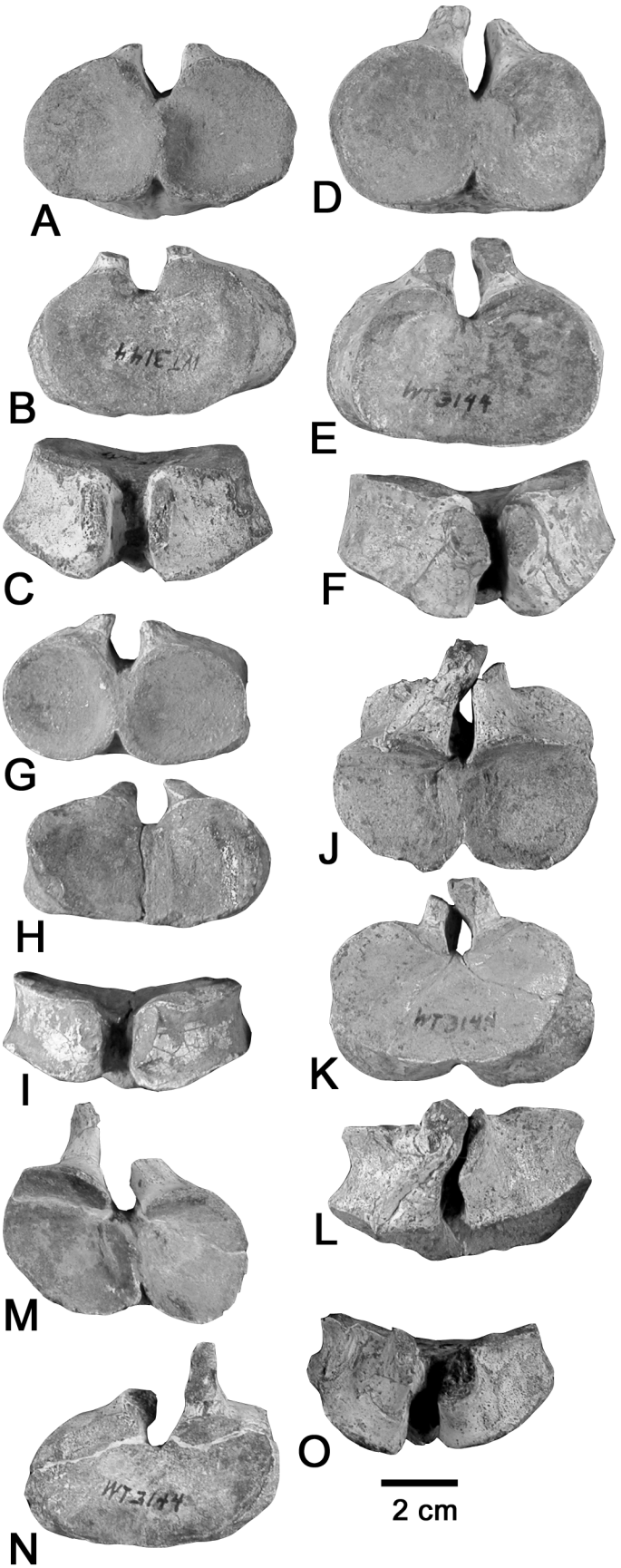

FIGURE 37. *Koskinonodon perfectum* atlas vertebrae from the Rotten Hill bonebed, WT 3144, five atlantes in **A**, **D**, **G**, **J**, **M**, anterior, **B**, **E**, **H**, **K**, **N**, posterior and **C**, **F**, **I**, **L**, **O**, dorsal views.

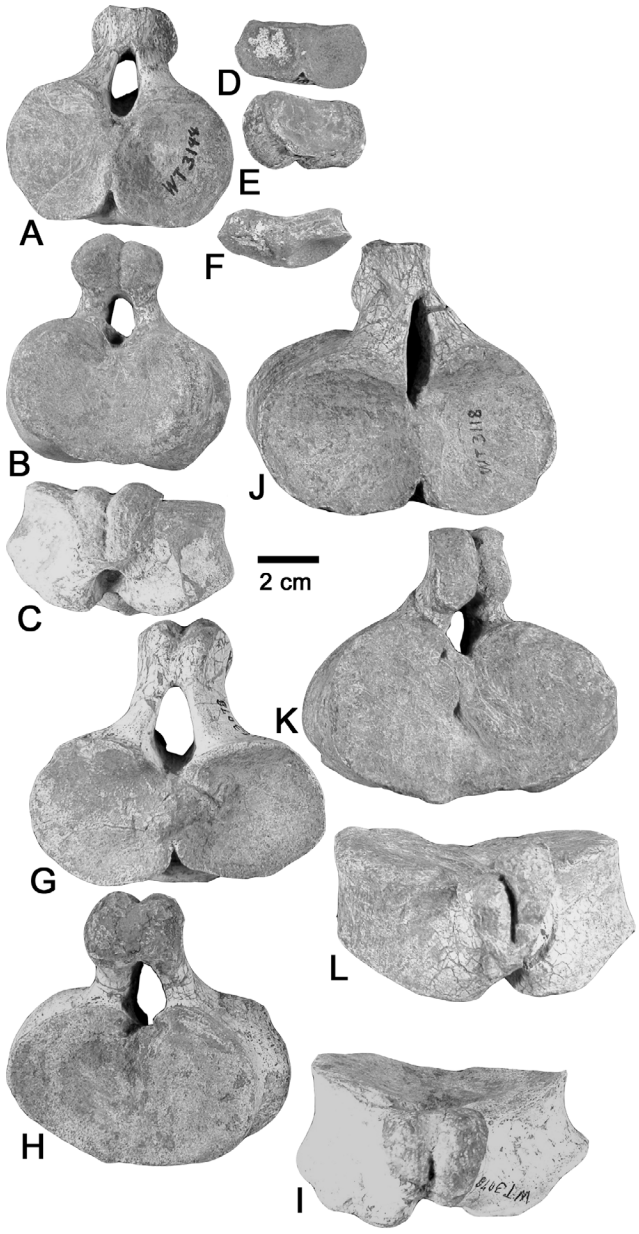

FIGURE 38. *Koskinonodon perfectum* atlas vertebrae from the Rotten Hill bonebed. **A-C**, WT 3148, atlas. **D-I**, WT 3078, two atlases. **J-L**, WT 3118, atlas. Atlantes in **A**, **D**, **G**, **J**, anterior, **B**, **E**, **H**, **K**, posterior and **C**, **F**, **I**, **L**, dorsal views.

The postorbital canals originate near the center of the supratemporals and proceed anteriorly onto the postorbitals, where they curve laterally onto the jugals, forming a half-loop. They continue posteriorly onto the quadratrojugals from which they bend medially onto the squamosals. On the squamosals, the canals curve posterolaterally forming another, smaller half-loop, and exit the skull just medial to the squamosal-quadratojugal suture. Presumably, the lateral line organs continued from this point for some distance down the side of the animal as they do in many extant fish and amphibians.

The supraorbital canals originate on the postfrontals, posteromedial to the orbits. They continue anteriorly onto the prefrontals where they curve laterally across the anteromedial border of the orbit. They then describe a gently anteromedial arcuate path across the dorsal process of the maxillae and onto the nasals just posterior to the external nares. The canals proceed medially around the external nares and cross the premaxillae to exit the skull roof anteromedial to the external nares.

The infraorbital canals closely parallel the maxillary-jugal suture along the sides of the skull, proceeding anteriorly until they form a

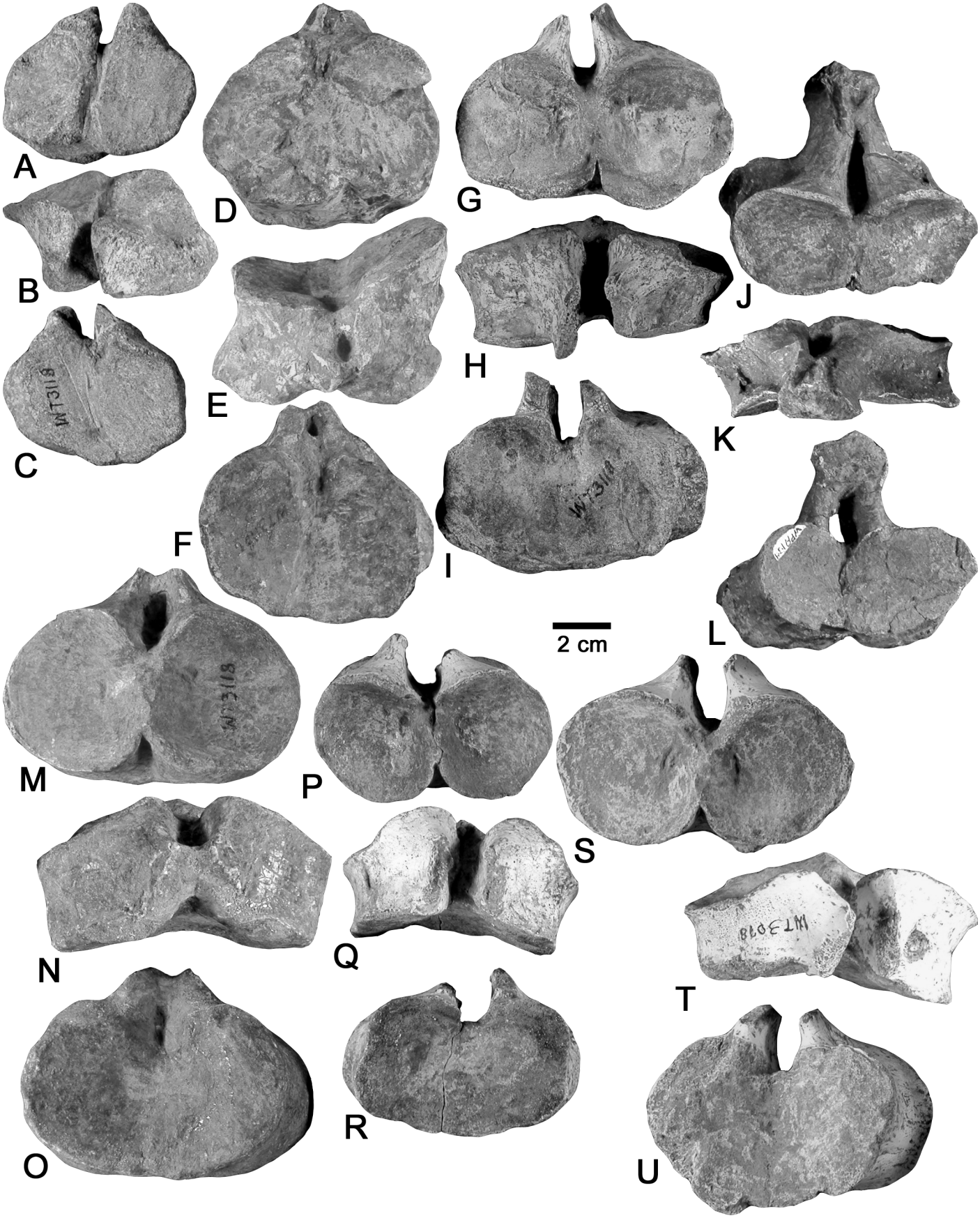

FIGURE 39. *Koskinonodon perfectum* atlas vertebrae from the Rotten Hill bonebed. **A-I**, **J-L**, WT 1341, atlas. **M-O**, WT 3118, four atlantes. **P-R**, WT 2973, atlas. **S-U**, WT 3078, atlas. Atlantes in **A**, **D**, **G**, **J**, **M**, **P**, **S**, anterior, **B**, **E**, **H**, **K**, **N**, **Q**, **T**, dorsal and **C**, **F**, **I**, **L**, **O**, **R**, **U**, posterior view.

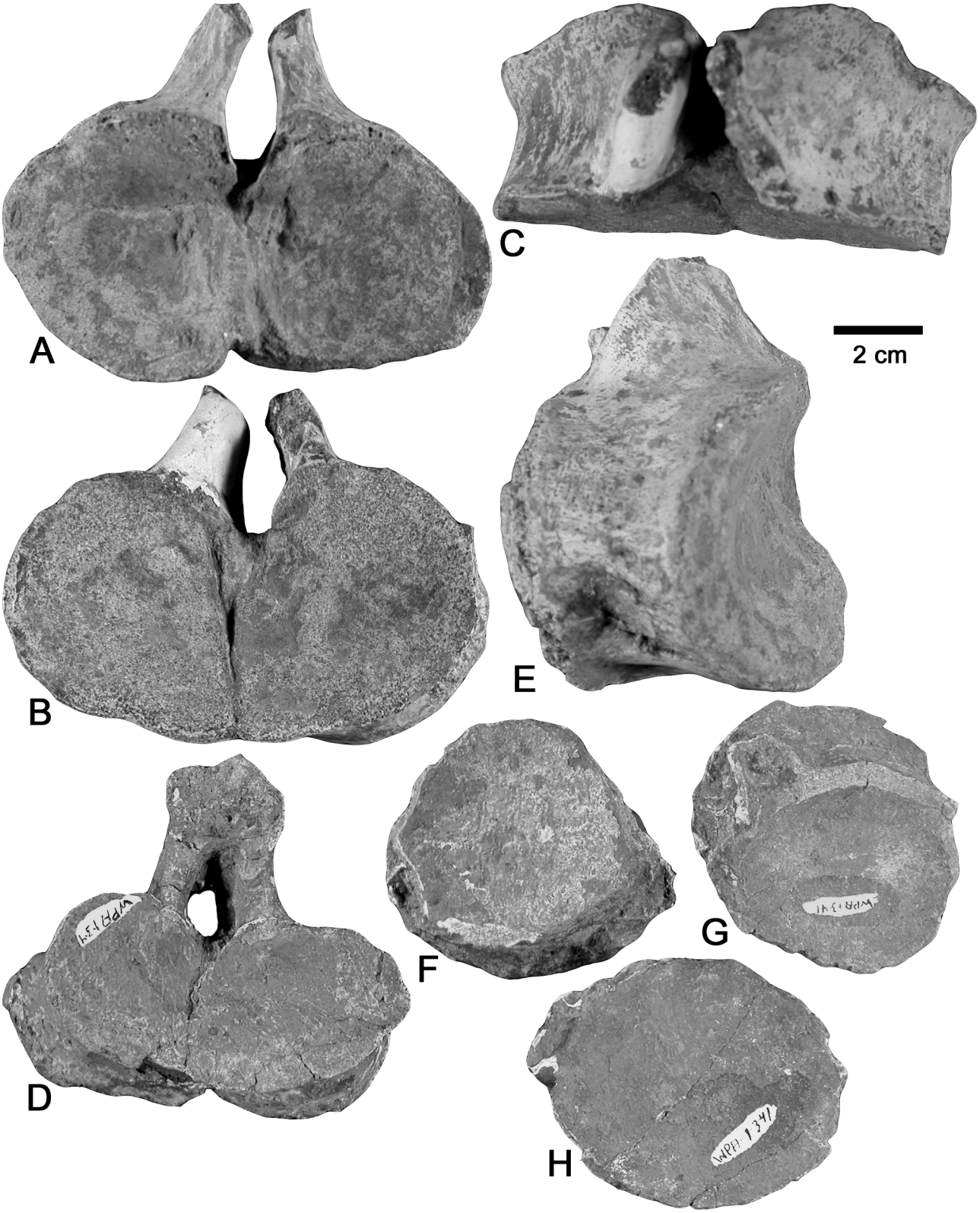

FIGURE 40. *Koskinonodon perfectum* cervical vertebrae from the Rotten Hill bonebed. **A-C**, WT 2975, atlas in **A**, anterior, **B**, posterior, and **C**, dorsal view. **E-H**, WT 1341, one atlas and three cervical centra. **D-E,**, atlas in **D**, posterior view and **E**, lateral view. **F-H**, three cervical centra in articular view.

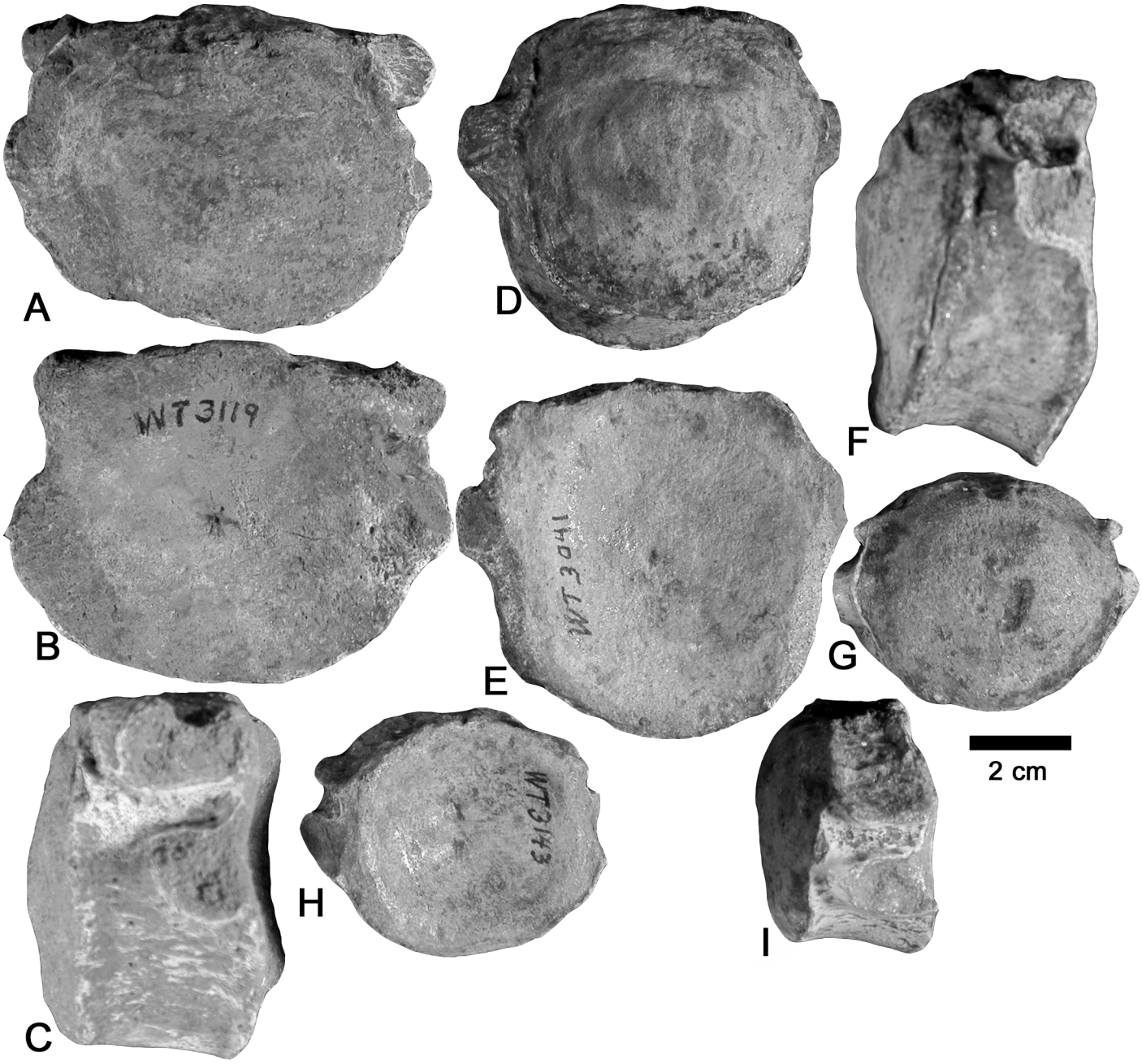

FIGURE 41. *Koskinonodon perfectum* cervical vertebrae from the Rotten Hill bonebed. **A-C**, WT 3119, cervical vertebra. **D-F**, WT 3041, cervical vertebra. **G-I**, WT 3143, cervical vertebra. Three cervical vertebrae in **A**, **D**, **G**, anterior, **B**, **E**, **H**, posterior and **C**, **F**, **I**, left lateral views.

Z-shaped flexure that brings them medially up onto the snout near the front of the lacrimals. They cross the dorsal process of the maxillae and proceed laterally around the external nares. They cross the premaxillae and exit the skull roof anterolateral to the external nares.

Upper Dentition

The dentition of *Koskinonodon* is impressive. Nearly 300 teeth are present in the marginal toothrows of the skull and on the palate. More than 100 additional teeth are contained in the lower jaws (Figs. 35-36). In the Rotten Hill *Koskinonodon* population nearly all of the teeth are broken off near the base of the crown (Figs. 27-34).

A minimum of four palatal tusks are present; two on the vomers and two on the palatines (e.g., Figs. 28B, C, F). These occur in emplacement pits that are large enough to contain two tusks, but generally only one is present unless, apparently, tooth replacement is underway. Typically, these tusks are 3-5 mm or more in diameter.

The premaxillary marginal tooth row comprises approximately 14 teeth on each premaxilla (Fig. 28B). These are the largest of the marginal teeth, being ~ 2 mm in diameter depending on the size of the specimen. Immediately posterior to the premaxillae, a short toothrow crosses the vomers in an anteriorly curved arc between the vomer tusk emplacement pits. This row contains approximately six teeth on each vomer that are of about the same size as the anterior maxillary teeth.

A row of approximately 25 very small, needle-like teeth originates posteromedially to the vomer tusk emplacement pits and follows the medial border of the nares, crossing from the vomers to the palatines. This tooth row curves laterally around the posterior margin of the choanae and ends before reaching the palatine tusk emplacement pits.

From the external nares posteriorly to the adductor fossae, the marginal toothrow is doubled. The maxillae contain the lateral marginal toothrow, and the palatines and ectopterygoids contain the medial marginal toothrow. The maxillary toothrow begins lateral to the vomer

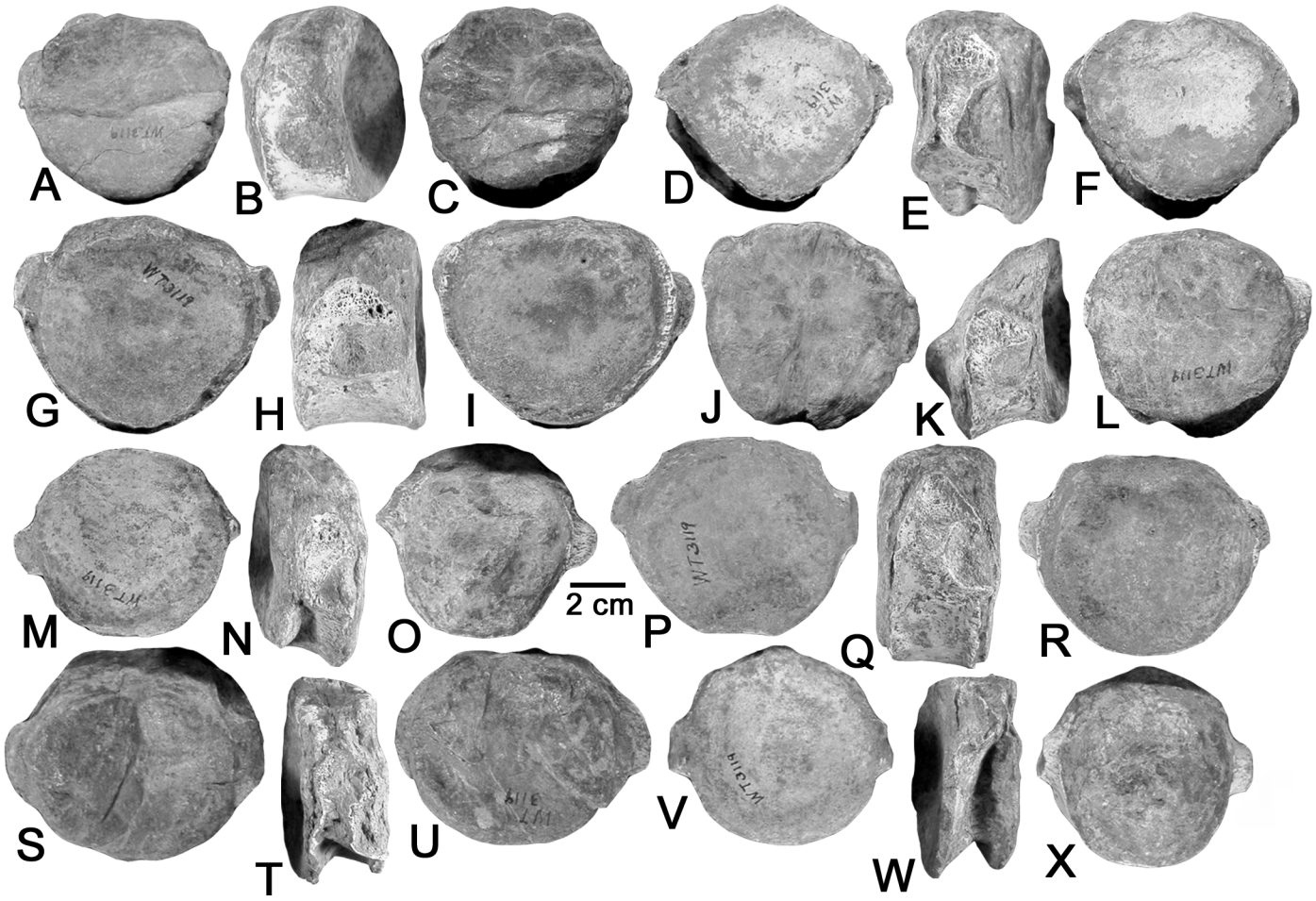

FIGURE 42. *Koskinonodon perfectum* dorsal vertebrae from the Rotten Hill bonebed. **A-X**, WT 3119, six centra in **A**, **D**, **G**, **J**, **M**, **P**, **S**, **V**, anterior, **B**, **E**, **H**, **K**, **N**, **Q**, **T**, **W**, left lateral and **C**, **F**, **I**, **L**, **O**, **R**, **U**, **X**, posterior views.

tusk emplacement pits and proceeds posteriorly as the teeth continually diminish in diameter from ~ 2 mm to ~ 0.5 mm. Approximately 55 teeth are present in each maxilla. The medial marginal toothrow originates on the palatine medial to the choanae and parallels the maxillary toothrow for the remainder of its length. Approximately 40 teeth similar in size to the maxillary teeth are present in this toothrow on each side of the skull. As in the maxillae, these teeth diminish in size from the anterior end of the row to the posterior end of the row.

Premaxilla

The premaxilla makes up the anteriormost portion of the skull and is one of the few elements that is part of both the dorsal and ventral surfaces of the skull (Figs. 27-34). In both dorsal and ventral view, the premaxilla consists of two processes, a medial process and a lateral process. As just described, there are approximately 14 marginal tooth positions in each premaxilla (Fig. 28B).

In dorsal view, the medial process extends posteriorly to form the anteromedial margin of the external nares and contacts the anterior nasal. The lateral process extends posterolaterally, forming the anterolateral margin of the external nares and contacting the anterior maxilla. Overall, the premaxilla forms the anterior half of the margin of the external nares. The anterior premaxilla is rounded, giving the anterior end of the skull a wide, arcuate shape.

In ventral view, the medial process of the premaxilla extends posteriorly to the posterior margin of the anterior palatal fenestra and borders the anterior vomer. The lateral process extends posterolaterally to the vomerine tusk pair where it contacts the anterior maxilla and forms the anterior half of the lateral margin of the anterior palatal fenestra.

The sutural patterns of the premaxilla vary little throughout the skulls that we examined. The premaxilla-nasal suture is typically sigmoidal and extends from the midline posterolaterally to the external nares (e. g., Figs. 28A, 30E). Only two variants have been noted, a slightly more triangular shape, without any sigmoidal flexure (Fig. 28E) and a more arcuate suture (Fig. 30A). Both of these variants are represented by single specimens, so we consider them rare and intraspecific in nature.

The dorsal premaxilla-maxilla suture is a straight line that extends from the lateral margin of the external nares to the lateral margin of the skull. The only variation of the suture is the angle at which it extends, ranging from extending mediolaterally, an angle of ~0° (Fig. 30A, E), to extending anterolaterally at an angle of ~45° (Fig. 28A, E).

The medial premaxilla-vomer suture is typically a straight line extending mediolaterally between the anterior palatal fenestra (Figs. 28F, 30B). Two variants are recognized: (1) the medial portion of the suture is rounded anteriorly (Fig. 30H); and (2) the medial portion of the suture is rounded posteriorly (Figs. 28B, 30B).

The ventral premaxilla-maxilla and lateral premaxilla-vomer suture show no distinguishable variation. The premaxilla-maxilla suture is straight, extending mediolaterally with little to no change in angle. The lateral premaxilla-vomer suture is a posterolateral suture that parallels the curve of the lateral skull margin.

Premaxillary apertures—The premaxillae contain the anterior portion of the premaxillary apertures. The posterior portion of these apertures is bordered by the anterior vomers. The premaxillary apertures are penetrations through the anteriormost portion of the snout, opening from anteromedial to the vomer tusk emplacement pits on the palate side into the anteromedial external nares on the skull roof side (Figs. 27-34). These apertures apparently accomodate the large symphyseal tusks of the mandibles when the mouth is closed.

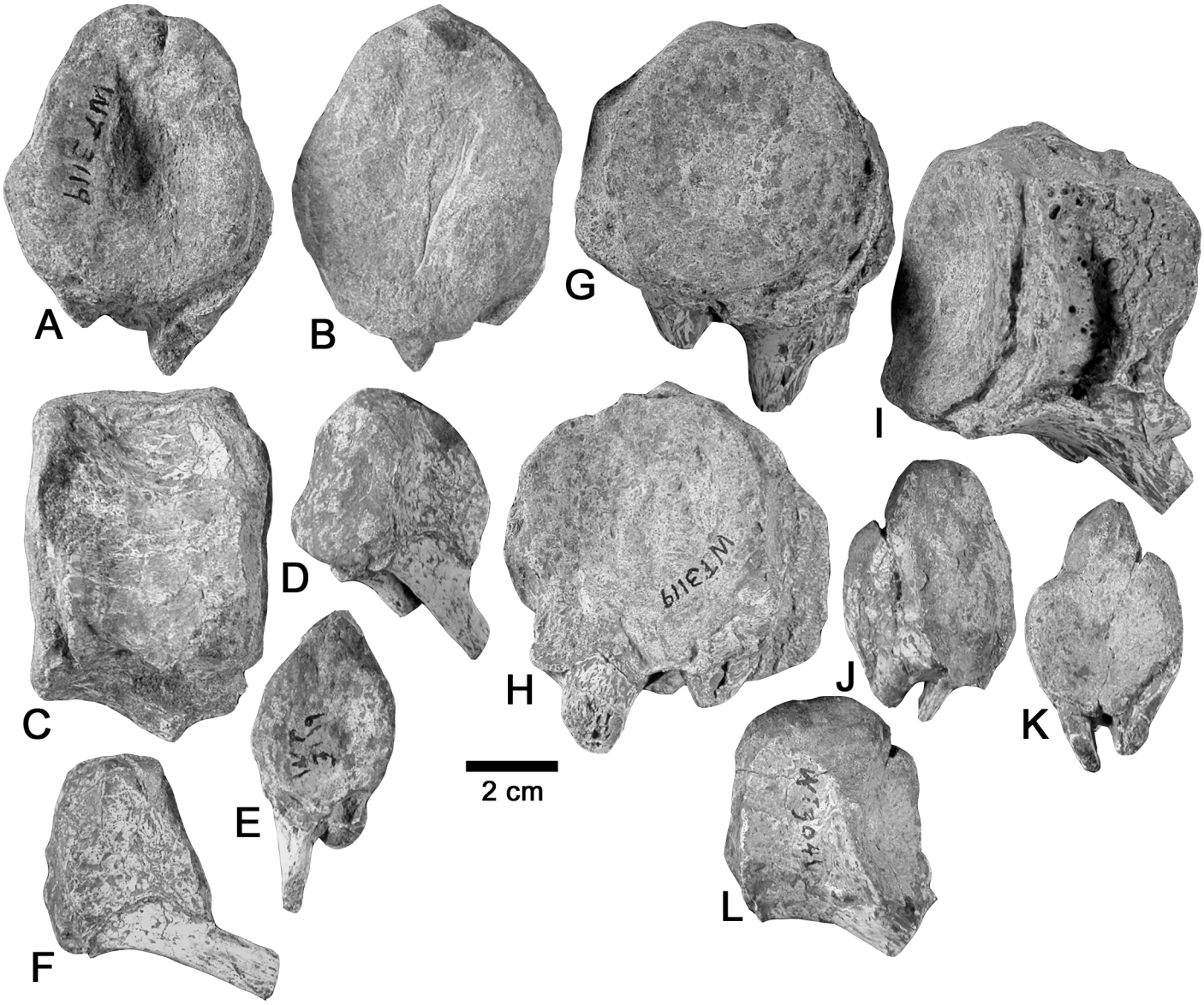

FIGURE 43. *Koskinonodon perfectum*, four caudal vertebrae from the Rotten Hill bonebed. **A-I**, WT 3119, three caudal vertebrae. **J-L**, WT 3041, caudal vertebra. Four caudal vertebrae in **A**, **G**, **J**, anterior, **B**, **E**, **H**, **K**, posterior and **C**, **D, F**, **I**, **L**, left lateral views.

Maxilla

The maxilla, like the premaxilla, is part of both the dorsal and ventral sides of the skull (Figs. 27-34). Dorsally, the maxilla is subrectangular with a long posterior process extending along the lateral margin of the skull. Ventrally, the maxilla consists of anterior, medial, and posterior processes. As described previously, the marginal dentition of the maxilla consists of approximately 55 tooth positions, which decrease in size posteriorly from ~2 mm to ~0.5 mm.

On the dorsal side of the skull the maxilla is located posterior to the lateral process of the premaxilla and is bordered medially by the nares and posteriorly by the prefrontal and lacrimal. The anterolateral portion of the maxilla forms the posterior half of the lateral and the lateral half of the posterior margin of the external nares. The posterior process of the maxilla extends along the lateral margin of the skull and borders the lateral margin of the lacrimal and the lateral margin of the anterior two-thirds of the jugal.

Ventrally, the anterior process of the maxilla extends anteromedially, parallel to the curvature of the lateral skull margin, and contacts the lateral process of the premaxilla. The medial process forms the anterolateral margin of the external nares. The extensive posterior process forms the lateral margin of the palatine and forms the lateral margin for the anterior half of the ectopterygoid.

The dorsal sutures of the maxilla show minimal variation. The anterior portion of the maxilla-lacrimal suture is typically rounded anteriorly (Figs. 28E, 30A, C, E, 32A), with a single variant, a flattened, straight-line suture (Fig. 30G). The lateral portion of the maxilla-lacrimal suture and maxilla-jugal sutures are straight-line sutures running parallel to the lateral skull margin and show no variation. Typically, the suture is straight and is angled at 45° or less (Figs. 28A, 30A, C, G, 32A). There are two variants: a suture that is rounded and extends anteriorly (Fig. 30E) and a rounded suture that extends posteriorly (Fig. 28E). The premaxilla-maxilla suture was discussed previously.

The ventral sutures of the maxilla show less variation than the dorsal sutures. The maxilla-vomer suture is a straight-line suture that parallels the lateral margin of the skull. On some specimens, the suture is slightly more interdigitated, so that it is slightly curved (Figs. 28F, H, 30B, F, H). However, this can vary within a single skull; compare the left and right sutures of Figure 28B. The maxilla-palatine suture is a straight-line suture in which the anteriormost end curves medially into the margin of the internal nares. This curvature into the narial margin is also variable, as the suture gently curves into the narial margin (Figs. 28C, F, 30B) or it curves posteriorly before entering the narial

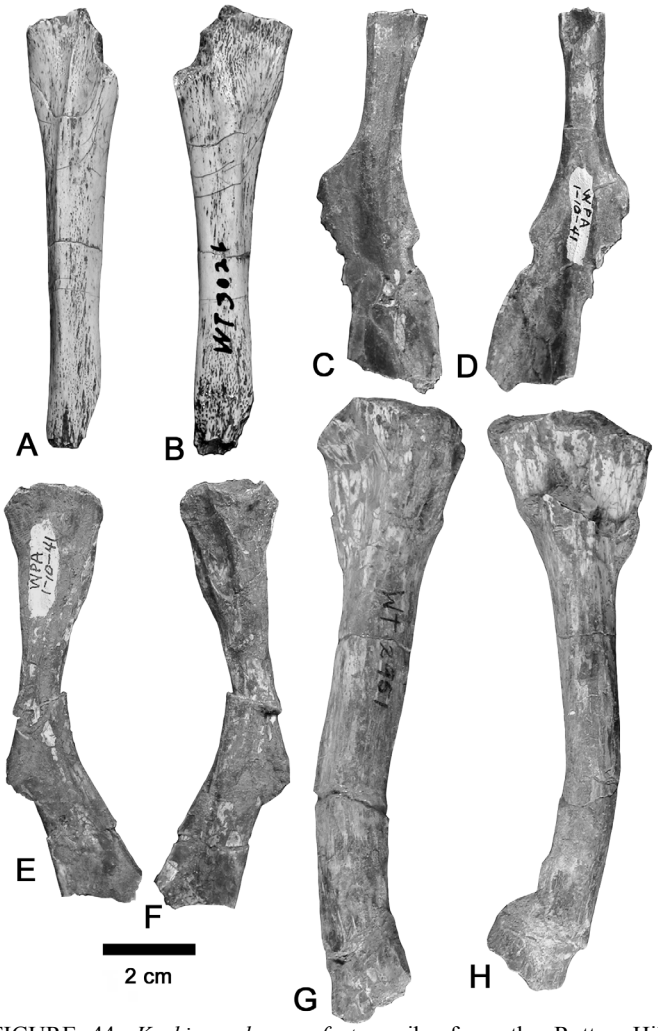

FIGURE 44. *Koskinonodon perfectum* ribs from the Rotten Hill bonebed. **A-B**, WT 3026, distal rib fragment in **A**, dorsal and **B**, ventral views. **C-F**, WT 1-10-41, right ribs in **C**, **E**, dorsal and **D**, **F**, ventral views. **G-H**, WT 2951, left rib in **G**, dorsal and **H**, ventral views.

margin (Figs. 28D, F, H, 30H, 32B), making the suture rounded. The maxilla-ectopterygoid suture shows no variation. The ventral maxilla-premaxilla suture was discussed previously.

Nasal

Overall, the nasal is polygonal. It has a narrower anterior process than posterior, and forms the posteromedial margin of the external nares. The nasal is posterior and medial to the external nares, medial to the medial process of the maxilla, anterior and medial to the prefrontal and anterior to the frontal.

The sutures of the nasal show moderate amounts of variation. Variants of the nasal-premaxilla and nasal-maxilla sutures were discussed previously. The nasal-prefrontal suture is typically a gently curved to straight-line suture (Figs. 28A, 30A, C, E, G, 32A); the only variant is a suture that is highly curved to irregular along its length (Fig. 28E). However, the typical morphology and variant can be found within the same skull; compare the left and right suture of Figure 28E. The nasal-frontal suture is typically angled at 45° (Figs. 28A, 30A) but has a flatter, nearly straight-line variant (Figs. 28E, 30G). However, both sutural patterns can be found in a single skull; compare the left and right sides of Figure 30A.

Lacrimal

The lacrimal is an elliptical to subrectangular bone; its posterior margin forms the anterolateral margin of the orbit. It is bordered anteriorly and laterally by the maxilla, medially by the prefrontal, and posterolaterally by the jugal. Its posterior margin forms the anterior margin of the orbit.

The only sutural variation is the lacrimal-prefrontal suture, which is typically an anteroposterior straight line or slightly curved suture (Figs. 28A, E, 30A, C, 32C, 34A, C, E), with the only variant a laterally directed curve to the posterior suture (Fig. 30E, G). The morphology of the lacrimal itself varies considerably, especially how much of the margin of the orbit it comprises. The lacrimal can either occupy a relatively small portion of the anterolateral margin of the orbit (Figs. 28E, 30E, 34A, E) or nearly the entire lateral margin of the orbit (Figs. 28A, 30C, G, 32A, C, 34C). This variation is considerable, though none of the skulls examined showed both variants within a single specimen.

The relationship of the lacrimal to the orbit has long been considered an important taxonomic character in metoposaurids. Thus, Romer (1947) noted that *Metoposaurus diagnosticus* differs from North American metoposaurids in excluding the lacrimal from the orbit. Colbert and Imbrie (1956) also noted this character in *M. diagnosticus* but failed to note that one of the population samples that they analyzed *("Buettneria" bakeri)* from North America also has this feature. Thus, Colbert and Imbrie (1956) placed all "*B." bakeri* in the same subspecies *(Eupelor fraasi jonesi)* as other metoposaurids that have a lacrimal that enters the orbit margin.

It is important to note that the "*Buettneria" bakeri* sample consists of a quarry (population) sample in which all specimens have a lacrimal excluded from the orbit (Case 1931, fig. 1, 1932, figs. 2-5, pl. 1, figs. 1, 4). However, Roy Chowdhury (1965) argued that because one of Colbert and Imbrie's subspecies contained individuals with lacrimals both included and excluded from the orbit margin, the position of the lacrimal is therefore a variable character within a metoposaur taxon. But, as Hunt (1993) stressed, and as the Rotten Hill *Koskinonodon* sample confirms, the position of the lacrimal relative to the orbit is not variable in any known metoposaurid population sample. Furthermore, no metoposaurid specimens show the variability within one individual that is evident in some capitosauroids (e. g., *Parotosuchus wadei:* Cosgriff, 1972; Kamphausen and Morales, 1981) in which cranial bones (frontal in this case) show incorporation and exclusion from the orbital margin on opposite sides of the same specimen. Dutuit (1976, p. 49) argued that the lacrimal position is of poor taxonomic utility because it is difficult to determine the lacrimal in all specimens. However, in most well-preserved metoposaurid skulls, the position and shape of the lacrimal is evident.

Prefrontal

The prefrontal is a polygonal bone that shows considerable variation in its morphology. It is bordered anteriorly by the maxilla and nasal, laterally by the lacrimal and orbit, medially by the frontal and nasal, and posteriorly by the postfrontal. The prefrontal forms the anteromedial margin of the orbit.

The sutural patterns of the prefrontal are highly variable. The prefrontal-maxilla, prefrontal-nasal and prefrontal-lacrimal sutures were discussed previously. The prefrontal-postfrontal suture has three variants: a nearly straight-line mediolateral suture (Figs., 30A, C, 34A, E), an angled suture that runs posteromedially from the lateral margin of the orbit (Figs. 30G, 32A, 34C) and a wedge-shaped suture that contacts an anterior postfrontal that is V-shaped (Fig. 28E). The prefrontal-frontal suture is an anteroposterior straight-line suture in all skulls examined. As in the lacrimal, the extent to which the prefrontal forms the orbit margin is variable. Typically, the prefrontal forms the medial half of the anterior margin and approximately half the medial margin of the orbit (Figs. 28A, E, 30G, 32A). Variants are the prefrontal forming the medial two-thirds of the anterior margin or forming up to two-thirds of the medial margin of the orbit (Figs. 30A, 34A).

Frontal

The frontal is a subrectangular to polygonal bone with considerable variation in its lateral and posterior sutural patterns. The frontal is bordered anteriorly by the nasal, laterally by the prefrontal and postfrontal and posteriorly by the parietal.

Overall, the morphology of the frontal varies throughout the skulls examined. One morphology is an anterior expansion of the frontal, with the greatest width being adjacent to the prefrontal-postfrontal suture. This gives the frontal a shape that approaches a diamond (Fig. 28E). A second morphology is an overall tapering of the frontal along its length, with the greatest width being adjacent to the nasal-prefrontal suture. This gives the frontal a polygonal shape (Figs. 28A, 30A, C, E). A third morphology is a rectangular frontal that only tapers along the posterior third of its length (Figs. 30G, 32A, 34C).

The frontal-nasal and frontal-prefrontal sutures were discussed

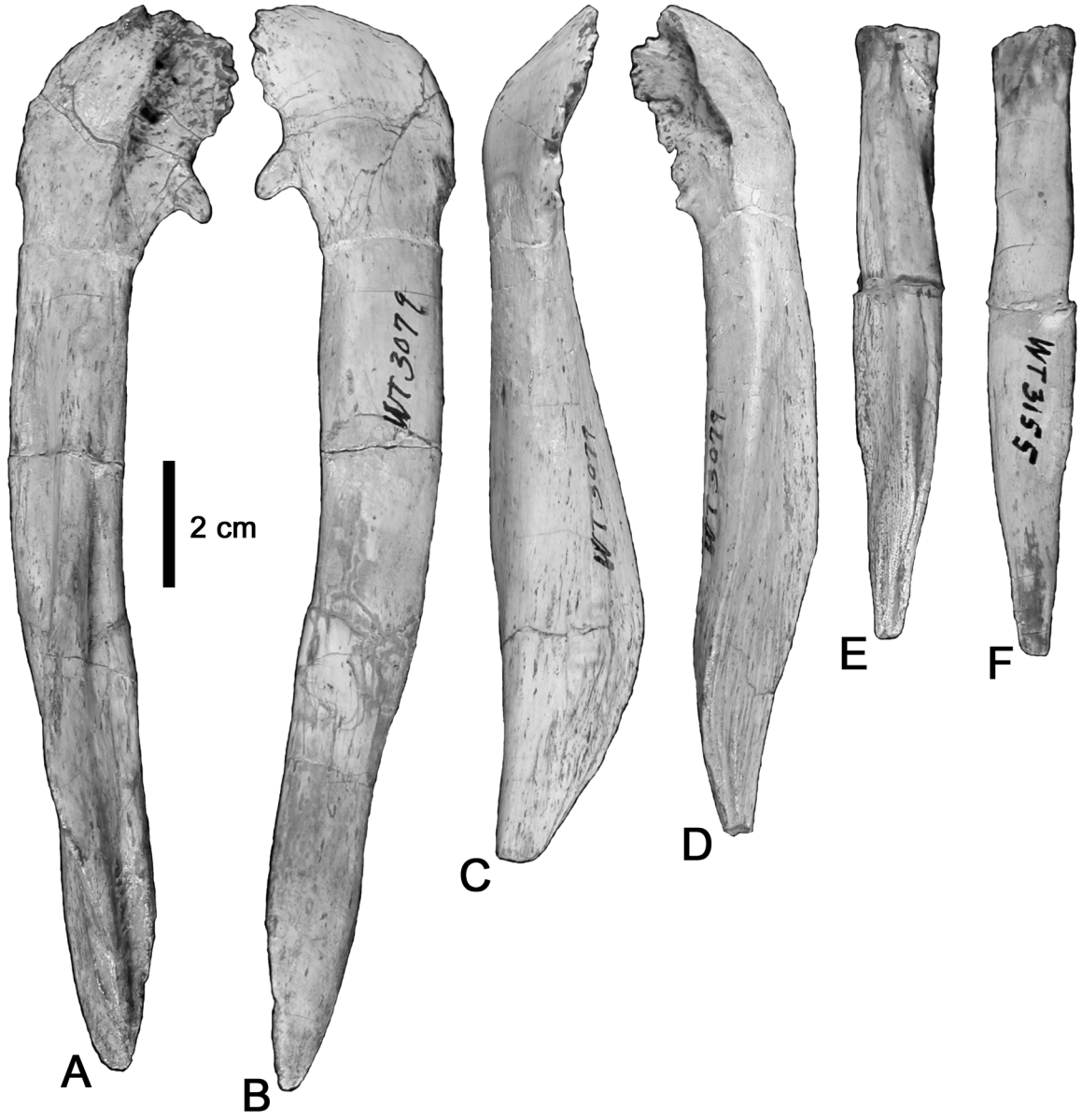

FIGURE 45. *Koskinonodon perfectum* cleithra from the Rotten Hill bonebed. **A-D**, WT 3079, two cleithra, **A**, left cleithrum in ventral view and **B**, dorsal view. **C**, small right cleithrum in lateral view and **D**, ventral view. **E-F**, WT 3155, proximal left cleithrum in **E**, ventral view and **F**, dorsal view.

previously. The frontal-postfrontal suture is typically a straight-line suture running posteromedially from the junction of the pre- and postfrontal. A single variant is a more erratic suture that exhibits some curvature (Figs. 28A, E, 30G). The frontal-parietal suture is highly variable. Typically, the suture is a v-shape, with a wedge-shaped posterior frontal sutured between medial and lateral prongs of the anterior parietal (Figs. 28A, E, 30E, G, 34A, C). Two variants are present in the Rotten Hill sample: the suture is a diagonal, with the anterior parietal located lateral to the posterior frontal (Figs. 28E, 30A), and the suture is rounded and extends posteriorly (Figs. 30C, 32A, C, 34E). However, the wedge-shaped and diagonal sutures are present together on a single skull; compare the left and right sides of Figures 28E and 30A.

Postfrontal

The postfrontal is a polygonal to subrectangular bone with minimal variation in its medial and lateral sutures. It is bordered anteriorly by the prefrontal and posterior orbit, medially by the frontal and parietal, laterally by the jugal and posteriorly by the supratemporal and parietal. The anterolateral postfrontal forms the posteromedial margin of the orbit.

The morphology of the postfrontal varies between subrectangular and polygonal due to the variation in the postfrontal-prefrontal suture, discussed previously, and the postfrontal-supratemporal suture, discussed here. The postfrontal-frontal suture was discussed previously. The postfrontal-postorbital suture is typically a straight-line suture extending posteriorly at a diagonal from the posterior orbit (Figs. 30A, C, E, 32A), but in a few specimens the suture is curved (bulges) along the middle of its length (Figs. 28A, E, 30G). The postfrontal suture with the parietal and supratemporal is typically wedge-shaped, with the postfrontal-parietal and postfrontal-supratemporal sutures being approximately equal in length (Figs. 28A, E, 30C, E, G, 32A, 34E). The only variant is seen in specimens that exhibit a triangular suture between these three elements in which the postfrontal-parietal suture is the primary suture, and the postfrontal and supratemporal only meet at their posteriormost and anteriormost points, respectively (Fig. 34A).

Postorbital

The postorbital is a subrectangular to polygonal bone with moderate variation in its medial and lateral sutures and considerable variation in its posterior sutures. The postorbital is bordered anteriorly by the posterior margin of the orbit, medially by the postfrontal, laterally by the jugal and posteriorly by the supratemporal and squamosal. The anterior edge of the postorbital forms the posterior margin of the orbit.

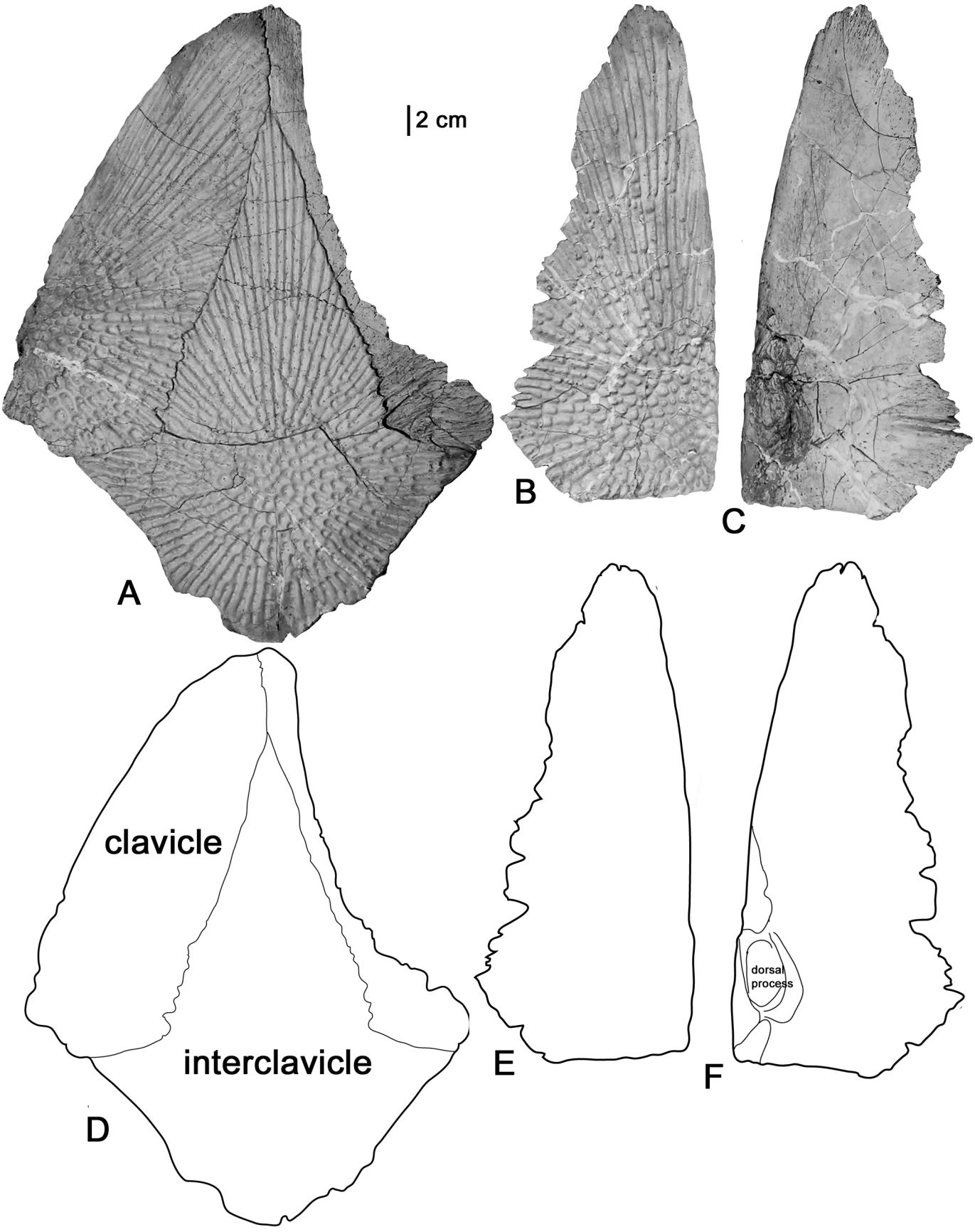

FIGURE 46. *Koskinonodon perfectum* pectoral elements from the Rotten Hill bonebed. **A-F**, PPHM X 2000.10.43, **A**, articulated interclavicle and right clavicle in ventral view, **B-C**, left clavicle in **B**, ventral and **C**, dorsal view. **D-F** are outline drawings of A-C.

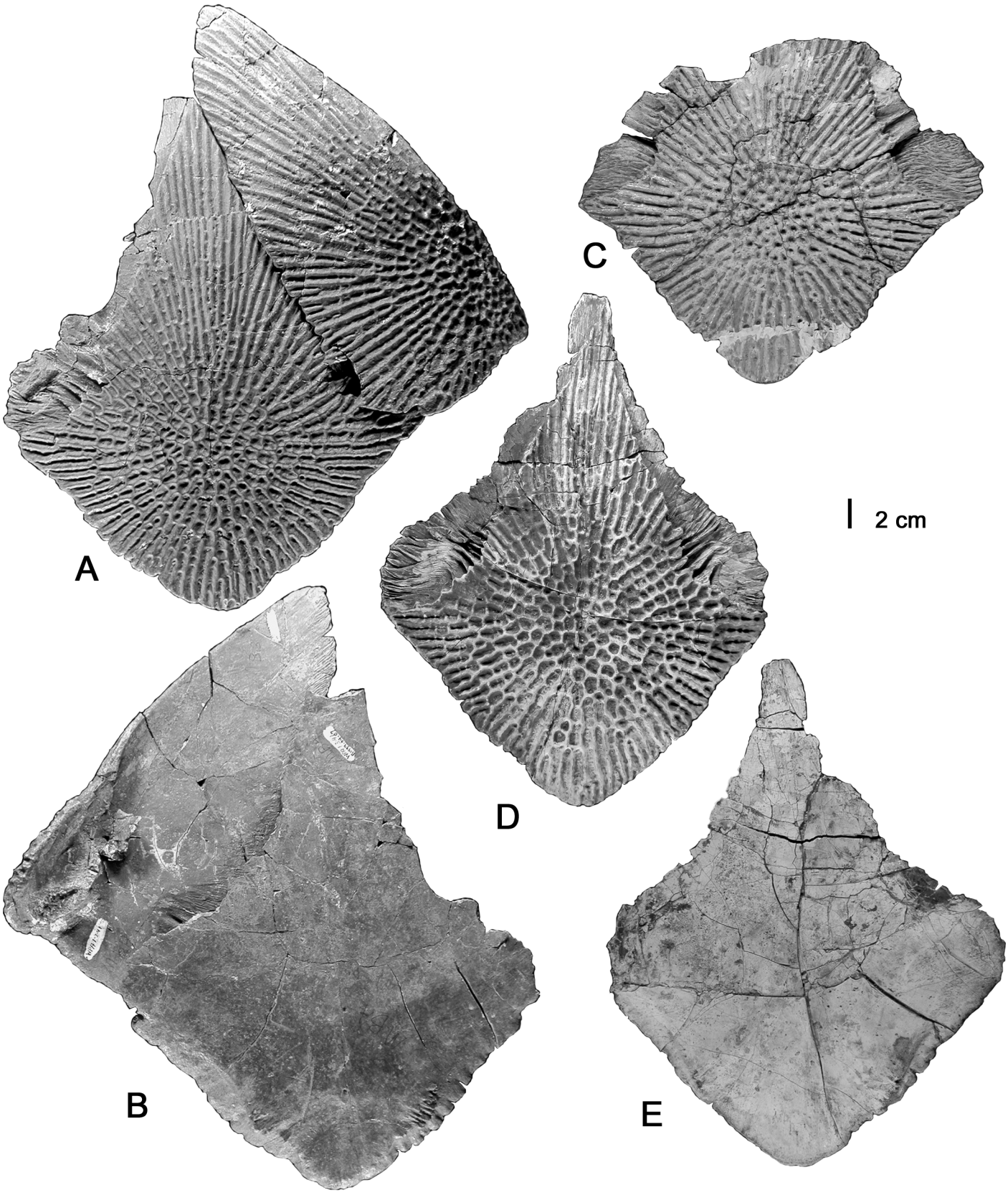

FIGURE 47. *Koskinonodon perfectum* pectoral elements from the Rotten Hill bonebed. **A-B**,WT 1.3.41/R 1999.34.07, articulated interclavicle and left clavicle in **A**, ventral and **B**, dorsal views. **C**, WT 3120, interclavicle in ventral view. **D-E**, WT 3063, interclavicle in **D**, ventral, and **E**, dorsal views.

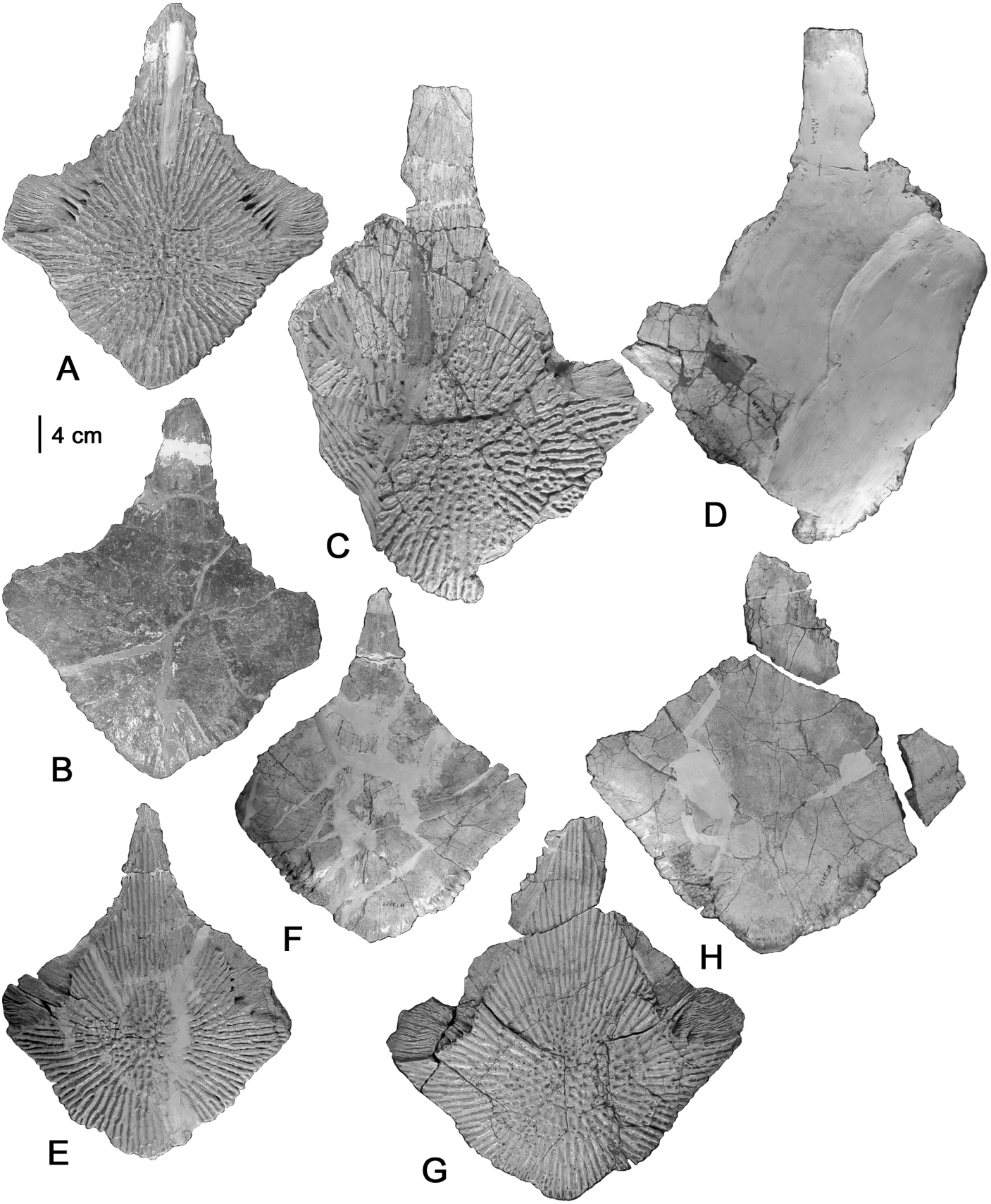

FIGURE 48. *Koskinonodon perfectum* interclavicles from the Rotten Hill bonebed. **A-B**, WT 2946, interclavicle in **A**, ventral and **B**, dorsal views. **C-D**, WT 2964, interclavicle in **C**, ventral and **D**, dorsal views. **E-H**, WT 3057, interclavicles in **E**, **G**, ventral and **F**, **H**, dorsal views.

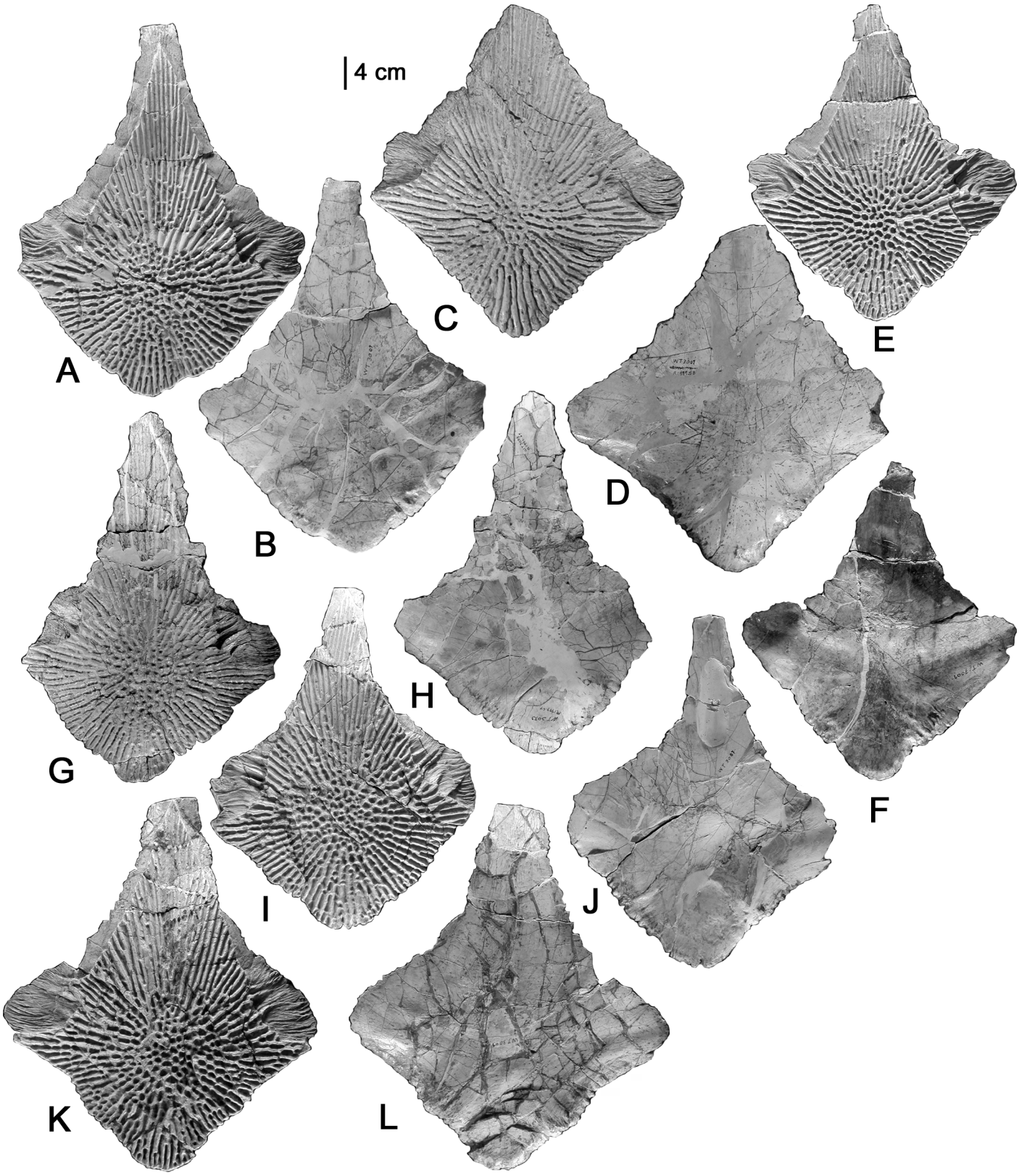

FIGURE 49. *Koskinonodon perfectum* interclavicles from the Rotten Hill bonebed, WT 3007, interclavicles in **A**, **C**, **E**, **G**, **I**, **K**, ventral and **B**, **D**, **F**, **H**, **J**, **L**, dorsal views.

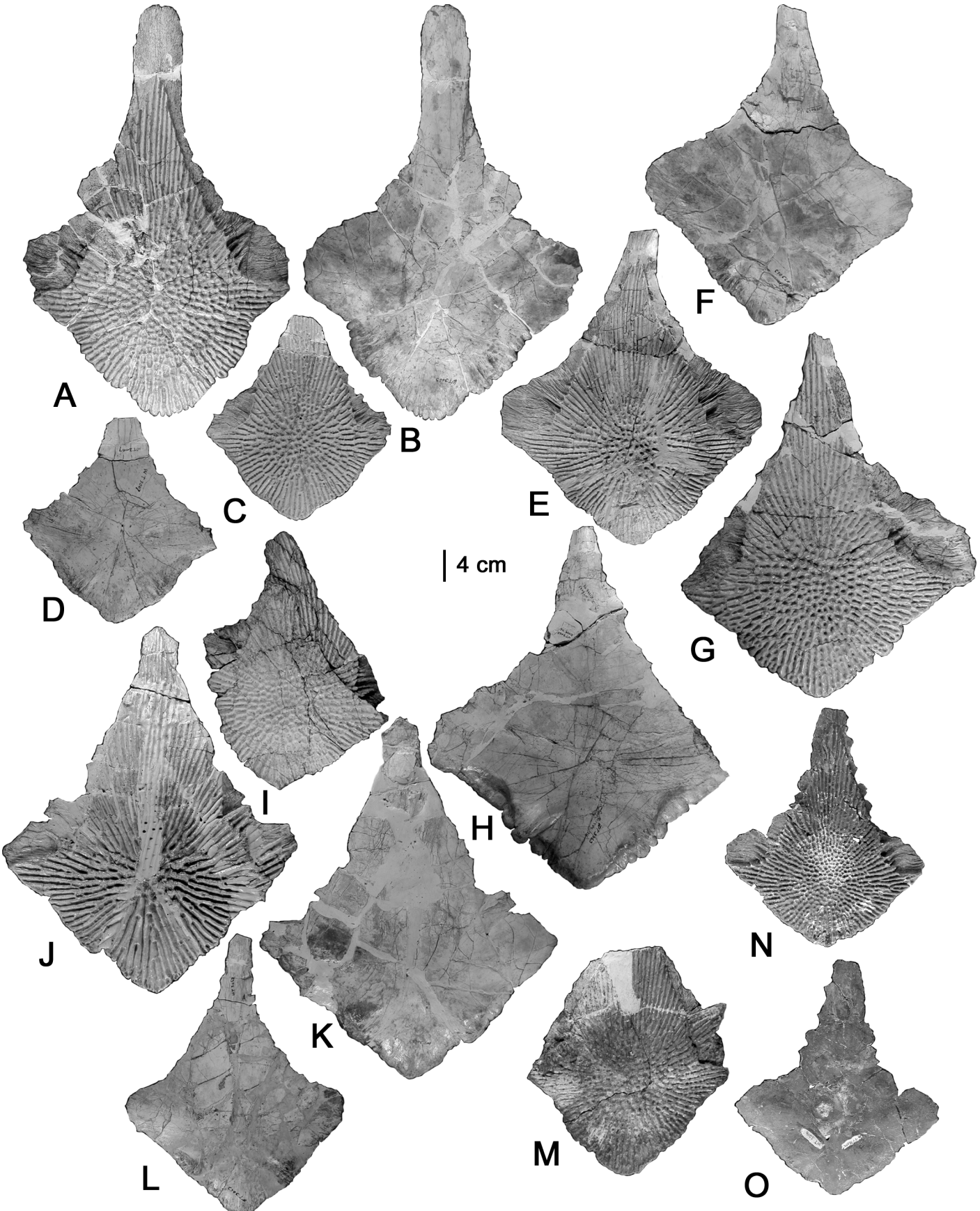

FIGURE 50. *Koskinonodon perfectum* interclavicles from the Rotten Hill bonebed. **A-D**, WT 3007, interclavicles in **A**, **C**, ventral and **B**, **D**, dorsal views. **E-L**, WT 3063, interclavicles in **E**, **G**, **I, J**, ventral and **F**, **H**, **K**, **L**, dorsal views. **M**, WT 3072, interclavicle in ventral view. **N-O**, WT 3240, interclavicle in **N**, ventral and **O**, dorsal views.

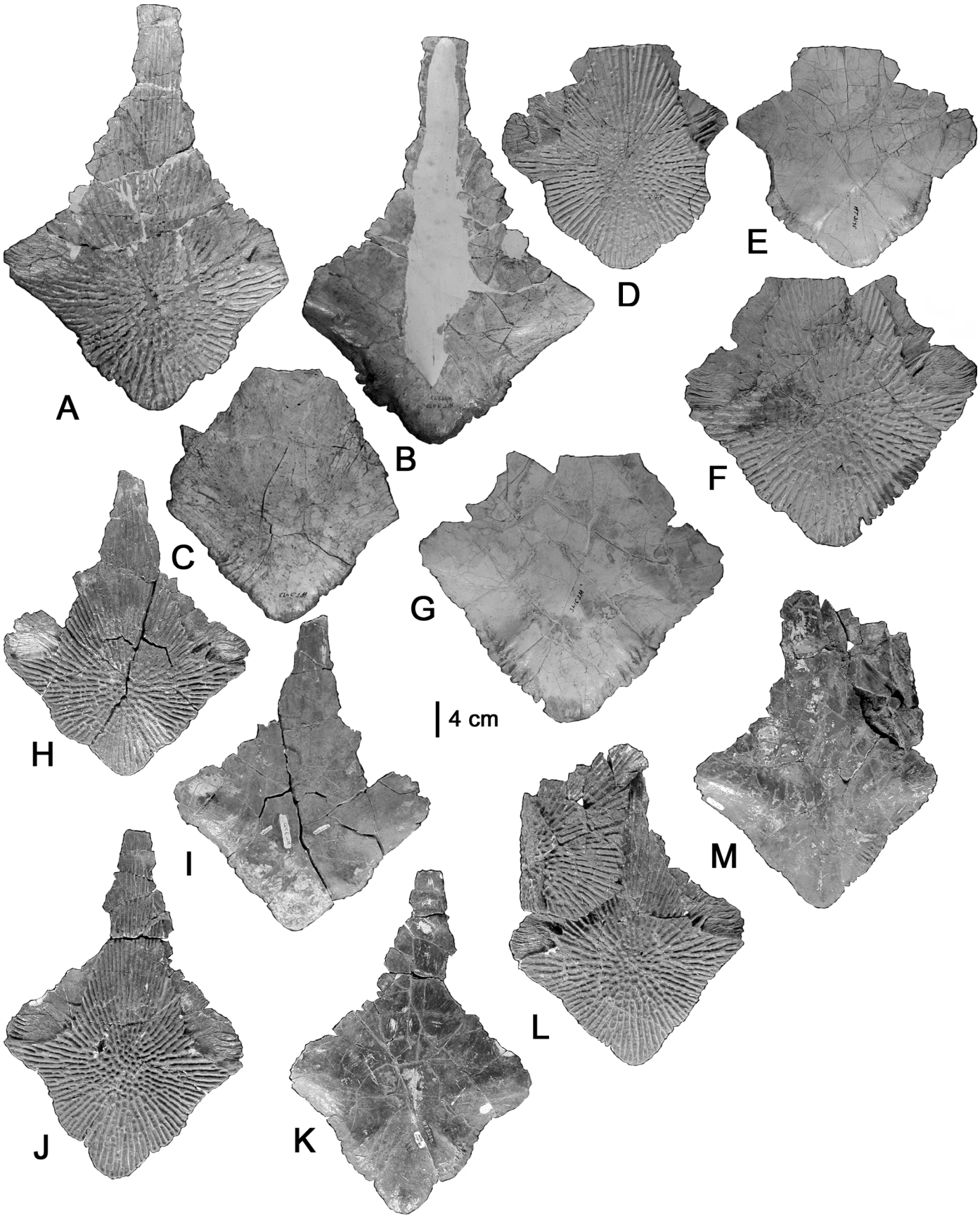

FIGURE 51. *Koskinonodon perfectum* interclavicles from the Rotten Hill bonebed. **A-B**, WT 3073, interclavicle in **A**, ventral and **B**, dorsal views. **C**, WT 3073, interclavicle in dorsal view. **D-G**, WT 3145, interclavicles in **D**, **F**, ventral and **E**, **G**, dorsal views. **H-I**, WT 3235, interclavicle in **H**, ventral and **I**, dorsal views. **J-K**, WT 3200, interclavicle in **J**, ventral and **K**, dorsal views. **L-M**, WT 3199, articulated interclavicle and right clavicle in **L**, ventral and **M**, dorsal views.

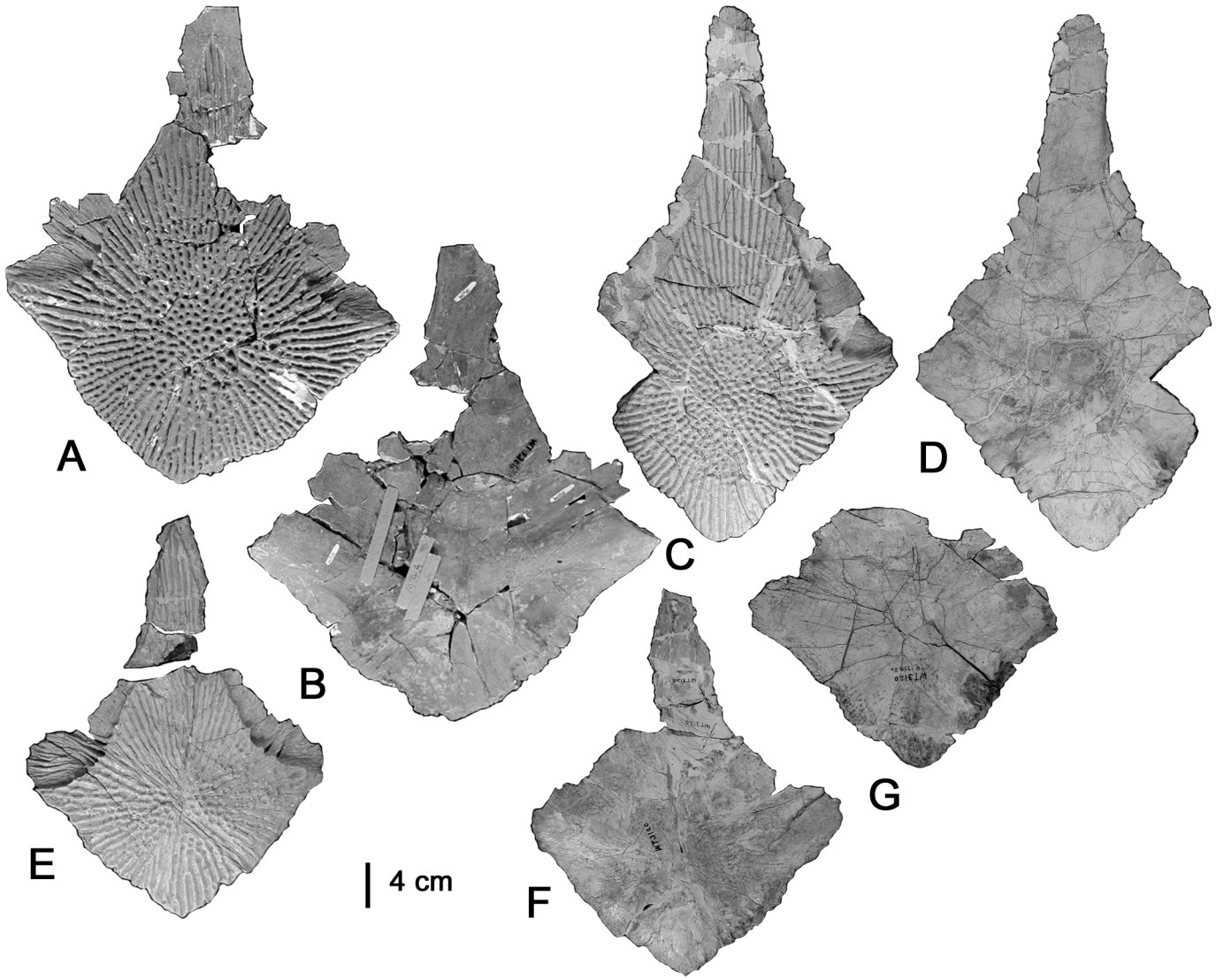

FIGURE 52. *Koskinonodon perfectum* interclavicles from the Rotten Hill bonebed. **A-B**, WT 3206, interclavicle in **A**, ventral and **B**, dorsal views. **C-D**, 1999.35.141, interclavicle in **C**, ventral and **D**, dorsal views. **E-G**, WT 3120, **E-F**, interclavicle in **E**, ventral and **F**, dorsal views, **G**, interclavicle in dorsal view.

The anterior postorbital forms the middle of the posterior margin of the orbit, and this feature shows no variation. The postorbital-postfrontal suture was discussed previously. The postorbital-jugal suture is typically a straight-line suture that runs posteriorly from the posterior margin of the orbit with some minor curvature of the suture in a few specimens (Figs. 28A, E, 30C, G, 32A, 34A, C). Straight-line and curved sutures can be present in the same skull; compare the left and right sutures of Figures 30A, E, G. The postorbital sutures with the supratemporal and squamosal are typically wedge shaped (Figs. 28E, 30A, C, G, 32A). The variant is a single skull with a posteriorly-directed, rounded suture (Fig. 30E).

Jugal

The jugal is a polygonal bone with a jugal-quadratojugal suture that is moderately variable and an anterior suture that is highly variable. The jugal is bordered anteriorly by the lacrimal, medially by the lateral orbit and postorbital, laterally by the maxilla and lateral margin of the skull and posteriorly by the squamosal and quadratojugal. The anteromedial jugal forms the posterolateral margin of the orbit.

The jugal-lacrimal, jugal-postorbital and jugal-maxilla sutures were discussed previously. However, the anterior jugal shows three distinct morphologies: (1) the jugal-lacrimal suture is at or posterior to the middle of the orbit (Figs. 28A, 30C, 34A); (2) the lateral edge of the jugal-lacrimal suture extends to the level of the anterior margin of the orbit (Figs. 28E, 30G); and (3) the lateral edge of the jugal-lacrimal suture extends anterior to the level of the anterior margin of the orbit (Fig. 30A). However, these last two morphologies can be present together in the same skull; compare the left and right sides of Figures 30A and E. The jugal's suture with the squamosal and quadratojugal is typically wedge shaped (Figs. 28E, 30A, C, G). The only variant is a single specimen with a rounded, posteriorly-directed suture (Fig. 30E).

Parietal

The parietal is a subrectangular bone with minimal sutural variation. It is bordered anteriorly by the frontal, laterally by the supratemporal, medially by the midline suture and posteriorly by the postparietal. The posteromedial portion of the parietal forms the lateral margin of the opening for the pineal foramen.

The parietal-frontal and parietal-postfrontal sutures were discussed previously. The parietal-supratemporal suture is an anteroposteriorly directed straight-line suture that displays no notable variation. The parietal-postparietal suture is a mediolaterally directed straight-line suture that, like the parietal-supratemporal suture, displays no significant variation.

Supratemporal

The supratemporal is a pentagonal bone that, like most of the other posterior skull elements, displays minimal variation. The supratemporal

is bordered anteriorly by the postorbital, medially by the parietal and postparietal, laterally by the squamosal and posteriorly by the tabular.

The supratemporal-parietal, supratemporal-postfrontal and supratemporal-postorbital sutures are discussed above. The supratemporal-squamosal suture is typically an anteroposteriorly directed straight-line suture (Figs. 30A, E, G, 32A, 34A). Two specimens have a lateral offset along the posterior half of this suture (Figs. 28A, E). The supratemporal-postparietal suture is a diagonally directed straight-line suture with no significant variation. The supratemporal-tabular suture is a mediolaterally directed straight-line suture. The only variant is a single specimen with an anteriorly-directed, rounded suture (Fig. 28A).

Squamosal

The squamosal is a pentagonal bone with minimal sutural variation. It is bordered anteriorly by the postorbital and jugal, medially by the supratemporal, laterally by the quadratojugal and posteriorly by the posterior margin of the skull. The posterior squamosal forms the anterior and lateral margins of the otic notch.

The squamosal-supratemporal and squamosal-jugal sutures were discussed previously. The squamosal-tabular suture is a diagonally directed, straight-line suture and shows no significant variation. The squamosal-quadratojugal suture is typically an anteroposteriorly directed suture with varying degrees of sigmoidal curvature (Figs. 28A, E, 30A, E, 34A, E); the only variant is a single specimen that has a straight-line suture (Fig. 30C).

Quadratojugal

The quadratojugal is a polygonal element that shows moderate sutural variation. It is bordered anteriorly by the jugal, medially by the squamosal and laterally and posteriorly by the lateral and posterior margin of the skull. The quadratojugal-jugal and quadratojugal-squamosal sutures were discussed previously.

Postparietal

The postparietal is a square to subrectangular bone with moderate sutural variation. It is bordered anteriorly by the parietal and supratemporal, medially by the midline suture, laterally by the tabular and posteriorly by the posterior margin of the skull.

The postparietal-parietal and postparietal-supratemporal sutures were discussed previously. The postparietal-tabular suture is typically an anteroposteriorly directed, straight-line suture. The only variant is a slight curvature of the posterior half of this suture; this curvature can be either directed medially (Fig. 30A) or laterally (Fig. 30E).

Tabular

The tabular is a subrectangular bone with moderate sutural variation. The tabular is bordered anteriorly by the supratemporal, medially by the postparietal, laterally by the squamosal and posteriorly by the posterior margin of the skull. The posterolateral portion of the tabular forms the medial margin of the otic notch. The tabular-supratemporal, tabular-squamosal and tabular-postparietal sutures were all discussed previously.

Vomer

The vomer is a polygonal bone with a single posterior process. It is bordered anteriorly by the premaxilla (where it encloses the posterior half of the premaxillary aperture), medially by the anterior process

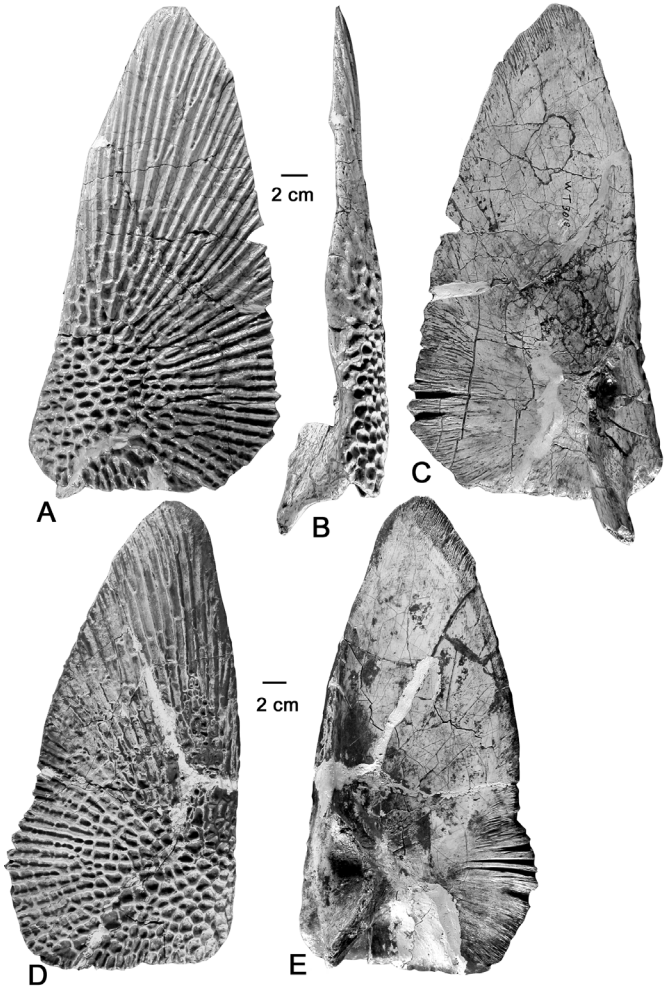

FIGURE 53. *Koskinonodon perfectum* clavicles from the Rotten Hill bonebed. **A-C**, WT 3018, right clavicle in **A**, ventral, **B**, lateral and **C**, dorsal views, **D-E**, 35197, left clavicle in **D**, ventral and **E**, dorsal views.

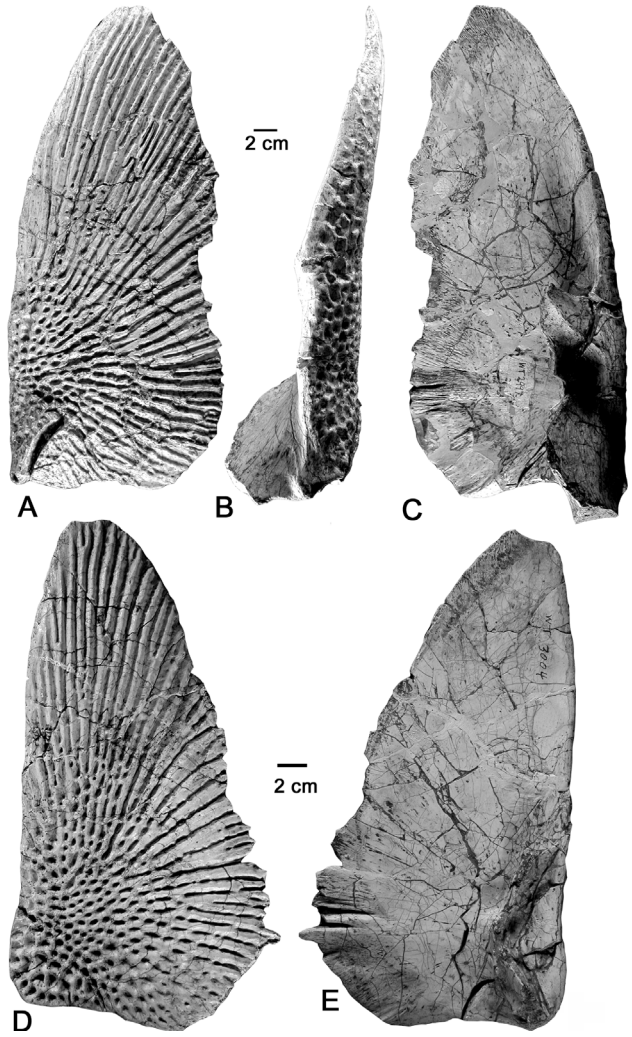

FIGURE 54. *Koskinonodon perfectum* clavicles from the Rotten Hill bonebed. **A-C**, WT 2997, right clavicle in **A**, ventral, **B**, lateral and **C**, dorsal views, **D-E**, WT 3004, right clavicle in **D**, ventral and **E**, dorsal views.

of the parasphenoid and the midline suture, laterally by the maxilla, palatine and internal nares and posteriorly by the palatal vacuity. The vomer forms the majority of the medial margin of the internal nares and the anteromedial margin of the palatal vacuity.

The posterior process of the vomer is wedge shaped and fits between the anteriormost portion of the anterior process of the parasphenoid and the anteromedial margin of the palatal vacuity. The vomerine tusk pair is located along the lateral edge of the vomer between the anterior palatal fenestra and the choana. As the name implies, these teeth are usually paired. However, in at least one specimen the anterior tusk was broken off and was not replaced but had an overgrowth of bone covering the socket.

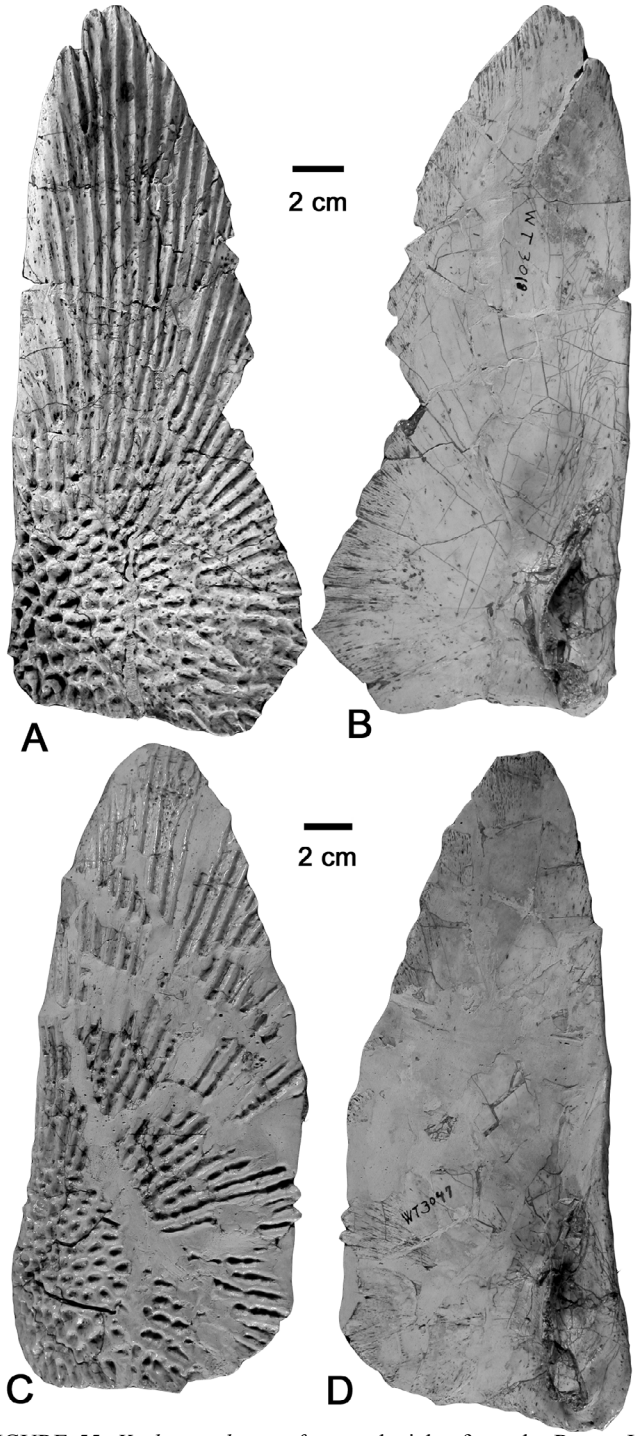

FIGURE 55. *Koskinonodon perfectum* clavicles from the Rotten Hill bonebed. **A-B**, WT 3018, right clavicle in **A**, ventral and **B**, dorsal views, **C-D**, WT 3047, right clavicle in **C**, ventral and **D**, dorsal views.

The vomer-premaxilla and vomer-maxilla sutures were discussed previously. The vomer-parasphenoid suture shows two distinct morphologies: (1) the suture is an anteroposteriorly directed straight-line suture due to a mediolaterally thin anterior process of the parasphenoid (Figs. 28B, C, F, 30B, 32B, 34D, F); and (2) the suture is a diagonally directed straight-line suture due to a wider triangular anterior process of the parasphenoid, which is apparently a hallmark of the more brachycephalic skulls (Figs. 28H, 30D, H). The vomer-palatine suture is typically a diagonally directed straight-line suture (Figs. 28B, C, F, 30B, D, F, H, 32B). However, in two specimens one of the vomer-palatine sutures is anteriorposteriorly directed (Figs. 28B, F).

Palatine

The palatine is a Y-shaped bone with an anterior and a medial process. It is bordered anteriorly and laterally by the maxilla, medially by the lateral margin of the choana and the vomer and posteriorly by the ectopterygoid and the palatal vacuity. The medial palatine forms the posterior half of the lateral margin of the choana, and the posterolateral palatine forms the anterolateral margin of the palatal vacuity.

The anterior process of the palatine extends half the length of the choana along its lateral margin and contains a palatal tusk pair. These tusks, like those of the vomer, are typically paired due to ongoing replacement, but in two specimens anomalies are present: (1) only a single tusk is present on one side of a skull (Fig. 30B); and (2) the posterior tusk of the pair is located at the posterior end of the narial

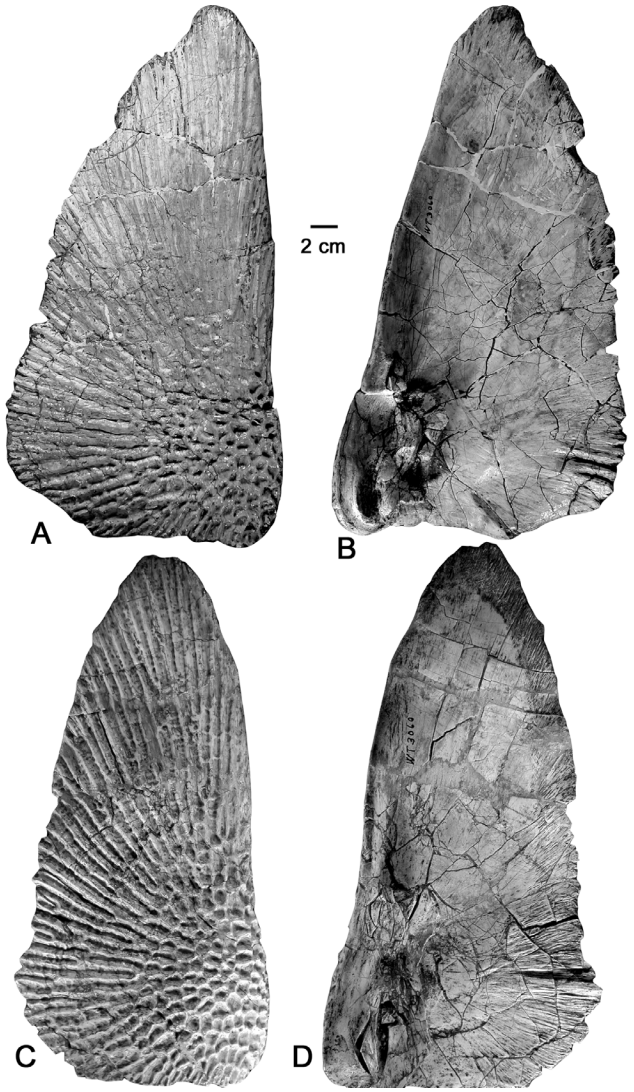

FIGURE 56. *Koskinonodon perfectum* clavicles from the Rotten Hill bonebed. **A-B**, WT 3060, left clavicle in **A**, ventral and **B**, dorsal views, **C-D**, WT 3060, left clavicle in **C**, ventral and **D**, dorsal views.

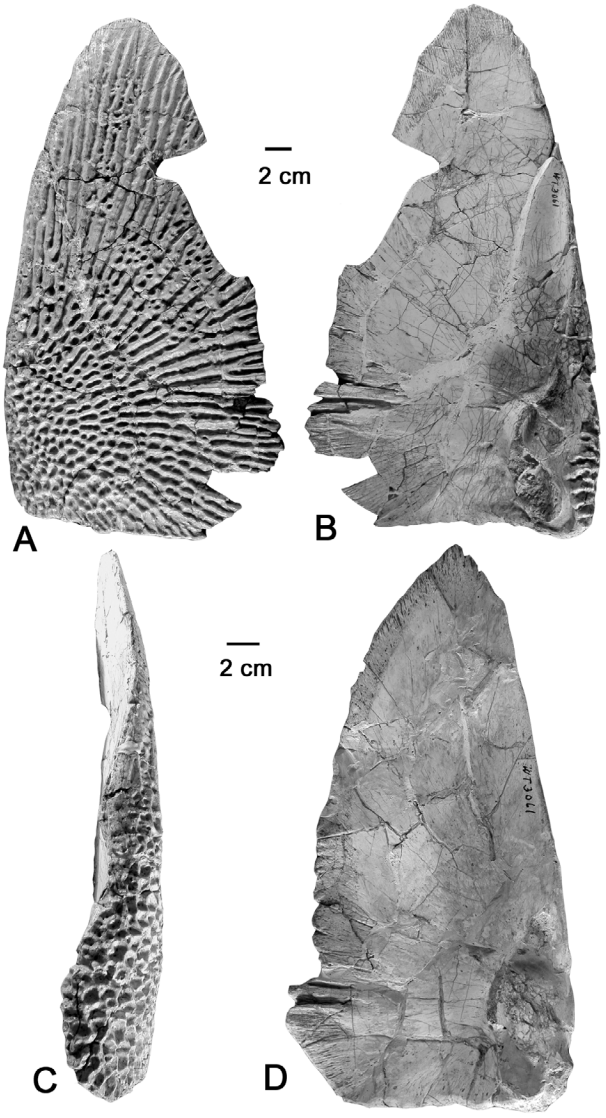

FIGURE 57. *Koskinonodon perfectum* clavicles from the Rotten Hill bonebed. **A-D**, WT 3061. **A-C**, right clavicle in **A**, ventral, **B**, dorsal and **C**, lateral view. **D**, right clavicle in dorsal view.

opening (Fig. 30F). The medial process of the palatine extends between the posterior choana and the anterior palatal vacuity to contact the lateral vomer.

The palatine-maxilla and palatine-vomer sutures were discussed previously. The palatine-ectopterygoid suture is a mediolaterally directed straight-line suture that is located at the same level as the posterior margin of the orbit. Some of these sutures are slightly inclined at a shallow angle.

Ectopterygoid

The ectopterygoid is a rectangular to triangular palatal element with moderate sutural variation. It is bordered anteriorly by the palatine, medially by the pterygoid and palatal vacuity, laterally by the maxilla and posteriorly by the subtemporal window.

Pterygoid

The pterygoid connects the upper jaw to the braincase and quadrate as a long strut of bone sutured anteriorly to the ectopterygoid, posterolaterally to the quadrate and posteromedially to the parasphenoid and the exoccipital. The ventral aspect of the pterygoid is slightly concave, and its antero-medial portion forms part of the postero-lateral margin of the palatal vacuity. In occipital view, the pterygoid forms most of the anterior otic vestibule.

Parasphenoid

The parasphenoid divides the palatal vacuities medially as a long, relatively thin plate of bone, its cultriform process. The anterior end of the cultriform process forms a long, triangular indentation between the vomers, to which it is sutured well anterior to the orbits. This process is particularly broad in the brachycephalic skull (Figs. 29H, 30H). The posterior portion of the parasphenoid is a rectangular to trapezoidal basal plate that floors the posterior portion of the braincase and separates the exoccipitals, forming the floor of the foramen magnum. It is sutured laterally to the pterygoids and posteriorly to the exoccipitals. The ventral aspect of the basal plate is slightly concave.

Quadrate

The quadrate is at the postero-lateral edge of the skull in ventral view and is dominated by the trochlear jaw joint. It is sutured to the pterygoid medially, the squamosal dorsally and the quadratojugal laterally. The jaw joint is a short and wide ginglymus at the postero-lateral corner of the ventral skull. Its relative width varies considerably (e.g., compare Figs. 28F and 30D).

Exoccipital

The exocciptals project posteriorly from the medial edge of the skull and are sutured to the parasphenoid, which separates them medially, and pterygoid. Their posterior projections comprise the two columnar occipital condyles.

Lower Jaw

Two, well-preserved lower jaw arcades are illustrated here (Figs. 35-36). The left side is represented by 2000.10.110 (Fig. 35) and the right by WT 3152 (Fig. 36). Seen laterally, the lower jaw of *Koskinonodo*n is thickest and highest at the coronoid and hamate processes just anterior to the jaw joint and thinner and shallower anteriorly. The large retroarticular process is composed of the angular, prearticular, articular and surangular. The anterior part of the jaw is composed primarily of the dentary, dorsally, and the postsplenial and splenial, ventrally. The external surface bears an extensive reticulate ornamentation of "boxes," ridges and grooves similar to the ornamentation of the dorsal surface of the skull. The boxes are centered near the ventral margin of the angular and radiate outward so that the lateral surfaces of the anterior part of the angular and the dentary bear elongate, narrow ridges separated by wide grooves.

Lower Jaw Dentition

In both illustrated jaws (and other preserved specimens) there is a single row of teeth. The mandibular teeth are generally larger than the corresponding teeth of the skull. In each lower jaw, the dentition comprises a large symphyseal tusk, 10-15 mm in diameter, approximately 48 marginal teeth that diminish in diameter from ~8 mm anteriorly to ~4 mm posteriorly, and a short row of small teeth medial to the posterior marginal toothrow and anterior to the adductor fossa. Most of the teeth are, based on the preserved tooth sockets, subcircular in cross-section.

Postcranial Osteology

In general, the postcranial osteology of metoposaurids has been well described and illustrated by Case (1922, 1932), Sawin (1945), Colbert and Imbrie (1956), Dutuit (1976), Hunt (1993), Long and Murry (1995) and Sulej (2007). Here, we describe and illustrate (Figs. 37-72) the metoposaur postcrania from the Rotten Hill bonebed, focusing on morphological variation among these bones.

Vertebral Column

Atlas—The atlas intercentrum (Figs. 37-40) is transversely oval in outline and has a fused neural arch. The anterior articular surface consists of two nearly circular, concave surfaces for articulation with the occipital condyles. The posterior surface is a single concave surface that is transversely elongate and ovoid for articulation with the axis. In cross section, the vertebral intercentrum is not rectangular but is slightly flexed so that it is more concave posteriorly. The periphery of the centrum is slightly concave, so that it is "waisted." There is a small cleft in the ventral midline of the centrum along its anterior edge (Fig. 37A, D, G, J). The posterior ventral edge is flat to slightly arcuate.

The neural canal is very narrow; it is a dorso-ventrally elongate ovoid channel with a pointed dorsal end. The neural arch is relatively short, with two thick neural spines that terminate in a broad, blunt and

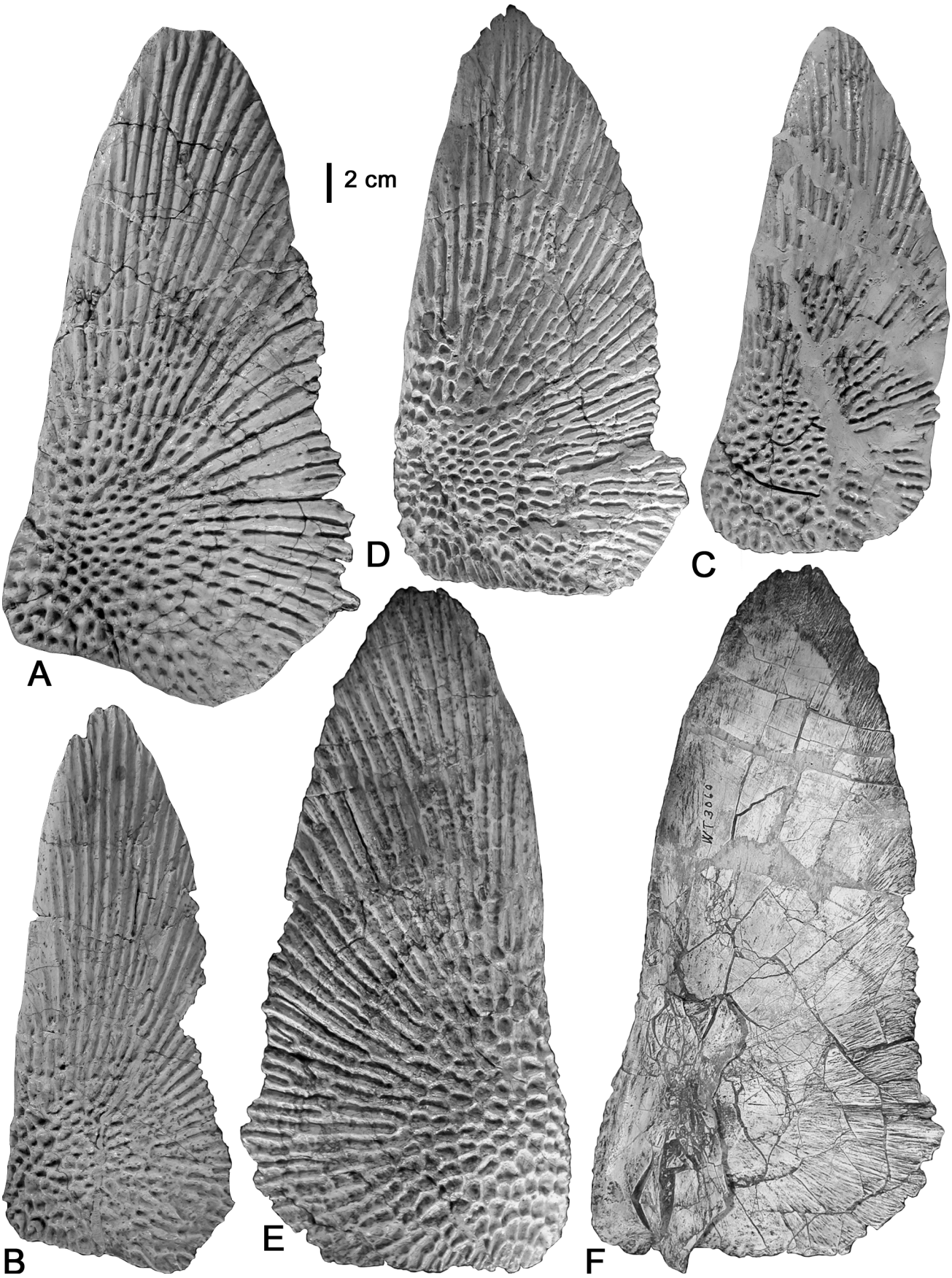

FIGURE 58. *Koskinonodon perfectum* clavicles from the Rotten Hill bonebed. **A**, WT 3004, right clavicle in ventral view. **B**, WT 3018, right clavicle in ventral view. **C**, WT 3047, right clavicle in ventral view. **D-F**, WT 3060, clavicles. **D**, right clavicle in ventral view, **E-F**, left clavicle in **E**, ventral and **F**, dorsal views.

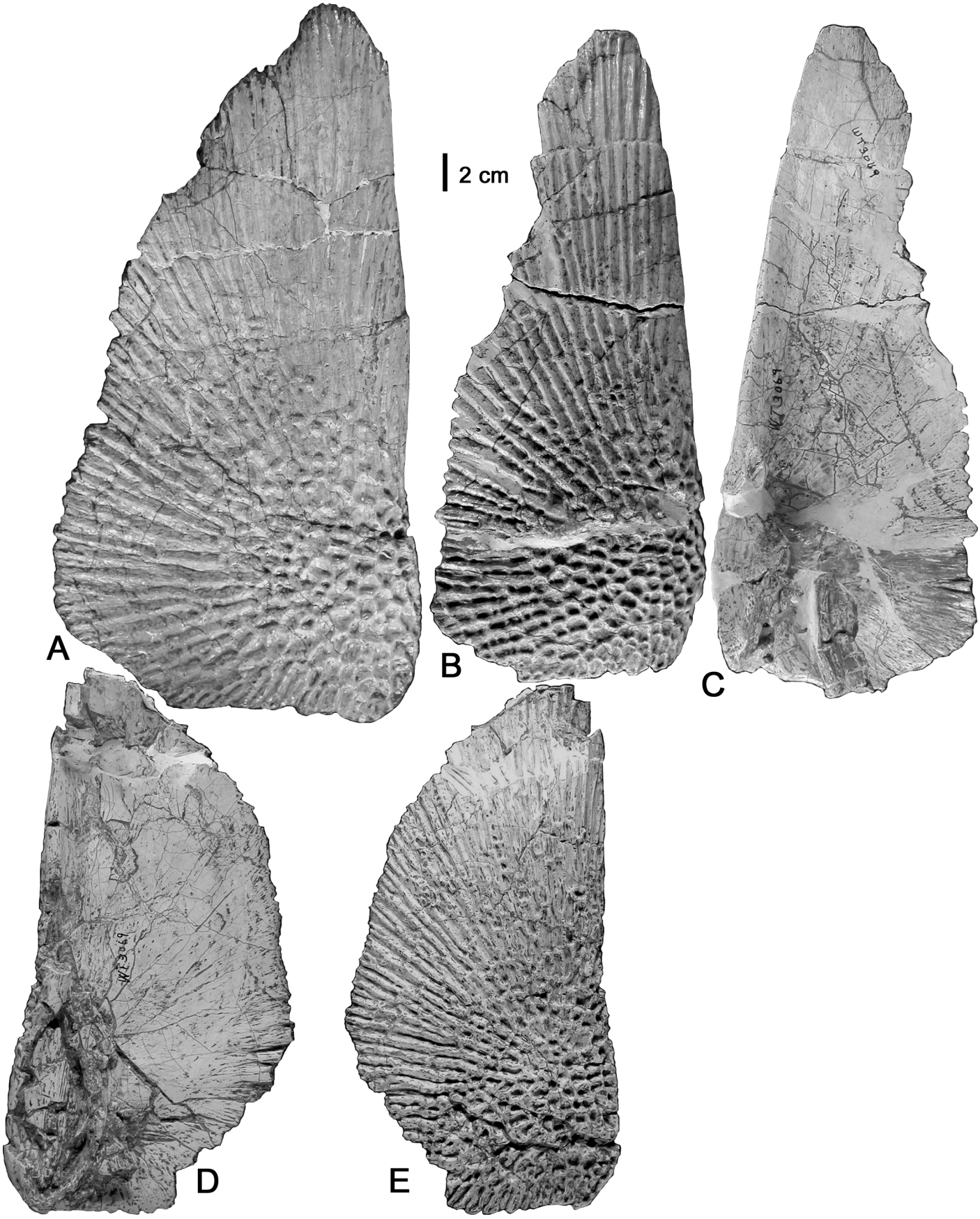

FIGURE 59. *Koskinonodon perfectum* clavicles from the Rotten Hill bonebed. **A**, WT 3060, left clavicle in ventral view. **B-E**, WT 3069, two left clavicles, **B-C**, left clavicle in **B**, ventral and **C**, dorsal views, **D-E**, left clavicle in **D**, dorsal and **E**, ventral views.

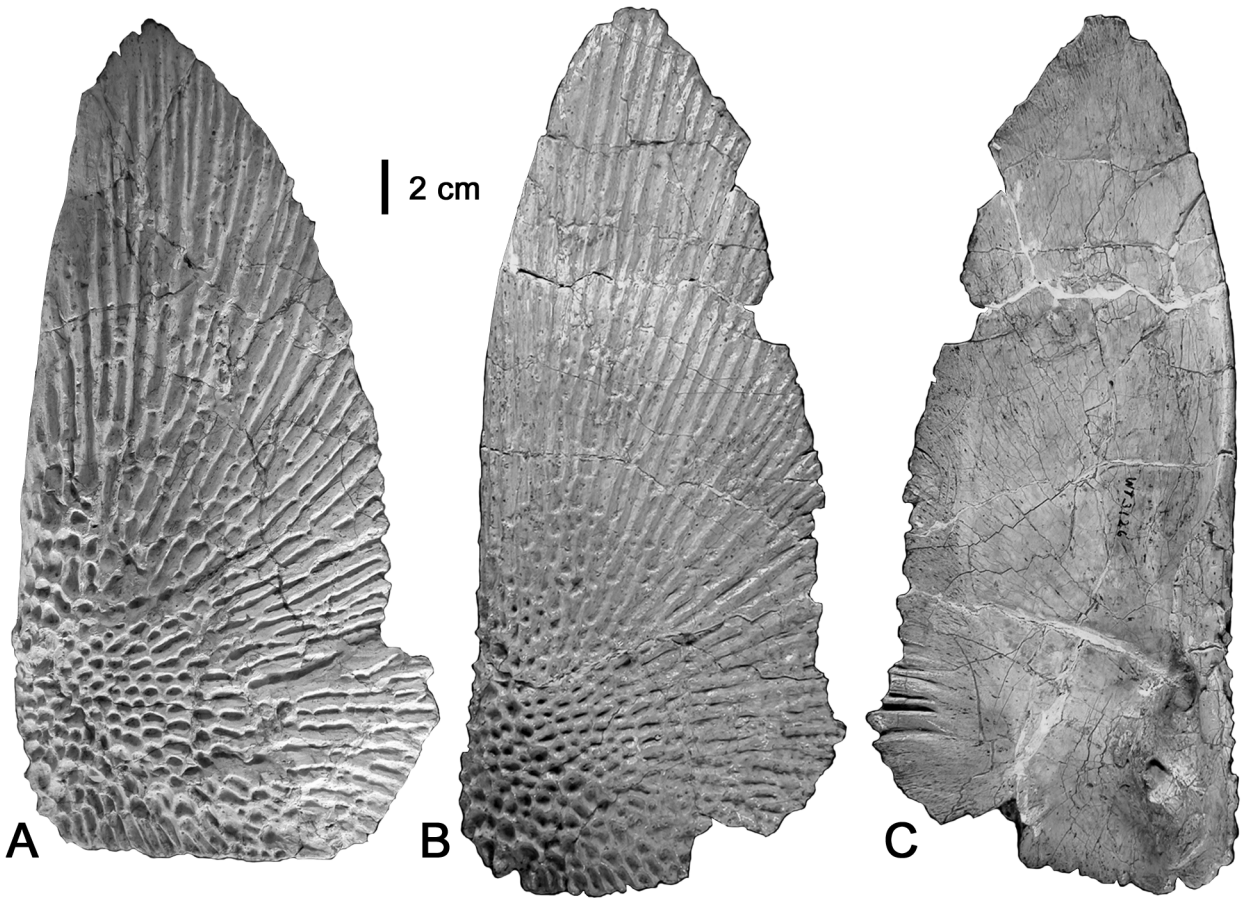

FIGURE 60. *Koskinonodon perfectum* clavicles from the Rotten Hill bonebed. **A**, WT 3061, right clavicle in ventral view. **B-C**, WT 3126, right clavicle in **B**, ventral and **C**, dorsal views.

slightly bilobed dorsal end.

Figures 37-40 capture a range of variation in atlas morphology, much of it due to taphonomic distortion or preservational completeness. Variation that reflects actual morphology is in overall intercentrum shape and the shape of the articular surfaces, which vary from more nearly circular to more ovoid. This variation appears to be largely ontogenetic, with the articular surfaces of small atlas intercentra more transversely ovoid (Fig. 37) and those of larger intercentra more nearly circular (Figs. 38-39). Some variation in the shape of the neural canal and the ventral notch is also evident but does not seem to be systematic.

The Rotten Hill atlas intercentra are very similar to the atlas of *Koskinonodon* illustrated by Sawin (1945, fig. 6a-b) and to those of *Metoposaurus diagnosticus* illustrated by Sulej (2007, fig. 22). Differences from the atlas intercentra of *Metoposaurus* are the wider and relatively taller neural canal, and the prominent cleft-like separation of the anterior articular surfaces in *M. diagnosticus*. We regard these as postcranial characters that distinguish *Koskinonodon* from *Metoposaurus* (see above). Also, the atlas intercentra of *Dutuitosaurus ouazzoui* (Dutuit, 1976, fig. 32a, c, d, pl.19, fig. a) have much deeper anterior articular facets than those of *Koskinonodon* (and *Metoposaurus*), another diagnostic feature.

Cervical vertebrae—A few intercentra are cervical vertebrae posterior to the axis (Figs. 40F-H, 41). These intercentra are weakly procoelous and have a single diapophysis and parapophysis that are vertically stacked, with the more ventral parapophysis more robust. The intercentra are round to nearly square in cross section and have slightly concave (waisted) lateral and ventral aspects.

Dorsal vertebrae—The few dorsal intercentra preserved (Fig. 42) do not have fused neural arches. They are nearly round to hexagonal in cross section. In articular view, the dorsal surface is nearly flat, and the ventral surface rounded and convex. The anterior articular surface is shallowly concave, and the posterior articular surface is slightly convex. The centra thus are weakly procoelous. The lateral and ventral surfaces of the intercentrum are shallowly concave ("waisted"). There is a single diapophysis laterally and near the dorsal edge of the intercentrum. The shape of the diapophysis varies from a short, blunt, antero-posteriorly directed rectangular flange to a more complex surface that is actually two facets that face anteriorly and posteriorly. The more anterior intercentra have the simple diapophysis, whereas the more complex diapophyses are on the more posterior intercentra.

Caudal vertebrae—Several caudal vertebrae (Fig. 43) can be identified in the Rotten Hill collection by their haemal arches fused to the intercentra. Most of these intercentra are dorso-ventrally taller than wide. They are weakly amphicoelous and lack fused neural arches. Laterally, their sides are rather deeply concave and lack diapophyses. The haemal arches are rod-like and sharply inclined posteriorly (about 45º). Differences among these vertebrae appear to be either preservational (some are poorly preserved) or positional. As already noted by Hunt (1993, p. 81), *Koskinonodon* differs from *Dutuitosaurus* in lacking the deep notochordal notches in the caudal vertebrae that are part of the diagnosis of *Dutuitosaurus* (compare Fig. 43A to Dutuit, 1976, figs. 38a-b, 39b-c, pl. 30, figs. b, e).

Ribs

Complete ribs are uncommon in the Rotten Hill collection, and we illustrate some of the few that are preserved here (Fig. 44). Sulej (2007) identified nine kinds of ribs in *Metoposaurus diagnosticus*, and we are able to assign the Rotten Hill ribs to at least three of his categories, though we suspect they are oversplit. One rib (Fig. 44A-B) has a compressed angular end that is trihedral in cross section. A dorsal ridge runs diagonally across the proximal part of the rib. This rib can be assigned to type H of Sulej (2007).

A second rib type (Fig. 44C-D) has a narrow, rod-like proximal end and widens to a concavo-convex, plate-like distal end. A small anterior process and a larger posterior uncinate process are present, identifying this rib as an anterior dorsal (also see Dutuit, 1976, fig. 43).

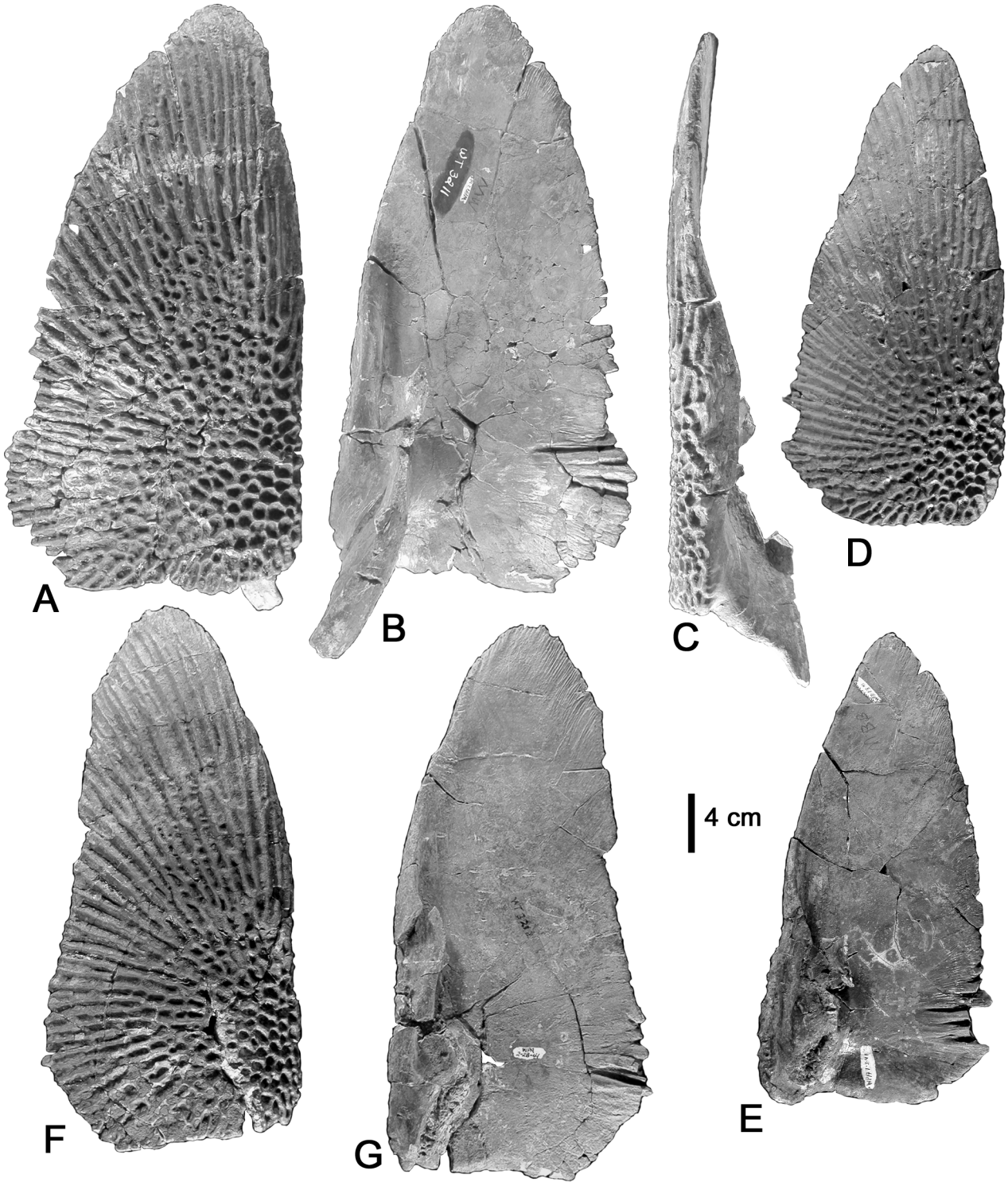

FIGURE 61. *Koskinonodon perfectum* clavicles from the Rotten Hill bonebed. **A-C**, WT 3211, left clavicle in **A**, ventral, **B**, dorsal and **C**, lateral views. **D-E**, WT 3212, left clavicle in **D**, ventral and **E**, dorsal views. **F-G**, WT 1341, left clavicle in **F**, ventral and **G**, dorsal views.

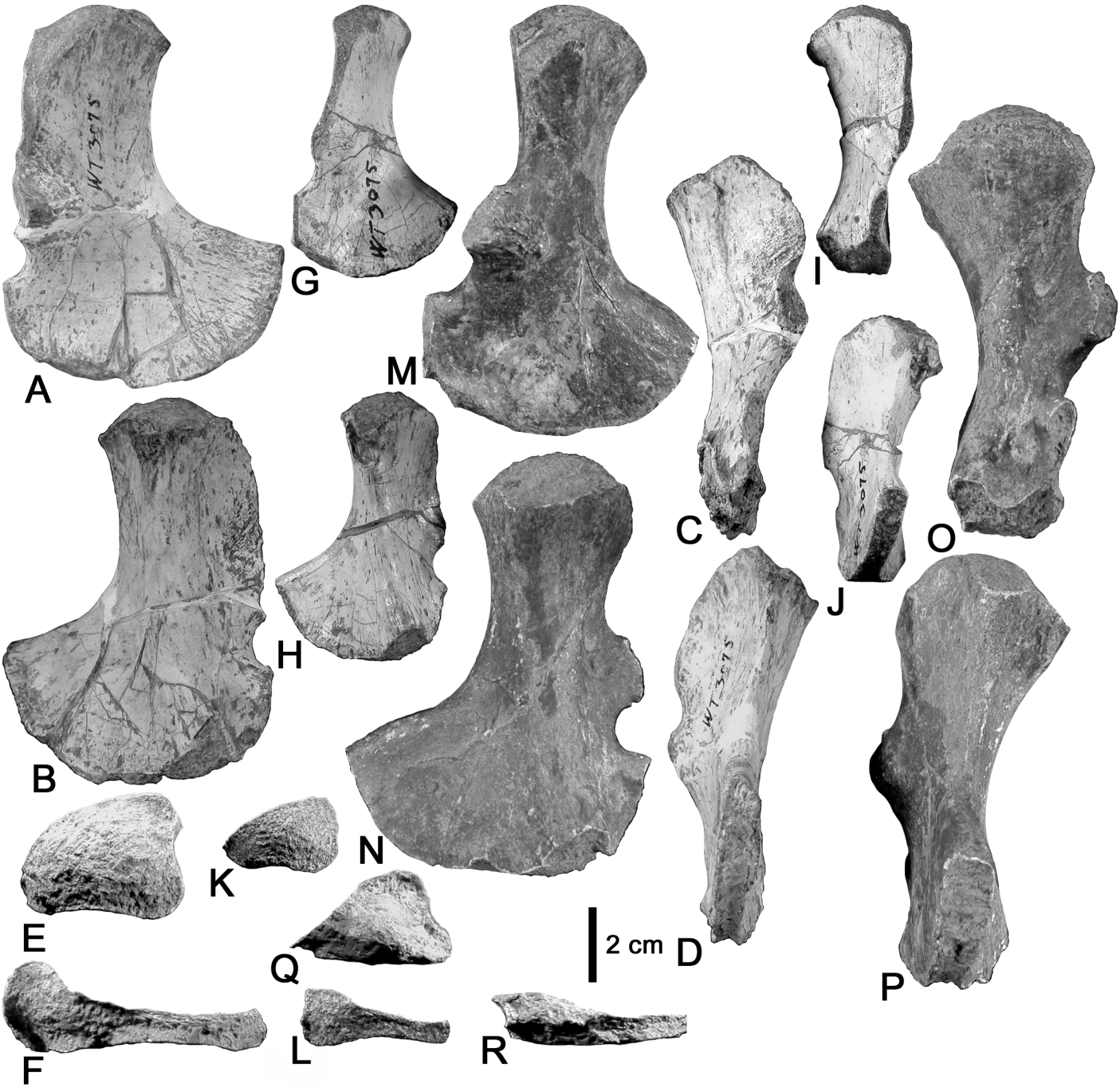

FIGURE 62. *Koskinonodon perfectum* humeri from the Rotten Hill bonebed. **A-R**, WT 3075, three humeri in **B, H**, **N,** dorsal view, **A, G, M** ventral view, **C**, **I**, **O**, anterior view, **D**, **J**, **P**, posterior view, **E**, **K**, **Q**, proximal view and **F**, **L**, **R**, distal view.

This belongs to type C of Sulej (2007). Another rib (Fig. 44E-F) has a bent shaft. It has a thick trihedral head and two ridges dorsally delineate a shallow sulcus. The distal end is a flat flange of bone, and a single uncinate process is present. This is type D of Sulej (2007). Another rib (Fig. 44G-H) is wide proximally and has a slightly curved shaft that expands distally, though not as wide as proximally. This is most similar to Sulej's (2007) type E ribs.

Scapulocoracoid

No scapulocoracoids of *Koskinonodon perfectum* are present in the Rotten Hill collection.

Cleithrum

Two complete cleithra (Fig. 45A-D) and one incomplete cleithrum (Fig. 45E-F) are in the Rotten Hill collection. The head of the cleithrum has a rugose and concave surface for articulation with the scapula. The shaft is trihedral in cross section and slightly curved. The clavicular articular surface is a groove or lineated shelf of bone. These Rotten Hill cleithra are very similar to that of *Koskinonodon* illustrated by Sawin (1945, fig. 8c-d), some of those of *Metoposaurus* illustrated by Sulej (2007, figs. 48-49) and that of *Dutuitosaurus* illustrated by Dutuit (1976, fig. 53, pl. 23, figs. C-J).

Interclavicle

This bone (Figs. 46A, D, 47-52) is diamond-shaped viewed ventrally, with the most acute angle of the diamond pointing anteriorly. The external (ventral) surface is ornamented, whereas the internal surface is covered with essentially smooth cortical bone. The antero-lateral sides of the diamond are the articular surfaces for the clavicles (Figs. 46A, D, 47A-B).

The Rotten Hill bonebed has yielded a large sample (68) of interclavicles that allow us to assess variation, particularly with regard

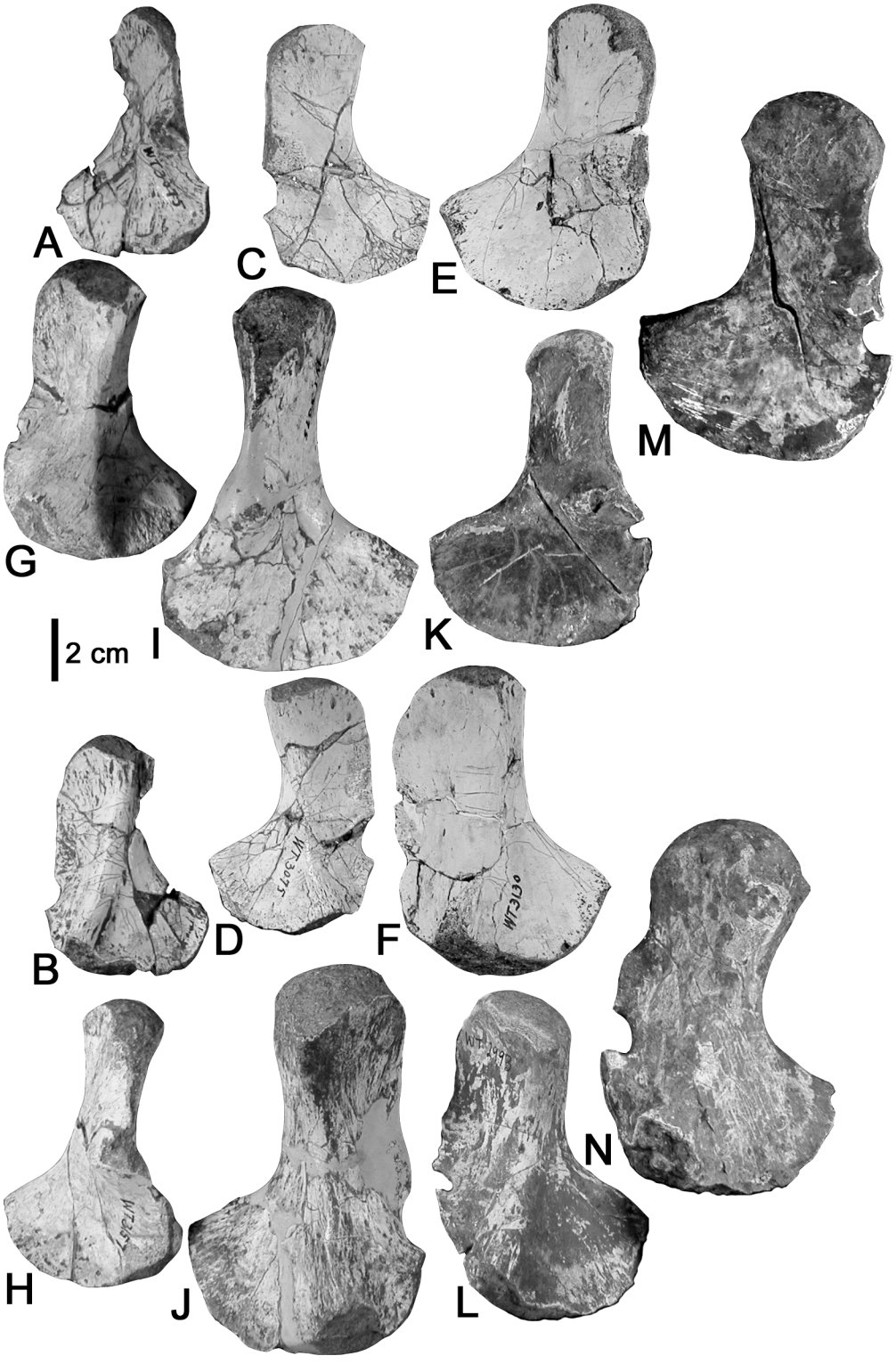

FIGURE 63. *Koskinonodon perfectum* humeri from the Rotten Hill bonebed. **A-D**, **I-J**, WT 3075, three humeri in **B, C, J**, dorsal and **A, D, I**, ventral views. **E-F**, WT 3130, humerus in **E**, ventral and **F**, dorsal view. **G-H**, WT 3157, humerus in **G**, dorsal and **H**, ventral view. **K-L**, WT 2993, humerus in **K**, ventral and **L**, dorsal view. **M-N**, WT uncataloged, humerus in **M**, ventral and **N**, dorsal view.

to ornamentation. The ornamentation is of two basic types—reticulate and ridge-and-groove (cf. Rinehart and Lucas, 2013b). As Rinehart and Lucas (2013b, p. 525) stated "the reticulate texture is a network of raised, reticulate ridges that enclose approximately flat-bottomed, interlocking polygonal cells….the vast majority of these cells are four-, five- or six-sided, creating honeycomb- or waffle iron-like texture." Rinehart and Lucas (2013b, p. 525) described the ridge-and-groove texture as comprising "raised, parallel to sub-parallel ridges separated by round-bottomed grooves." On the interclavicles of the Rotten Hill *Koskinonodon*, the reticulate texture occupies the posterior central part of the external surface, and the ridge-and-groove texture radiates outward from it. Variation in the texture takes the form of different proportions of the reticulate and the ridge-and-groove texture, most simply seen as interclavicles that have more extensive areas of

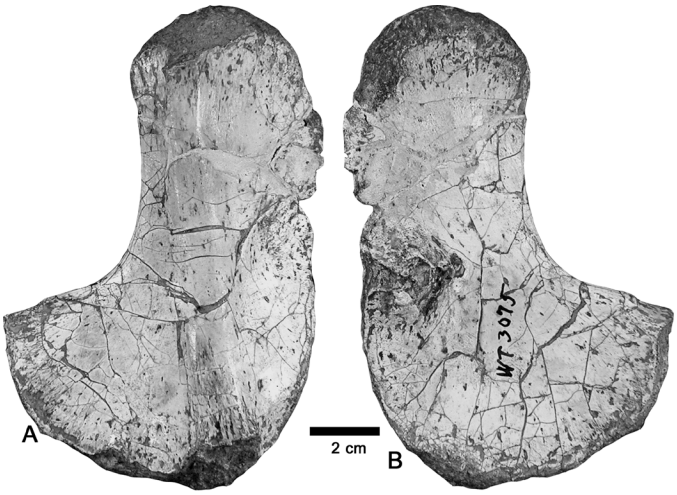

FIGURE 64. *Koskinonodon perfectum* humerus from the Rotten Hill bonebed. **A-B**, WT3075, pathologic right humerus in **A**, dorsal and **B**, ventral views.

reticulate texture contrasted with those that have relatively limited areas of reticulate texture.

Koskinonodon differs from *Metoposaurus* in having a much greater area of reticulate texture on the interclavicle (Hunt, 1993; see also Colbert and Imbrie, 1956, fig. 10). However, one specimen from Rotten Hill (Fig. 49C) overlaps the morphology of *Metoposaurus* in the limited area of reticulate sculpture. *Dutuitosaurus* is more similar to *Koskinonodon* in this feature than *Metoposaurus* (Dutuit, 1976, figs. 48-50; pl. 22, figs. D-e; pl. 23, fig. a-b; pl. 24). The "length-to-pits" measurement we employ in our analysis of interclavicles (described in the morphometrics section below) was intended to capture this feature when comparisons are made across taxa, as those with more ridge-and-groove structures tend to have a shorter "length to pits" than do those with extensive areas covered with reticulate structures.

Clavicle

The metoposaurid clavicle (Figs. 46B-C, E-F, 53-61) forms an acute triangle in external or internal view. Like the interclavicle, the external surface of the clavicle is ornamented with two kinds of texture: reticulate (anteriorly and antero-laterally) and ridge-and-groove (posteriorly and antero-medially). The reticulate texture extends onto the lateral edge of the clavicle (Figs. 53B, 54B, 57C, 61C).

The internal aspect of the clavicle is mostly smooth cortical bone except along the antero-medial, medial and antero-medial edges where finely ridged bone comprises the sutural surface that articulates with the interclavicle. The external surface of the clavicle is slightly convex, especially towards its lateral edge, whereas the internal surface is correspondingly concave.

The dorsal process of the clavicle is a flange of bone that projects from the postero-medial portion of the internal surface. This flange is concave laterally (Figs. 53B-C, 61B-C). On many clavicles the dorsal process is broken and only preserved as a low, blunt flange (Figs. 61F-G) or a plate of bone (Fig. 54B-C).

This process is much smaller/less prominent than in *Metoposaurus* (Sulej, 2007, fig. 43). *Koskinonodon* has a relatively extensive area of reticulate sculpture on the clavicle compared to *Metoposaurus* (Colbert and Imbrie, 1956, figs. 10, 11; Hunt, 1993, fig. 3). The clavicle of *Koskinonodon* is also relatively longer and narrower and has a more pointed anterior end than that of *Metoposaurus*. These features of the clavicle diagnose *Koskinonodon* from *Metoposaurus* (see above). The clavicles of *Koskinonodon* and *Dutuitosaurus* (Dutuit, 1976, figs. 50-51; pl. 22, figs. a-b) are very similar. However, note that Dutuit's (1976, fig. 50) drawing of the articulated interclavicle and clavicles of *Dutuitosaurus* is misleading because it shows unusually short and broad clavicles attached to a disproportionately small interclavicle.

Humerus

A relatively large number (20) of humeri (Figs. 62-64) are in the Rotten Hill collection. These bones vary considerably in size and completeness of preservation. In general, the humerus of *Koskinonodon* from Rotten Hill has a blunt, tubercular proximal head with a convex articular surface. The distal end of the humerus is a broad, sweeping and arcuate plate extending from the entepicondyle to the supinator crest.

The head is wider than the shaft in some specimens (Fig. 62M-N), but in others a large, plate-like deltopectoral crest along the posterior edge of the proximal humerus makes the shaft wider than the head (Fig. 62A-B). There is substantial variation in this feature, and the humeri fall into two groups: (1) those with prominent deltopectoral crests, which have weakly developed supinator processes (Fig. 62A-B); this is most common among the smaller humeri; and (2) less common humeri with weak development of the deltopectoral crest, limited to development of the biceps tubercle and a more prominent supinator process (Fig. 62M-N). The humerus illustrated by Sawin (1945, fig. 10a-b) is of the latter type, but it is not characteristic of *Koskinonodon*. The differences are not strictly size related, as a comparison of Figure 62A and M reveals. Perhaps most unusual among the Rotten Hill humeri is a very long humerus in which the deltopectoral crest extends down the shaft, and no notch separates it from the supinator crest (Fig. 64).

The *Metoposaurus* humeri described by Sulej (2007, fig. 50) lack the degree of variation in humeral morphology seen in the Rotten Hill sample of *Koskinonodon*. The few illustrated humeri of *Dutuitosaurus* (Dutuit, 1976, fig. 50; pl. 26, figs. a-d) fall within the range of variation of the *Koskinonodon* humeri. The Rotten Hill sample suggests that the dominant morphology of the *Koskinonodon* humerus is that with a large and plate-like deltopectoral crest confluent with or only separated from the supinator crest by a small/shallow notch (Fig. 63A-B). The humerus morphology illustrated by Sawin (1945) thus is unusual and not characteristic of the genus.

Radius

Eight radii are preserved in the Rotten Hill collection, and we illustrate a selection (Fig. 65). The radius of *Koskinonodon* from Rotten Hill is a columnar bone with slightly expanded proximal and distal ends. The proximal end is nearly circular in cross section (cf. Sawin, 1945, fig. 10c), but in the Rotten Hill specimens it has been distorted by compression to a nearly teardrop shape (Fig. 65Q). The lateral surface of the shaft is convex, and the medial aspect is concave towards the proximal and distal ends. The anterior tuberculum is just distal to the head on the anterior edge of the bone, but it only forms a crest that extends toward the mid-shaft constriction. The radius of *Koskinonodon* based on the Rotten Hill specimens and illustrated by Sawin (1945, fig. 10c-d) does not differ significantly from that of *Metoposaurus* (Sulej, 2007, figs. 54-55) or of *Dutuitosaurus* (Dutuit, 1976, fig. 59, pl. 26, figs. l-p).

Ulna

One of the two ulnae in the Rotten Hill collection is illustrated here (Fig. 66). This bone corresponds well to the ulna of *Koskinonodon* illustrated by Sawin (1945, fig. 10e-f). Thus, it is a columnar bone with a proximal end much wider than the distal end. The shaft is compressed medio-laterally, so that the cross section is not as round as that of *Koskinonodon* depicted by Sawin (1945, fig. 10e-f) or Sulej (2007, figs. 57a-e, g-i) illustrated in *Metoposaurus*. This is likely due to taphonomic distortion of the Rotten Hill specimen. The ulna of *Dutuitosaurus* illustrated by Dutuit (1976, fig. 60, pl. 26, figs. e-f) also has a round cross section. Undistorted, the medial side of the ulna is the flat side, where it faces the radius. What Sulej (2007, fig. 57) called the olecranon process is a thin ridge along the lateral edge of the ulna.

Manus

No bones that we could confidently assign to the metoposaur manus were identified in the Rotten Hill collection.

Ilium

Seventeen ilia that cover a wide size range are available in the Rotten Hill collection (Fig. 67). Like previously illustrated metoposaur ilia (e. g., Sawin, 1945, fig. 10m-p; Sulej, 2007, figs. 58-59), the ilia from Rotten Hill have a long and narrow dorsal shaft, and a widened acetabular base. The sacral rib facet, which is the dorsal terminus of the ilium, is a rugose and somewhat trapezoidal surface (Fig. 67C, F, I, L). This surface is slightly expanded from the shaft. The acetabular end is thick and trihedral with a concave acetabulum and a flattened/convex ischial facet.

The ilium of *Metoposaurus* differs from that of *Koskinonodon* in terms of having a more s-shaped curve (greater curvature of the dorsal surface of the shaft) and in having torsion of the shaft (Sulej, 2007, figs. 58-59). The ilium of *Dutuitosaurus* (Dutuit, 1976, fig. 66, pl. 27, figs.

i-m, pl. 28, figs. a-b) is similar to that of *Koskinonodon*.

Ischium

Three ischia are available in the Rotten Hill collection, and one is illustrated (Fig. 68). In ventro-lateral or medio-dorsal view, it is a half-moon-shaped bone that has a gently concave dorsal edge and a broadly convex ventral edge. Key features include a set of foramina and grooves on the medio-dorsal surface for insertion of the interischial ligament, a shallow fossa dorso-posteriorly and the rugose anterior edge for articulation with the ilium. It is morphologically very similar to the ischia of *Koskinodon* illustrated by Sawin (1945, fig. 10q-r), of *Metoposaurus* illustrated by Sulej (2007, fig. 60-61) and of *Dutuitosaurus* illustrated by Dutuit (1976, fig. 63; pl. 27, figs. a-d).

Femur

Fifteen femora covering a wide size range are available in the Rotten Hill collection (Figs. 69-70). A characteristic, relatively large femur (Fig. 69) has a poorly developed proximal head that is nearly flat proximally (not the more convex head illustrated by Sawin, 1945, fig. 10g-h), and a trihedral, relatively straight and narrow shaft that widens to the broad, flange-like distal end, which is convex dorsally. The axes of the proximal and distal ends are rotated ~ 90º relative to each other. A well-developed trochanter is about one-third of the way down the shaft from the proximal end. The distal articular surface is asymmetrical—a larger fibular condyle and a smaller tibial condyle (Fig. 69F).

Smaller femora (Fig. 70) are proportionately more robust (lower length:width ratios) than the relatively gracile larger femur. However, no obvious variation in morphology corresponds to differences in size. The Rotten Hill femora do not differ from the range of femoral variation illustrated by Sulej (2007, figs. 63-64) for *Metoposaurus* or of the variation in femora of *Dutuitosaurus* illustrated by Dutuit (1976, fig. 67, pl. 27, figs. e-h)

Tibia

Five tibiae are available in the Rotten Hill collection (Fig. 71), and they closely resemble the tibia of *Koskinonodon* illustrated by Sawin (1945, fig. 10i-j). Thus, the tibia is broadly similar to that of *Metoposaurus* (Sulej, 2007, figs. 65-66) and *Dutuitosaurus* (Dutuit, 1976, fig. 69; pl. 28, figs. i-p), but it differs in being a much flatter bone in cross section with a much more expanded dorsal end and a more broadly arcuate proximal end. This gives the tibia of *Koskinonodon* a much more "hourglass" shape than that of *Metoposaurus* or *Dutuitosaurus*.

Both tibiae illustrated here (Fig. 71) are nearly the same size and have an arcuate proximal end, so that the shaft is dramatically waisted. The cnemial crest is a low ridge on the antero-ventral edge of the bone. The distal end is expanded to form a convex to bipartite articular surface for the astragalus. The cross sections proximally and distally are antero-medially compressed.

Fibula

Three fibulae are available in the Rotten Hill collection (Fig. 72). The fibula of *Koskinonodon* is a relatively short and robust bone with expanded proximal and distal ends, with the distal end widest. The proximal and distal ends have a flattened, ellipsoidal cross section. The entire fibula is flattened latero-medially and has broadly concave anterior

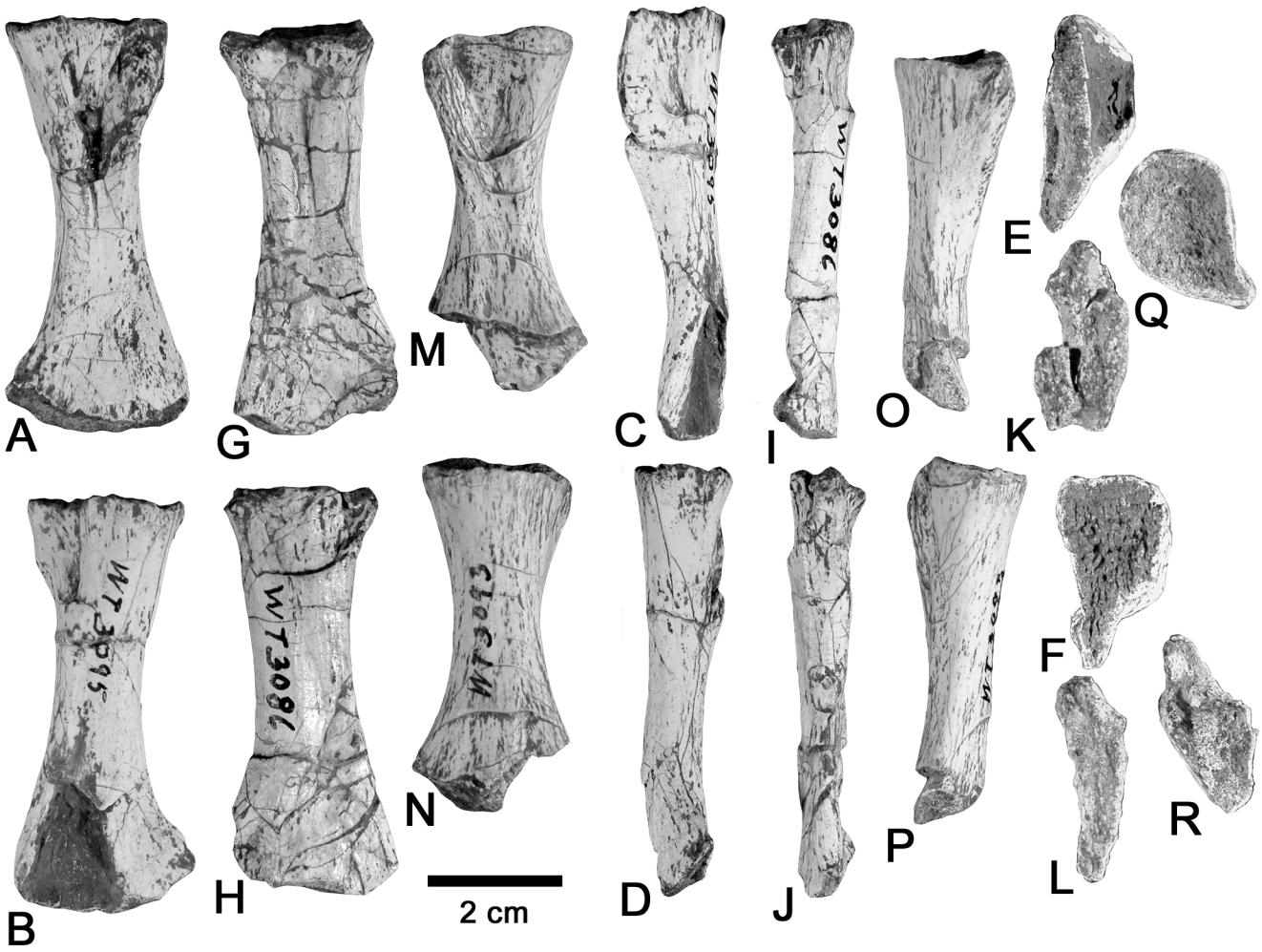

FIGURE 65. *Koskinonodon perfectum* radii from the Rotten Hill bonebed. **A-F**, WT 3095, radius in lateral (**A**, **G**, **M)**, medial (**B, H, N**), posterior (**C, I, O**), anterior (**F, J, P**), proximal (**E, K, Q**) and distal (**F, L, R**) views.

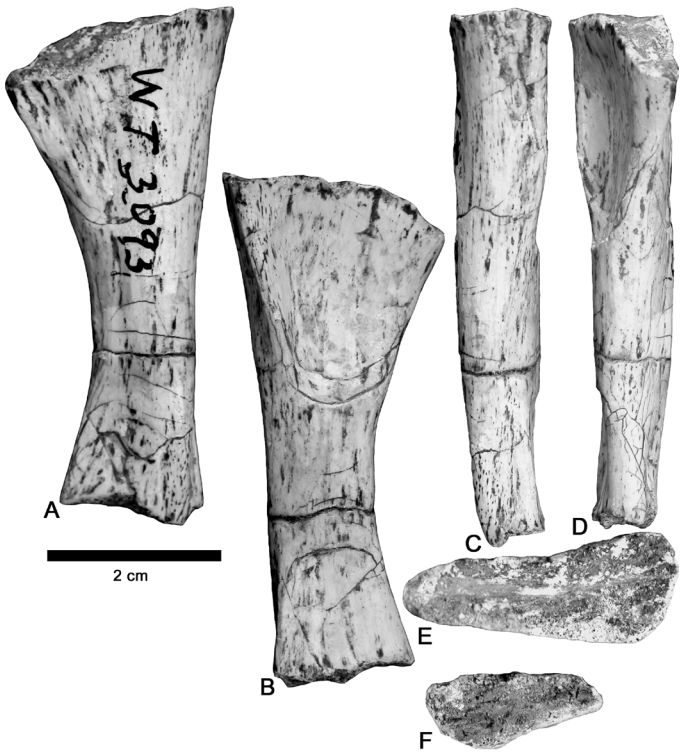

FIGURE 66. *Koskinonodon perfectum,* WT 3093, left ulna from the Rotten Hill bonebed in **A**, lateral, **B**, medial, **C**, ventral, **D**, dorsal, **E**, proximal and **F**, distal views.

and posterior edges, so the proximal and distal ends are widened. The anterior edge is more deeply concave than the posterior edge and the proximal end wider than the distal end. There is a prominent tuberosity antero-medially located on the distal end.

The Rotten Hill fibulae have a relatively shorter and thicker shaft than the fibula of *Koskinonodon* illustrated by Sawin (1945, fig. 10k-l), of *Metoposaurus* illustrated by Sulej (2007, figs. 67-68) and of *Dutuitosaurus* illustrated by Dutuit (1976, fig. 70; pl. 28, fig. d-h).

Pes

No bones unambiguously from the metoposaur pes were identified in the Rotten Hill collection.

KOSKINONODON: MORPHOMETRICS AND ALLOMETRICS

Morphometric Database

Most of the Rotten Hill *Koskinonodon perfectum* measurements were collected at the PPHM collection. Clavicles, interclavicles, skulls, lower jaws, atlas vertebrae, and limb bones were measured. Additionally, 11 skulls, 13 lower jaws, and numerous other elements were borrowed for study, photography, and measurement at NMMNH. Some Rotten Hill elements were also measured at the Texas Memorial Museum, Austin, TX, and at the American Museum of Natural History, New York, NY. The institutional locations of these various elements are indicated by the specimen numbers on the database pages. All measurements are included in the morphometric database (Appendix 2). Summary descriptive statistics, including minimum and maximum sizes, central tendencies, standard deviation and other statistics for the lengths and widths of each group of bones are tabulated in Appendix 3. At a minimum, all limb elements were measured for length, and proximal and distal widths. Sketches define the measurement protocols for the skulls and shoulder girdle elements (Fig. 73).

Metrics and Allometry

A study of whole-body allometry (e.g., limb length or skull length versus total body length throughout growth) is not possible using the Rotten Hill metoposaur data because the quarry consists entirely of disarticulated material. Therefore, we do, as much as possible, describe the differential growth of each of the bones.

Disarticulation appears to be the norm in the large metoposaur assemblages. Examples include the Krasiejów, Poland *Metoposaurus* deposit (Sulej, 2007), and the *Koskinonodon* quarries located at Lamy, New Mexico (Romer, 1939; Lucas et al., 2010) and Rotten Hill, Texas. To our knowledge, only the *Dutuitosaurus* quarry (Dutuit's Quarry 13) in Morocco has produced numerous fully articulated specimens (Dutuit, 1976). Unfortunately, these articulated animals span only a small size range, so a whole-body allometry assessment over anything approximating an ontogenetic growth series would be very difficult.

In the allometric power function of Huxley (1932):

$$y = \beta x^{\alpha},$$

the exponent, α, is the relative growth coefficient. If $\alpha > 1$, y grows proportionately more than x, and the curve is concave-up; for $\alpha = 1$, y and x grow in isometry, and the plot line is straight; and for $\alpha < 1$, y grows proportionately less than x, and the curve is concave-down (Gould, 1966).

The quality of the curve fits is reflected in the correlation coefficient, R^2. R^2 is also known as the coefficient of determination, and as such shows the percentage of variation observed in the dependent variable, y, that "is explained" by the value of the independent variable, x (Hammer and Harper, 2006). We show plots of both linear and log-transformed data to most fully exemplify the relationships. The linear plots show, at a glance, the size relationships of the various elements, while the "log-space" plots show allometry, the relative growth rates that reflect shape change throughout ontogeny. Curve fit equations in the figures show the absolute and relative growth functions. In the allometry plots, the x coefficient is the allometric constant, Huxley's α.

Here, we briefly describe the metrics and relative growth of each element in the Rotten Hill sample.

Skull length—The range of skull lengths in the sample varies from 302 to 560 mm. We divided the skull into various zones beginning at the snout tip and proceeding posteriorly to include the entire skull (e.g., prenarial, narial, narial-orbital, etc.) (Fig. 73C). The relationship of the length of these various skull zones to midline length throughout the size range of the sample is shown graphically and described by the curve fit equations (Fig. 74A).

Relative growth of the skull zones is also shown graphically and defined by linear equation fits to the natural log-transformed data. On the snout, the prenarial length grows in strong positive allometry, increasing proportionately much more than total skull length (α = 1.94), but narial and narial-orbital lengths grow in moderate negative allometry (α = 0.79 and 0.83, respectively). The result is that the entire preorbital snout grows in weak negative allometry (α = 094). The postorbital skull zone grows in approximate isometry (α = 1.03). Thus, there is a weak tendency for the orbits to migrate forward on the skull throughout growth.

Skull width—Skull widths, measured at the greatest point (across the quadratojugals), range from 254 to 498 mm. Skull width, measured at various points along the skull length, is shown in a plot of these metrics (Fig. 74C).

A plot of width allometry shows considerable shape change throughout growth (Fig. 74D). The anteriormost skull, measured across the anterior nares, shows strong positive allometry, growing at a much higher rate than length (α = 1.68). Farther posteriorly, at the anterior orbits, the width increases in positive allometry, but proportionately less than at the snout tip (α = 1.2). At the point of greatest width, across the posterior skull, width continues to increase but in slightly less positive allometry (α =1.16). Thus, throughout growth the skull width increases in positive allometry along its entire length. The anteriormost skull parts widen most aggressively with respect to length, and this trend decreases continuously proceeding posteriorly until, at the posterior skull, width increases in weak positive allometry. In general, the younger animals have a more triangular skull, with a more pointed snout, whereas in older individuals the snout becomes more roundly broadened, assuming a more "bullet" shape.

Comparison with a previous study—Colbert and Imbrie (1956) studied and compared skull growth in five populations of *Koskinonodon perfectum* from the western United States using multivariate methods; a remarkable feat in the pre-computer age. Samples from Arizona, Wyoming, New Mexico, and Texas were included in their work. Their data included two sites in Texas: Howard County and Potter County; the latter is the Rotten Hill site. Their analysis showed that differential skull growth varied significantly between these five localities, with the two Texas localities being the most similar. Our current findings agree well with their analysis of the Rotten Hill metoposaur skulls, which showed allometric growth of the skull width and weak negative

allometric growth in preorbital length (Colbert and Imbrie, 1956, fig. 16). Interestingly, Colbert and Imbrie (1956, table 2) appear to have had more skulls (15) available to them for measurement, and one of their individuals is much wider (550 mm) than any we measured, although we measured at least one skull longer than they did, so there could be as many as 16 measurable skulls from the site.

Lower jaws—Lower jaw lengths were measured around the arc of the jaw; jaw heights indicate the maximum height, which is generally at the hamate process. Lengths ranged from 376 to 654 mm, and heights from 55 to 135 mm. The metric relationships are shown (Fig. 74E). Lower jaw height grows in weak positive allometry, increasing proportionately slightly more than length ($\alpha = 1.15$) (Fig. 74F).

A scatterplot of tooth count versus jaw length (Fig. 74G) shows that, in general, tooth count increases as jaw length increases. However, the increase is not directly proportional to length; as length increases by ~ 42% over the range of sizes in the sample, the tooth count only increases ~13%, from ~ 45 to ~ 52 tooth positions. Additionally, there is high variance in the data, and correlation of the curve fit is low. Because the correlation is low, it is not possible to predict the exact tooth count from even the most accurate jaw measurement, but the approximate number may be estimated by the curve fit equation (Fig. 74G).

Atlas vertebrae—The range of 17 measurable atlas lengths in the Rotten Hill metoposaurs is from 9 to 42 mm. Anterior height and width metrics are plotted against length (Fig. 75A). Both width and height grow with strong negative allometry, increasing proportionately less than length in the atlas ($\alpha = 0.55$ and 0.58, respectively) (Fig. 75B).

Interclavicles—Fifty-nine interclavicles range in length from 282 to 510 mm and in width from 216 to 400 mm. A plot of interclavicle metrics shows the relationship of width, length along the midline to the clavicle, and length to the pitted texture area (Fig. 75C). Width grows in negative allometry, increasing proportionately less than length ($\alpha = 0.65$). The interclavicle becomes proportionately narrower as it grows. The relative growths of length to clavicle and length to pits (defined in Fig. 73) show negative allometry ($\alpha = 0.85$ and 0.4, respectively) (Fig. 75D).

Clavicles—Forty-six clavicles in the study sample vary in length from 256 to 398 mm and in width from 105 to 210 mm (Appendix 2). The width-to-length relationship (Fig. 73A) is defined over the size range of the Rotten Hill sample (Fig. 76E). Width grows in positive allometry, increasing proportionately more than length; thus, the clavicle becomes relatively wider throughout growth ($\alpha = 1.2$).

Ischia—Only three ischia, ranging in length from 45 to 59 mm, are present. The length-to-width relationship of this small sample is shown (Fig. 75G). Width grows proportionately less than length ($\alpha = 0.83$), although, with such a small sample, confidence in this statistic is very low (Fig. 75H).

Ilia—Ilium length varies from 41 to 106 mm in the Rotten Hill sample (N=14). Ilium proximal and distal widths are compared to length (Fig. 75I). Proximal width grows proportionately more than length ($\alpha = 1.58$); distal width of this element grows proportionately less than length ($\alpha = 0.91$) (Fig. 75J).

Humeri—Twenty humeri in the sample vary in length between 65 and 136 mm. Proximal and distal widths versus length are shown (Fig. 75K). Proximal width grows in near isometry with respect to length ($\alpha = 1.06$), whereas distal width grows in weak negative allometry ($\alpha = 0.92$).

Radii—There are only eight radii in the population, and only five of these are completely measurable. Attempted plots of metrics and allometry show high variance and low correlation (R^2). We consider these data uninformative and do not present them here.

Ulnae—Only two ulnae are present. We did not attempt to analyze such a small sample.

Femora—The sample contains 18 femora varying in length from 90 to 151 mm. Proximal and distal widths and other metrics versus length (Fig. 75M) show some scatter but reasonable correlation. Both the proximal and distal widths grow in negative allometry with respect to length, with the distal width being more negative ($\alpha = 0.93$ and 0.73, respectively) (Fig. 75N). Strength indicators—midshaft circumference and midshaft diameter (average of major and minor diameters; the femur cross section being elliptical)—both grow in relatively strong negative allometry ($\alpha = 0.78$ and 0.76, respectively) (Fig. 75N). Thus, the femora become more gracile throughout growth.

Tibiae—Five tibiae are present; lengths range from 53 to 73 mm. Proximal and distal width-to-length relationships are plotted (Fig. 75O). The proximal and distal widths grow in negative allometry, increasing proportionately less than length ($\alpha = 0.88$ and 0.58, respectively); scatter is moderately high in the data. As in the femora, the tibiae become more gracile throughout growth.

Fibulae—Four fibulae vary in length over the range of 41 to 55 mm. High scatter in the data precludes analysis of these elements.

Comparison to the Lamy, NM population—We compare distal width metrics and differential growth in the humeri of the Rotten Hill *Koskinonodon perfectum* and the Lamy population using data from Olsen (1951) for 20 of the Lamy metoposaurs. Distal width is plotted against length for both populations (Fig. 76A). The curve fits are very similar, although scatter is higher in the Rotten Hill sample. We tested for coincidence of the regression lines (Zar, 1999; Glantz, 2005). The complete coincidence test results and the results of subsequent t-tests are shown in Appendix 4. In the overall test of coincidence the two regression lines are shown to be statistically different (better described by two lines than by one) at the 95% confidence level but not at the 99% level. Subsequent t-tests showed that the most significant portion of the difference between the regressions is in the slopes, not the intercepts. The slopes define the rates of growth, while the intercepts are of questionable biological significance (Olsen, 1951). So, the most significant part of the difference in the humerus relative distal width growth curves of *K. perfectum* from Lamy and from Rotten Hill is the relative rate of growth. Relative growth is then addressed allometrically; both populations show negative allometry, but the Lamy population is slightly more negative (Fig. 76B). The distal humerus width of the Rotten Hill population grows slightly faster with respect to length than that of the Lamy population.

Finally, we show the size ranges and distal width versus length for *Koskinonodon perfectum* limb bones from the Lamy amphibian quarry (Fig. 76C). Symbols marking the ends of the regression lines show the shortest and longest elements of each type. The raw data are from Olsen's (1951; tables 1-2) published size range and linear regression coefficients. Comparing the maximum and minimum lengths of the Rotten Hill limb elements (Appendix 3) to the size range of the Lamy limb elements (Fig. 76C) shows general similarity in the two groups. Comparison of the limb bone distal width versus length regression lines between the Rotten Hill (Fig. 75K, M, O) and Lamy populations (Fig. 76C) shows, as was seen in the comparison of humeri (Fig. 76A), that there are overall similarities, especially in size, but the two populations are not identical in their differential growth.

Allometry: Summary and Discussion

Skulls—The preorbital snout length grows in weak negative allometry with respect to the midline length, whereas the postorbital portion grows in approximate isometry. Skull width grows aggressively in the anteriormost part, but width increases less rapidly proceeding posteriorly. However, we find that the width of all skull areas increases proportionately more than length throughout growth, in general agreement with Davidow-Henry (1989).

Shoulder girdle—The interclavicle width grows in negative allometry, whereas the clavicle width grows in positive allometry. Thus, as the animal grows, the clavicles account for relatively more of the shoulder girdle width, and the interclavicle accounts for relatively less.

Limb bones—In general, a straight line relationship exists between the lengths and widths of the limb bone and the pelvic girdle bone metrics. Proximal and distal widths grow in negative allometry in the femora and tibiae.

Both Olsen (1951) and Sulej (2007) noted similar negative limb bone allometry in *Koskinonodon* and *Metoposaurus,* respectively. They both proposed that this allometry indicated adaptation to an aquatic habitat. Sulej (2007) also posed the question of how metoposaurs could be so nearly cosmopolitan in the Late Triassic world, because their land mobility would be compromised by their delicate limbs, and, as amphibians, they probably could not swim in salt water (though some workers dispute this conclusion; see, e.g., Holman, 2006, fig. 4 and associated text). Sulej (2007) speculated that perhaps they moved overland on their bellies seal-like, with undulating body ripples assisted a bit by the limbs. Both these authors assessed limb bone allometry by comparing proximal and distal widths to lengths, but the limb bone ends do not determine the bone's resistance to bending moments, i.e., its strength. Olsen (1951) stated that (at least the proximal) end widths are probably an indicator of how much area is required for muscle attachment. We do not see why this is less so for the distal ends as well. In addition, Sulej's (2007) idea of seal-like locomotion in metoposaurs is problematic because while the musculature of marine mammals is adapted for propulsive motion in the dorso-ventral plane, the musculature of amphibians is designed to provide serpentine motions in

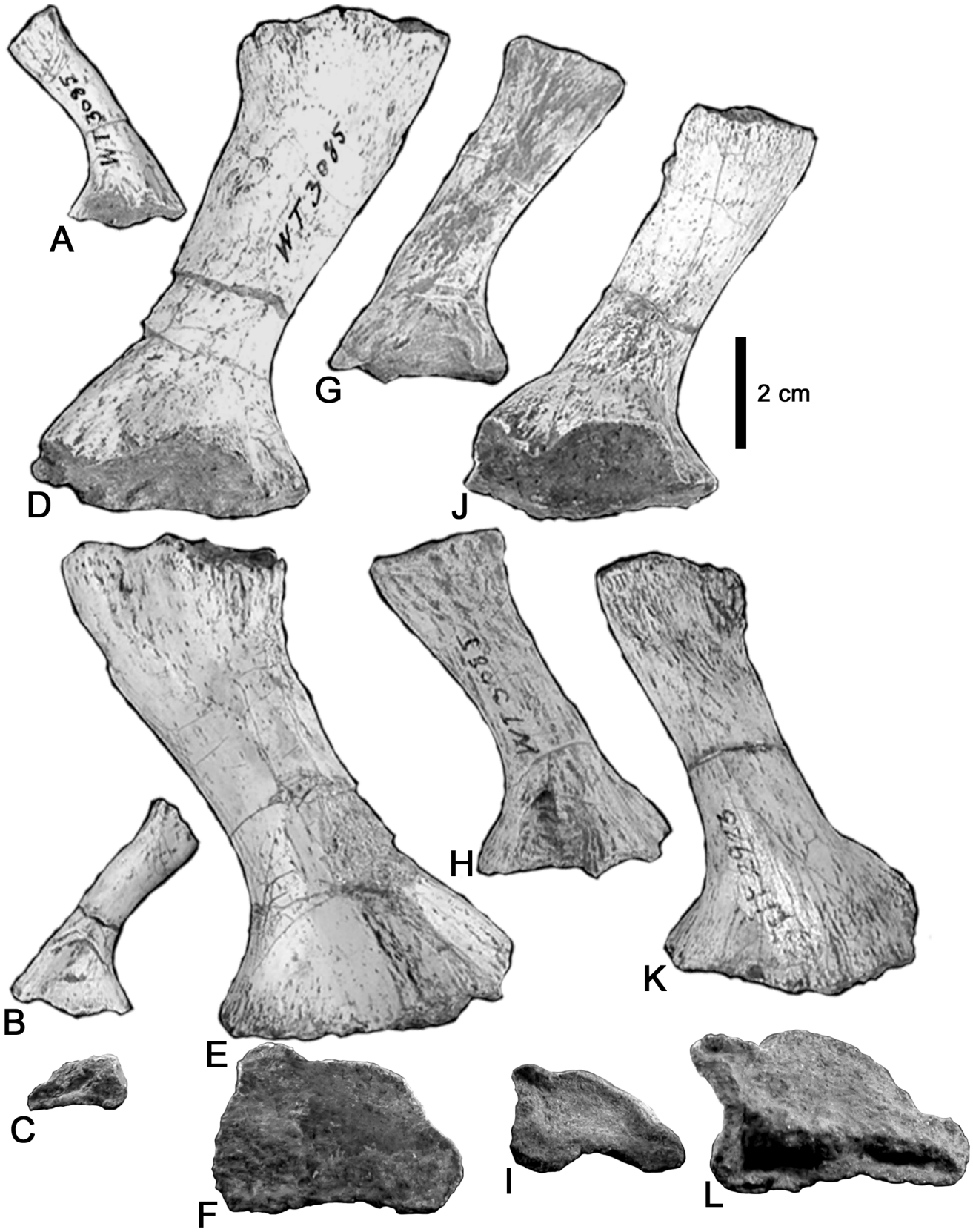

FIGURE 67. *Koskinonodon perfectum* ilia from the Rotten Hill bonebed. **A-I**, WT 3085, **A-C**, right ilium in **A**, lateral, **B**, medial and **C**, ventral view. **D-I**, two left ilia in **D**, **G**, lateral, **E**, **H**, medial and **F**, **I**, ventral views. **J-L**, WT 2923, left ilium in **J**, lateral, **K**, medial and **L**, distal view.

the lateral plane to propel the animal. Thus, seal-like locomotion in an amphibian would be very difficult to achieve. Furthermore, there is no trace fossil evidence of this behavior in spite of the rich Upper Triassic vertebrate ichnofossil record.

In order to establish a more definitive assessment of limb allometry and its effects on these animals, we undertook to carefully measure the allometry of the stress- and strength-defining metrics of the limbs; the length (an indicator of size, or stress) and midshaft diameter (an indicator of strength) (McGowan, 1999). We reiterate and expand here on Rinehart et al. (2008). Femora were chosen for our analysis. Humeri were not included because the complex shape of the humerus does not readily lend itself to a clear-cut measurement of midshaft diameter. The lower arm and leg bones are paired, but because of disarticulation of the specimens it is unclear which specimens were originally paired in the living animals. The load-bearing capacity of these bone pairs as they existed in the live animals therefore cannot be calculated, so we have excluded them from this study. We show a plot of detailed femur allometry of the Rotten Hill *Koskinonodon* femora (Fig. 75N) that includes both the proximal and distal widths plus midshaft diameter and circumference. The average midshaft diameter allometric constant is 0.76, and the allometric constant of a related quantity, midshaft circumference, is 0.78; these values are extremely similar, and both strongly negative.

The strength of a bone is proportional to its cross sectional area, and area is the square of a linear dimension, l; $A = l^2$. But volume, which is proportional to the weight (stress) applied to the bone, is governed by length cubed; $V = l^3$. Based on these relationships, McGowan (1999) has shown that the diameter of the bone must increase as the square root of the volume, that is,

$$SQRT\ l^3 = l^{3/2} = l^{1.5}$$

for the stress level to remain constant throughout growth. Thus, the allometric constant must equal or exceed 1.5 for the strength of the limbs to keep up with the increasing stress of the animal's weight.

McMahon (1975) and Alexander (1977) showed that the limb bones of cursorial ungulates generally maintain an allometric growth factor near 1.5. Most animals, however, do not. In a wide variety of animals (shrews to elephants) the limb bone diameters grow in near isometry. These animals accommodate the increasing stress on their limb bones behaviorally. Larger animals tend to keep more feet on the ground during locomotion (adult elephants do not gallop) and to hold the legs straighter, so they are more column-like and thus reduce shear stress (Biewener, 1983). Following Olsen (1951) and Sulej (2007), we hypothesize that *Koskinonodon* accommodated the increasing stress on its limb bones by becoming more fully aquatic.

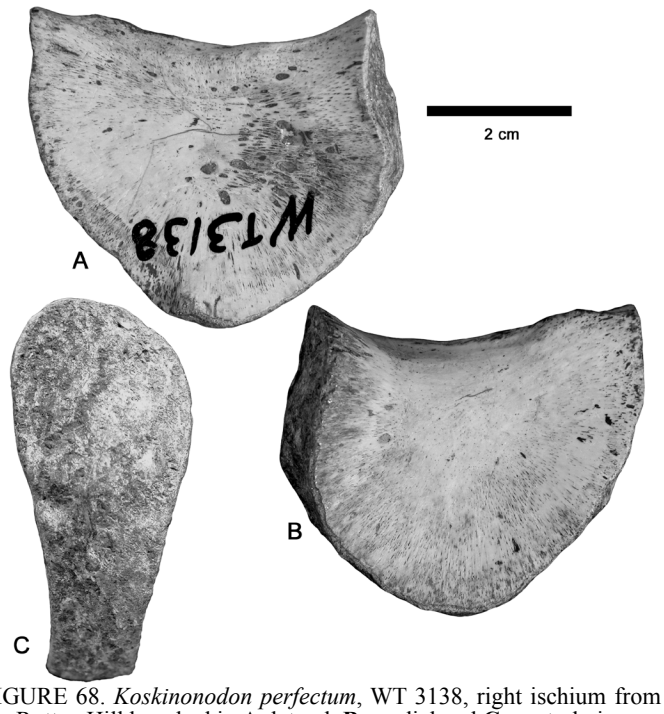

FIGURE 68. *Koskinonodon perfectum*, WT 3138, right ischium from the Rotten Hill bonebed in **A**, lateral, **B**, medial and **C**, ventral views.

To exemplify the stress-strength relationship in *Koskinonodon* femora, we graphed three power equations (Fig. 77A):

$$Y = X^{1.5},$$
$$Y = X^{1},$$

and

$$Y = X^{0.76}$$

which show, respectively, the positive allometric increase in diameter necessary to accomodate stress due to increasing mass, the approximately isometric strength increase observed in most animal limb bones, and the negative allometric strength increase in *Koskinonodon* femora. Figure 77B (dashed line) shows the difference between the power curves with 1.5 and 0.76 exponents. This quadratic function represents the accumulating unbalanced (by an opposing strength) stress in *Koskinonodon* femora throughout growth. The curve is concave-up, so excess stress increases slowly in the small animals but increases very rapidly in larger animals. Note that the excess stress curve does not cross the isometric growth line (solid, Y = X line: Fig. 77B) until considerable size is reached, so small animals have sufficient bone strength while large animals have passed the point where behavioral modification accommodates increasing stress. The stress and strength units in Figure 77A and 77B are arbitrary, but the curve shapes are pertinent.

Based on the preceding analysis, we agree with Olsen (1951) and Sulej (2007) that these metoposaurs must have become increasingly aquatic throughout growth. When midshaft diameters are used in the analysis, the negative allometry of limb bone growth shows itself to be much more dramatic than is indicated when proximal and distal widths are used. In addition, we hypothesize that the stress-strength data show that adult *Koskinonodon* were unable to support themselves on land; they were probably water-bound and entirely natatorial, while the juveniles were more terrestrial or littoral. This idea provides a possible answer to Sulej's (2007) question regarding dispersal of the metoposaurs over land: the juveniles may have easily traveled overland before their limbs became too feeble for the purpose. Schneider (2004) has pointed out that even if the amphibians were only moderately terrestrial, they may not have had long distances (1-2 km) to cross between the headwaters of some major Triassic river systems. This factor would certainly have aided in wide metoposaur dispersal.

Note in Figure 77B that because the limb bone stress curve is concave-up, stress does not increase out of control until the animals have reached some moderate size. We further propose that there was probably an ecological separation of the adults and juveniles that is evidenced by, and possibly enforced by, decreasing relative limb bone strength. Ecological separation of adults and juveniles is known in some extant amphibians (e.g., Hellbenders, genus *Cryptobranchus*) (AmphibiaWeb, 2006), among which it reduces competition for resources between the groups and reduces conspecific predation on the juveniles. These same benefits may have been present in *Koskinonodon* populations.

Ecological separation of adult and juvenile metoposaurs may help explain another odd circumstance regarding fossil metoposaur populations. Several well-populated assemblages of metoposaurs have been described from diverse locations: Lamy, NM, *Koskinonodon* (Romer, 1939; Lucas et al., 2010), N > 60; Rotten Hill, TX, *Koskinonodon*, N > 60; Argana, Morocco, *Dutuitosaurus* (Dutuit, 1976b), N > 70; Krasiejów, Poland, *Metoposaurus* (Sulej, 2007), N > 66. To the best of our knowledge, not a single very small metoposaur is reported from any of these localities, even though population dynamics demands that the juveniles must outnumber the adults. Rarely are skulls under 200 mm long seen in any of these assemblages. The vast majority have skulls greater than 300 mm long and shoulder girdles at least 300 mm across. These are not small juvenile animals.

Isolated occurrences of small juvenile metoposaur skulls are known from the Chinle Group and these are identifiable at the generic level (Davidow-Henry, 1989; Morales, 1993; Zanno et al., 2002). Therefore, these metoposaurs did not undergo any structural change between skull lengths of a few cm and adulthood that would have rendered the juveniles unrecognizable. *So, where are the juveniles that pertain to these large populations of metoposaurs, and why is there such a large preservational preference for the adults?* The idea that the juveniles were ecologically separated from the adults and were largely terrestrial offers an explanation; the adults, in their aquatic environment, were much more likely to be buried in sediment and

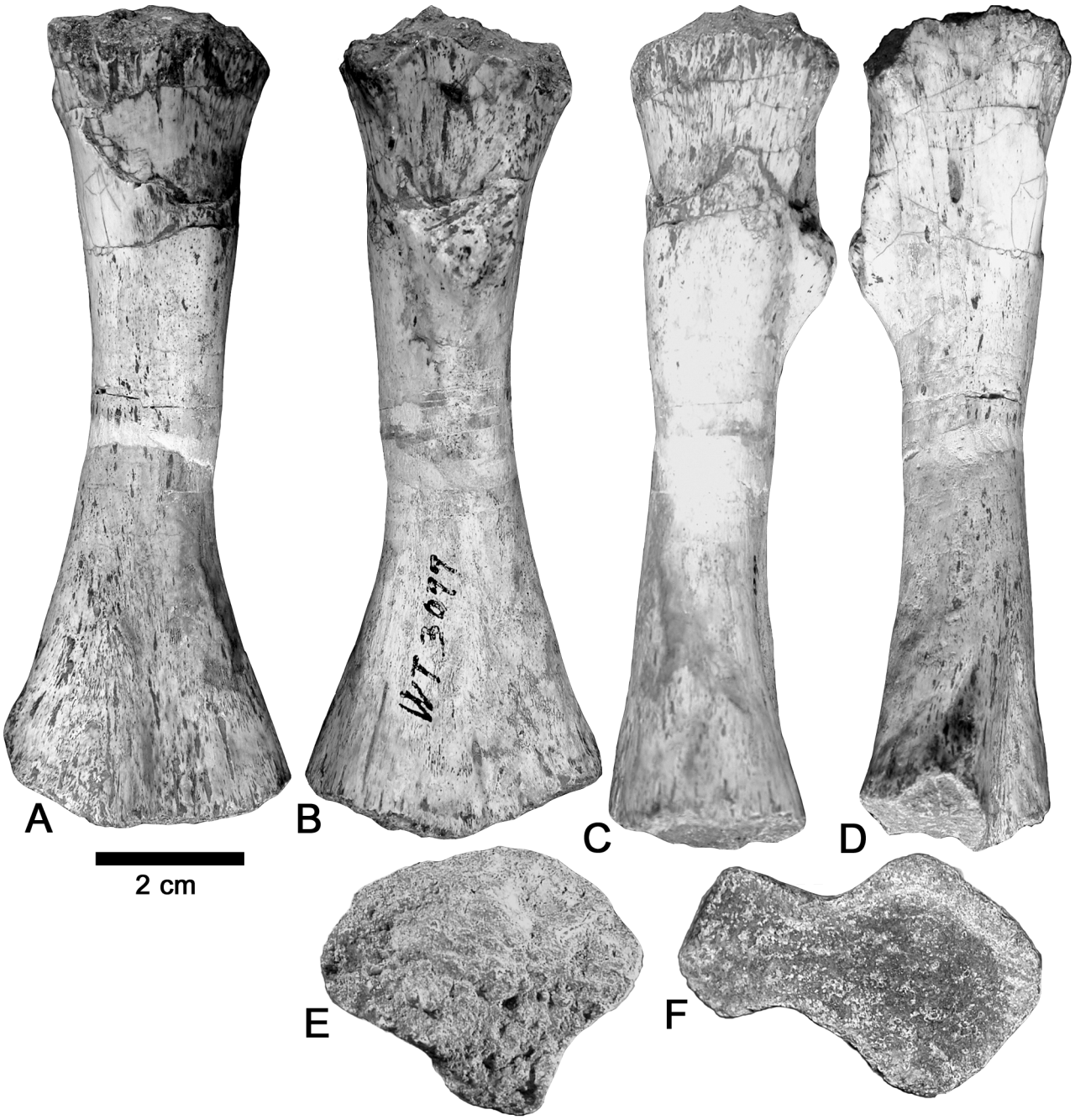

FIGURE 69. *Koskinonodon perfectum,* WT 3077, right femur from the Rotten Hill bonebed in **A**, dorsal, **B**, ventral, **C**, anterior, **D**, posterior, **E**, proximal and **F**, distal view.

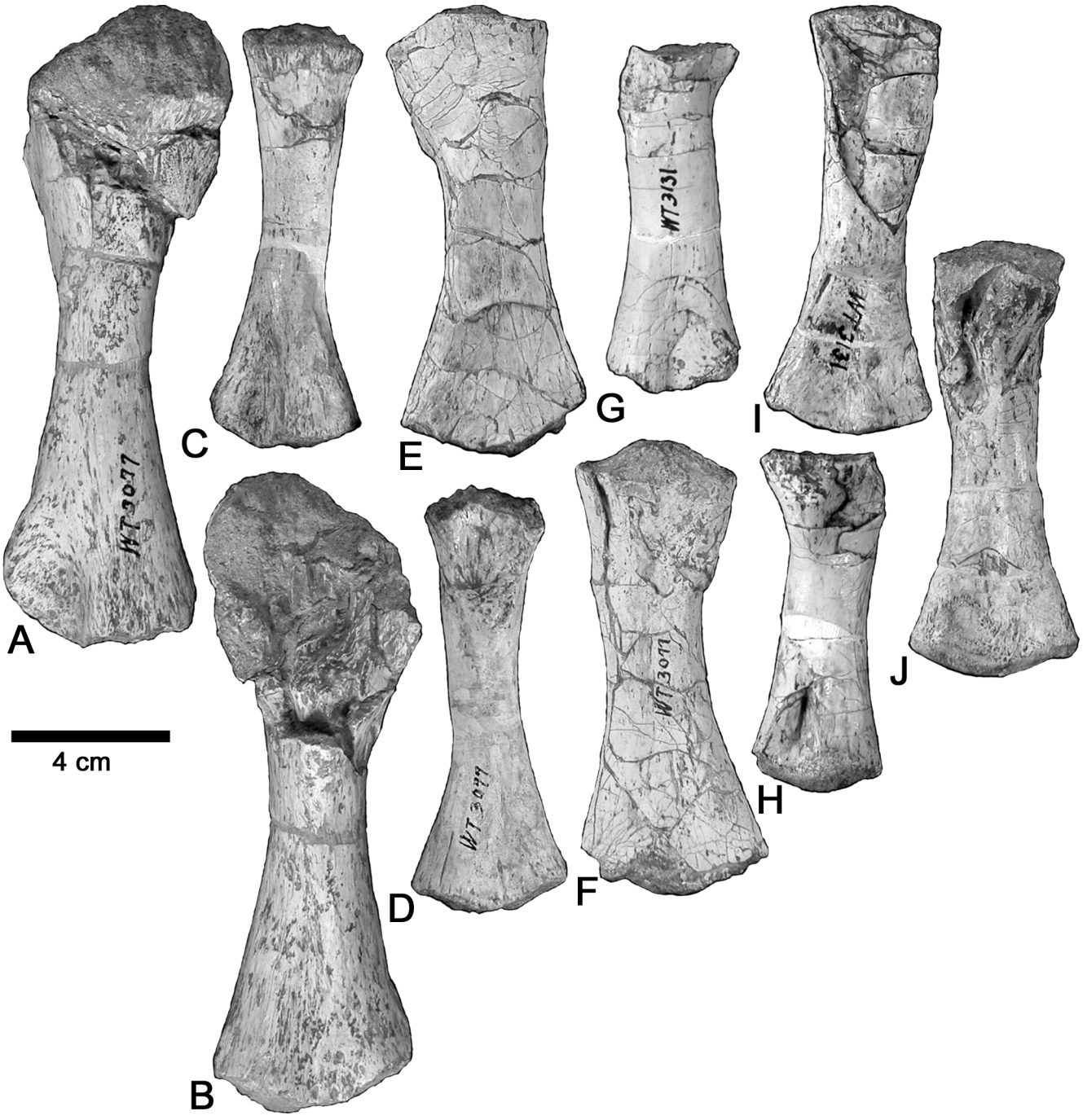

FIGURE 70. *Koskinonodon perfectum* femora from the Rotten Hill bonebed. **A-F**, WT 3077, three femora in **A**, **C**, **E**, dorsal and **B**, **D**, **F**, ventral view. **G-J**, WT 3131, two femora in **G**, **I**, dorsal and **H**, **J**, ventral view.

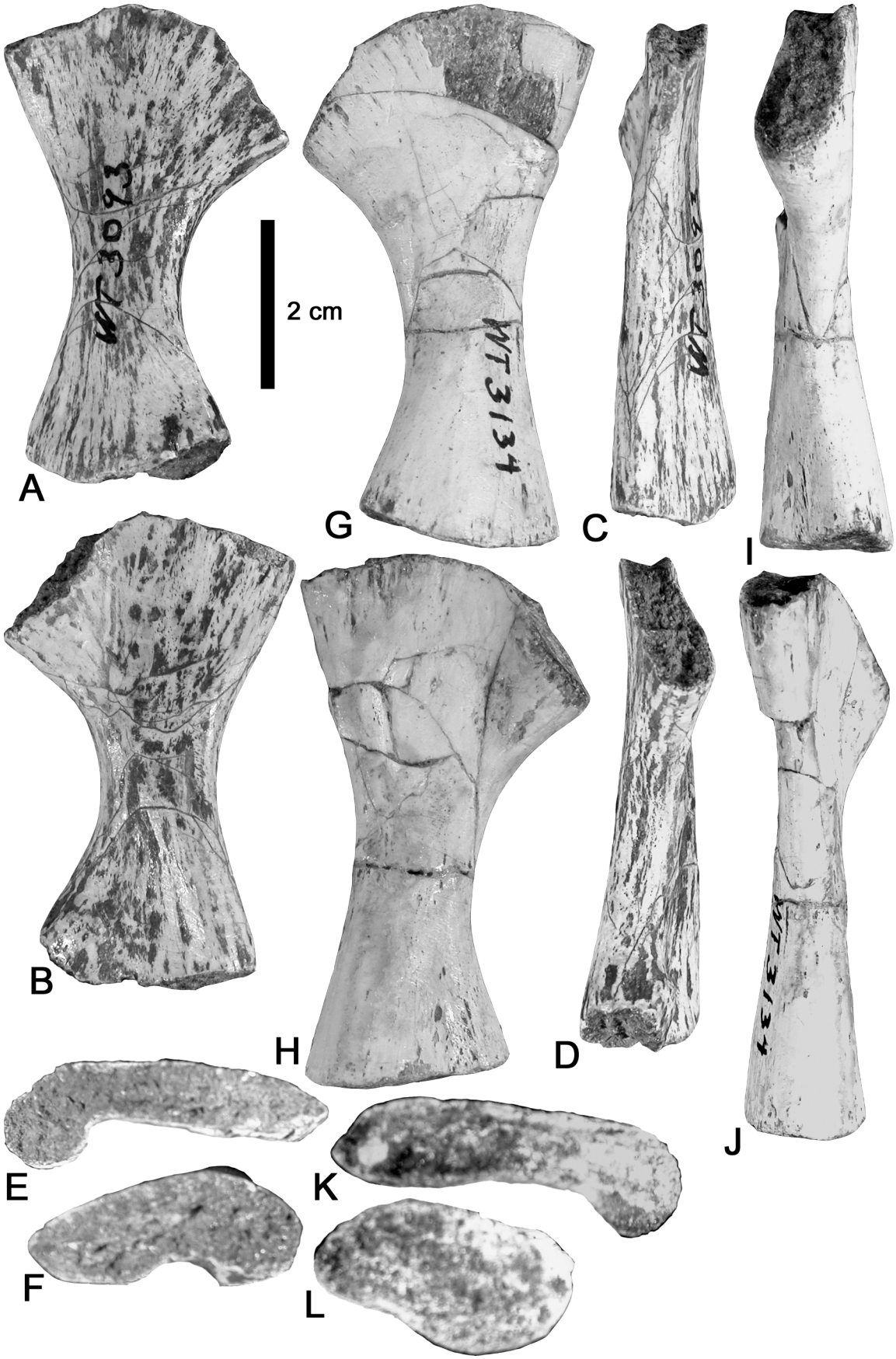

FIGURE 71. *Koskinonodon perfectum* tibiae from the Rotten Hill bonebed. **A-F**, WT 3093, left tibia. **G-L**, WT 3134, right tibia. Tibiae in **A**, **G**, medial, **B**, **H**, lateral, **D**, **I**, anterior, **C**, **J**, posterior, **E**, **K**, proximal and **F**, **L**, distal views.

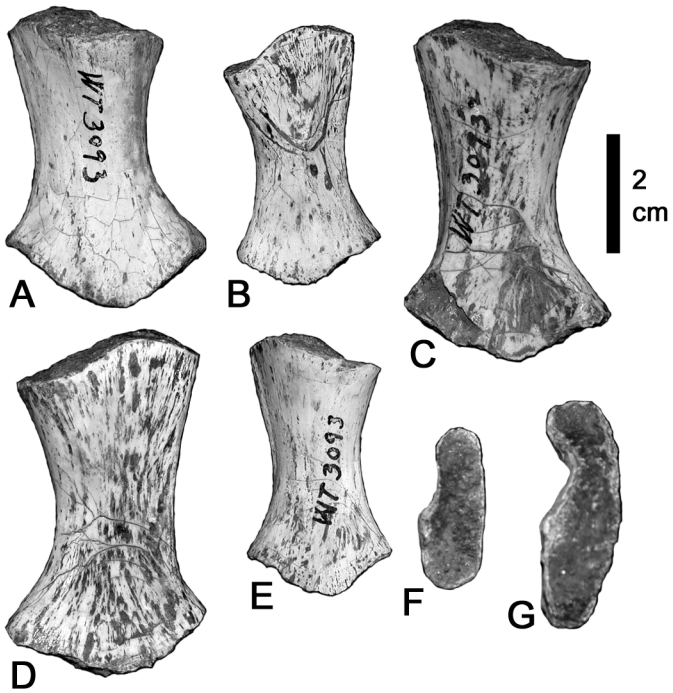

FIGURE 72. *Koskinonodon perfectum* fibulae from the Rotten Hill bonebed. **A-G**, WT 3093, three fibulae in **A**, **C, D**, lateral view, **B, E,** medial view, **F,** proximal view and **G**, distal view.

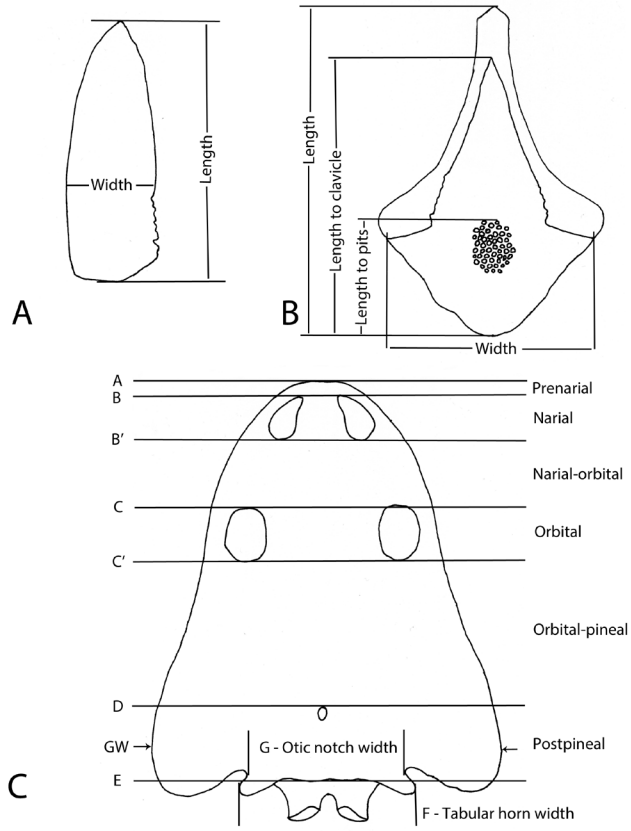

FIGURE 73. Measurement protocols. **A**, Clavicle; **B**, Interclavicle; and **C**, Skull; in which A = tip of snout; B = anterior limit of nares; B′ = posterior limit of nares; C = anterior limit of orbits; C′ = posterior limit of orbits; D = anterior limit of pineal foramen; E = posterior limit of midline suture; F = width across tabular horns; G = width across antero-medial limits of otic notches; A-B = prenasal length; A- C = preorbital length; A-D = prepineal length; A-E = skull length (midline length); GW = greatest width.

preserved than the juveniles in their more terrestrial environment away from the sedimentary processes of lakes and rivers. In the section on Growth, Variation, and Age Distribution we will discuss the ecological separation idea further and offer more evidence that the large assemblages of metoposaurs represent only adults, probably breeding populations.

GROWTH, VARIATION, AND AGE DISTRIBUTION

Introduction

Bonebeds such as Rotten Hill provide a rare but excellent opportunity to analyze ontogeny, growth, variation, and paleoecology (Brinkman et al., 2007). It is relatively rare for enough individuals to be present in a fossil sample to support statistical analysis. The large population of metoposaurs at Rotten Hill invites the use of statistical methods that require large populations for maximum accuracy. Properly applied, statistical methods can yield information on growth, demographics, ontogenetic life stages, sexual dimorphism, and other quantities and qualities (e.g., Stoddart, 1980; Oxnard, 1987; Bennett, 1995; Carrano, 1999; Rinehart and Lucas, 2001; Rinehart et al., 2001, 2002a, b, 2005, 2009; Lucas and Rinehart, 2005; Brinkman et al., 2007). Here, we attempt here to extract growth, variation, and age distribution from the Rotten Hill *Koskinonodon perfectum* data and to infer lifestyle information from these data.

Probablity Plotting

Harding (1949) showed that probability plots could be used to resolve the component modes of multimodal distributions. This method, and extensions and variants of it, have been used to define size groups and produce growth and demographic data for extant wild animal populations (e.g., Semlitsch, 1980), and we used it here to test for statistical size groupings in the metoposaur data. Statistically distinct size groups, which represent the component modes of the multimodal distribution of sizes that make up a population, plausibly correspond to age groups (Hunt, 1967; Raup and Stanley, 1971; Andrews, 1982; Bennett, 1995; Brinkman et al., 2007) and may thus be used to generate growth curves and age distributions, as we have in the past for the Triassic theropod *Coelophysis* (Rinehart et al., 2009).

It follows that if a breeding season exists in a group of animals, each yearly hatching or birthing (cohort) will constitute a statistical size group that, if indeterminate growth is present, remains distinct from older and younger cohorts throughout its lifetime. If the population is killed all at once, a "snapshot" of its yearly age groups may be preserved in the fossil record. Thus, in catastrophic assemblages, the age groups should be very apparent, whereas in attritional assemblages they may be less evident, but possibly still statistically resolvable. In animals that have indeterminate growth, the size groups may remain statistically separable for the lifespan of the animal if enough members of the size group survive. In animals that have determinate (asymptotic) growth, however, the size groups representing younger animals tend to "catch up" to those of the older animals that are approaching their growth asymptote. Ultimately, individual variation exceeds yearly growth, the size groups mix very thoroughly, and become statistically inseparable near the asymptote. In this case, only the asymptote itself may be resolved.

Other factors may create or accentuate the yearly size groups and produce stepwise growth curves. These include, among others, seasonal abundance of food, seasonal weather patterns (e.g., wet and dry seasons), estivation, and, after sexual maturity, the periodic alternation of energy resources between growth and reproduction (Andrews, 1982; Zug, 1993). Such size groups may be evident and resolvable, even in attritional assemblages (Brinkman et al., 2007).

Probability Plotting the Metoposaur Data

Clavicle width and interclavicle width were chosen for statistical testing because they provide the largest sample populations, and therefore the best resolution. These bones are also robust and relatively resistant to deformation that might skew measurements. As outlined above, probability plotting was used to test for and resolve size (= age) groups in the data. A very brief explanation of the probability plotting method is included here. It is by no means comprehensive and only attempts to elaborate on the specifics pertinent to interpreting the current *Koskinonodon perfectum* data.

Probability plotting is a simple, powerful, graphic method of comparing a data set to a statistical distribution function (King, 1971). A probability plot shows the probability (x axis) that a random observed

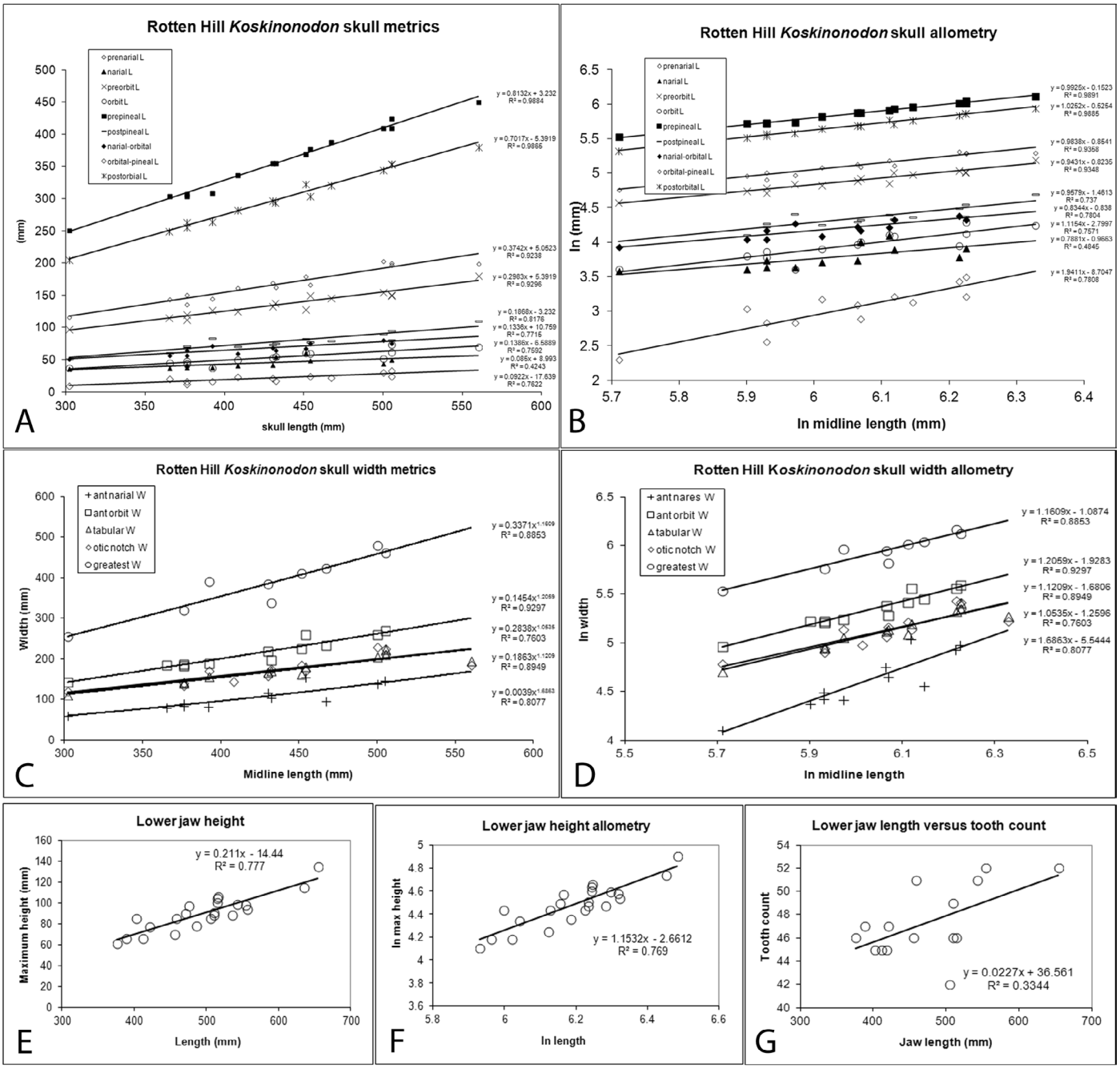

FIGURE 74. Scatterplots with linear curve fits showing metrics and allometry of the Rotten Hill *Koskinonodon perfectum* skulls and lower jaws. All measurements are in mm. **A**, Various skull length zone metrics versus midline length. **B**, Allometry of various skull metric zones. **C**, Skull width metrics measured at various landmarks versus skull midline length. **D**, Skull width allometry. **E,** Lower jaw height as a function of length. **F,** Lower jaw height allometry. **G,** Lower jaw tooth count versus jaw length.

variable will be less than or equal to a given value (y axis). Probability calculations are simple, and the plots are easily made by hand, but here we used KaleidaGraph (1997) graphic analysis software. The probability data are plotted against a scale that is related to a specific distribution function (e.g., normal, log normal, extreme value, etc.). Straight line fits of the data on a specific probability scale indicate that the data are distributed according to the function that is related to that scale. Departures from a straight line fit indicate that the data are skewed, truncated, multi-modal, or do not fit the distribution function. Each of these deviations produces a unique characteristic shape on the plot that may be further explored to reveal information about the nature of the distribution and the process or circumstances that produced it (Kock and Link, 1970; King, 1971).

Normal (Gaussian) probability plots of *Koskinonodon perfectum* clavicle and interclavicle widths (Fig. 78A-B) have several short "plateaus" that vary from horizontal to somewhat inclined. These indicate that the overall distribution of widths comprises several component modes (King, 1971). Smooth curves drawn through the data points show that the plateaus are connected by steep jogs that contain, when viewed from left to right, concave-up to concave-down inflections. These inflection points indicate the approximate "boundaries" of the component distributions (Harding, 1949; Peck, 1987; Knoop and Owen, 1994). Theoretically, the distributions expand infinitely in either direction from the mean, but given a finite data set, the inflection points provide a very good approximation of each component mode. Only the concave-up to concave-down inflections are used to show the component mode boundaries; concave-down to concave-up inflections (in the center of the plateaus) indicate the approximate mean of the components.

We separate the overall distributions (Fig. 78A-B) into their

TABLE 3. *Koskinonodon perfectum* clavicle width size (age) groups from the Rotten Hill sample. N = 46.

Age Group	Mean clavicle width (μ)	Standard deviation (σ)	Curve fit quality (R^2)	Population of group
1	109.67	3.34	0.967	6
2	126.9	4.48	0.931	10
3	139.33	2.43	0.957	12
4	150.78	3.57	0.939	9
5	159.5	1.46	0.906	8
6	165.89	1.84	0.849	9
7	175.67	1.24	0.894	12
8	187.0	2.08	0.922	5
9	200.5	0.81	0.62	4
10	209.5	0.74	1.0	2

TABLE 4. *Koskinonodon perfectum* interclavicle width size (age) groups from the Rotten Hill sample. N = 59.

Age Group	Mean interclavicle width (μ)	Standard deviation (σ)	Curve fit quality (R^2)	Population of group
1	219.0	4.47	1.0	2
2	239.33	2.07	0.75	3
3	254.67	2.52	0.95	9
4	274.0	7.46	0.963	8
5	292.56	3.04	0.797	9
6	309.87	3.93	0.913	8
7	330.0	4.96	0.905	5
8	341.8	2.34	0.847	5
9	360.5	4.56	0.767	4
10	376.0	3.75	0.952	4
11	397.5	3.72	1.0	2

components at the inflection points (marked by short horizontal bars in the figure) and replot each component (Fig. 78C-D). The straight line curve-fits to the components indicate that they have been correctly resolved and that they are distributed normally (Peck, D. S., 1988, pers. comm.). The upper- and lowermost components that contain only two members are, of course, very rough approximations. The mean value and standard deviation (σ) of each component may be read directly off the plot. The mean value occurs at the 50% probability point; +σ and -σ occur at the 84% and 16% probability points, respectively (King, 1971). For maximum accuracy, we used the coefficients of the linear curve fits (Fig. 78C-D) provided by the graphic analysis software.

Mean values, standard deviations, the population of each resolved size group, and the coefficient of variation are given for clavicle widths (Table 3) and interclavicle widths (Table 4). We have thus resolved the component modes that make up the overall distributions of widths, and for each of them we provide the three factors that uniquely define a distribution: shape (here, the normal or Gaussian bell curve), center (mean value in a symmetrical distribution), and width or variation (standard deviation). The coefficient of variation (CV), also provided (Tables 4-5), is a dimensionless quantity that is the standard deviation divided by the mean value and multiplied by 100 so as to express it as a percent of the mean.

$$CV = (\text{std. dev.}/\text{mean}) \cdot 100$$

This quantity is of greater utility than standard deviation when comparing variation in animals of different sizes because the size units have been removed (Simpson et al., 1960). The coefficient of variation within the resolved cohorts is quite small, typically 1% to 3%, and in a few cases less than 1%.

Analysis of variance (ANOVA) tests were applied to determine if there is a statistically significant difference between all of the resolved size groups (Zar, 1999). Holm's multiple comparison test was employed because it is the most accurate test where: (1) the data are normally distributed, (2) the groups are of unequal size, (3) and there are more than three or four groups to compare (Glantz and Slinker, 2001; Glantz, 2005). Complete statistical reports of the Holm's tests are given in Appendix 4. All of the resolved component size groups show statistically significant differences from each other at the 95% confidence level ($P \leq 0.05$).

Growth, Variation, and Age Distribution

We hypothesize that the most parsimonious interpretation of the existence of discrete size classes (the component modes) in both the clavicle and interclavicle data is that they represent the various cohorts that make up the total population. There are 10 resolvable component modes resolved from the clavicle data and 11 from the interclavicle data. We treat the mean values of these component modes as representative of the mean sizes of the yearly age groups and plot a growth curve for *Koskinonodon perfectum* based on clavicle and interclavicle widths (Fig. 79A). We do not assume isometric growth of these elements, but consider them to be generally indicative of overall growth in the animals.

TABLE 5. Life-stage sizes of various aquatic (cryptobranchid) and terrestrial (plethodontid) salamanders. All measurements in mm. Maximum length represents the largest recorded individual. Lengths are total length unless specified; SVL = snout-to-vent length. SML/HL, and LAL/SML are the growth factors between hatching and sexual maturity, and sexual maturity and large adult size (the largest normally encountered, not the absolute record holder), respectively. References: *Cryptobranchus alleganiensis, Necturus maculosus* and *Andrias japonicus*, (AmphibiaWeb, 2006); *Bolitoglossa rostrate* and *Plethodon cinereus* (Houck, 1977); *Chioglossa lusitanica* (Lima et al., 2000).

Taxon	Common name and/or -comment	Hatch Length	Sex Maturity Length	SML/ HL	Large Adult Length	LAL/SML	Max. Length
Cryptobranchus alleganiensis	Hellbender-aquatic	~ 29	~ 300	10.3	740	~ 2.5	
Necturus maculosus	Mudpuppy-aquatic	~ 23	~ 200	8.7	490	~ 2.5	
Andrias japonicus	Giant Japanese salamander -aquatic	30	~ 350	11.7	1020	~ 2.9	1440
Bolitoglossa rostrata	-terrestrial, female size		58 (SVL)		64 (SVL)	1.1	
Chioglossa lusitanica	Golden-striped salamander -terrestrial		~ 35		~ 47	1.3	
Plethodon cinereus	-terrestrial, female size		65 (SVL)		70 (SVL)	1.1	

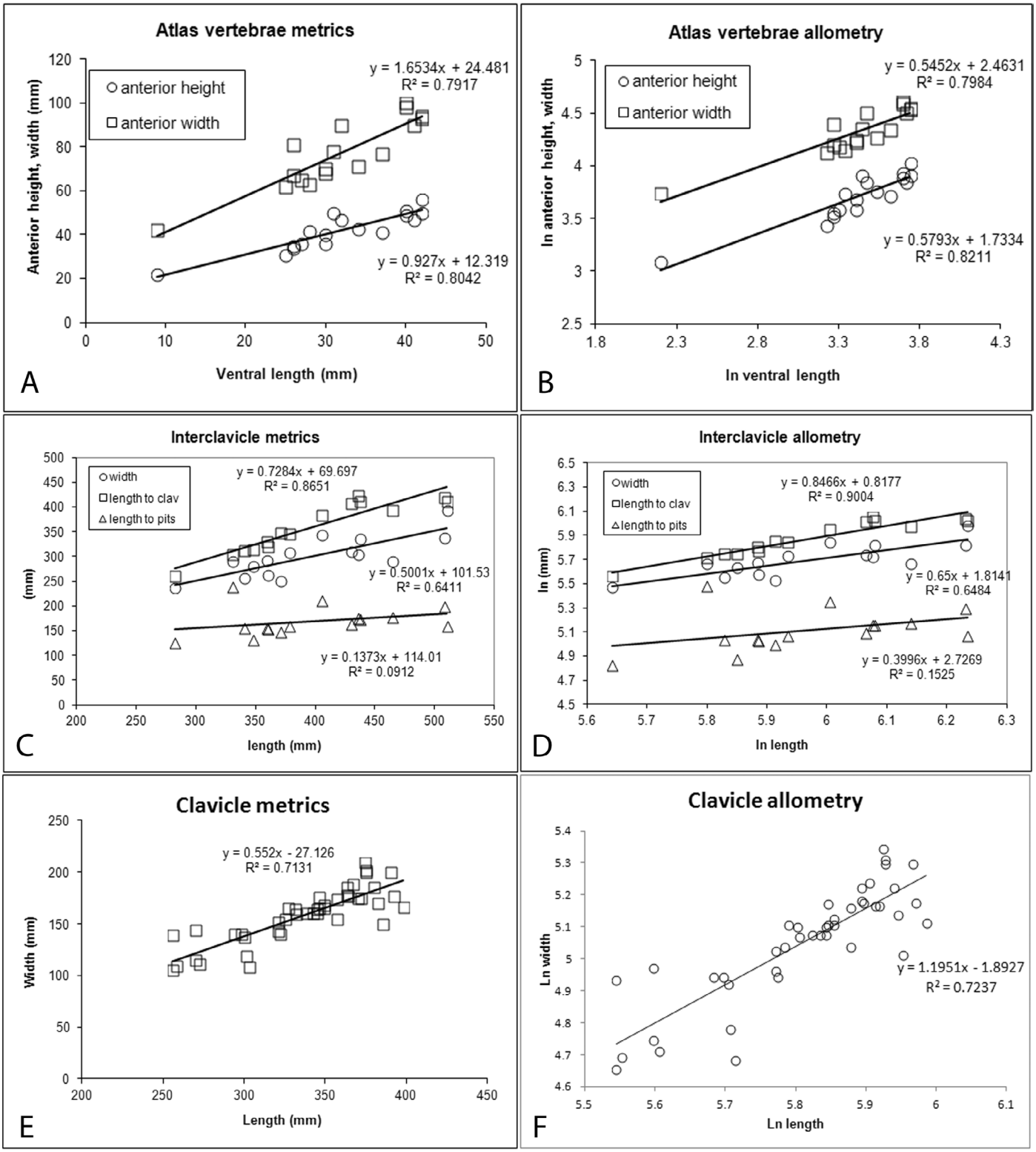

FIGURE 75. Postcranial metrics and allometry of *Koskinonodon perfectum* from the Rotten Hill bonebed. **A,** Atlas anterior height and width versus length. **B,** Atlas height and width allometry. **C,** Interclavicle various metrics versus length. **D,** Allometry of various interclavicle metrics. **E,** Width as a function of length in the clavicles. **F,** Clavicle width allometry. **G,** Ischium width as a function of length. **H,** Ischium width allometry. **I,** Ilium proximal and distal widths as a function of length. **J,** Ilium width allometry. **K,** Humerus proximal and distal widths as a function of length. **L,** Allometry of humerus proximal and distal widths. **M,** Various femur metrics versus length. **N,** Femur allometry. **O,** Tibia proximal and distal widths versus length. **P,** Allometry of the tibia proximal and distal widths.

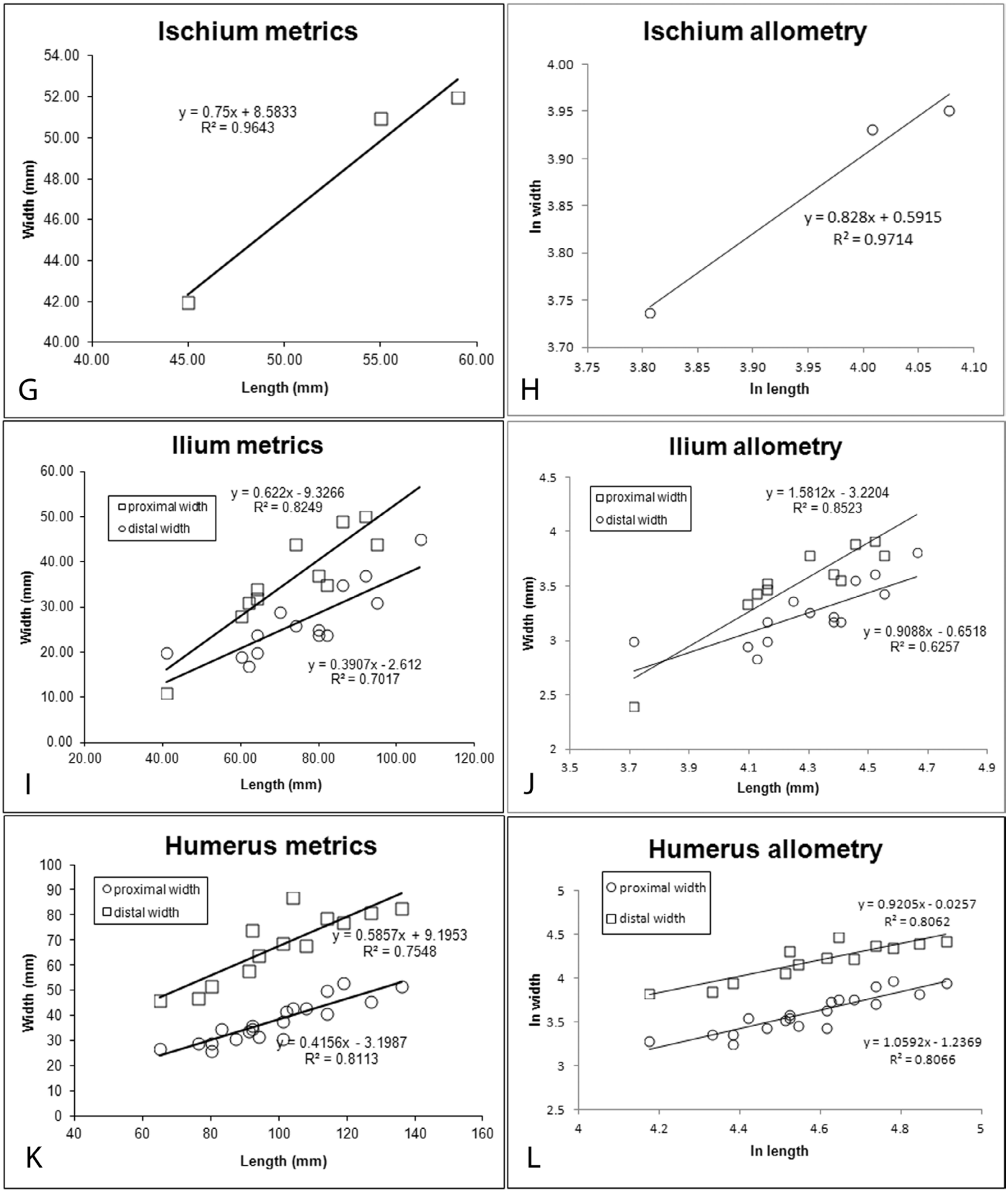

FIGURE 75 (Continued).

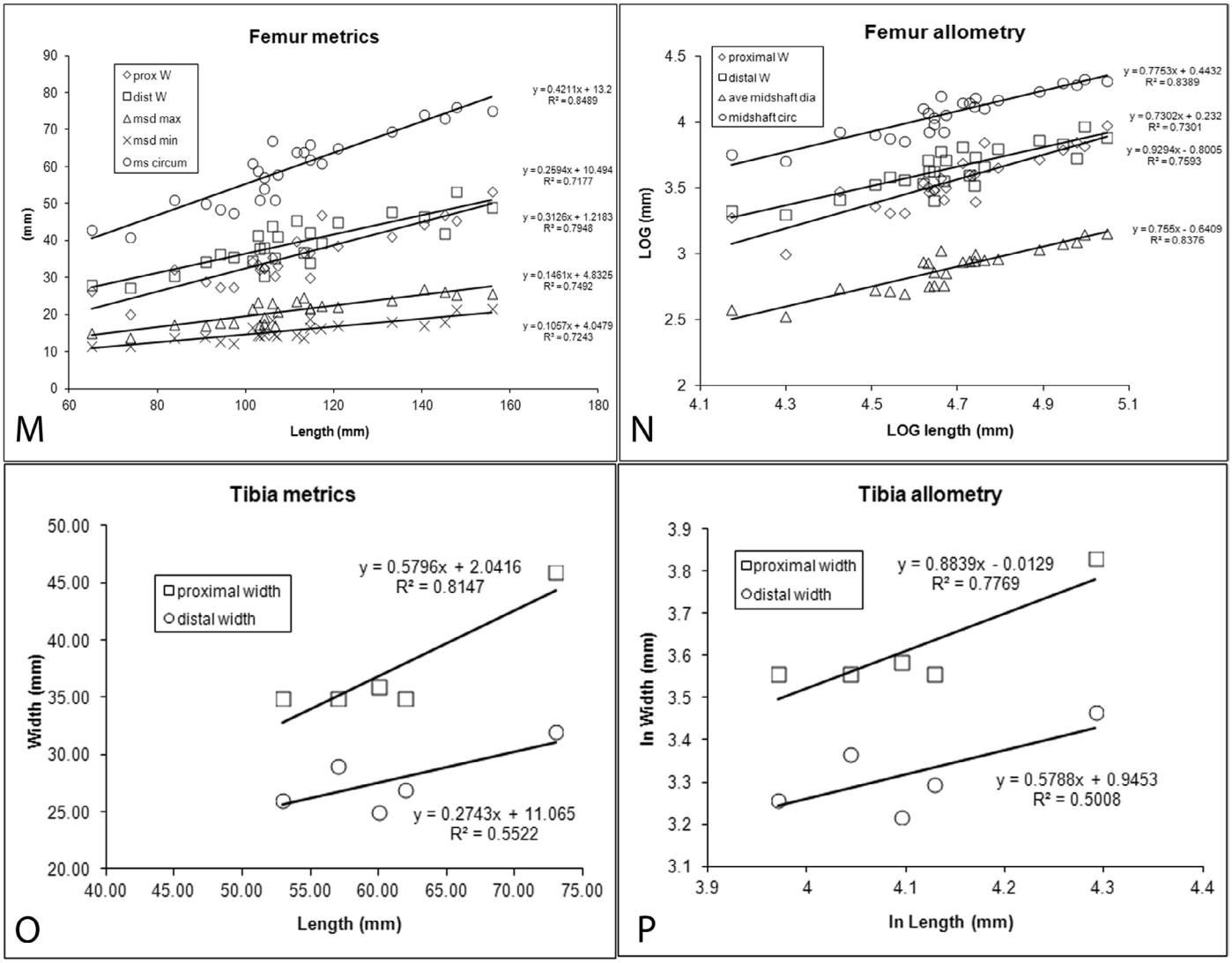

Figure 75 (Continued).

Both elements show straight-line growth. Growth is defined by the slope-intercept equations in Figure 79A over the range of ~ 110 to ~ 210 mm for the clavicle widths, and ~ 219 to ~ 398 mm for the interclavicle widths. This range apparently represents 10 and 11 years, respectively. The size increases by a factor of ~ 1.9 and ~ 1.8, respectively, for the clavicles and interclavicles during this time period. Mass typically increases as the cube of the linear dimensions (Gould, 1966; Thompson, 1942), so the mass of the animals in this study may have increased by a factor of 6 (1.8^3) or 7 (1.9^3) over the size range.

We use the population of each of the age groups in both the clavicle and interclavicle data (Tables 3-4) to produce an age distribution plot (Fig. 79B). Both clavicle- and interclavicle-based age distributions show similar overall form (dashed line in Fig. 79B). Initially, there is a one or two year build-up in the population; then a largely stable period of four or five years represented by an approximately horizontal plateau; finally, a drop-off to near zero population occurs in another four or five years.

Discussion

Indeterminate growth in *Koskinonodon perfectum* is indicated by both the probability plots (Fig. 78A-B) and the growth curves (Fig. 79A). If growth were determinate, the probability plots would show truncation of the size distributions at the growth asymptote by bending over toward the horizontal. No such truncation is seen in the plots. Likewise, in determinate growth the growth curves would not be linear, but would show an asymptotic approach to a maximum size.

As shown by the growth curves, the smallest size groups of the Rotten Hill metoposaurs have clavicles that average 109.7 mm wide, and interclavicles that average 219 mm wide (Tables 3-4), so the smallest animals in the sample would have a shoulder girdle over 30 cm wide. These would not represent small juveniles; the smallest animals are missing from the sample. We suggest that the age distribution in Figure 79B represents only sexually mature animals. Other hypotheses, such as collection bias or taphonomic bias, will also be addressed, but we feel that these can be ruled out. Thus, the following discussion focuses on the hypothesis of niche separation of juveniles and adults.

In some modern amphibians, separation of the juveniles and adults by a feeding strategy or other ecological factor is the norm, and there is evidence for this type of separation in some fossil populations (Olson, 1951; Cruickshank and Skews, 1980). Such separation may reduce predation of the juveniles by conspecifics, which is common in some extant amphibians such as the large aquatic salamanders (AmphibiaWeb, 2006).

Being of similar body plan and habitat, salamanders may be a reasonable analog for metoposaurs. We offer comparisons to extant salamander populations in support of the idea that only adults are present in the Rotten Hill data. Although the large aquatic salamanders may be better suited for comparison, these are difficult to study, and little detailed information is available in the literature and databases; therefore, we have included some terrestrial species.

The overall shape of an age distribution of a wild, adult breeding population of *Chioglossa lusitanica* (golden-striped salamander) is very similar to our metoposaur age distribution (Lima et al., 2001). We replotted the Lima et al. (2001) data for direct comparison to our *Koskinonodon perfectum* data (Fig. 79C). These animals mature 3 years after hatching, and have a lifespan of ~ 8 years. Their adult (breeding

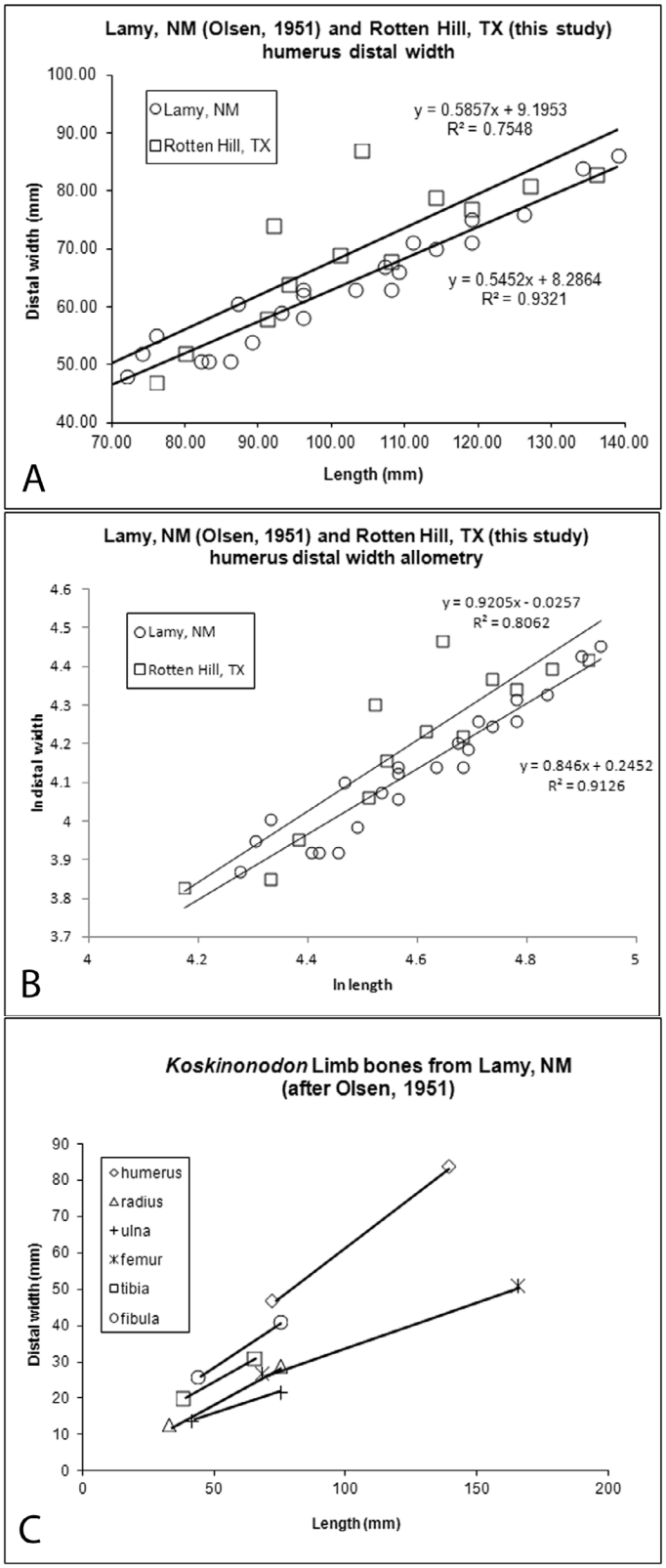

FIGURE 76. Comparison of Lamy amphibian quarry and Rotten Hill quarry *Koskinonodon perfectum* limb bones. **A**, Humerus proximal and distal width versus length in the two populations. **B**, Comparison of relative growth in the humerus of both populations. **C**, Size range and metrics of *Koskinonodon* bones from Lamy, NM. The raw data for the Lamy quarry are from Olsen's (1951, tables 1-2) published size range and linear regression coefficients.

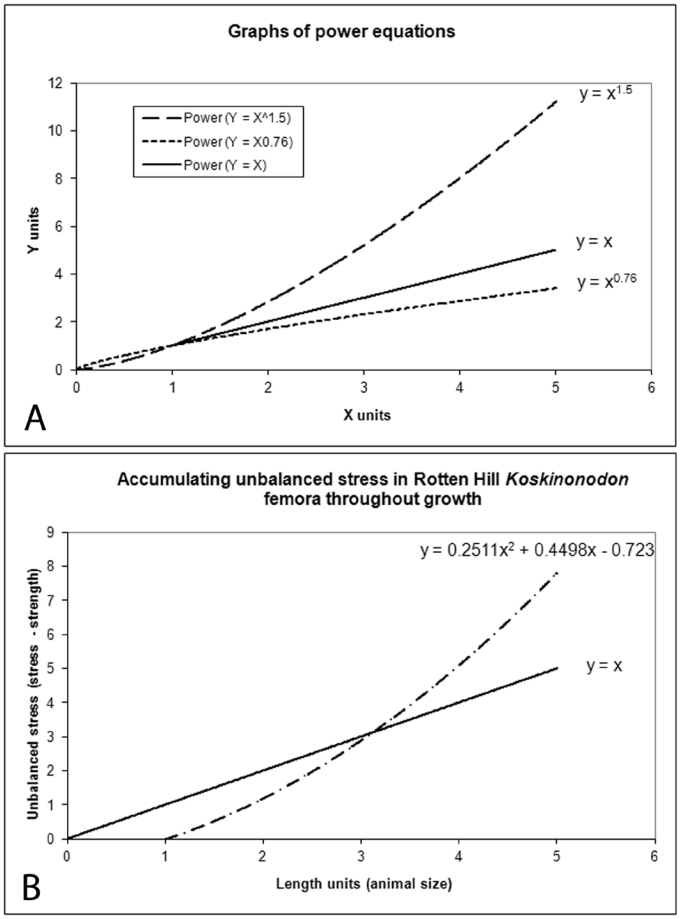

FIGURE 77. Power curves exemplify the stress-strength relationship in *Koskinonodon perfectum* femora throughout growth. The exponent of the power curve equals the allometric growth constant. **A,** An exponent of 1.5 (dashed line), producing a concave-up curve, is required to maintain constant stress throughout growth. This curve shows femur stress accumulating at a constantly increasing rate throughout growth. An exponent of approximately 1 (solid line), is observed in most animals and requires behavioral changes during growth to accommodate increasing stress. An exponent of 0.76 is observed in *K. perfectum* and indicates an extreme deficiency in strength to meet the increasing stress. This concave-down curve continually flattens and shows that the inability of the femora to support the animal worsens at an increasing rate throughout growth. **B,** This (dashed) curve shows the rate at which excess stress (stress that is not balanced by an opposing strength) would accumulate in the femora of *K. perfectum* if they had to support the animal throughout growth. In these graphs, the units are arbitrary, the curve shapes are pertinent.

population) age distribution shows a one year buildup, followed by a three year stable period, and finally a two year decline to zero population. The most significant difference in the age distributions of this wild salamander population and that of the metoposaurs is the timescale; the overall shapes are strikingly similar (compare Figs. 79B and C). Presumably, in both the metoposaurs and salamanders the short population buildup period represents the time during which newly matured, young adults are joining the group. The stable plateau would represent animals in the "prime-of-life;" the strong, young to middle-aged adult size range. The declining population period no doubt represents the onset of senescence and succumbing to predation, accumulated traumas, injuries, or disease.

We also compared the life-stage size ranges of some extant salamanders to that of the Rotten Hill metoposaurs. Data were collected for several species of large aquatic and smaller terrestrial salamanders (Table 5). In each of the large aquatic species (Hellbenders, Mudpuppies, and giant Japanese salamanders, the genera *Cryptobranchus*, *Necturus*, and *Andrias*, respectively) length increases by a factor of ~ 10 between

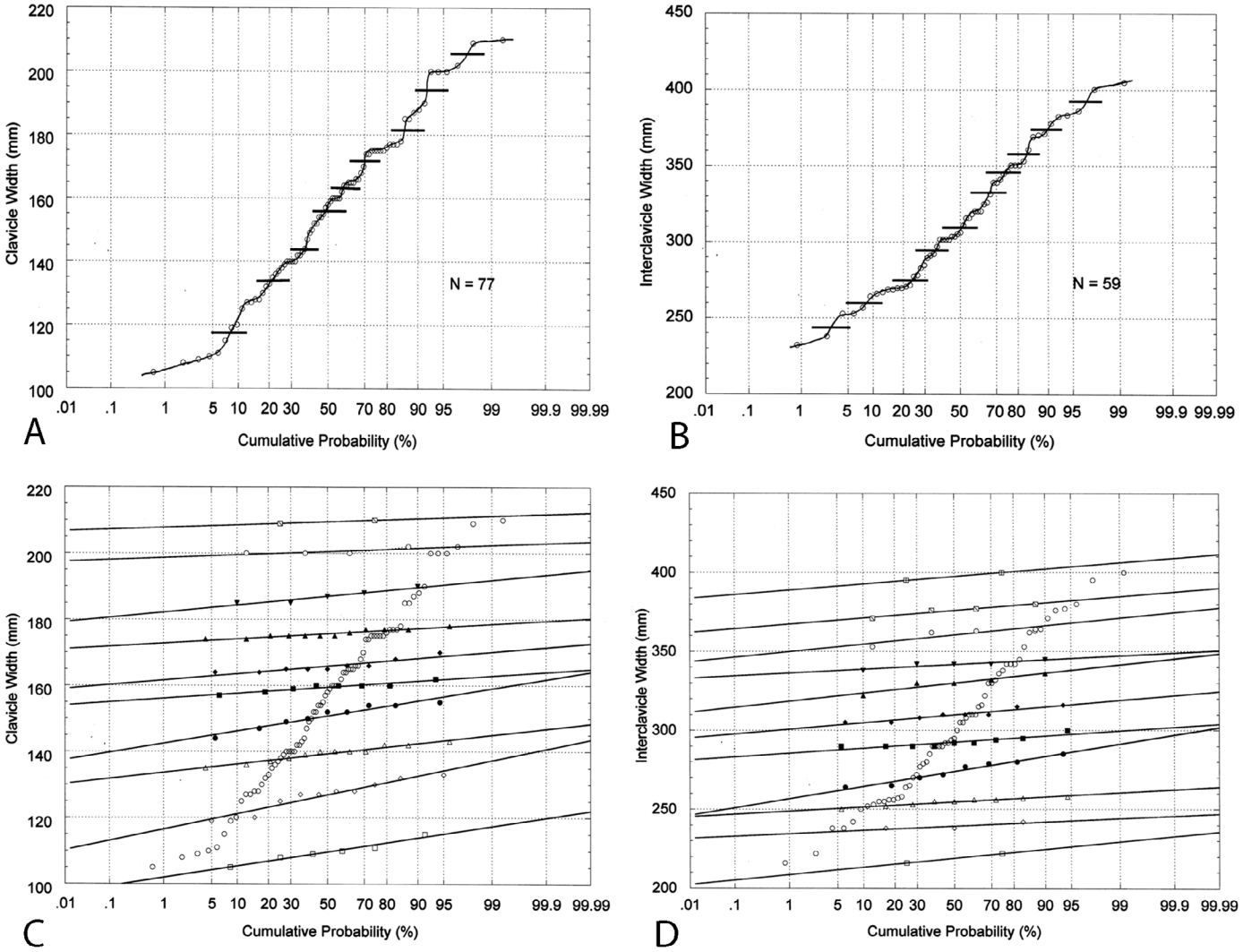

FIGURE 78. Probability plots showing the multimodal distribution of clavicle and interclavicle widths of *Koskinonodon perfectum*. **A,** Clavicle widths with a smooth curve drawn through the data points and the concave-up to concave-down inflections marked by horizontal bars. **B,** Interclavicle widths with a similar smooth curve and inflection markers. **C,** Probability plot showing the multimodal distribution of all clavicle widths with overlying resolved component modes and their linear curve fits. **D,** Probability plot of interclavicle widths with resolved component modes.

hatching and sexual maturity (column SML/HL) (AmphibiaWeb, 2006). Between sexual maturity and large adult size, length increases by a factor of ~ 2.5 to ~2.9 for the large aquatic animals and 1.1 to 1.3 for the smaller terrestrial varieties (column LAL/SML) (AmphibiaWeb, 2006). Recalling that the metoposaur clavicle and interclavicle growth data show width increasing by a factor of 1.8 to 1.9 over the range of sizes, we see the growth factor of the Rotten Hill metoposaurs bracketed by the adult growth factor of extant salamanders (Fig 79D).

The skulls of very small *Koskinonodon perfectum* are recognizable at the species level (Davidow-Henry, 1989; Morales, 1993; Zanno et al., 2002), so there is no evidence of a global metamorphosis that would render the small juveniles unrecognizable. The Rotten Hill quarry contains many very small bony elements belonging to other species. If small juvenile metoposaurs had been present in the Rotten Hill quarry, their presence would be obvious. We hypothesize, based on comparison to the adult growth factor of salamanders and the shape of wild adult population age distributions, that the Rotten Hill sample represents only breeding adults. The age axis in Figure 79B then represents age after sexual maturity and indicates that the animals survived at least 10 or 11 years after maturity, perhaps longer. It seems that there is an enforced separation of adults and juveniles in these animals. No doubt, some individuals could have reached extraordinary size as seen in the maximum size of the Giant Japanese salamander *Andrias japonicus* and its Chinese counterpart, *Andrias davidanus*, in which 1.8 m-long individuals have been reported (AmphibiaWeb, 2006). Such extreme outliers, however, would not be expected in our sample size of ≤ 68, although it may account for truly gigantic temnospondyls such as the specimen documented by Steyer and Damiani (2005).

We show a growth curve that is typical of reptiles and amphibians that have indeterminate growth (after Zug, 1993) (Fig. 80). We thus infer that the Rotten Hill metoposaurs show indeterminate growth and that they reside on the straight line portion of the curve above the "knee" where sexual maturity occurs.

Comparison to *Dutuitosaurus*—Steyer et al. (2004) studied growth in *Dutuitosaurus ouazzoui,* which is similar in overall size to *Koskinonodon perfectum*. Similar size is apparent in the skull lengths. The average skull length of *D. ouazzoui* is 465 mm (N = 15) (Dutuit, 1976, table 3), whereas in the *K. perfectum* Rotten Hill sample, the average skull length is 433 mm (N = 14); ~ 7% smaller. Based on histology and external morphology, Steyer et al. (2004) placed the demarcation between juvenile and adult femora in *D. ouazzoui* at ~ 100 mm length. Our *K. perfectum* femora span the length range from 90 to 151 mm, which again supports the idea that juveniles are not present; considering the fact that *K. perfectum* appears to be slightly smaller than *D. ouazzoui*, the evidence is even more convincing.

Similar to our growth curve based on the statistical method, Steyer et al.'s (2004) histological study produced a practically straight-line growth plot for *Dutuitosaurus*. They chose a second order polynomial

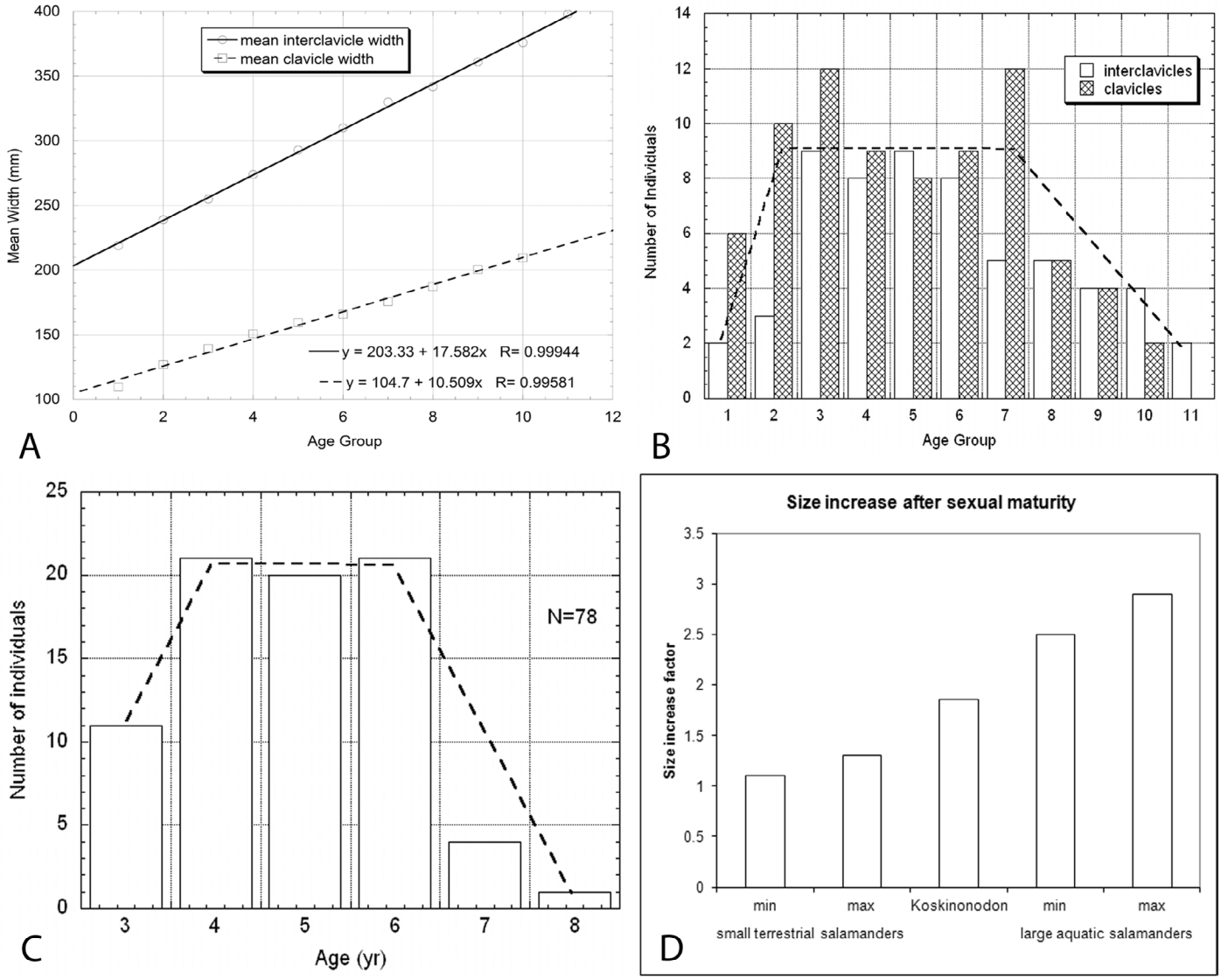

FIGURE 79. Growth, age distribution and size increase of *Koskinonodon perfectum* after sexual maturity. **A,** Clavicle and interclavicle growth curves based on the resolved age groups (~years after joining the Rotten Hill population, not absolute numerical age). **B,** Age distribution of the Rotten Hill metoposaurs based on the populations of the resolved age groups in clavicles (crosshatched) and interclavicles (clear). **C,** Age distribution in an extant salamander population for comparison to the metoposaur data. **D,** Maximum and minimum size increase factor in small terrestrial and large aquatic salamanders compared to that of the Rotten Hill *Koskinonodon* population.

as a very slightly better fit to the data than the straight line equation, but the difference in R^2 between the two fits was only 0.016, and, given the sample size, this value is well inside the error bars.

The femoral lengths reported in the *Dutuitosaurus* data range from 63 to 157 mm, yielding a growth factor of 157/63 = 2.49 over a period of 10 years (span of 2 to 12 estimated LAGs in the histology study) (Steyer et al., 2004, table 1, fig. 5). Our growth factor of 1.8 or 1.9 over a period of 10 or 11 years in *Koskinonodon perfectum* is somewhat lower but generally similar.

Summary—We have extracted age groups (cohorts) from biometric data of *Koskinonodon perfectum* using probability plots. The resolved age groups produce a growth curve that is linear and that shows a relative growth and relative size range that coincide well with the adult size ranges of extant salamanders and the histologically determined growth of *Dutuitosaurus*. An age distribution derived from the resolved metoposaur age group populations has distinct similarity to the age distribution of some extant adult salamanders. Size variation within the cohorts, expressed as CV, is small, typically 1% to 3%.

We hypothesize that the relatively large size of the smallest individuals in the Rotten Hill *Koskinonodon perfectum* population, the size range, growth rate, and age distribution shape all indicate that only a sexually mature breeding population is present. There is, no doubt, a mechanism such as feeding strategy, greater terrestriality, or other ecological factor that enforced separation of adults and juveniles, probably resulting in reduced predation of juveniles by conspecific adults and reduction of competition for food resources between the immature and mature groups.

CONCLUSIONS

1. Rotten Hill is a Late Triassic bonebed in the Texas Panhandle discovered by Floyd V. Studer in 1926, and collected primarily by WPA-funded excavations during the late 1930s-early 1940s.
2. The Rotten Hill bonebed is in the upper part of the Tecovas Formation (Chinle Group) and is of Adamanian (late Carnian) age. Forensic taphonomic analysis indicates it is a mass death assemblage that was hydraulically concentrated.
3. The Rotten Hill bonebed is a low diversity multitaxic and monodominant bonebed; the vast majority of the bones are of the metoposaurid *Koskinonodon perfectum*.
4. It closely resembles other Chinle Group metoposaurid-dominated bonebeds that suggest aggregation of a group of metoposaurids (cause unknown), followed by catastrophic mortality, complete disarticulation and disassociation of the skeletons and culminated by rapid transport and burial.
5. Fossil taxa from the Rotten Hill bonebed are the unionoidan *Plesioelliptio* sp., the coprolite ichnogenera *Alacocopros*, *Eucoprus*

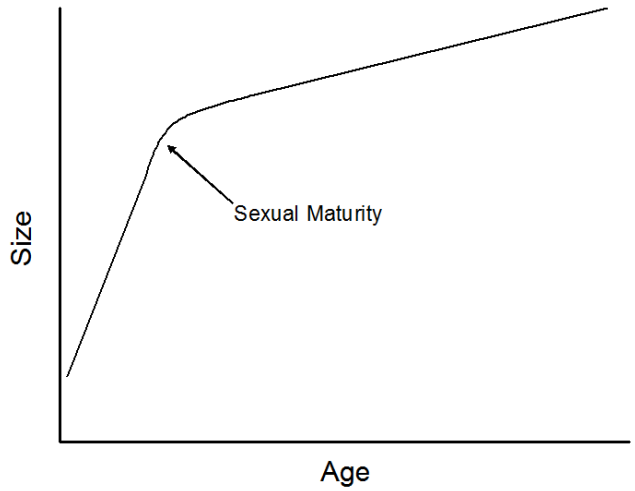

FIGURE 80. A generic indeterminate growth curve similar to that proposed for the Rotten Hill *Koskinonodon* population (after Zug, 1993).

and *Heteropolacopros*; various fishes; a rhynchosaur; a sphenodontid; the archosauriform *Vancleavea;* the trilophosaurs *Spinosuchus* and *Trilophosaurus*; the "rauisuchian" cf. *Postosuchus*, the phytosaur *Smilosuchus*; the aetosaurs *Desmatosuchus* and cf. *Stagonolepis*; a shuvosaurid; and the metoposaurids *Apachesaurus gregorii* and *Koskinonodon perfectum*.

6. Numerous skulls, lower jaws, vertebrae, girdle and limb bones of *Koskinonodon perfectum* represent a minimum number of 68 individuals. We describe the osteology and variation of these bones, which allows us to present a revised diagnosis of *Koskinonodon* that employs new postcranial characters to differentiate it from other metoposaurid genera.

7. We also compiled and analyzed a morphometric database of the Rotten Hill *Koskinonodon* to conclude that bone growth varied from isometry to allometry and suggest a loss in limb robustness during ontogeny that likely indicates a transition from a partly terrestrial to a more aquatic lifestyle.

8. Probability plotting of clavicle and interclavicle measurements in the Rotten Hill *Koskinodonon* sample identifies 10-11 groups that we interpret as yearly age groups and use to plot a growth curve. This indicates indeterminate growth in *K. perfectum* and that the Rotten Hill sample represents a population of breeding adults that survived at least 10-11 years after reaching sexual maturity. This type of growth curve is characteristic of some living salamanders.

9. We infer that *Koskinonodon perfectum* employed some mechanism such as feeding strategy, or another ecological factor that enforced separation of adults and juveniles, probably to reduce predation of juveniles by conspecifics and reduce the competition for food resources between the size classes.

ACKNOWLEDGMENTS

We owe a heavy debt to Jeff Indek and his volunteers for access to and loans of the Rotten Hill specimens, as well as access to the records and archives of the Panhandle Plains Historical Museum. Greg Gunnell made possible study of the UMMP collection, and Mark Norrell granted access to the AMNH collection. Julien Kimmig, Silvio Renesto and Robert Sullivan provided helpful reviews of the manuscript.

REFERENCES

Alexander, R. M., 1977, Allometry of the limbs of antelopes (Bovidae): Journal of Zoology, London, v. 183, p. 125-146.

AmphibiaWeb, 2006, Information on amphibian biology and conservation (web application), Berkeley, CA: AmphibiaWeb.

Andrews, R. M., 1982, Patterns of growth in reptiles; *in* Gans, C., and Pough, F. H., eds., Biology of the Reptilia Vol. 13 Physiology D: London, Academic Press, p. 273-321.

Aslan, A. and Behrensmeyer, A. K., 1996, Taphonomy and time resolution of bone assemblages in a contemporary fluvial system: The East Fork River, Wyoming: Palaios, v. 11, p. 411-421.

Behrensmeyer, A. K., 1975, The taphonomy and paleoecology of Plio-Pleistocene vertebrate assemblages east of Lake Rudolph, Kenya: Bulletin of the Museum of Comparative Zoology, v. 146, p. 473-578.

Behrensmeyer, A. K., 1978, Taphonomic and ecologic information from bone weathering: Paleobiology, v. 4, p. 150-162.

Behrensmeyer, A. K., 1988, Vertebrate preservation in fluvial channels: Palaeogeography, Palaeoclimatology, Palaeoecology, v. 63, p. 188-199.

Behrensmeyer, A.K., 1991, Terrestrial vertebrate accumulations; *in* Allison, P. and Briggs, D.E.G., eds., Taphonomy: Releasing the Data Locked in the Fossil Record. Plenum Press, New York, p. 291-335.

Behrensmeyer, A.K., 2007, Bonebeds through time; *in* Rogers, R.R., Eberth, D.A. and Fiorillo, A.R., eds., Bonebeds: Genesis, Analysis, and Paleobiological Significance. University of Chicago Press, Chicago, p. 65-101.

Bennett, S. C., 1995, A statistical study of *Ramphorynchus* from the Solnhofen Limestone of Germany: Year-classes of a single large species: Journal of Paleontology, v. 69, p. 569-580.

Biewener, A. A., 1983, Allometry of quadrupedal locomotion: The scaling of duty factor, bone curvature and limb orientation to body size: Journal of Experimental Biology, v. 105, p. 147-171.

Blakey, R.C. and Gubitosa, R., 1983, Late Triassic paleogeography and depositional history of the Chinle Formation, southern Utah and northern Arizona; *in* Reynolds, M.W. and Dolly, E. D., eds., Mesozoic Paleogeography of West-central United States. SEPM, Rocky Mountain Section, Denver, p. 171-187.

Blakey, R. C. and Gubitosa, R., 1984, Controls of sandstone body geometry and architecture in the Chinle Formation (Upper Triassic) Colorado Plateau: Sedimentary Geology, v. 38, p. 51-86.

Blob, R. W., 1997, Relative hydrodynamic dispersal potentials of soft-shelled turtle elements: Implications for interpreting skeletal sorting of non-mammalian terrestrial vertebrates: Palaios, v. 12, p. 151-164.

Branson, E. B. and Mehl, M. G., 1929, Triassic amphibians from the Rocky Mountain region: The University of Missouri Studies, v. 4, p. 155-255.

Brinkman, D.B., Eberth, D.A. and Currie, P.J., 2007, From bonebeds to paleobiology: Applications of bonebed data; *in* Rogers, R.R., Eberth, D.A. and Fiorillo, A.R., eds., Bonebeds: Genesis, Analysis, and Paleobiological Significance. University of Chicago Press, Chicago, p. 221-263.

Browne, R.K., Li, H., Wang, Z., Okada, S., Hime, P., McMillan, A., Wu, M., Diaz, R., McGinnity, D., and Brigger, J.T., 2014, The giant salamanders (Cryptobranchidae): Part B. Biogeography, ecology and reproduction, Amphibian and Reptile Conservation, v. 5, p. 30-50.

Camp, C. L., 1930, A study of the phytosaurs with description of new material fro0m western North America: Memoirs of the University of California, v. 10, p. 1-161.

Camp, C. L. and Welles, S. P., 1956, Triassic dicynodont reptiles, Part I, the North American genus *Placerias*: Memoirs of the University of California, v. 13, p. 255-304.

Carrano, M. T., 1999, What, if anything, is a cursor? Categories versus continua for determining locomotor habit in mammals and dinosaurs: Journal of the Zoological Society of London, v. 247, p. 29-42.

Case, E. C., 1922, New reptiles and stegocephalians from the Upper Triassic of western Texas: Carnegie Institution Publication, v. 321, p. 84.

Case, E. C., 1927, The vertebral column of *Coelophysis* Cope: Contributions from the Museum of Paleontology, University of Michigan, v. 2, p. 209-222.

Case, E. C., 1931, Description of a new species of *Buettneria*, with a discussion of the brain case: Contributions from the Museum of Paleontology, University of Michigan, v. 3, p. 187-206.

Case, E.C., 1932. A collection of stegocephalians from Scurry County, Texas: Contributions of the Museum of Paleontology, University of Michigan, no. 4, p. 1-56.

Case, E. C. and White, T. E., 1934, Two new specimens of phytosaurs from the Upper Triassic of western Texas: Contributions of the Museum of Paleontology, University of Michigan, v. 4, p. 133-142.

Cavin, L., Suteethorn, V., Buffetaut, E., and Tong, H., 2007, A new Thai Mesozoic lungfish (Sarcopterygii, Dipnoi) with an insight into post-Palaeozoic dipnoan evolution: Zoological Journal of the Linnean Society, v. 149, p. 141-177.

Colbert, E. H., 1989, The Triassic dinosaur *Coelophysis*: Museum of Northern Arizona Bulletin, v. 57, 160 p.

Colbert, E.H. and Imbrie, J., 1956, Triassic metoposaurid amphibians: Bulletin of the American Museum of Natural History, v. 110, p. 405-452.

Cosgriff, J. W., 1972, *Parotosaurus wadei*, a new capitosaurid from New South Wales: Journal of Paleontology, v. 47, p. 1094-1101.

Cruickshank, A. R. I. and Skews, B. W., 1980, The functional significance of nectridean horns (Amphibia: Lepospondyli): Proceedings of the Royal

Society, London, v. B 209, p. 513-537.
Davidow-Henry, B., 1989, Small metoposaurid amphibians from theTriassic of western North America and their significance, *in* Lucas, S. G., and Hunt, A. P., eds., Dawn of the Age of Dinosaurs in the American Southwest: Albuquerque, New Mexico Museum of Natural History and Science, p. 278-292.
Deevey, E. S., Jr., 1947, Life tables for natural populations of animals: Quarterly Review of Biology, v. 22, no. 4, p. 283-314.
Desojo, J. B., Heckert, A. B., Martz, J. W., Parker, W. G., Schoch, R. R., Small, B. J., and Sulej, T., 2013, Aetosauria: A clade of armoured pseudosuchians from the Late Triassic continental beds: Geological Society, London, Special Publications, v. 379, p. 203-239.
Dodson, P. 1971. Sedimentology and taphonomy of the Oldman Formation (Campanian), Dinosaur Provincial Park, Alberta (Canada). Palaeogeography, Palaeoclimatology, Palaeoecology, v. 10, p. 21-74.
Dorst, J., 1974, The Life of Birds, 2 vols. Columbia University Press, New York, 1600 pp.
Dubiel, R. F., 1989, Depositional environments of the Upper Triassic Chinle Formation in the eastern San Juan Basin and vicinity, New Mexico: U. S. Geological Survey, Bulletin 1801B, p. 1-22.
Dunay, R. E., and Fisher, M. J., 1974, Late Triassic palynofloras of North America and their European Correlatives: Review of Palaeobotany and Palynology, v. 17, p. 179-186.
Dunay, R. E., and Fisher, M. J., 1979, Palynology of the Dockum Group (Upper Triassic), Texas, U.S.A.: Review of Palaeobotany and Palynology, v. 28, p. 61-82.
Dutuit, J.-M., 1976, Introduction a l'étude paléontologique du Trias continental Marocain. Description des premiers stegocephales recueillis dans le couloir d'Argana (atlas occidental): Mémoires du Muséum National d'Histoire Naturelle, Série C, Sciences de le terre, v. 36, p. 1-253.
Eberth, D.A. Shannon, M., Noland, B.G., 2007a, A bonebed database: Classification, biases, and patterns of occurrence; *in* Rogers, R.R., Eberth, D.A. and Fiorillo, A.R., eds., Bonebeds: Genesis, Analysis, and Paleobiological Significance. University of Chicago Press, Chicago, p. 103-219.
Eberth, D.A., Rogers, R.R., and Fiorillo, A.R., 2007b, A practical approach to the study of bonebeds; *in* Rogers, R.R., Eberth, D.A. and Fiorillo, A.R. eds., Bonebeds: Genesis, Analysis, and Paleobiological Significance. University of Chicago Press, Chicago, p. 265-331.
Erickson, G. M., Olson, K. H. 1996. Bite marks attributable to *Tyrannosaurus rex*: Preliminary description and implications. Journal of Vertebrate Paleontology, v. 16, p. 175-178.
Finch, W. I. and Wright, J. C., 1983, Measured stratigraphic sections of uranium-bearing Upper Triassic rocks of the Dockum basin, eastern New Mexico, West Texas, and the Oklahoma Panhandle with brief discussion of stratigraphic problems: U. S. Geological Survey, Open-file Report 83-701, 118 p.
Finch, W. I., Wright, J. C. and Davis, B. O., 1976, Unevaluated preliminary geologic cross section of uranium-bearing Upper Triassic rocks extending from Ute Reservoir, New Mexico, to Palo Duro Canyon, Texas: U. S. Geological Survey, Open-file Report 76-205, 1 sheet.
Fiorillo, A. R., 1984, An introduction to the identification of trample marks: Current Research University of Maine, v. 1, p. 47-48.
Fiorillo, A. R., 1987, Trample marks: Caution from the Cretaceous: Current Research in the Pleistocene, v. 4, p. 73-75.
Fiorillo, A. R., 1991, Prey bone utilization in predatory dinosaurs: Palaeogeography, Palaeoclimatology, Palaeoecology, v. 88, p. 157-166.
Fiorillo, A. R., Padian, K. and Musikasintorn, C., 2000, Taphonomy and depositional setting of the *Placerias* quarry (Chinle Formation, Late Triassic, Arizona): Palaios, v. 15, p. 373-386.
Glantz, S. A., 2005, Primer of Biostatistics: New York, McGraw-Hill, Inc., 520 p.
Glantz, S. A., and Slinker, B. K., 2001, Applied Regression and Analysis of Variance: New York, McGraw-Hill, Inc., 949 p.
Good, S. C., 1993, Molluscan paleobiology of the Upper Triassic Chinle Formation, Arizona and Utah [Ph.D. dissertation]: University of Colorado, Boulder, 276 p.
Good, S. C., 1998, Freshwater bivalve fauna of the Late Triassic (Carnian-Norian) Chinle, Dockum, and Dolores formations of the southwest United States; *in* Johnston, P. A. and Haggart, J. W., eds., Bivalves: An eon of evolution, Calgary, University of Calgary Press, p. 223-249.
Gould, C. N., 1907, The geology and water resources of the western portion of the Panhandle of Texas: U.S. Geological Survey Water-Supply and Irrigation Paper, v. 191, p. 70.
Gould, S. J., 1966, Allometry and size in ontogeny and phylogeny: Biological Reviews, v. 41, p. 587-640.
Gregory, J. T., 1945, Osteology and relationships of *Trilophosaurus*: University of Texas Publication, v. 4401, p. 273-359.
Gregory, J. T., 1980, The otic notch of metoposaurid labyrinthodonts; *in* Jacobs, L. L., ed., Aspects of Vertebrate History: Essays in Honor of Edwin Harris Colbert: Flagstaff, Museum of Northern Arizona Press, p. 125-136.
Hammer, Ø., and Harper, D.A.T., 2006, Paleontological Data Analysis, Blackwell Publishing - Replika Press Pvt. Ltd., Hong Kong, 351 p.
Harding, J. P., 1949, The use of probability paper for the graphical analysis of polymodal frequency distributions: Journal of the Marine Biological Association of the United Kingdom, v. 28, p. 141-153.
Hausdorf, B., 2008, Comments on the proposed conservation of *Buettneria* Case, 1922 (Amphibia): Bulletin of Zoological Nomenclature, v. 64, p. 217.
Heckert, A.B., 2004, Late Triassic microvertebrate from the lower Chinle Group (Otischalkian-Adamanian: Carnian), southwestern U.S.A.: New Mexico Museum of Natural History and Science, Bulletin 27, 170 p.
Heckert, A. B., 2008, Comments on the proposed conservation of *Buettneria* Case, 1922 (Amphibia): Bulletin of Zoological Nomenclature, v. 65, p. 310-313.
Heckert, A. B., and Lucas, S. G., 2000, Taxonomy, phylogeny, biostratigraphy, biochronology, paleobiogeography, and evolution of the Late Triassic Aetosauria (Archosauria:Crurotarsi): Zentralblatt für Geologie und Paläontologie Teil I 1998 Heft 11-12, p. 1539-1587.
Heckert, A. B., and Lucas, S. G., 2002, Historical taxonomy of the Late Triassic aetosaurs *Typothorax* and *Desmatosuchus* (Archosauria: Crurotarsi), including a lectotype designation for *Desmatosuchus haplocerus*: New Mexico Museum of Natural History and Science, Bulletin 21, p. 193-204.
Heckert, A. B., and Lucas, S. G., 2006, Micro- and small vertebrate biostratigraphy and biochronology of the Upper Triassic Chinle Group, southwestern USA: New Mexico Museum of Natural History and Science, Bulletin 37, p. 94-104.
Heckert, A. B., Jenkins, H. S., Hunt, A. P., and Lucas, S. G., 2013, Mandibles of juvenile phytosaurs (Archosauria:Crurotarsi) from the Upper Triassic Chinle Group of Texas and New Mexico, USA: New Mexico Museum of Natural History and Science, Bulletin 61, p. 228-236.
Heckert, A. B., Lucas, S. G., Hunt, A. P., and Spielmann, J. A., 2007a, Late Triassic aetosaur biochronology revisited: New Mexico Museum of Natural History and Science, Bulletin 41, p. 49-50.
Heckert, A. B., Lucas, S. G., Spielmann, J. A., and Hunt, A. P., 2007b, Biostratigraphic utility of the Upper Triassic aetosaur *Tecovasuchus* (Archosauria: Stagonolepididae), an index taxon of St. Johnsian (Adamanian: Late Carnian) time.: New Mexico Museum of Natural History and Science, Bulletin 41, p. 51-57.
Heckert, A. B., Lucas, S. G., Sullivan, R. M., Hunt, A. P., and Spielmann, J. A., 2005, The vertebrate fauna of the Upper Triassic (Revueltian: early-mid Norian) Painted Desert Member (Petrified Forest Formation: Chinle Group) in the Chama Basin, northern New Mexico: New Mexico Geological Society, Guidebook 56, p. 302-318.
Heckert, A. B., Mitchell, J. S., Schneider, V. P., and Olsen, P. E., 2012, Diverse new microvertebrate assemblage from the Upper Triassic Cumnock Formation, Sanford subbasin, North Carolina, USA: Journal of Paleontology, v. 86, p. 368-390.
Heckert, A. B., Zeigler, K. E., Lucas, S. G., Rinehart, L. F., and Harris, J. D., 2000, Preliminary description of coelophysoids (Dinosauria:Theropoda) from the Upper Triassic (Revueltian:early-mid Norian) Snyder quarry, north-central New Mexico: New Mexico Museum of Natural History and Science, Bulletin 17, p. 27-32.
Hill, A., 1979, Disarticulation and scattering of mammal skeletons: Paleobiology, v. 5, p. 261-274.
Hollocher, K., and Hollocher, T. C., 2012, Early process in the fossilization of terrestrial feces to coprolites, and microstructure preservation: New Mexico Museum of Natural History and Science, Bulletin 57, p. 79-92.
Holman, J.A., 2006, Fossil Salamanders of North America. Bloomfield, Indiana University Press, 232 p.
Holz, M. and Barberena, M. C., 1994, Taphonomy of the south Brazilian Triassic paleoherpetofauna: Pattern of death, transport and burial: Palaeogeography, Palaeoclimatology, Palaeoecology, v. 107, p. 179-197.
Houck, L. D., 1977, Life history patterns and reproductive biology of neotropical salamanders; *in* Taylor, D. H., and Guttman, S. I., eds., The Reproductive Biology of Amphibians: New York, Plenum Press, p. 475.
Huber, P., Lucas, S.G. and Hunt, A.P., 1993, Late Triassic fish assemblages of the North American Western Interior: Museum of Northern Arizona, Bulletin 59, p. 51-66.
Hunt, A. P., 1987, Phanerozoic trends in nonmarine taphonomy: Implications for Mesozoic vertebrate taphonomy and paleoecology: Geological Society of America Abstracts with Programs, v. 9, p. 171.
Hunt, A. P., 1989, Cranial morphology and ecology among phytosaurs; *in* Lucas,

S. G., and Hunt, A. P., eds., Dawn of the Age of Dinosaurs in the American Southwest: Albuquerque, New Mexico Museum of Natural History, p. 349-354.

Hunt, A.P., 1993, Revision of the Metoposauridae (Amphibia: Temnospondyli) and description of a new genus from western North America: Museum of Northern Arizona, Bulletin 59, p. 67-97.

Hunt, A. P. and Downs, A., 2002, Taphonomy of the Late Triassic Canjilon quarry (Petrified Forest Formation: Chinle Group), north-central New Mexico: Data from new excavation: New Mexico Museum of Natural History and Science, Bulletin 21, p. 291-296.

Hunt, A.P. and Lucas, S.G., 1991, A new rhynchosaur from the Upper Triassic of West Texas, and the biochronology of Late Triassic rhynchosaurs: Palaeontology, v. 34, p. 927-938.

Hunt, A.P. and Lucas, S.G., 1993, Taxonomy and stratigraphic distribution of Late Triassic metoposaurid amphibians from Petrified Forest National Park, Arizona: Journal of the Arizona-Nevada Academy of Science, v. 27, p. 89-96.

Hunt, A. P. and Lucas, S. G., 2010, Crocodylian coprolites: New Mexico Museum of Natural History and Science, Bulletin 51, p. 219-226.

Hunt, A. P. and Lucas, S. G., 2012, Descriptive terminology of coprolites and recent feces: New Mexico Museum of Natural History and Science, Bulletin 57, p. 153-160.

Hunt, A. P., Chin, K., and Lockley, M. G., 1994, The palaeobiology of vertebrate coprolites; *in* Donovan, S. K., ed., The palaeobiology of trace fossils: Chichester, John Wiley and Sons, p. 221-240.

Hunt, A. P., Lucas, S. G., and Heckert, A. B., 2005a, Definition and correlation of the Lamyan: A new biochronological unit for the nonmarine late Carnian (Late Triassic): New Mexico Geological Society, Guidebook 56, p. 357-366.

Hunt, A. P., Lucas, S. G. and Lockley, M. G., 1998, Taxonomy and stratigraphic and facies significance of vertebrate coprolites of the Upper Triassic Chinle Group, western United States: Ichnos, v. 5, p. 225-234.

Hunt, A. P., Lucas, S. G. and Spielmann, J. A., 2005b, The holotype specimen of *Vancleavea campi* from Petrified Forest National Park, Arizona, with notes on the taxonomy and distribution of the taxon: New Mexico Museum of Natural History and Science, Bulletin 29, p. 59-66.

Hunt, A. P., Lucas, S. G. and Spielmann, J. A., 2013, Triassic vertebrate coprolite ichnofaunas: New Mexico Museum of Natural History and Science, Bulletin 61, p. 237-258.

Hunt, A. P., Lucas, S. G., Milàn, J. and Spielmann, J. A., 2012, Vertebrate coprolite studies: Status and prospectus: New Mexico Museum of Natural History and Science, Bulletin 57, p. 5-24.

Hunt, A. P., Lucas, S. G., Spielmann, J. A., and Lerner, A. J., 2007, A review of vertebrate coprolites of the Triassic with descriptions of new Mesozoic ichnotaxa: New Mexico Museum of Natural History and Science, Bulletin 41, p. 88-107.

Hunt, A. S., 1967, Growth, variation, and instar development of an agnostid trilobite: Journal of Paleontology, v. 41, p. 203-208.

Huxley, J. S., 1932, Problems of relative growth. New York, Dial Press, 276 p.

ICZN, 2010, Opinion 2255 (Case 3420) *Buettneria* Case, 1922 (Amphibia): Generic name not conserved: Bulletin of Zoological Nomenclature, v. 67, p. 263-265.

Irmis, R. B., Nesbitt, S. J., Padian, K., Smith, N. D., Turner, A. H., Woody, D., and Downs, A., 2007, A Late Triassic dinosauromorph assemblage from New Mexico and the rise of dinosaurs: Science, v. 317, p. 358-361.

KaleidaGraph, 1997, Graphic analysis software, Version 3.09, Synergy Software.

Kamphausen, D., and Morales, M., 1981, *Eocyclotosaurus lehmani*, a new combination for *Stenotosaurus lehmani* Heyler, 1969 (Amphibia): Neues Jahrbuch für Geologie und Paläontologie Monatshefte, v. 1981, p. 651-656.

Karsch, F., 1889 (for 1888), Orthopterologische Beiträge: III. Berliner Entomologische Zeitung, v. 32, p. 415-464.

Kaye, F. T., and Padian, K., 1994, Microvertebrates from the *Placerias* quarry: A window on Late Triassic vertebrate diversity in the American Southwest; *in* Fraser, N. C., and Sues, H.-D., eds., In the shadow of dinosaurs: Early Mesozoic tetrapods: Cambridge, Cambridge University Press, p. 171-196.

Kemp, A., 1997, A revision of Australian Mesozoic and Cenozoic lungfish of the family Neoceratodontidae (Osteichthyes; Dipnoi) with a description of four new species: Journal of Paleontology, v. 71, p. 713-733.

Kimmig, J., 2009, Functional morphology and systematic palaeontology of the Phytosauria (Achosauria; Crurotarsi) and the development of their Late Triassic habitats [M. S. thesis]: London, Imperial College London, 118 p.

King, J. R., 1971, Probability charts for decision making. New York, Industrial Press Inc., 290 p.

Knoop, P. A., and Owen, R. M., 1994, Computer software for identifying compositional subpopulations in marine sediment geochemical data using threshold value analysis: Marine Georesources and Geotechnology, v. 12, p. 11-24.

Kock, J. G. S. and Link, R. F., 1970, Statistical analysis of geological data. New York, Dover Publications, 438 p.

Lehman, T. and Chatterjee, S., 2005, Depositional setting and vertebrate biostratigraphy of the Triassic Dockum Group of Texas: Journal of Earth Systems Science, v. 114, p. 325-351.

Lima, V., Arntzen, J. W. and Ferrand, N. M., 2000, Age structure and growth pattern in two populations of the golden-striped salamander *Chioglossa lusitanica* (Caudata, Salamandridae): Amphibia-Reptilia, v. 22, p. 55-68.

Lima, V., Arntzen, J. W. and Ferrand, N. M., 2001, Age structure and growth patterns of the golden-striped salamander *Chioglossa lusitanica* (Caudata, Salamanderidae): Amphibia-Reptilia, v. 22, no. 1, p. 55-68.

Lintze, C., 2003, The Stamper Site, 34TX1, Texas County Oklahoma Part I: The historical context and excavators: Oklahoma Archeology, v. 51, no. 2, p. 13-22.

Long, R. A., and Ballew, K. L., 1985, Aetosaur dermal armor from the Late Triassic of southwestern North America, with special reference to material from the Chinle Formation of Petrified Forest National Park: Museum of Northern Arizona Bulletin, v. 47, p. 45-68.

Long, R. A., and Murry, P. A., 1995, Late Triassic (Carnian and Norian) tetrapods from the southwestern United States: New Mexico Museum of Natural History and Science, Bulletin 4, 254 p.

Long, R. A., Lucas, S. G., Hunt, A. P. and McCrea, R. T., 1989, Charles Camp: Collecting Late Triassic vertebrates in the American Southwest during the 1920's and 1930's; *in* Lucas, S. G. and Hunt, A. P., eds., Dawn of the age of dinosaurs in the American Southwest: Albuquerque, New Mexico Museum of Natural History, p. 65-71.

Lucas, S. G., 1993, The Chinle Group: Revised stratigraphy and biochronology of Upper Triassic nonmarine strata in the western United States: Museum of Northern Arizona, Bulletin 59, p. 27-50.

Lucas, S. G., 1997, The Upper Triassic Chinle Group, western United States, nonmarine standard for Late Triassic time; *in* Dickins, J. M., Yang, Z., Yin, H., Lucas, S. G., and Acharyya, S. K., eds., Permo-Triassic of the Circum-Pacific: Cambridge, Cambridge University Press, p. 200-228.

Lucas, S. G., 1998, Global Triassic tetrapod biostratigraphy and biochronology: Palaeogeography, Palaeoclimatology, Palaeoecology, v. 143, p. 347-384.

Lucas, S. G., 2010, The Triassic timescale based on nonmarine tetrapod biostratigraphy and biochronology; *in* Lucas, S. G., ed., The Triassic Timescale: London, The Geological Society, Special Publications 334, p. 447-500.

Lucas, S. G., 2013, Plant megafossil biostratigraphy and biochronology, Upper Triassic Chinle Group, western USA: New Mexico Museum of Natural History and Science, Bulletin 61, p. 354-365.

Lucas, S. G., and Anderson, O. J., 1993, Triassic stratigraphy in southeastern New Mexico and southwestern Texas: New Mexico Geological Society, Guidebook 44, p. 231-235.

Lucas, S. G., and Hunt, A. P., 1993, Tetrapod biochronology of the Chinle Group (Upper Triassic), western United States: New Mexico Museum of Natural History and Science, Bulletin 3, p. 327-329.

Lucas, S. G. and Rinehart, L. F., 2005, Nonmarine bivalves from the Lower Permian (Wolfcampian) of the Chama Basin, New Mexico: New Mexico Geological Society, Guidebook 56, p. 283-287.

Lucas, S. G., Anderson, O. J., and Hunt, A. P., 1994, Triassic stratigraphy and correlations, southern High Plains of New Mexico-Texas: New Mexico Bureau of Mines & Mineral Resources, v. 150, p. 105-126.

Lucas, S. G., Heckert, A. B., and Kahle, R., 2002, Postcranial anatomy of *Angistorhinus*, a Late Triassic phytosaur from West Texas: New Mexico Museum of Natural History and Science, Bulletin 21, p. 157-164.

Lucas, S.G., Rinehart, L.F. and Spielmann, J.A., 2008, Comments on the proposed conservation of *Buettneria* Case, 1922 (Amphibia): Bulletin of Zoological Nomenclature, v. 65, p. 218-219.

Lucas, S. G., Spielmann, J. A., and Hunt, A. P., 2007a, Taxonomy of *Shuvosaurus*, a Late Triassic archosaur from the Chinle Group, American Southwest: New Mexico Museum of Natural History and Science, Bulletin 41, p. 259-261.

Lucas, S. G., Spielmann, J. A., and Rinehart, L. F., 2013, Juvenile skull of the phytosaur *Redondasaurus* from the Upper Triassic of New Mexico, and phytosaur ontogeny: New Mexico Museum of Natural History and Science, Bulletin 61, p. 389-400.

Lucas, S.G., Rinehart, L.F., Spielmann, J.A. and Hunt, A., 2007b, Case 3420; *Buettneria* Case, 1922 (Amphibia): Proposed conservation: Bulletin of Zoological Nomenclature, v. 64, p. 252-254.

Lucas, S. G., Rinehart, L. F., Krainer, K., Spielmann, J. A., and Heckert, A. B., 2010, Taphonomy of the Lamy amphibian quarry: A Late Triassic bonebed in New Mexico, USA: Palaeogeography, Palaeoclimatology,

Palaeoecology, v. 298, p. 388-398.
Lucas, S. G., Tanner, L. H., Kozur, H. W., Weems, R. E., and Heckert, A. B., 2012, The Late Triassic timescale: Age and correlation of the Carnian-Norian boundary: Earth-Science Reviews, v. 114, p. 1-18.
Marshall, W. B., 1929, New fossil land and fresh-water mollusks from the Reynosa Formation of Texas: Proceedings of the U. S. National Museum, v. 76, p. 1-6.
Martin, M., 1979, *Arganodus atlantis* et *Ceratodus arganensis*, deux nouveaux Dipneustes du Trias supérieur continental marocain: Comptes Rendus Academie des Sciences, Paris, Sciences de la Terre et des Planetes, Serie D, v. 289, p. 89-92.
Martz, J. W., and Small, B. J., 2006, *Tecovasuchus chatterjeei*, a new aetosaur (Archosauria: Stagonolepididae) from the Tecovas Formation (Carnian, Upper Triassic) of Texas: Journal of Vertebrate Paleontology, v. 26, p. 308-320.
McGowan, C., 1999, A Practical Guide to Vertebrate Mechanics. New York, NY, Cambridge University Press, 301 p.
McGowen, J. H., Granata, G. E., and Seni, S. J., 1979, Depositional framework of the lower Dockum Group (Triassic), Texas Panhandle: Texas Bureau of Economic Goelogy, Report of Investigations, v. 97-1979, p. 1-60.
McMahon, T. A., 1975, Allometry and biomechanics: Limb bones in adult ungulates: American Naturalist, v. 109, p. 547-563.
Mead, J. I., and Swift, S. L., 2012, Late Pleistocene (Rancholabrean) dung deposits of the Colorado Plateau, western North America: New Mexico Museum of Natural History and Science, Bulletin 57, p. 337-342.
Miall, A.D., 1996, The geology of fluvial deposits. Berlin, Springer, 582 p.
Milner, A. R. C., Kirkland, J. I. and Birthisel, T. A., 2006, The geographic distribution and biostratigraphy of Late Triassic-Early Jurassic freshwater fish faunas of the southwestern United States: New Mexico Museum of Natural History and Science, Bulletin 37, p. 522-529.
Morales, M., 1993, A small metoposaurid partial skull from the Chinle Formation near St. Johns, Arizona: New Mexico Museum of Natural History and Science, Bulletin 3, p. 353.
Mueller, B.D., 2007 *Koskinonodon* Branson and Mehl, 1929, a replacement name for the preoccupied temnospondyl *Buettneria* Case, 1922: Journal of Vertebrate Paleontology, v. 27, p. 225.
Munthe, K. and McLeod, S. A. 1975. Collection of taphonomic information from fossil and recent vertebrate specimens with a selected bibliography. Paleobios, v. 19, p. 1-12.
Murry, P. A., 1982, Biostratigraphy and paleoecology of the Dockum Group (Triassic) of Texas [Ph.D. dissertation]: Dallas, Southern Methodist University, 459 p.
Murry, P.A., 1986, Vertebrate paleontology of the Dockum Group, western Texas and eastern New Mexico; *in* Padian, K., ed., The beginning of the age of dinosaurs: Faunal change across the Triassic-Jurassic boundary: Cambridge, Cambridge University Press, p. 109-137.
Murry, P. A., 1989a, Geology and paleontology of the Dockum Formation (Upper Triassic), West Texas and eastern New Mexico; *in* Lucas, S. G., and Hunt, A. P., eds., Dawn of the Age of Dinosaurs in the American Southwest: Albuquerque, New Mexico Museum of Natural History, p. 102-148.
Murry, P.A., 1989b, Microvertebrate fossils from the Petrified Forest and Owl Rock Members (Chinle Formation) in Petrified Forest National Park and vicinity, Arizona; *in* Lucas, S.G. and Hunt, A.P., eds., Dawn of the Age of Dinosaurs in the American Southwest: Albuquerque, New Mexico Museum of Natural History, p. 249-277.
Mutter, R. J., and Heckert, A. B., 2006, Re-investigation of enigmatic fish bones known as colobodontid/perlidid toothplates from the Upper Triassic Chinle Group (Southwestern U.S.A.): New Mexico Museum of Natural History and Science, Bulletin 37, p. 530-542.
Nesbitt, S. J., 2007, The anatomy of *Effigia okeeffeae* (Archosauria, Suchia), theropod-like convergence, and the distribution of related taxa: Bulletin of the American Museum of Natural History, v. 302, 84 p.
Nesbitt, S. J., 2011, The early evolution of archosaurs: Relationships and the origin of major clades: Bulletin of the American Museum of Natural History, v. 392, p. 1-292.
Nesbitt, S. J., Smith, N. D., Irmis, R. B., Turner, A. H., Downs, A., and Norell, M. A., 2009a, A complete skeleton of a Late Triassic saurischian and the early evolution of dinosaurs: Science, v. 326, p. 1530-1533.
Nesbitt, S. J., Stocker, M. R., Small, B. J., and Downs, A., 2009b, The osteology and relationships of *Vancleavea campi* (Reptilia:Archosauriformes): Zoological Journal of the Linnean Society, v. 157, p. 815-864.
Nesbitt, S. J., Flynn, J. J., Pritchard, A. C., Parrish, J. M., Ranivoharimanana, L., and Wyss, A. R., 2015, Postcranial osteology of *Azendohsaurus madagaskarensis* (?Middle to Upper Triassic, Isalo Group, Madagascar) and its systematic position among stem archosaur reptiles: Bulletin of the American Museum of Natural History, v. 398, p. 1-126.
Newell, A. J. 1993. Depositional environment of the Late Triassic Bull Canyon Formation (New Mexico): Implications for 'Dockum Formation' paleogeography. New Mexico Museum of Natural History and Science, Bulletin 3, 359-368.
Okada, S., Utsunomiya, T., Okada, T., Felix, Z.I., and Ito, F., 2008, Characteristics of Japanese giant salamander (*Andrias japonicus*) populations in two small tributary streams in Hiroshima Prefecture, western Honshu, Japan, Herpetological Conservation and Biology, v. 3, pp. 192-202.
Olsen, R., 1951, Size relations in the limb bones of *Buettneria perfecta*: Journal of Paleontology, v. 25, p. 520-524.
Olson, E. C., 1951, *Diplocaulus*, a study in growth and variation: Fieldiana: Geology, v. 11, p. 57-154.
Oxnard, C. E., 1987, Fossils, teeth and sex: New perspectives on human evolution. Hong Kong, Hong Kong University Press, 280 p.
Parker, W. G., 2005, A new species of the Late Triassic aetosaur *Desmatosuchus* (Archosauria: Pseudosuchia): Comptes Rendus Palevol, v. 4, p. 327-340.
Parker, W. G., 2008, Description of new material of the aetosaur *Desmatosuchus spurensis* (Archosauria: Suchia) from the Chinle Formation of Arizona and a revision of the genus *Desmatosuchus*: Paleobios, v. 28, p. 1-40.
Parker, W. G., Stocker, M. R., and Irmis, R. B., 2008, A new desmatosuchine aetosaur (Archosauria: Suchia) from the Upper Triassic Tecovas Formation (Dockum Group) of Texas: Journal of Vertebrate Paleontology, v. 28, p. 692-701.
Pearl, R., and Miner, J.R., 1935, Experimental studies on the duration of life XIV. The comparative mortality of certain lower organisms, American Naturalist, v. 10, p. 60-79.
Pearl, R., and Parker, S.L., 1921, Experimental studies on the duration of life, I. Introductory discussion of the duration of life in *Drosophila*: American Naturalist, v. 55, p. 481-509.
Peck, D. S., 1987, Accelerated testing handbook. Portola, CA, Technology Associates, 136 p.
Raup, D. M. and Stanley, S. M., 1971, Principles of paleontology. San Francisco, W. H. Freeman and Company, 481 p.
Rinehart, L. F. and Lucas, S. G., 2001, A statistical analysis of a growth series of the Permian nectridean *Diplocaulus magnicornis* showing two-stage ontogeny: Journal of Vertebrate Paleontology, v. 21, p. 803-806.
Rinehart, L. F., Heckert, A. B., and Lucas, S. G., 2002a, Probability plots, populations, and paleobiology: What to do with Lagerstätten: Journal of Vertebrate Paleontology, v. 22, supplement to no. 3, p. 100A.
Rinehart, L. F., Lucas, S. G., and Heckert, A. B., 2002b, Probability plots distinguish morphological groupings in biometric data: Analysis of *Coelophysis* and comparison to other Diapsida: New Mexico Geology, v. 24, p. 62.
Rinehart, L. F. and Lucas, S. G., 2013a, A population of *Antediplodon dockumensis* (Bivalvia: Unionoida: Hyriidae) from the Revuletian (Upper Triassic: early-mid Norian) Bull Canyon Formation of West Texas: Growth, allometry, productivity and ecology: New Mexico Museum of Natural History and Science, Bulletin 61, p. 500-523.
Rinehart, L. F. and Lucas, S. G., 2013b, The functional morphology of dermal ornamentation in temnospondyl amphibians: New Mexico Museum of Natural History and Science, Bulletin 61, p. 524-532.
Rinehart, L. F., Heckert, A. B. and Lucas, S. G., 2002b, Stasis in bivalve growth and population ecology: Age distribution, growth curves, and biomass of a population of Revueltian (Upper Triassic: Early-mid Norian) unionids from West Texas: Geological Society of America, Abstracts with Programs, v. 34, p. 354.
Rinehart, L. F., Lucas, S. G. and Heckert, A. B., 2001, Preliminary quantification of the robust and gracile forms of *Coelophysis* using probability plots: Geological Society of America, Abstracts with Programs, v. 33, p. A-55.
Rinehart, L.F., Lucas, S.G., Heckert, A.B., and Hunt, A.P., 2008, Preliminary analysis of growth and age structure of *Buettneria* (Amphibia: Metoposauridae) assemblages fom the Upper Triassic of Texas and New Mexico, New Mexico Geology, v. 30, p. 56.
Rinehart, L. F., Rasnitsyn, A. P., Lucas, S. G. and Heckert, A. B., 2005, Instar sizes and growth in the middle Permian monuran *Dasyleptus brongniarti* (Insecta: Machilida: Dasyleptidae): New Mexico Museum of Natural History and Science, Bulletin 30, p. 270-272.
Rinehart, L.F., Lucas, S.G., Heckert, A.B., Spielmann, J.A. Celeskey, M., 2009. The paleobiology of *Coelophysis bauri* (Cope) from the Upper Triassic (Apachean) Whitaker quarry, New Mexico, with detailed analysis of a single quarry block: New Mexico Museum of Natural History and Science, Bulletin 46, 260 p.
Rogers, R.R. and Kidwell, S.M., 2007. A conceptual framework for the genesis and analysis of vertebrate skeletal concentrations; *in* Rogers, R.R., Eberth, D.A., Fiorillo, A.R., eds., Bonebeds: Genesis, Analysis, and Paleobiological Significance. University of Chicago Press, Chicago, p. 1-63.

Romer, A.S., 1939, An amphibian graveyard: Scientific Monthly, v. 49, p. 337-339.
Romer, A. S., 1947, Review of the Labyrinthodontia: Bulletin of the Museum of Comparative Zoology, 99, 368 p.
Roy Chowdhury, T., 1965, A new metoposaurid amphibian from the Upper Triassic Maleri Formation of central India: Philosophical Transactions of the Royal Society of London, B, v. 250, p. 1-52.
Sander, P. M. 1987. Taphonomy of the Lower Permian Geraldine bonebed in Archer County, Texas: Palaeogeography, Palaeoclimatology, Palaeoecology, v. 61, p. 221-236.
Sawin, H. J., 1945, Amphibians from the Dockum Triassic of Howard County, Texas: University of Texas, Publication 4401, p. 361-399.
Schneider, J.W., 2004, Appalachen-Mauretaniden-Varisciden-Fragen zur Paläobiogeographie kontinentaler Biota: Geobiologie [JT Paläontologische Gesellschaft Göttingen], v. 74, p. 20-25.
Schoch, R. R. and Milner, A. R., 2000, Sterospondyli: Stem-Sterospondyli, Rhinesuchidae, Rhytidostea, Trematosauroidea, Capitosauroidea, Encyclopedia of Paleoherpetology: München, Verlag Dr. Friedrich Pfeil, 203 p.
Semlitsch, 1980, Geographic and local variation in population parameters of the slimy salamander *Plethodon glutinosus*: Herpetologica, v. 36, p. 6-16.
Simroth, H., 1888, Uber die azorisch-portugiesische Nacktschnekenfauan und ihre Beziehungen (Vorlaufe Mittheilung): Zoologischer Anzeiger, v. 11, p. 86-90.
Simroth, H., 1910, Lissopode Nackschnecken von Madagaskar, den Comoren un Mauritius; *in* Voeltzkow, A., ed., Reise in Ostafrika (1903-1905): Stuttgart, E. Schweizerbart'sche Verlagsbuchhandlung, p. 577-622.
Simpson, G. G., Roe, A., and Lewontin, R. C., 1960, Quantitative Zoology. New York, Harcourt, Brace and World, Inc., 440 p.
Soto, M., and Perea, D., 2010, Late Jurassic lungfishes (Dipnoi) from Uruguay, with comments on the systematics of Gondwanan ceratodontiforms: Journal of Vertebrate Paleontology, v. 30, p. 1049-1058.
Spielmann, J. A. and Lucas, S. G., 2012, Tetrapod fauna of the Upper Triassic Redonda Formation, east-central New Mexico: The characteristic assemblage of the Apachean land-vertebrate faunachron: New Mexico Museum of Natural History and Science, Bulletin 55, 119 p.
Spielmann, J.A., Lucas, S.G., Hunt, A.P. and Heckert, A.B., 2006, Reinterpretation of the holotype of *Malerisaurus langstoni*, a diapsid reptile from the Upper Triassic Chinle Group of West Texas: New Mexico Museum of Natural History and Science, Bulletin 37, p. 543-547.
Spielmann, J. A., Lucas, S. G., Heckert, A. B., Rinehart, L. R. and Richards, H. R. III, 2009, Redescription of *Spinosuchus caseanus* (Archosauromorpha: Trilophosauridae) from the Upper Triassic of North America: Palaeodiversity, v. 2, p. 283-313.
Spielmann, J. A., Lucas, S. G., Rinehart, L. F., and Heckert, A. B., 2008, The Late Triassic archosauromorph *Trilophosaurus*: New Mexico Museum of Natural History and Science, Bulletin 43, 177 p.
Spielmann, J. A., Lucas, S. G., and Huber, P., 2013a, New record of *Spinosuchus caseanus* (Archosauromorpha:Trilophosauridae) from the Late Triassic (Adamanian) of West Texas: New Mexico Museum of Natural History and Science, Bulletin 61, p. 573-576.
Spielmann, J. A., Lucas, S. G., Heckert, A. B., and Krzyzanowski, S. E., 2013c, *Trilophosaurus* (Archosauromorpha:Trilophosauridae) postcrania from the Upper Triassic Blue Mesa Member of the Petrified Forest Formation (Carnian:Adamanian), Arizona, USA: New Mexico Museum of Natural History and Science, Bulletin 61, p. 567-572.
Spielmann, J. A., Lucas, S. G., Heckert, A. B., Rinehart, L. F., and Hunt, A. P., 2007, Taxonomy and biostratigraphy of the Late Triassic archosauromorph *Trilophosaurus*: New Mexico Museum of Natural History and Science, Bulletin 40, p. 231-240.
Spielmann, J. A., Lucas, S. G., and Hunt, A. P., 2013b, The first Norian (Revueltian) rhynchosaur: Bull Canyon Formation, New Mexico, U.S.A.: New Mexico Museum of Natural History and Science, Bulletin 61, p. 562-566.
Steyer, J. S. and Damiani, R., 2005, A giant brachyopoid temnospondyl from the Upper Triassic or Lower Jurassic of Lesotho: Bulletin Societe Geologique de France, v. 176, p. 243-248.
Steyer, J. S., Laurin, M., Castanet, J., and Ricqles, A. D., 2004, First histological and skeletochronological data on temnospondyl growth: Palaeoecological and palaeoclimatological implications: Palaeogeography, Palaeoclimatology, Palaeoecology, v. 206, p. 193-201.
Stocker, M. R. and Butler, R. J., 2013, Phytosauria: Geological Society, London, Special Publication 379, p. 91-117.
Stoddart, D. M., 1980, Methods of sex-identification of subfossil bones: Journal of the Zoological Society of London, v. 192, p. 543-546.
Studer, F. V., 1951, Triassic fossil locale; *in* The Panhandle Geological Society field trip May 5, 1951 Antelope Creek Pueblo and Triassic fossil site Hutchinson and Potter Counties, Texas, p. 17-21.
Studer, F. V., 1958, Road log; *in* The Panhandle Geological Society field trip November 1, 1958 to Saddleback Pueblo and Rotten Hill Triassic fossil site Hutchinson and Potter Counties Texas, p. 2-7.
Sulej, T. 2007. Osteology, variability, and evolution of *Metoposaurus*, a temnospondyl from the Late Triassic of Poland: Palaeontologia Polonica, v. 64, p. 29-139.
Taborda, J. R. A., Heckert, A. B., and Desojo, J. B., 2015, Intraspecific variation in *Aetosauroides scagliai* Casamiquela (Archosauria: Aetosauria) from the Upper Triassic of Argentina and Brazil: Evidence of sexual dimorphism?: Ameghiniana, v. 52, p. 173-187.
Tanner, L.H. and Lucas, S.G., 2006. Calcareous paleosols of the Upper Triassic Chinle Group, Four Corners region, southwestern United States: Climatic implications: Geological Society of America, Special Paper 416, p. 53-74.
Thompson, D. W., 1942, On Growth and Form. New York, Dover Publications, Inc., [1992], 1116 p.
Voorhies, M. R., 1969, Taphonomy and population dynamics of an early Pliocene vertebrate fauna, Knox County, Nebraska: University of Wyoming Contributions to Geology, Special Paper 1, p. 1-69.
Walls, K. D., 2007, The Ecology and Behavior of Amphibians. Chicago, University of Chicago Press, 1148 p.
Zanno, L. E., Heckert, A. B., Krzyzanowski, S. E., and Lucas, S. G., 2002, Diminutive metoposaurid skulls from the Upper Triassic Blue Hills (Adamanian: latest Carnian) of Arizona: New Mexico Museum of Natural History and Science, Bulletin 21, p. 121-125.
Zar, J. H., 1999, Biostatistical analysis. Singapore, Pearson Education, 663 p.
Zeigler, K. E., Heckert, A. B., and Lucas, S. G., 2003a, An illustrated atlas of the phytosaur (Archosauria: Parasuchidae) postcrania from the Upper Triassic Snyder quarry (Petrified Forest Formation, Chinle Group): New Mexico Museum of Natural History and Science, Bulletin 24, p. 89-103.
Zeigler, K. E., Lucas, S. G., and Heckert, A. B., 2002a, The Late Triassic Canjilon quarry (Upper Chinle Group, New Mexico) phytosaur skulls: evidence of sexual dimorphism in phytosaurs: New Mexico Museum of Natural History and Science, Bulletin 21, p. 179-188.
Zeigler, K. E., Lucas, S. G., and Heckert, A. B., 2002b, Taphonomy of the Late Triassic Lamy amphibian quarry (Garita Creek Formation: Chinle Group), central New Mexico: New Mexico Museum of Natural History and Science, Bulletin 21, p. 279-283.
Zeigler, K. E., Lucas, S. G., and Heckert, A. B., 2003b, Variation in the Late Triassic Canjilon quarry (Upper Chinle Group, New Mexico) phytosaur skulls: Evidence of sexual dimorphism: Paläontologische Zeitschrift, v. 77, p. 341-351.
Zug, G. R., 1993, Herpetology: An introductory biology of amphibians and reptiles. New York, Academic Press, Inc., 527 p.

APPENDIX 1—WPA REPORTS ON THE ROTTEN HILL EXCVATIONS

QUARTERLY REPORT
PALEONTOLOGICAL PROJECT
OCTOBER 1, 1940 TO DECEMBER 31,,1940 [sic]
WP NO. 15525
OP NO. 65-1-66-2757
STATE APPLICATION NO. 40670

QUARTERLY REPORT ON PALEONTOLOGICAL PROJECT # 15523, ENDING DECEMBER, 31, 1940.

The projects current operations continued in the Triassic quarry located twenty-five miles north west of Amarillo, Texas, on the Herring Ranch. Nine new workers were added to the field crew in November, but due to the emergency work required in Amarillo, Texas, a large percentage of the crew was transferred to the emergency project. As a result our field operations were slowed down. However, the men were transferred back to the projects in less than two weeks and operations returned to normal.

According to most authorities, it is a rare thing to find a quarry in Triassic formations; however, as I have stated before, we were most fortunate in discovering a quarry which has proven most productive.

The quarry is of a fine clay deposit and the fossils found represent water-loving animals. Mostly stegocephalian material is found, including a great number of skulls which are in an excellent state of preservation. The distinguishing characteristics of this animal are an elongated sculpture on the frontal and post orbital regions, an incomplete sensory canal system, and the extension of the palatal vacuities anterior to the orbits. There is also the presence of an accessory row of small teeth of the inner side of the dentary adjacent to the symyshysis. Several of the stegosephalians skulls have been restored and are now ready for exhibit. It is hoped that enough parts of this animal will be found to mount a complete skeleton.

A great deal more phytosaur material has been found, including vetrebrae [sic], scapulae, pelvis, foot-bones and lower jaws. Ten spines of desmanasuchus [sic] have also been found. Most of these specimens have been catalogued; being either put on exhibit or in the study collections.

Mr. Charles A. Pryor, a movietone photographer from Hollywood, California, visited our project and became so interested that he decided to make a motion picture of the work being done by our project, both in the field and laboratory. He made thousands of feet of film. The film was the[n] edited and called “Before the Dawn of Man.” This motion picture is now being shown in colleges and High Schools [sic] throughout the United States. He included in this picture several scenes of animated animals which were made by Robert Lewis Bedford, one of the greatest prehistoric animators in the United States.

The field crew lost a great deal of time in December due to bad weather, even so approximately 3500 specimens have been excavated. A great deal of this is fragmental material.

QUARTERLY REPORT
PALEONTOLOGICAL PROJECT
JULY 1, 1940 TO SEPTEMBER 30, 1940
WP NO. 15525
OP NO. 65-1-66-2757
STATE APPLICATION NO. 40670

QUARTERLY REPORT
PALEONTOLOGICAL PROJECT NO. 15525
ENDING SEPTEMBER 30, 1940

Paleontological Project no. 15525 closed all quarries in Dealey County, Texas, on July 26, 1940. August 1, 1940 the project began operations in a Triassic formation twenty-five miles northwest of Amarillo, Texas. The Triassic was a period during the Mesozoic Era, the Age of Reptiles. This era was made up of three periods; Triassic, Jurassic and Cretaceous. The Mesozoic Era was dominated by reptiles and during this time the most outlandish and monstrous forms lived. They inhabited not only the earth [sic] but also the sea and the air. The most interesting of these were the land-dwelling dinosaurs, marine ichthyosaurs and the flying dragon, known as pterodactyls. The dinosaurs were extremely variable in both size and form, some were no larger than a toad, others were the largest animals that have ever walked the earth [sic]. Some were flesh eater and others vegetarians.

Very little work has been done in the Triassic beds of the panhandle of West Texas; therefore, it is the purpose of our project to collect and preserve this pre-historic [sic] material. Erosion is continually in the process of uncovering these fossils, and a consequence gradually destroying them. It is extremely important when these specimens are found, through either erosion or artificial means, that they are carefully recovered and taken into the laboratory where they can be properly cared for. If this is not done, they are lost and the history they represent can never be regained. Therefore, through the efforts of our project a gap of paleontological knowledge is being largely filled.

On August 11th a complete lower jaw of a phytosaur was found. The specimen was in very good condition and was approximately forty-two inches long. A good many of the teeth were missing. On August 26th a skull of the phytosaur was found. The skull was found approximately one-half mile from that of [sic] the lower jaw, but they seem to belong to the same species and will be displayed together. These two specimens have been cleaned by the laboratory crew and are now ready for exhibit as soon as the proper stand has been made. A great deal more phytosaur material was found this month, including vertebrae, scapulae, pelvis, humerus, femur, feet bones and ribs. Work continued through August and September in these Triassic beds. They show great promise of a rich assemblage of reptile material.

We were very fortunate in finding a quarry. According to Mr. William F. Reed “The discovery of a new bone quarry in the Triassic is an event of more than passing interest to the paleontological world. The Triassic by and large affords notoriously poor collecting. In fact, the main part of our knowledge concerning the life of this period derives from a very few productive localities scattered throughout the United States. The total amount of material collected from these few localities is discouragingly small. The life picture is incomplete. Consequently, each new find carries the prospect of yielding previously unknown forms, and of adding new links to the chains in vertebrate life. The Herring Ranch quarry seems to be located in the fine, muddy deposits of a semi-stagnant body of water adjacent to the main course of one of the westward-flowing rivers of Triassic time. The bones are disarticulated and belong almost entirely to water-loving types of animals; remains of many different individuals are crowded together as if parts of numerous carcasses had been drifted together by a current, or dragged together by carnivores. Further excavating will be necessary in order to determine the exact extent and probable nature of the deposit. At present, it may be said to be roughly tabular, or lenticular, about two or three feet thick, and to extend for at least thirty feet horizontally. It is composed mainly of very fine clay, with some sandy lenses. The clay is badly slickensided and preserves little evidence of its original bedding.” Twenty-four large casts have been removed from this quarry, approximately five hundred teeth and six hundred fragments of ribs, leg bones, pelvis, etc.

On September 1, 1940, Mr. William F. Reed arrived from the University of Chicago to take over the duties as Head of the Department of Geology and Anthropology at West Texas College and to be the Sponsor’s Representative. Mr. Reed has had much valuable study and experience with Triassic reptiles and will be most helpful to our project as a technical advisor.

On September 16, 1940, we placed a very interesting collection of specimens on exhibit at the Tri-State Fair at Amarillo, Texas. Hundreds of people visited the exhibit and passed many favorable comments.

We were very fortunate in having several distinguished visitors visit the project this quarter. Dr. Everett C. Olson, Department of Paleontology of the University of the University of Chicago, was accompanied by Mr. Ernest DuBois, graduate student in paleontology at the University of Chicago; Mr. Greyson Meade, Department of Work Projects Administration project working the Triassic near Big Springs, Texas; Richard L. Lewis, State supervisor state-wide Paleontological Survey, Austin, Texas; and W. N. McAnulte, in change of the laboratory work for the state-wide Paleontological Survey, Austin, Texas.

Summary of the Fossil material Collected from the Herring Ranch Lease
up to September 30, 1940, and from Dalhart in September, 1940

Herring Ranch

Phytosaur

Skull	One specimen; perfect; about 45 inches long (2900)
Lower jaws	**Two parts; one pair large and heavy, about 42 inches long, and seemingly belonging to the same species as the skull (2699); the other pair lighter, shorter, and badly eroded (2898).**
Vertebrae	**About twenty good centra (2930). Five neural arches in good condition (2924, 2951, 2952, 2953, 2954). Numerous spines (1918).**
Shoulder Girdle	**Two complete scapulae (2902, 2912); base of another scapula (2911). One small coracoid, complete (2901[sic]; one large coracoid, complete except for posterior ventral margin, and with base of scapula attached (2908); symphysial portion of another small coracoid (2907). One partially complete interclavicle (2917). Two clavicles, both lacking scapular extremities, one (2904) much longer and heavier than the other (2910); shaft of a third clavicle (2922).**
Pelvic Girdle	**Fragments of right side of one pelvis, including acetabular portion of ilium and connecting portion of ischium (2927).**
Fore Limb	**One perfect humerus, length 13 inches (2928); distal end of a much larger humerus (2925). One perfect ulna, length 10 inches (2903); proximal and distal ends, respectively, of two other ulnas (2915, 2916).**
Hind Limb	**One femur, complete except for distal end, originally about twenty inches long (2914). One tibia? (2906), one fibula? (2913).**
Ribs	**Four sacrals (2904, 2905, 2919, and 2920); portions of eight thoracic ribs sufficiently complete to permit assignment to a specific place in the series (2922).**
Gastralia	**Portions of four abdominal ribs (2922). Four lateral splints (2932).**
Dermal scutes	**Twenty-four dorsal scutes (2958); sixteen ventral scutes (2359).**

Desmatosuchus

Dermal Armor One large spine, - fifth cervical of case (2939); four smaller spines (2961).

Stegocephalians

Skull	**Three partial pterygoids (2965, 2966, 2967). Tip of snout, including both premaxillaries (2968). Portion of left side of skull, including lacrimals, and parts of maxillary, nasal, prefrontal, palatine, and vomer (2969). Part of vomer (2970). Fragment [sic] including portions of transverse, palatine, maxillary, and jugal. Palatine (2971).**
Lower Jaw	**One complete speicmen (2943); anterior portion, including symphysis, of another (2947).**
Vertebrae	**Five axes (2946, 2974, 2973, 2975, 2976). Twenty-two centra (2972).**
Shoulder Girdle	**Five perfect clavicles (2536, 2940, 2941, 2942, 2947); lateral margin of another clavicle (2944); portion adjoining cleithral buttress of another (2937). Four interclavicles, all sufficiently complete to permit comparative measurements (2946, 2962, 2963, 2964).**

Lungfish

Skull and Lower Jaw	**Three teeth (2926).**

Dalhart

Elephant

Skull	**One tooth and one tusk (2960).**

QUARTERLY REPORT
PALEONTOLOGICAL PROJECT
JANUARY 1, 1941 to MARCH 31, 1941
WP NO. 15523
OP NO. 65-1-66-2757
STATE APPLICATION NO. 40670

QUARTERLY REPORT ON PALEONTOLOGICAL PROJECT # 15523, ENDING MARCH 31, 1941. DISTRICT #26.

It is a well recognized [sic] fact that the Panhandle of West Texas is unusually rich in pre-historic remains. Institutions from as far East as New England and as far West as California have been collecting here since 1895. It has been the desire of the West Texas State College, through its Department of Paleontology to collect some of this material with which West Texas is so abundantly endowed. Erosion is continually uncovering these fossils representing the pre-history of Texas, and as a consequence gradually destroying them. Therefore, it is highly important that these specimens be collected and preserved before they are destroyed. Once they are lost, the history that they represent can never be regained. Thus through the efforts of our project these specimens are being collected and preserved, and a gap in Paleontological knowledge is largely being filled. Some of the specimens collected during the operation of this project have been prepared and are now on exhibit in the museum at Canyon, Texas. Other material has been carefully stored away and cataloged [sic]. Thus it furnishes and will continue to furnish a source of work for the students interested in the science of paleontology, and be a source of many fine new exhibits for the museum. All of the material collected is not of a spectacular nature such as one would use in a display. However, it is all important [sic] scientifically. All the material collected on the project is filed and cataloged [sic] according to the location from which it came, the geological horizon in which it is found, and the year in which it is collected. As a result of our projects during the past five years, there are now on hand extensive scientific collections from the Lower, Middle, and Upper Pliocene and the Lower Pleistocene. Our collections are becoming much more complete by the present work

the project is doing. During the past year we have been operating in the Triassic period, the beginning of the era of Middle Life, the so-called Mesozoic era, better known as the age of reptiles. Warm-blooded animals as we know them today did not exist; no feathered birds flew through the air and flowering plants were unknown. Reptiles, cold-blooded, scale-covered, beasts were beginning their development, and in the future were to dominate the earth, sea and air. As has been stated before, it is most unusual to find a quarry in Triassic beds, but we have been very fortunate to locate a quarry which [sic] has been proven most productive. This quarry located twenty-five miles N. W. of Amarillo, Texas on the Herring Ranch, is of a fine clay deposit and the fossils found are disarticulated and belong almost entirely to water-loving animals. Many different individuals are found crowded together, and todate [sic] over ten thousand specimens have been found. As would be expected a large number of these are fragments, however, a large majority are complete specimens. It is our opinion that there are numerous quarries in this locality. With this in mind we are continually searching for new beds. The more experienced workers have been advanced far enough in the work to be allowed to conduct the search for new localities. The importance of the work is stressed and these men given extensive field instructions.

The Laboratory [sic] work has been confined for the most part to the cleaning and restoring of the fossils as they are brought in from the field. We now have cleaned and prepared enough parts of the Stegocephalian material to assemble a complete skelton [sic] for exhibit. This should be ready for exhibit in the very near future.

The project operated with a crew of forty three workers (for)[sic] the greater part of this quarter, but that number has been reduced to twenty two, due to the quota reduction. 40245 hours have been worked and 16, 454.60 dollars have been spent.

The work our project is doing is highly justified; first, from the standpoint of rehabilitation of the men employed; secondly, from the demonstrated desirability of the work through the material results achieved; and thirdly, the lasting value of the data and the specimens collected, together with the scientific and educational value they represent.

Summary of Fossil Material Collected from the
Herring Ranch Lease up to March 31, 1941

HERRING RANCH

PHYTOSAUR

Skull	**Snout fragment (3099 [sic].**
Lower Jaws	**End of lower jaw (3092).**
Vertebrae	**Two neural arches in good condition (3105). Fourteen centra (3098) [sic]**
Metacarpals	**Three metacarpals in good condition (3084).**
Phalanges	**Three phalanges in good condition (3083).**
Shoulder Girdle	Three fragments of coracoids (3091) [sic] One end of scapula (3102). Seven complete clavicles (3079). Six clavicle fragments (3080).
Scutes	**Two dermal scutes (3100); Five fragmentary scutes (3033); Ten ventral scutes in perfect condition (3101). Eleven armor fragments (3034)**
Ribs	**Two ribs (3094); Ten ribs in good condition (3035).**
Fore Limb	**One complete ulna (3082). Two ends of humerus (3104). Two unknown limb bones (3103).**
Hind Limb	Four complete femurs (3081). Twelve coracoids and femur fragments (3031).

STEGOCEPHALIAN

Vertebrae	**Thrity-one centra (3038). Twenty one good centra (3039). Six perfect neural arches (3020); Four neural arches (3111). Four axis, three complete (3078). Seven neural arches (3087). Thirty-five vertebral centra (3097).**
Lower Jaws	**Six left jaws complete (3072); Nine [sic] left jaws, very few teeth (3064); Ten right jaws (3065); Three right jaws (3071); Fifteen lower jaws (3008); One lower jaw (3110); nineteen large fragments of lower jaw (3024); Large fragments of lower jaws (3066).**
Skull	**Eight complete skulls in good condition (3011); One skull (3108); Two skulls, incomplete (3068); Three skull fragments (3074). One incomplete parasphenoid and pterygoid (3090). Two incomplete pterygoids (3089). Seven exoccipitals (3113); Eight exoccipitals in good condition (3088). Six pterygoids, fragmentary (3005); Four fragments of parasphenoid (3006). One skull fragment (3003). Seven incomplete maxillary (3009). Two palatine fragments (3021). Two fragments of pterygoids (3022). Twelve small skull fragments (3025). Fourteen maxillary fragments (3023).**
Metacarpals	**One good metacarpal (3017).**
Shoulder Girdle	**Eleven perfect interclavicles (3007); Twelve outer clavicles, good condition (3018); One outer clavicle (3004); Two right clavicles in good condition (3106) [sic] One left clavicle in good condition (3107); Three interclavicle fragments (3109); Twenty-three large fragments of outer clavicles (3023); Thirteen clavicle fragments (3030); Nine left clavicles in good condition (3060); Nine right clavicles (3061); Sixteen innerclavicles in good condition (3063); Nine large fragments of clavicles (3062); Eight right clavicles in good condition (3069); Nine left clavicles in good condition (3070); Three interclavicles (3073).**
Pelvis Girdle	**One good ilium (?)(3014); Twelve ilium (?)(3085); Four ilium fragments (3029). Twenty-six small unidentified bones (3095 [sic] Six small unidentified bones (3112).**
Hind Limb	**Two femurs in perfect condition (3015). One perfect fibula (3012); Eleven fibula [sic] in good condition (3093). Fourteen complete femurs (3077).**
Fore Limb	**One perfect ulna (3016). Two good humerus (3010); Twelve humerus (3075); Five fragments of humerus (3076); Two good ulna [sic].**
Ribs	**Ten complete ribs in perfect condition (3019); Forty-five good ribs (3026); One hundred six rib fragments with good end (3027); Nineteen complete ribs (3096).**

Summary of the Fossil Material Collected from the Herring Ranch Lease
up to October 1, 1940, and from Delhart in September, 1940

Herring Ranch

Phytosaur

Skull	One specimen; perfect; about 45 inches long (2900).
Lower Jaws	**Two pairs: one pair large and heavy, about 42 inches long, and seemingly belonging to same species as the skull (2899); the other pair lighter, shorter, and badly crushed (2898).**
Vertebrae	**About twenty good centra (2930). Five neural arches in good condition (2924, 2931, 2932, 2933, 2934). Numerous spines (2918).**
Shoulder Girdle	**Two complete scapulae (2902, 2912); base of another scapula (2911). One small caracoid, complete (2901); one larger coracoid, complete except for posterior ventral margin, and with base of scapula attached (2908); symphysial portion of another small coracoid (2907). One practically complete interclavicle (2917). Two clavicles, both lacking scapular extremities, one (2964) much larger and heavier than the other (2910); shaft of a third clavicle (2922).**
Pelvic Girdle	**Fragments of right side of one pelvis, including acetabular portion of ilium and connecting portion of ischium (2927).**
Fore Limb	**One perfect humerus, length 13 inches (2928); distal end of a much larger humerus (2925). One perfect ulna, length 10 inches (2903); proximal and distal ends, respectively, of two other ulnas (2915, 2916).**
Hind Limb	**One femur, complete except for distal end, originally about twenty inches long (2914);. One tibia? (2906). One fibula? (2913).**
Foot Bones	**Part of one metacarpal (2926). Two phalanges (2929).**
Ribs	**Four sacrals (2904, 2905, 2919, and 2920). Portions of eight thoracic ribs sufficiently complete to permit assignment to a specific place in the series (2922).**
Gastralia	**Portions of four abdominal ribs (2922). Four lateral splints (2922).**
Dermal Scutes	**Twenty-four dorsal scutes (2958); Sixteen ventral scutes (2959).**

Desmatosuchus

Dorsal Armor	One large spine, - fifth cervical of Case (2939); four smaller spines (2961).

Stegocephalians

Skull	Three partial pterygoids (2965, 2966, 2967). Tip of snout, including both premaxillaries (2968). Portion of left side of skull, including lacrimal, and parts of maxillary, nasal, prefrontal, palatine, and vomer (2969). Part of vomer (2970). Fragment including portions of transverse, palatine, maxillary, and jugal. Palatine (2971).
Lower Jaw	One complete specimen (2943); anterior portion, including symphysis, of another (2947).
Vertebrae	Five axes (2948, 2974, 2973, 2975, 2976). Twenty-two centra (2972).
Shoulder Girdle	Five perfect clavicles (2938, 2940, 2941, 2942, 2947); lateral margin of another clavicle (2944); portion of adjoining cleithral buttress of another (2937). Four interclavicles, all sufficiently complete to permit comparative measurements (2946, 2962, 2963, 2964).

Lungfish

Skull and Lower Jaw	Three teeth (2986).

Dalhart

Elephant

Skull	One tooth and one tusk (2960).

APPENDIX 2—MORPHOMETRIC DATABASE OF THE ROTTEN HILL METOPOSAURIDS

Morphometric database of the Rotten Hill metoposaur clavicles, interclavicles, lower jaws, skulls, atlas vertebrae and limb elements. Measurements throughout are in millimeters. Some are estimated. Estimates with lower confidence are indicated by "e" notation.

clavicles

N = 79

specimen	width	length	specimen	width	length
3211L	188	367	2001.38		301
3212L	178	363	2001.219	110	
3238	177	392	1999.35.297		360
3233	130		1999.35.123	175	
3186	105	256	3023L	155	
3188	125		3023L	157	
3191	128		3023L	190	
3190	115	270	3023L	160	
3211	185	363	3126	140	322
3212	177	364	3069	144	270
WPA 1-3-41	152	321	3060	200	375
3126	127		3040	202	375
3126	175		3061	150	385
3070	127		3069	200	390
2997	166	398	3126	143	321
3070	133		3146	160	345
3061	160	342	2947	187	
3061R	209	374	3018	168	349
3061 small	140	294	2938	164	345
3053R	147		2940	160	338
3053L	139	256	2941	176	346
3070R	175	370	3060	175	372
1999.35.207	149		3069	170	382
3060	159	332	3069		383
3058	142		3069	119	301
3070	175		3059	166	
3062	138		3018R	111	272
3069	108	303	3018	136	
3060	185	380	3054	135	
3106	137	300	3021	142	
3034	140	298	3062	162	
3063	152		1999.35.197	174	357
3063	154	357	3018	164	331
3047	154	325	3070	165	349
1999.35.231	140		3062	120	
3139	132		3047	109	258
3139	128		3010?	158	
3070R	200		2000.11.71	174	
1999.35.80	210		2000.76.1	165	346
3018	177				
3004	165	327			

interclavicles
N = 67

specimen	length	width	length to clavicle	length to end pits
UMMP 7265				
UMMP 3841	330	290	303	240
UMMP 12887	510	395	412	160
WT3120		256	330	200
3168				112
3063			320	164
3063	508	338	419	200
1999.35.330		255	290	124
1999.35.141	464	290	393	177
3057		377	400	197
3127		257		163
3063	360	264	320	153
2962		342		203
1999.35.300			388	192
2946		332	372	167
3032		295		
3030		285		
3127		279		157
3109		272		163
3145		322		193
3073		270		163
3057	359	292	330	155
3030				248
3145		250		142
1999.146		342	429	161
2996				169
1999.36.84		255	324	150
1999.35.85		290	374	171
3063		362	433	161
3163		380		195
3127		216		122
3120		256		137
3120		265		159

specimen	length	width	length to clavicle	length to end pits
3073	430	310	408	163
3163		305	338	165
3063		364	445	200
3057		292	338	155
3007		371		198
3030A		342		205
3030B		353		203
3073	435	305	424	175
3057		310	205	
3007a		242	144	
1999.34.07		294	343	160
1999.35.01			200	
3007A	437	336	412	174
3007B		315	366	155
3007C		316	398	186
3007D		376	428	196
3063A		363		175
3063B	378	308	345	160
3063C		310		233
2964		400	515	220
3030a		238		150
3030b				132
3063d		277	310	145
3063e			377	
3007e		290	384	194
3007f		222		145
3007g		300	397	175
3007h		253	340	150
3240	282	238	260	125
3239		330		193
3235	347	280	314	131
3199 w/clav	340	258	312	155
3206	405	345	384	212
3200	370	252	347	148
3239		330		220

lower jaws
a,b,c,… notation added by NMMNH
N = 55

Specimen	comments	total arc length	max height	height at articulation	tooth count
3237		470	90	67	
3013			75	45	
3152			88	42	
3065a			102	74	
3064a		402	85	68	45
3037a			106	88	
1999.35.16			114	85	
3152			92	66	
3064right		455	70	68	46
3064left			88	66	
3064left		505	85	76	42
3065a		535	88	67	
3008a		500		58	
3065c			98	83	
3167		634	115	92	
3037b		556	94	74	
1999.35.299		515	106	85	
1999.35.200			88		
1999.35.300a			89	80	
1999.35.300b			88	59	
3064b			78	59	
3064c			120	84	
3064d	TC >42	475	97	59	
3072a		388	66	41	47
3008(l)a			114	68	
3008ra			55	45	
3008(l)b			95	70	
3008rb		514	104	52	
3008rc			67	50	
3008rd			84		
3037c			86	72	
3072b			117	74	
1999.35.322		485	78	50	
3024r			82	67	
3024l				46	
2000.10.16			77	66	
3024				60	
3110			115		
3065d		458	85		51
3041			75	48	
3065e				51	
3008b		418			45
3027			77	46	
2000.11.31			78		
WT3128		376	61	51	46
X2000.10.20	fragment				
WT3008a		411	66	47	45
WT3152		509	91	65	46

2000.10.110		654	135	92	52
WT3008b		542	99	76	51
WT3072		554	98	82	52
WT2957	fragment				
WT3241		420	77	49	47
WT3071a		514	100	74	46
WT3071b		509	88	63	49

skulls
N = 25

equivalent Colbert & Imbrie, (1956) notations			**AL**			**SL**						**GW**
NMMNH notations	**AB**	**AB'**	**AC**	**AC'**	**AD**	**AE**	**AF**	**width B**	**width C**	**width E**	**width F**	**width G**	**GW**
specimen													
UMMP 7475	24	65	125	175	337	408	446			345		145	
UMMP 8854			180	250	450	560	580			495	195	185	
UMMP 21326	33		150	212	410	505	520			460	210	225	
3011-3	17	55	112	156	307	376	392	90	183	305	140	135	
3011	25	74	150	210	377	454	480	155	260	430	180	170	
3011 incomplete	19	57	122	71				92	175				
3057	17	78	158	227	423			130	285	470			
3003									279				
2001.20									270				
2001.23													395
3068-2													498
3068-1													458
3011-2	25	76	145	202	374			125	245				440
3114	21	58	115	160	304	365	390	80	186				
WT 3055	13	55	120	168	304	376	385	84	187	311	142	141	319
WT 3011	10	46	97	134	151	302	317	61	143	252	110	120	254
WT 3166-1	17	55	127	164	309	392	407	83	190	370	157	170	390
WT 3067-2	31	75	155	207	410	500	510	139	260	420	205	230	480
PPHM 6	18	73	138	193	356	432	451	105	198	315	170	175	338
PPHM 5	25	75	151	224	425	505	529	146	271	370	224	210	460
WT 3011-1		60	128	189	369	451	473		226	395	162	184	411
PPHM 3									196	295	137	145	295
WT 3151									270	412		190	430
PPHM 9	19	56	124	170	351			94	195			162	310
WT 3067	22	64	133	186	356	430	454	116	219	378	167	158	384

atlas

a,b,c… notation added by NMMNH
N = 17

specimen	width ant face	length ventral centerline	height ant cup	estimate
1341	81	26	34	
2973	77	37	41	
2975	98	40	51	
3078sm	42	9	22	
3078lg	100	40	49	
3078m	90	32	47	
3118	93	42	50	
3144	71	34	43	
3118a	94	42	56	
3118b	90	41	47	
3118c	78	31	50	e
3118d	63	28	42	e
3144a	68	30	36	
3114b	70	30	40	
3114c	65	27	36	
3114d	67	26	35	
3114e	62	25	31	

humeri

a,b,c… notations added by NMMNH

N = 20

Specimen	length	prox width	dist width	estimate
3130a	94	32	64	
3157	91	34	58	
3075a	92	35		
uncat a	104	43	87	
uncat b	114	50	79	
3075b	92	36	74	
3075c	127	46	81	e
3075d	65	27	46	
3075e	80	29	52	
3130b	114	41		
3175f	102	42		
3175g	76	29	47	
2993	101	31	69	
3010	83	35		
3075h	101	38		
3075i	119	53	77	
3075j	80	26		
3075k	87	31		
2100	136	52	83	
3011	108	43	68	

radii

a,b,c… notation added by NMMNH

N = 8

specimen	length	proximal width	distal width	estimate
3095a	60	24	27	
3086	59	22	25	
3095b	55	22	23	
3095c	59	26	26	
3095d	52	33		
3093	67	27		e
3095e	82		31	
3011	80	35	22	

ulnae

N = 2

Specimen	length	proximal width	distal width
3093	56	26	15
3011	75	36	27

femora

a,b,c… notation added by NMMNH

N = 19

specimen	length	proximal width	distal width	estimate
3077a	105	26	37	
3077b	129	39	46	
3148	119	30	42	
3077c	109	40	47	
3131a	101	32	31	e
3131b	102	31	41	
3131c	109	35	47	
3137	151	46	57	e
3131d			31	
3277	112	40	47	
3099	100	27	36	
3131e	108	35	42	
3131f	95	32		
3131g	90	30	34	
3011	92	26	36	
3077d	91	26	36	
3077e	116	49	55	e
3077f	100	34	41	
3011mount	125		55	

tibiae

a,b,c… notation added by NMMNH

N = 5

specimen	length	proximal width	distal width
3134a	60	36	25
3093a	62	35	27
3093b	53	35	26
3134b	57	35	29
3011	73	46	32

fibulae

a,b,c… notation added by NMMNH

N = 4

specimen	length	proximal width	distal width
3093a	45	35	26
3093b	46	30	27
3093c	55	34	29
3093d	41	24	23

ilia

a,b,c… notation added by NMMNH

N = 17

specimen	length	proximal width	distal width
3085a	92	50	37
3132a	64	32	20
3085b	64	34	24
2923	74	44	26
3085c	80	37	24
3085d	95	44	31
3085e	82	35	24
3085f	60	28	19
3085g	70		29
3149	62	31	17
3029a		45	
3132b	80		25
3029b		36	
3132c		29	
3085h	41	11	20
3132d	86	49	35
3011	106		45

ischia

a,b… notation added by NMMNH

N = 3

specimen	length	maximum width
3138a	55	51
3096	59	52
3138b	45	42

APPENDIX 3—DESCRIPTIVE STATISTICS OF THE ROTTEN HILL METOPOSAURID DATABASE

Descriptive statistics of the basic bone groups in the Rotten Hill metoposaur database. Count indicates the number of measurements of each class, not the number of bones in the sample.

Skulls and Lower jaws:

	Skull lengths	Skull widths	Lower jaw lengths	Lower jaw heights
Mean	432.5714	398.4286	491.625	90.125
Standard Error	18.5086	15.97909	14.36718	2.406335
Median	431	411	502.5	88
Mode	505	460	514	88
Standard Deviation	69.25284	73.22539	70.38454	16.67158
Sample Variance	4795.956	5361.957	4953.984	277.9415
Kurtosis	-0.25074	-1.04117	0.267445	0.126836
Skewness	0.046857	-0.40703	0.430318	0.349504
Range	258	244	278	80
Minimum	302	254	376	55
Maximum	560	498	654	135
Sum	6056	8367	11799	4326
Count	14	21	24	48

Atlas and shoulder girdle:

	Atlas lengths	Atlas widths	Clavicle lengths	Clavicle widths	Interclavicle lengths	Interclavicle widths
Mean	31.76471	77	337.5	155.7013	397	302.5763
Standard Error	2.044594	3.799187	5.873773	2.908203	17.06319	5.918954
Median	31	77	345.5	158	378	295
Mode	26	90	363	175	#N/A	290
Standard Deviation	8.430076	15.66445	39.83787	25.51938	66.08544	45.46435
Sample Variance	71.06618	245.375	1587.056	651.2386	4367.286	2067.007
Kurtosis	1.983476	-0.16091	-0.60326	-0.55674	-0.55824	-0.72389
Skewness	-1.00016	-0.33382	-0.58788	0.021876	0.286338	0.257675
Range	33	58	142	105	228	184
Minimum	9	42	256	105	282	216
Maximum	42	100	398	210	510	400
Sum	540	1309	15525	11989	5955	17852
Count	17	17	46	77	15	59

Pelvic girdle:

	Ilium lengths	Ilium proximal widths	Ilium distal widths	Ischium lengths	Ischium widths
Mean	75.42857	36.07143	26.85714	53	48.33333
Standard Error	4.499956	2.732515	2.098815	4.163332	3.179797
Median	77	35.5	24.5	55	51
Mode	64	44	24	#N/A	#N/A
Standard Deviation	16.8373	10.22414	7.853046	7.211103	5.507571
Sample Variance	283.4945	104.533	61.67033	52	30.33333
Kurtosis	0.179052	1.564433	0.713158		
Skewness	-0.14619	-0.86272	1.013925	-1.15207	-1.66803
Range	65	39	28	14	10
Minimum	41	11	17	45	42
Maximum	106	50	45	59	52
Sum	1056	505	376	159	145
Count	14	14	14	3	3

Limb bones:

	Hum length	Hum prox width	Hum dist width	Rad length	Rad prox width	Rad dist width	Femur length	Femur prox width	Femur dist width	Tibia length	Tibia Prox width	Tibia dist width	Fib length	Fib prox width	Fib dist width
Mean	98.3	37.65	68.076	64.25	27	25.66	108.6	34	42.27	61	37.4	27.8	46.75	30.75	26.25
Standard Error	4.009	1.85	3.832	3.962	1.952	1.308	3.631	1.67	1.89	3.36	2.158	1.240	2.955	2.496	1.25
Median	97.5	35.5	69	59.5	26	25.5	106.5	32	41.5	60	35	27	45.5	32	26.5
Mode	92	35	#N/A	59	22	#N/A	109	26	47	#N/A	35	#N/A	#N/A	#N/A	#N/A
Standard Deviation	17.932	8.273	13.817	11.209	5.163	3.20	15.41	6.88	8.020	7.516	4.827	2.77	5.909	4.99	2.5
Sample Variance	321.58	68.45	190.9	125.64	26.66	10.26	237.4	47.37	64.33	56.5	23.3	7.7	34.92	24.92	6.25
Kurtosis	-0.191	-0.827	-1.128	-0.718	-0.987	0.681	2.107	-0.009	-0.70	1.82	4.83	0.129	2.18	-0.002	0.93
Skewness	0.291	0.466	-0.406	0.882	0.762	0.78	1.27	0.784	0.429	1.130	2.19	0.926	1.18	-1.06	-0.56
Range	71	27	41	30	13	9	61	23	26	20	11	7	14	11	6
Minimum	65	26	46	52	22	22	90	26	31	53	35	25	41	24	23
Maximum	136	53	87	82	35	31	151	49	57	73	46	32	55	35	29
Sum	1966	753		514	189	154	1954	578	761	305	187	139	187	123	105
Count	20	20		8	7	6	18	17	18	5	5	5	4	4	4

APPENDIX 4--TEST FOR COINCIDENCE IN THE REGRESSION LINES

Test for coincidence in the regression lines of distal humerus width on humerus length in the Lamy, NM metoposaur population (Line 1) and the Rotten Hill population (Line 2). Critical value of F corresponding to $P < 0.05$ is 3.30, $P < 0.01$ is 5.34 (Glantz, 2005, Table 3-1).

--- Compare Two Regressions ---

	Line 1	Line 2	Single Regression
n:	23	13	36
Slope:	0.545	0.586	0.560
y Int:	8.286	9.195	8.578
SE Slope:	0.032	0.101	0.046
SE Int:	3.292	10.312	4.757
SE Est:	2.839	7.146	5.263
r:	0.965	0.869	0.900
t:	16.975	5.819	12.067
DF:	21	11	34
P:	0.000	0.000	0.000

Overall Test of Coincidence:
$F = 4.613$ with 2 numerator and 32 denominator degrees of freedom; $P = 0.017$

Comparison of slopes: $t = 0.468$ with 32 degrees of freedom; $P = 0.643$
Comparison of intercepts: $t = 0.103$ with 32 degrees of freedom; $P = 0.919$
Results of Analysis of Variance (ANOVA) tests for statistically significant difference between the resolved component modes in the clavicle data. Holm's multiple comparison test is used.

One Way ANOVA
Data Table: Rotten Hill metoposaur clavicle size groups
Factor A: 10 Groups
E, F, G, N, H, I, J, K, L, M

Analysis of Variance Results

Source	DF	SS	MS	F	P
Total	76	49494.13	651.23855		
A	9	48990.619	5443.4021	724.32948	< .0001
Error	67	503.51111	7.5150912		

Holm's Multiple Comparison

Comparison	Mean Difference	|t|		2-Padjusted Alpha	Significant?
N vs J	-24.8889	20.5893	0	0.001111	yes
N vs I	-15.1111	11.6933	0	0.001136	yes
N vs L	-49.7222	30.183	0	0.001163	yes
N vs K	-36.2222	23.6892	0	0.00119	yes
G vs M	-70.1667	33.5124	0	0.00122	yes
G vs J	-36.3333	32.4649	0	0.00125	yes
G vs I	-26.5556	1.968	0	0.001282	yes
G vs L	-61.1667	38.6463	0	0.001316	yes
G vs K	-47.6667	32.6662	0	0.001351	yes
N vs M	-58.7222	27.4016	0	0.001389	yes
I vs M	-43.6111	20.3503	0	0.001429	yes
I vs L	-34.6111	21.0101	0	0.001471	yes
J vs M	-33.8333	16.1592	0	0.001515	yes
J vs L	-24.8333	15.6902	0	0.001562	yes
I vs K	-21.1111	13.8066	0	0.001613	yes
H vs K	-27.5	17.5964	0	0.001667	yes
H vs J	-16.1667	12.9203	0	0.001724	yes
H vs M	-50	23.0708	0	0.001786	yes
H vs L	-41	24.4231	0	0.001852	yes
E vs K	-77.3333	46.5869	0	0.001923	yes
E vs J	-66	48.1512	0	0.002	yes
E vs M	-99.8333	44.602	0	0.002083	yes
E vs L	-90.8333	51.3315	0	0.002174	yes
E vs I	-56.2222	38.9128	0	0.002273	yes
E vs G	-29.6667	21.6437	0	0.002381	yes
E vs F	-17.2333	12.1736	0	0.0025	yes
E vs H	-49.8333	33.6596	0	0.002632	yes
E vs N	-41.1111	28.454	0	0.002778	yes
F vs N	-23.8778	18.9571	0	0.002941	yes
F vs L	-73.6	45.3813	0	0.003125	yes
F vs K	-60.1	40.0264	0	0.003333	yes
G vs H	-20.1667	16.1171	0	0.003571	yes
F vs M	-82.6	38.8989	0	0.003846	yes
F vs J	-48.7667	41.5466	0	0.004167	yes
F vs I	-38.9889	30.9541	0	0.004545	yes
F vs H	-32.6	25.0703	0	0.005	yes

F vs G	-12.4333	10.5925	6.661e-16	0.005556	yes
K vs M	-22.5	9.8099	1.377e-14	0.00625	yes
G vs N	-11.4444	9.4674	5.618e-14	0.007143	yes
I vs J	-9.77778	8.0886	1.666e-11	0.008333	yes
J vs K	-11.3333	7.7668	6.337e-11	0.01	yes
K vs L	-13.5	7.3411	3.702e-10	0.0125	yes
N vs H	-8.72222	6.5479	9.676e-09	0.01667	yes
H vs I	-6.38889	4.7962	9.387e-06	0.025	yes
L vs M	-9	3.7909	0.0003243	0.05	yes

Results of Analysis of Variance (ANOVA) tests for statistically significant difference between the resolved component modes in the interclavicle data. Holm's multiple comparison test is used.

One Way ANOVA
Data Table: Rotten Hill metoposaur interclavicle size groups
Factor A: 11 Groups
m1, m2, m3, m4, m5, m6, m7, m8, m9, m10, m11

Analysis of Variance Results

Source	DF	SS	MS	F	P
Total	58	119886.41	2067.007		
A	10	118948.34	11894.834	608.64942	< .0001
Error	48	938.06389	19.542998		

Holm's Multiple Comparison

Comparison	Mean Difference	|t|		2-P adjusted Alpha	Significant?
m4 vs m8	-67.8	26.9025	0	0.0009091	yes
m4 vs m7	-56	22.2203	0	0.0009259	yes
m4 vs m9	-86.5	31.9525	0	0.0009434	yes
m4 vs m11	-123.5	35.3371	0	0.0009615	yes
m4 vs m10	-102	37.6781	0	0.0009804	yes
m4 vs m6	-35.875	16.2303	0	0.001	yes
m3 vs m8	-87.1333	35.3371	0	0.00102	yes
m3 vs m7	-75.3333	30.5516	0	0.001042	yes
m3 vs m9	-105.833	39.8388	0	0.001064	yes
m3 vs m11	-142.833	41.3308	0	0.001087	yes
m3 vs m10	-121.333	45.6735	0	0.001111	yes
m6 vs m8	-31.925	12.6676	0	0.001136	yes
m7 vs m10	-46	15.5116	0	0.001163	yes
m6 vs m9	-50.625	18.7005	0	0.00119	yes
m6 vs m11	-87.625	25.0722	0	0.00122	yes
m6 vs m10	-66.125	24.4261	0	0.00125	yes
m5 vs m11	-104.944	30.3671	0	0.001282	yes
m5 vs m7	-37.4444	15.1857	0	0.001316	yes
m7 vs m11	-67.5	18.2498	0	0.001351	yes
m5 vs m8	-49.2444	19.9712	0	0.001389	yes
m5 vs m10	-83.4444	31.411	0	0.001429	yes
m5 vs m9	-67.9444	25.5763	0	0.001471	yes
m1 vs m6	-90.875	26.0021	0	0.001515	yes
m8 vs m11	-55.7	15.0595	0	0.001562	yes
m2 vs m6	-70.5417	23.57	0	0.001613	yes
m2 vs m5	-53.2222	18.0588	0	0.001667	yes
m1 vs m11	-178.5	40.3778	0	0.001724	yes
m1 vs m8	-122.8	33.2012	0	0.001786	yes
m1 vs m7	-111	30.0109	0	0.001852	yes
m1 vs m10	-157	41.0085	0	0.001923	yes
m1 vs m9	-141.5	36.9599	0	0.002	yes
m1 vs m4	-55	15.7372	0	0.002083	yes
m2 vs m11	-158.167	39.1931	0	0.002174	yes
m3 vs m6	-55.2083	25.701	0	0.002273	yes
m3 vs m5	-37.8889	18.1812	0	0.002381	yes
m2 vs m10	-136.667	40.477	0	0.0025	yes
m2 vs m8	-102.467	31.7386	0	0.002632	yes
m2 vs m7	-90.6667	28.0836	0	0.002778	yes
m1 vs m5	-73.5556	21.2843	0	0.002941	yes
m2 vs m9	-121.167	35.8863	0	0.003125	yes
m2 vs m4	-34.6667	11.5831	1.554e-15	0.003333	yes
m8 vs m10	-34.2	11.5325	1.998e-15	0.003571	yes
m1 vs m3	-35.6667	10.3206	8.926e-14	0.003846	yes
m7 vs m9	-30.5	10.2849	1.001e-13	0.004167	yes
m9 vs m11	-37	9.6644	7.649e-13	0.004545	yes
m3 vs m4	-19.3333	9.0002	7.086e-12	0.005	yes
m4 vs m5	-18.5556	8.6381	2.432e-11	0.005556	yes
m5 vs m6	-17.3194	8.0627	1.771e-10	0.00625	yes
m6 vs m7	-20.125	7.9854	2.317e-10	0.007143	yes
m8 vs m9	-18.7	6.3058	8.538e-08	0.008333	yes
m10 vs m11	-21.5	5.6158	9.63e-07	0.01	yes
m2 vs m3	-15.3333	5.2027	4.028e-06	0.0125	yes
m1 vs m2	-20.3333	5.0385	7.069e-06	0.01667	yes
m9 vs m10	-15.5	4.9585	9.284e-06	0.025	yes
m7 vs m8	-11.8	4.2204	0.0001077	0.05	yes